

*Smith*

(NASA-CR-133616) FEASIBILITY STUDY OF A  
110 WATT PER KILOGRAM LIGHTWEIGHT SOLAR  
ARRAY SYSTEM Final Report (General  
Electric Co.) 345 p HC \$17.75 CSCL 10A

N73-29006

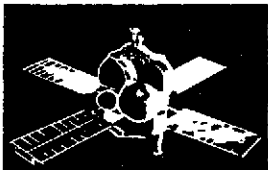
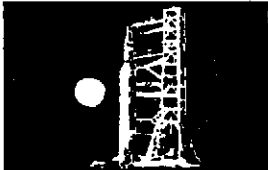
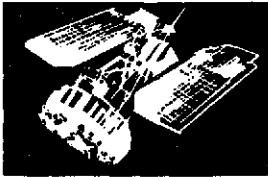
Unclas

G3/03 11478

GE Document No. 73SD4256

May 25, 1973

**SPACE  
DIVISION**

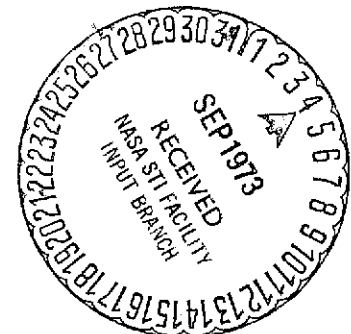


# FINAL REPORT FEASIBILITY STUDY OF A 110 WATT PER KILOGRAM LIGHTWEIGHT SOLAR ARRAY SYSTEM

Reproduced by  
NATIONAL TECHNICAL  
INFORMATION SERVICE  
US Department of Commerce  
Springfield, VA. 22151

Prepared for:  
Jet Propulsion Laboratory

Prepared Under:  
Contract 953387



GENERAL  ELECTRIC

FINAL REPORT  
FEASIBILITY STUDY  
OF A  
110 WATT PER KILOGRAM  
LIGHTWEIGHT SOLAR ARRAY SYSTEM

PREPARED FOR  
JET PROPULSION LABORATORY  
CALIFORNIA INSTITUTE OF TECHNOLOGY  
PASADENA, CALIFORNIA

PREPARED UNDER: CONTRACT 953387

JPL PROJECT MANAGER: E. SEQUEIRA

PREPARED BY: N.F. SHEPARD  
C.V. STAHLER  
K.L. HANSON  
A. SCHNEIDER  
L.E. BLOMSTROM  
W.T. HANSEN  
A. KIRPICH

THIS WORK WAS PERFORMED FOR THE JET  
PROPULSION LABORATORY, CALIFORNIA  
INSTITUTE OF TECHNOLOGY, AS SPONSORED  
BY THE NATIONAL AERONAUTICS AND SPACE  
ADMINISTRATION UNDER CONTRACT NAS7-100

**GENERAL  ELECTRIC**

**SPACE SYSTEMS ORGANIZATION**

Valley Forge Space Center

P. O. Box 8555 • Philadelphia, Penna. 19101

"This report contains information prepared by the General Electric Company, Space Systems Organization, under JPL Subcontract. Its content is not necessarily endorsed by the Jet Propulsion Laboratory, California Institute of Technology, or the National Aeronautics and Space Administration."

## ABSTRACT

This final report summarizes the results of a study to assess the feasibility of a 10,000 watt solar array panel which has a minimum power-to-mass ratio of 110 watt/kg. The application of this ultralightweight solar array to three possible missions was investigated. With the interplanetary mission as a baseline, the constraining requirements for a geosynchronous mission and for a manned space station mission are presented. A review of existing lightweight solar array system concepts revealed that changes in the system approach are necessary to achieve the specified 110 watt/kg goal. A comprehensive review of existing component technology is presented in the areas of thin solar cells, solar cell covers, welded interconnectors, substrates and deployable booms. Advances in the state-of-the-art of solar cell and deployable boom technology were investigated. System level trade studies required to select the optimum boom bending stiffness, system aspect ratio, bus voltage level, and solar cell circuit arrangement are reported. Design analysis tasks included the thermal analysis of the solar cell blanket, thermal stress analysis of the solar cell interconnectors/substrate, and the thermostructural loading of the deployed boom.

A new "V" stiffened solar array concept was conceived and analyzed. This solar array geometry results in increased system stiffness with no increase in total system weight (or reduced weight with the same deployed frequency requirement). A subscale model of this "V" stiffened geometry was fabricated along with a similar model of the conventional planar blanket geometry. These models provide a graphical illustration of the stiffening effect of the "V" geometry.



## TABLE OF CONTENTS

<u>Section</u>	<u>Page</u>
1.0 INTRODUCTION . . . . .	1-1
2.0 SUMMARY . . . . .	2-1
3.0 TECHNICAL DISCUSSION . . . . .	3-1
3.1 Study Objectives and Ground Rules . . . . .	3-1
3.1.1 Design Requirements . . . . .	3-1
3.1.1.1 General . . . . .	3-1
3.1.1.2 Interplanetary Mission . . . . .	3-2
3.1.1.3 Geosynchronous Mission . . . . .	3-6
3.1.1.4 Manned Space Station Mission . . . . .	3-9
3.1.1.5 Comparison of Requirements . . . . .	3-13
3.1.2 State-of-the-Art Philosophy . . . . .	3-17
3.2 Configuration Study Results . . . . .	3-18
3.2.1 Recommended Design Baseline . . . . .	3-18
3.2.1.1 Description . . . . .	3-18
3.2.1.2 Performance . . . . .	3-36
3.2.1.3 Critical Technical Problems . . . . .	3-37
3.2.2 Changes to Baseline Required for Geosynchronous Mission . . . . .	3-40
3.2.2.1 Description . . . . .	3-40
3.2.2.2 Performance . . . . .	3-42
3.2.3 Changes to Baseline Required for Manned Space Station Mission . . . . .	3-42
3.2.3.1 Description . . . . .	3-42
3.2.3.2 Performance . . . . .	3-44
3.3 State-of-the-Art Discussion . . . . .	3-46
3.3.1 State-of-the-Art Baseline . . . . .	3-46
3.3.1.1 Solar Array System Designs . . . . .	3-46
3.3.1.2 Components . . . . .	3-57
3.3.2 State-of-the-Art Advances . . . . .	3-101
3.3.2.1 COMSAT Violet Solar Cell . . . . .	3-101
3.3.2.2 Boron/Aluminum BI-STEM . . . . .	3-101
3.3.2.3 Graphite/Epoxy Boom . . . . .	3-112
3.3.3 Variations in Performance Due to State-of-the-Art Improvements . . . . .	3-114
3.4 Trade-offs, Analyses, and Studies . . . . .	3-116
3.4.1 Parametric Analysis of Solar Cell Blanket . . . . .	3-116
3.4.1.1 General . . . . .	3-116
3.4.1.2 Solar Cell Radiation Degradation . . . . .	3-117
3.4.1.3 Results of Trade Studies . . . . .	3-117
3.4.1.4 Discussion of Results . . . . .	3-129

## TABLE OF CONTENTS (Cont)

<u>Section</u>	<u>Page</u>
3.4.2 Parametric Analysis of Bus Strip	
Distribution System . . . . .	3-133
3.4.2.1 General . . . . .	3-133
3.4.2.2 Method of Analysis . . . . .	3-133
3.4.2.3 Results of Analysis . . . . .	3-136
3.4.3 Planar Solar Array Aspect Ratio Trade Study . . . . .	3-139
3.4.3.1 Introduction . . . . .	3-139
3.4.3.2 Optimum Boom and Blanket Tension	
Analysis . . . . .	3-139
3.4.3.3 Deployment and Support Structure Analysis . . . . .	3-146
3.4.3.4 Study Results . . . . .	3-149
3.4.4 Solar Cell Blanket Configuration Trade Study . . . . .	3-152
3.4.4.1 Introduction . . . . .	3-152
3.4.4.2 Definitions and Nomenclature . . . . .	3-152
3.4.4.3 Candidate Blanket Configurations . . . . .	3-154
3.4.5 Analysis of a "V"-Stiffened Solar Array . . . . .	3-160
3.4.5.1 Introduction . . . . .	3-160
3.4.5.2 RA250 In-Plane Test and Analysis . . . . .	3-162
3.4.5.3 Symmetric Vibration Analysis . . . . .	3-165
3.4.5.4 Assessment of Stiffening Effects . . . . .	3-169
3.4.5.5 Assessment of Reduced Stiffness . . . . .	3-172
3.4.6 Thermal Analysis of Solar Cell Blanket . . . . .	3-174
3.4.6.1 Introduction . . . . .	3-174
3.4.6.2 Solar Cell/Substrate Modeling . . . . .	3-174
3.4.6.3 Transmittance Properties of Kapton-H Film . . . . .	3-174
3.4.6.4 Results of Analysis . . . . .	3-180
3.4.6.5 Discussion of Results . . . . .	3-183
3.4.7 Thermal Stress Analysis of Solar Cell Blanket . . . . .	3-183
3.4.7.1 Introduction . . . . .	3-183
3.4.7.2 Material Properties . . . . .	3-185
3.4.7.3 Results of Analysis . . . . .	3-190
3.4.8 Thermostructural Analysis of Deployed ASTROMAST	
Boom . . . . .	3-194
3.4.9 Stowed Vibration and Loads Analysis . . . . .	3-199
3.4.9.1 Introduction and Summary . . . . .	3-199
3.4.9.2 Analytical Model . . . . .	3-199
3.4.9.3 Vertical Resonant Frequencies . . . . .	3-201
3.4.9.4 Lateral Vibration Analysis . . . . .	3-203
3.4.9.5 Vertical Response Analysis . . . . .	3-204
3.4.9.6 Summary of Results . . . . .	3-205

## TABLE OF CONTENTS (Cont)

<u>Section</u>	<u>Page</u>
3.5 "V"-Stiffened Solar Array Model Development . . . . .	3-209
3.5.1 Introduction . . . . .	3-209
3.5.2 Description of Model . . . . .	3-209
3.5.3 Model Test Results . . . . .	3-212
3.5.4 Discussion of Test Results . . . . .	3-215
3.6 Spacecraft Integration Studies . . . . .	3-216
3.6.1 Mounting Considerations . . . . .	3-216
3.6.1.1 Introduction . . . . .	3-216
3.6.1.2 Present Mounting Arrangement . . . . .	3-217
3.6.1.3 Alternate Mounting Arrangement . . . . .	3-218
3.6.2 Attitude Control Considerations . . . . .	3-218
3.6.2.1 Introduction . . . . .	3-218
3.6.2.2 Design Guidelines . . . . .	3-220
3.6.2.3 Discussion . . . . .	3-221
4.0 CONCLUSIONS. . . . .	4-1
5.0 RECOMMENDATIONS . . . . .	5-1
6.0 NEW TECHNOLOGY . . . . .	6-1
7.0 REFERENCES . . . . .	7-1

### Appendices

A	JPL Specification ES 506080B - Lightweight Solar Panel Subsystem, 110 Watts per Kilogram, Detail Specification for . . . . .	A-1
B	Solar Cell Radiation Damage vs 1- MeV Electron Fluence . . . . .	B-1
C	Preliminary Specification for an Ultralightweight Integrally Covered Solar Cell . . . . .	C-1
D	Preliminary Specification for a Canister Deployed Continuous Longeron ASTROMAST Boom . . . . .	D-1

# LIST OF ILLUSTRATIONS

<u>Figure</u>		<u>Page</u>
2-1	Baseline Solar Array Configuration . . . . .	2-2
3-1	Schematic of the Classes of Particulate Contaminants Associated with Ion Engines . . . . .	3-6
3-2	Variations in Earth-Sun Distance, Apparent Solar Declination and Eclipse Duration for a Geosynchronous Orbit . . . . .	3-7
3-3	Solar Flare Omnidirectional Proton Integral Energy Spectra for Interplanetary and Geosynchronous Missions . . . . .	3-9
3-4	Omnidirectional Trapped Electron Integral Energy Spectra for Geosynchronous Orbit . . . . .	3-10
3-5	Omnidirectional Trapped Proton Integral Energy Spectra for Geosynchronous Orbit . . . . .	3-10
3-6	Transient Heat Rates for $\beta = 0^\circ$ Orbit . . . . .	3-12
3-7	Drag Force with Normal Incidence on $100 \text{ m}^2$ Surface Area . . . . .	3-14
3-8	Omnidirectional Trapped Proton Integral Energy Spectra for 555 km, $i = 60^\circ$ Orbit . . . . .	3-14
3-9	Omnidirectional Trapped Electron Integral Energy Spectra for 555 km, $i = 60^\circ$ Orbit . . . . .	3-15
3-10	Solar Flare Omnidirectional Proton Integral Energy Spectra for 500 km, $i = 55^\circ$ Orbit . . . . .	3-15
3-11	Outline Drawing of Baseline Configuration . . . . .	3-19
3-12	Detail of Module Arrangement on Solar Cell Blankets . . . . .	3-23
3-13	Rear View of Solar Cell Blanket . . . . .	3-26
3-14	Flatpack Solar Array with Protective Interleafs . . . . .	3-28
3-15	Retractable Flatpack Concept . . . . .	3-28
3-16	Flatpack Solar Array Configuration . . . . .	3-30
3-17	Diagram of Retractable Scissors Assembly . . . . .	3-31
3-18	Solar Panel Frames . . . . .	3-33
3-19	Beginning-of-Life Solar Array I-V Characteristic . . . . .	3-38
3-20	Bulk Accumulation Regions for Mercury Atoms on Surfaces where Absorbed Monolayers Already Exist . . . . .	3-38

# LIST OF ILLUSTRATIONS (Cont)

<u>Figure</u>		<u>Page</u>
3-21	Effects of Uniform Molybdenum Film on Illuminated (Front) Surface of Solar Cell Panel . . . . .	3-39
3-22	Comparison of SERT II Results with Theoretical Predictions . . . . .	3-41
3-23	Solar Array I-V Characteristic in Geosynchronous Orbit at Two Seasons of the Year . . . . .	3-42
3-24	Beginning-of-Life Solar Array I-V Characteristic . . . . .	3-45
3-25	GE/JPL 30 watt/lb Roll-up Solar Array . . . . .	3-47
3-26	Hughes/AF Roll-up Solar Array . . . . .	3-48
3-27	RAE Flat-pack Solar Array . . . . .	3-49
3-28	Lockheed Space Station Solar Array . . . . .	3-51
3-29	CTS Flat-pack Solar Array . . . . .	3-52
3-30	Boeing/JPL Fold-out Solar Array . . . . .	
3-31	EOS Hollowcore Folding Solar Array (Phase II Demonstration Panels). . .	3-55
3-32	Bottom Wraparound Contact Configuration . . . . .	3-58
3-33	Baseline Solar Cell Electrical Performance . . . . .	3-60
3-34	I-V Characteristic for 125 $\mu\text{m}$ Thick, 10 ohm-cm Covered Ferranti Cell . . . . .	3-60
3-35	Integral Coverslip Cell Bow Versus Integral Coverslip Thickness . . .	3-64
3-36	Transmission of 150 $\mu\text{m}$ Slides after $2.5 \times 10^{14}$ 1-MeV Electrons/cm <sup>2</sup> . . . . .	3-65
3-37	Transmission of 150 $\mu\text{m}$ Slides after $5 \times 10^{15}$ 1-MeV Electrons/cm <sup>2</sup> . . .	3-65
3-38	Stress in the Integral Cover as a Function of Film Thickness for Silica and Two Borosilicate Glasses . . . . .	3-68
3-39	Effect of 2 keV Protons on Solar Cell Short-Circuit Current . . . . .	3-71
3-40	FEP Covered Submodules . . . . .	3-72
3-41	Circuit Interconnect Pattern . . . . .	3-73
3-42	FEP Covered Module . . . . .	3-74
3-43	Details of Lockheed Space Station Solar Array Substrates . . . . .	3-76
3-44	RAE Flat-pack Solar Array Substrate Configuration . . . . .	3-77

## LIST OF ILLUSTRATIONS (Cont)

<u>Figure</u>		<u>Page</u>
3-45	Normalized Cumulative Number of Solder Joints Showing Cracks after 400 Cycles from 75°C to the Indicated Lower Temperature Limit . . . . .	3-80
3-46	Contact Pull Strength Tab Configuration . . . . .	3-80
3-47	Contact Strength of Solar Cell Solder Joint . . . . .	3-81
3-48	Time to Solder Joint Rupture versus Applied Stress for Two Solder Alloys at Various Temperatures . . . . .	3-81
3-49	TRW Welded Aluminum Interconnector Configuration . . . . .	3-82
3-50	Thermal Stress in Welded Joints . . . . .	3-84
3-51	Cycles to Failure versus Temperature Range . . . . .	3-84
3-52	Hughes Aluminum Cell/Aluminum Interconnector Ultrasonically Welded Module . . . . .	3-85
3-53	Welded Ag Mesh Interconnector . . . . .	3-86
3-54	Photomicrograph of Welded Joint . . . . .	3-87
3-55	Hughes MCW-550 Impulse Welder . . . . .	3-87
3-56	Mechanical Strength of Welded Electrical Degradation versus Welding Voltages . . . . .	3-88
3-57	Laser Microwelder . . . . .	3-89
3-58	Results of Peel Tests on Thermal-Diffusion Bonded Solar Cell Joints . . . . .	3-89
3-59	Schematic of STEM Boom . . . . .	3-90
3-60	Schematic of BI-STEM Boom . . . . .	3-91
3-61	BI-STEM Deployable Boom and Actuator . . . . .	3-92
3-62	Schematic of Quasi-Biconvex Boom . . . . .	3-92
3-63	ASTROMAST Coilable Lattice Boom - Lunar Antenna Mast . . . . .	3-93
3-64	ASTROMAST Articulated Lattice Boom for Lockheed Space Station Solar Array . . . . .	3-94
3-65	BI-STEM Section . . . . .	3-95
3-66	BI-STEM Deployer Mass vs Boom Diameter . . . . .	3-96
3-67	Deployable Boom Mass vs Bending Stiffness . . . . .	3-98
3-68	Total Mass of Boom Plus Deployer vs Bending Stiffness . . . . .	3-99

# LIST OF ILLUSTRATIONS (Cont)

<u>Figure</u>		<u>Page</u>
3-69	Relative Flexural Modulus vs Temperature for "Scotchply" Type 1002 Unidirectional Fiberglass/Epoxy Composite . . . . .	3-99
3-70	Total Mass of an Articulated ASTROMAST with Steel Longerons vs Mast Diameter . . . . .	3-100
3-71	1-MeV Electrons Radiation Damage of COMSAT Violet Cells Compared with Conventional Cells . . . . .	3-102
3-72	Effects of Fiber Content on Composite Modulus of Elasticity . . . .	3-106
3-73	Transverse Elastic Modulus vs Content of 107 $\mu\text{m}$ BORSIC Fibers . . .	3-107
3-74	Transverse Tensile Strength of 50% Volume 107 $\mu\text{m}$ BORSIC/Aluminum . . . . .	3-108
3-75	Transverse Tensile Strength of 60% Volume 142 $\mu\text{m}$ BORSIC/6061 Aluminum . . . . .	3-109
3-76	B/Al Composite Tape Material. . . . .	3-110
3-77	Possible Configurations of B/Al Monolayer Tape . . . . .	3-111
3-78	Rockwell International Corp. Concept for a Graphite Composite Deployable Boom . . . . .	3-113
3-79	Effects of Improved Solar Cell Performance on System Power-to-Mass Ratio . . . . .	3-115
3-80	Damage Equivalent-Normally Incident (DENI) 1-MeV Electron Fluence with Infinite Backshielding for Interplanetary Mission . . . . .	3-118
3-81	Damage Equivalent-Normally Incident (DENI) 1-MeV Electron Fluence with Infinite Backshielding for Geosynchronous Mission . . . . .	3-118
3-82	Damage Equivalent-Normally Incident (DENI) 1-MeV Electron Fluence with Infinite Backshielding for Manned Space Station Mission . . . .	3-121
3-83	Solar Cell Blanket Mass for Interplanetary Mission (10 kw, BOL Output) . . . . .	3-123
3-84	Solar Cell Blanket Mass for Geosynchronous Mission (10 kw, BOL Output) . . . . .	3-126
3-85	Solar Cell Blanket Mass for Manned Space Station Mission (10 kw, BOL Output) . . . . .	3-128
3-86	Solar Cell Blanket Trade-off for Interplanetary Mission (7.5 kw, EOL Output) . . . . .	3-130

# LIST OF ILLUSTRATIONS (Cont)

<u>Figure</u>		<u>Page</u>
3-87	Solar Cell Blanket Trade-off for Geosynchronous Mission (7.5 kw, EOL Output) . . . . .	3-130
3-88	Solar Cell Blanket Trade-off for Manned Space Station Mission (7.5 kw, EOL Output) . . . . .	3-130
3-89	Minimum Possible Blanket Mass for 100 $\mu$ m Thick Cells . . . . .	3-131
3-90	Minimum Possible Blanket Mass for 125 $\mu$ m Thick Cells . . . . .	3-131
3-91	Schematic of Solar Cell Blanket Circuit Configuration . . . . .	3-134
3-92	Optimum Bus Strip Power Loss vs Voltage . . . . .	3-138
3-93	Total Bus Strip Mass at the Optimum vs Voltage . . . . .	3-138
3-94	Total Blanket Mass vs Blanket Aspect Ratio . . . . .	3-141
3-95	Finite-Element Model of Two Blankets, Single Boom Solar Array . . .	3-142
3-96	Continuous Fiberglass Longerons ASTROMAST Mass and Diameter as a Function of Bending Stiffness . . . . .	3-143
3-97	Steel BI-STEM Mass and Diameter as a Function of Bending Stiffness . . . . .	3-143
3-98	Symmetric and Anti-Symmetric Frequency vs Tension . . . . .	3-145
3-99	Symmetric and Anti-symmetric Frequency vs Tension . . . . .	3-145
3-100	Optimum Boom Stiffness and Tension vs Frequency . . . . .	3-147
3-101	Optimum Boom Stiffness and Tension vs Frequency . . . . .	3-148
3-102	Total Structural Mass vs Blanket Width and Strip Length . . . . .	3-149
3-103	Total System Mass vs Deployed Natural Frequency . . . . .	3-150
3-104	Total System Mass vs Deployed Natural Frequency . . . . .	3-150
3-105	Total System Mass vs Aspect Ratio . . . . .	3-151
3-106	Total System Mass vs Aspect Ratio . . . . .	3-151
3-107	Solar Cell Circuit Configuration . . . . .	3-153
3-108	Solar Cell Blanket Configuration . . . . .	3-155
3-109	Comparison of 2 and 10 ohm-cm Cells at Various Operating Temperatures . . . . .	3-157
3-110	"V" Configuration, Single Boom Solar Array Concept . . . . .	3-160



# LIST OF ILLUSTRATIONS (Cont)

<u>Figure</u>		<u>Page</u>
3-111	In-Plane Force-Deflection Characteristic . . . . .	3-163
3-112	Symmetric Models . . . . .	3-166
3-113	Edge View of Deflected Array . . . . .	3-167
3-114	Force Diagram of Outer End of Array . . . . .	3-167
3-115	Effect of Blanket Tension on Solar Array Frequency . . . . .	3-171
3-116	Effect of Boom Stiffness on "V" Configuration Solar Array Characteristics . . . . .	3-173
3-117	Solar Cell Thermal Model - 37 Nodes . . . . .	3-175
3-118	Infrared Transmittance of 50 $\mu$ m Thick Kapton-H Film. . . . .	3-177
3-119	Cool-down and Heat-up Transient Temperature History in Geosynchronous Orbit. . . . .	3-182
3-120	Solar Array Maximum Power Output vs Equilibrium Temperature . . . . .	3-184
3-121	Power-to-Mass Ratio of Baseline Solar Array Panel Configuration vs Temperature . . . . .	3-184
3-122	Linear Thermal Expansion of Solar Cell Blanket Materials . . . . .	3-186
3-123	Kapton Thermal Expansion Test Set-up . . . . .	3-187
3-124	Geometry of Wire Interconnectors at Room Temperature . . . . .	3-191
3-125	Thermal Distortion with Aluminum Interconnectors at 73.2°C Solar Cell Temperature . . . . .	3-192
3-126	Model of Interconnector Wire Loop Configuration . . . . .	3-193
3-127	Deployable Boom Orbital Thermostructural Loading . . . . .	3-195
3-128	Continuous Longeron ASTROMAST Diameter and Weight vs Bending Stiffness . . . . .	3-197
3-129	Continuous Longeron ASTROMAST Diameter and Weight vs Bending Strength . . . . .	3-198
3-130	Maximum Bending Moment vs Blanket Tension . . . . .	3-198
3-131	Analytical Models of Stowed Solar Array . . . . .	3-200
3-132	Results of Vertical Vibration Analysis . . . . .	3-202
3-133	Results of Lateral Vibration Analysis . . . . .	3-204

## LIST OF ILLUSTRATIONS (Cont)

<u>Figure</u>	<u>Page</u>
3-134 Vertical Response Analysis - Simple Supports at Ends . . . . .	3-206
3-135 Vertical Response Analysis - Simple Supports at Quarter Span . . . . .	3-206
3-136 Vertical Response Analysis - Cantilevered at Center . . . . .	3-207
3-137 Vertical Response Analysis - End and Center Supports . . . . .	3-207
3-138 Solar Array "V" Stiffened Demonstration Models . . . . .	3-210
3-139 Comparison of Static Tip Deflections of Planar and "V" Stiffened Models . . . . .	3-213
3-140 Model Vibration Test Results . . . . .	3-215
3-141 Constraints on Baseline Mounting Arrangement . . . . .	3-217
3-142 Static Deflection vs Frequency . . . . .	3-223

# LIST OF TABLES

<u>Table</u>		<u>Page</u>
2-1	Limiting Design Requirements . . . . .	2-1
2-2	Summary of Baseline Solar Array Panel Design Features for each Mission Application . . . . .	2-4
3-1	Mission Orbital Parameters . . . . .	3-1
3-2	Summary of Design Requirements for Interplanetary Mission from JPL Specification E5506080B . . . . .	3-3
3-3	Comparison of Key Design Requirements . . . . .	3-16
3-4	Significant Design Features of the Baseline Solar Array Panel Configuration . . . . .	3-21
3-5	Component Quantity Related to Level of Assembly . . . . .	3-24
3-6	Design Characteristics of Ferranti Type MS36 125 $\mu$ m Thick Solar Cells . . . . .	3-25
3-7	Mass Breakdown for Solar Cell Blanket (Total for Both Blankets) . . . . .	3-27
3-8	Design Characteristics of Articulated Steel Longerons ASTROMAST . . . . .	3-34
3-9	Total System Mass Summary . . . . .	3-36
3-10	Design Characteristics of Continuous Fiberglass Longerons ASTROMAST . . . . .	3-41
3-11	Total System Mass Summary for Manned Space Station Application . . . . .	3-44
3-12	Existing Lightweight Solar Array Types . . . . .	3-46
3-13	Comparison of Existing Lightweight Solar Array Designs . . . . .	3-56
3-14	Summary of Integral Cover Materials Deposited by HVIBS . . . . .	3-62
3-15	Comparison of Integral Cover Materials . . . . .	3-63
3-16	1-MeV Proton Irradiation Data . . . . .	3-66
3-17	Mass of Lockheed Space Station Solar Array Substrate . . . . .	3-77
3-18	Mass of RAE Flat-pack Solar Array Substrate . . . . .	3-78
3-19	Comparison of Soldered and Welded Solar Cell Interconnections . . . . .	3-79
3-20	Axial Tensile Strength of 142 $\mu$ m BORSIC/Al . . . . .	3-105
3-21	Properties of Aluminum Alloy Matrix Materials . . . . .	3-112
3-22	Six-Cusp Graphite/Epoxy Tubular Boom Properties for SEPS Solar Array Application . . . . .	3-113

# LIST OF TABLES (Cont)

<u>Table</u>		<u>Page</u>
3-23	Equivalent 1-MeV Electron Fluences for N/P Type Silicon Solar Cells in Low Altitude Circular Orbits in the Time Period 1977-1990 . . .	3-119
3-24	Solar Cell Blanket Weight Tradeoff for Interplanetary Mission . . . .	3-120
3-25	Baseline Solar Cell Maximum Power Output . . . . .	3-121
3-26	Minimum Possible Blanket Mass for 10,000 Watts, BOL, 1 AU, 55°C . . . . .	3-124
3-27	Solar Cell Blanket Mass Tradeoff for Geosynchronous Mission . . . .	3-125
3-28	Solar Cell Blanket Mass Tradeoff for Manned Space Station Mission . .	3-127
3-29	Summary of Blanket Mass vs Aspect Ratio Trade Study. . . . .	3-140
3-30	Possible Module Lengths . . . . .	3-156
3-31	Possible Circuit Arrangements for $N_{S/C} = 540$ . . . . .	3-158
3-32	Possible Blanket Configurations for $N_{P/M} N_{C/B} = 221$ . . . . .	3-159
3-33	Possible Blanket Configurations for $N_{P/M} N_{C/B} = 210$ . . . . .	3-161
3-34	Effect of Blanket Tension on Force-Deflection Characteristics of "V" Configuration Solar Array . . . . .	3-170
3-35	Effect of Boom Stiffness on Force-Deflection Characteristics of "V" Configuration Solar Array . . . . .	3-173
3-36	Material Thermal Properties . . . . .	3-176
3-37	Calculation of Kapton Transmittance for a 76.7°C (170°F) Black Body Radiation Spectrum . . . . .	3-179
3-38	Calculation of Total Average Kapton Transmittance . . . . .	3-181
3-39	Steady-State Temperature Distributions . . . . .	3-181
3-40	Mechanical Properties of Materials . . . . .	3-185
3-41	Raw and Reduced Data for Kapton Specimen Length . . . . .	3-188
3-42	Linear Coefficient of Thermal Expansion for Kapton-H Film (50 $\mu$ m Thick) . . . . .	3-190
3-43	Margins of Safety for Combined Bending and Axial Stresses in the Wires .	3-193
3-44	Summary of Maximum Loads and Responses for "1" g Excitation . . .	3-208
3-45	Design Parameters of Models . . . . .	3-211

## LIST OF TABLES (Cont)

<u>Tables</u>		<u>Page</u>
3-46	Summary of Vibration Test Results . . . . .	3-214
3-47	Alternative Mounting Arrangements . . . . .	3-219
3-48	Structural Rigidity Design Requirements for Large Lightweight Solar Array Programs . . . . .	3-222

SECTION 1  
INTRODUCTION

## SECTION 1

### INTRODUCTION

A program to study the feasibility of a 10,000 watt solar array panel system with an overall power-to-mass ratio of better than 110 watts/kg was initiated on May 5, 1972. This panel system would be one element of a multipanel solar array system on space vehicles for interplanetary, synchronous earth orbit, or manned space station missions. The power-to-mass ratio is interpreted to be the delivered beginning-of-life maximum power output at 1 AU divided by the total system mass which includes all elements of the deployment and support structure and mechanisms, but not the gimbaling or orientation related equipment. Thus, for the specified power output of 10,000 watts at 1 AU, the total panel system mass must be less than 90.9 kg.

The program has been organized into the following tasks:

<u>Task No.</u>	<u>Task Title</u>
1000	Design Requirements Definition and Analysis
2000	Investigation of Existing Array Technology
3000	Feasibility of Extending Existing Array Concepts to 110 Watts/kg
4000	Definition and Analysis of Improved Configurations
5000	State-of-the-Art Analysis, Projection and Advances

In Task 1000 the design requirements for each of the three missions were investigated with the results summarized in Section 3.1.1. This set of design requirements was used as a guide to the trade-off and analysis activity during the second quarter.

In Tasks 2000 and 3000, the use of existing concepts, configurations and technology was investigated and is reported in Section 3.3.1. The best features of these existing concepts were combined with recent advances in component technology to formulate a baseline configuration which has a power-to-mass ratio of better than 110 watt/kg. This configuration is described in Section 3.2.1.

Task 4000 involved the synthesis of advanced concepts and configurations to meet the system requirements. A promising new concept, called the "V" stiffened solar array, is described in Section 3.4.5. This concept provides increased stiffness to out-of-plane bending when compared to an equivalent planar geometry. This may allow a reduction in the boom stiffness (and weight) required to maintain a specified deployed natural frequency. A subscale model of the "V" stiffened solar array configuration was fabricated along with a similar model of a planar array geometry. Static load tests and "twang" tests were performed to obtain quantitative verification of the analytical results. This model development and testing activity is reported in Section 3.5.

Task 5000 consists of two major parts. One is concerned with the analysis and definition of the state-of-the-art with respect to the design of the candidate configurations. It was a goal of the study to base the design of the system upon components or devices which are commercially available on today's market. Preliminary component specifications were prepared for the two components which represent that greatest uncertainty in terms of development status. The specification for an ultralightweight integrally covered solar cell is contained in Appendix C, while Appendix D applies to a canister deployed, continuous longeron ASTROMAST. These specifications, which reflect the current performance requirements as related to this program application, are directed toward specific technical or design approaches. Comments on technical content and budgetary pricing information were solicited from the suppliers of these items.



## SECTION 2

### SUMMARY

## SECTION 2

### SUMMARY

The definition of solar array design requirements for the three mission applications resulted in the limiting requirements which are summarized in Table 2-1. All missions require a minimum deployed natural frequency of 0.04 Hz and a power-to-mass ratio of at least 110 watt/kg at the beginning-of-life. For the reference interplanetary mission, the limiting requirement is the thermal shock temperature range of  $-190^{\circ}\text{C}$  to  $+140^{\circ}\text{C}$ . For the geosynchronous application the upper limit of this range can be reduced to about  $+70^{\circ}\text{C}$ . The limiting design requirements for a possible manned space station application include full in-orbit retraction capability which is not needed for the other two missions. In addition, this

Table 2-1. Limiting Design Requirements

Mission	Limiting Design Requirements
All Missions	<ol style="list-style-type: none"> <li>1. <math>f \geq 0.04 \text{ Hz}</math></li> <li>2. Beginning-of-life (BOL) power-to-mass ratio <math>\geq 110 \text{ watt/kg}</math></li> <li>3. 10,000 watts at BOL</li> </ol>
Interplanetary	<ol style="list-style-type: none"> <li>1. Thermal shock temperature range = <math>-190^{\circ}</math> to <math>+140^{\circ}\text{C}</math></li> <li>2. Thermal shock cycles = 1000</li> </ol>
Geosynchronous	<ol style="list-style-type: none"> <li>1. Thermal shock temperature range = <math>-190</math> to <math>+70^{\circ}\text{C}</math></li> <li>2. Thermal shock cycles = 1000</li> </ol>
Manned Space Station	<ol style="list-style-type: none"> <li>1. Full in-orbit retraction required</li> <li>2. 0.035 g's for 0.3 sec</li> <li>3. <math>0.137 \text{ deg/sec}^2</math> for 2 sec</li> <li>4. Thermal shock temperature range = <math>-91^{\circ}</math> to <math>+80^{\circ}\text{C}</math></li> <li>5. Thermal shock cycles = 60,000</li> </ol>

application requires the deployed solar array to withstand certain loading conditions as specified in Table 2-1. The thermal shock environment is characterized by the large number of cycles associated with the postulated 10 year in-orbit useful life of such an array.

The baseline configuration which meets those requirements for the interplanetary and geosynchronous missions is shown in Figure 2-1. This concept consists of a single, central, deployable mast which supports two flexible solar cell blankets. The 10,000 watt beginning-of-life output is generated by 226,800 solar cells which are interconnected to supply power at a 193 vdc maximum power voltage. These solar cells are nominal 125  $\mu\text{m}$  thick, 2 x 2 cm, N/P silicon with a nominal base resistivity of 10 ohm-cm. A plated nickel-copper-nickel-gold bottom wraparound contact configuration is used in conjunction with an ultrasonically bonded aluminum wire interconnector system. The active solar cell surface is protected from low energy proton damage by a nominal 37  $\mu\text{m}$  thick integrally deposited coverglass. A Kapton-H film substrate supports the solar cell modules without the aid of a bonding adhesive. Holes in the substrate allow for this direct radiation heat transfer from the rear of the solar cells. The exposed portions of the rear cell contacts are coated with adhesive to provide the necessary low energy proton protection.

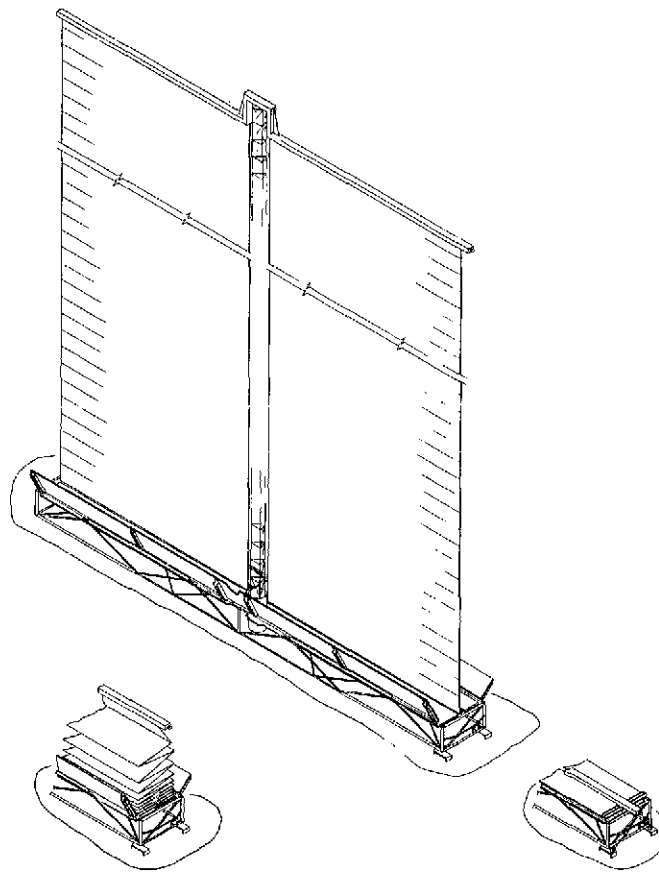


Figure 2-1. Baseline Solar Array Configuration

Tension in the solar cell blanket substrates maintains the deployed natural frequency above the minimum specified value of 0.04 Hz. The flexible solar cell blankets are stowed for launch by folding into a flat-pack package which is retained in compression between a bottom honeycomb panel and spring driven hinged honeycomb panel doors on the top. These doors are held closed during launch by the tubular leading edge member (LEM) which is attached to the deployable boom at the center and retained at each end by a launch retention cable mechanism. Solar array deployment is accomplished by firing redundant cable cutters at each end of the array which releases the end of the LEM and the restraint at each end of the supporting truss work. Application of power to the deployable boom actuator will cause the LEM to move off the door panels allowing them to swing open. Continued deployment of the boom will cause the LEM to pull each fold of the blankets from the stowed package. Interlayer cushions of Kapton-H film are retained by the bottom panel. At the end of the deployment travel, the further deployment of the blankets applies the required tension load by extending a spring mechanism at the base of each blanket.

The deployable boom is an ASTROMAST structure manufactured by SPAR Aerospace Products, Ltd. For this interplanetary mission application an articulated longeron mast, which is similar to the Lockheed Space Station Solar Array Mast, is required to meet the specified +140<sup>0</sup> C upper temperature extreme. The other two mission applications can utilize a continuous fiberglass longeron mast. Table 2-2 summarizes the significant design features of the baseline design as applied to the three mission types. The addition of retraction capability, in the form of a roll-up drum stowage system, in the manned space station design results in a total system mass which does not meet the 110 watt/kg goal.

Table 2-2. Summary of Baseline Solar Array Panel Design Features  
for each Mission Application

Parameter	Mission Application		
	Interplanetary	Geosynchronous	Manned Space Station
1. Deployed length (L')	18.565 m	18.565 m	18.565 m
2. Total width (W)	5.915 m	5.915 m	5.915 m
3. Blanket width (w)	2.830 m	2.830 m	2.830 m
4. System aspect ratio (L'/W)	3.14	3.14	3.14
5. Total gross blanket area	105.08 m <sup>2</sup>	105.08 m <sup>2</sup>	105.08 m <sup>2</sup>
6. Total number of solar cells (2 x 2 cm)	226 800	226 800	226 800
7. Lowest deployed natural frequency	0.04 Hz	0.04 Hz	0.04 Hz
8. Maximum equilibrium temperature at 1 AU	57°C	57°C	80°C
9. Solar cell base resistivity	10 ohm-cm	10 ohm-cm	2 ohm-cm
10. Electrical power output at BOL	V <sub>mp</sub> = 193 volts	V <sub>mp</sub> = 193 volts	V <sub>mp</sub> = 193 volts
• Maximum equilibrium temperature			
• 1 AU, AMO illumination	P <sub>max</sub> = 9860 watts	P <sub>max</sub> = 9860 watts	P <sub>max</sub> = 10060 watts
• Normal incidence			
• Measured at panel interface connector			
11. Total system mass	87.5 kg	86.8 kg	95.1 kg
12. Expected maximum power degradation at the end-of-mission (EOM)	30%	32%	20%
13. BOL power-to-mass ratio	112.7 watt/kg	113.6 watt/kg	105.8 watt/kg
14. EOM power-to-mass ratio	78.9 watt/kg	77.2 watt/kg	84.6 watt/kg

SECTION 3  
TECHNICAL DISCUSSION

SECTION 3  
TECHNICAL DISCUSSION

3.1 STUDY OBJECTIVES AND GROUND RULES

3.1.1 DESIGN REQUIREMENTS

3.1.1.1 General

The basic design requirements for the 110 Watt per Kilogram Solar Array Feasibility Study are given in JPL Specification ES506080 Revision B which is included as Appendix A of this report. The specification pertains to the interplanetary mission application. The requirements for the other two mission types, viz, geosynchronous and manned space station were derived as a task under this contract. Table 3-1 lists the assumed orbital parameters for each of these mission types.

Table 3-1. Mission Orbital Parameters

Mission Type	Orbit Altitude (km)	Orbit Inclination (deg)
Interplanetary	-----	--
Geosynchronous	35,700	0
Manned Space Station	500	55

In the following paragraphs, the requirements for each mission type, as they pertain to the solar array system, are presented. These requirements were not intended to place undue restrictions on the solar array system design, but only to act as a guide in the formulation of a design approach for each mission application. Where any design requirement was found to restrict a potentially attractive design approach, this requirement was reviewed to determine its impact on the ability to achieve the 110 watt/kg goal. The intent was to develop high performance design concepts which are viable candidates

for future missions of the three types being investigated. The design requirements will be representative rather than specific as a detailed design optimization cycle would be a part of any flight hardware application.

#### 3.1.1.2 Interplanetary Mission

##### 3.1.1.2.1 Specification Requirements

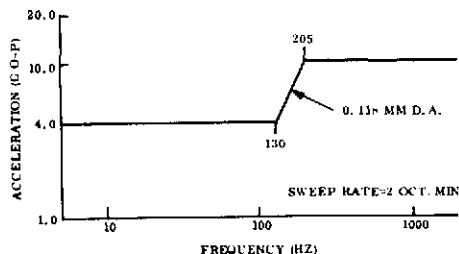
The significant requirements for this mission, as reflected by JPL Specification ES506080 Revision B, have been summarized in Table 3-2. During the course of review of these design requirements, sections of the JPL specification which need change or further clarification have been identified. These are listed and discussed below.

The solar panel lifetime, as stated in Section 3.2.3 of the specification, is three years with no greater than a 20 percent loss of power over this period. The effect of this requirement on the solar cell blanket was investigated and is reported in Section 3.4.1 of this report. The general conclusion regarding this 20 percent maximum degradation restriction is that it imposes shielding requirements which result in a total blanket mass which is too high in relationship to the total system power-to-mass ratio goal. For a nominal 125  $\mu\text{m}$  thick, 10 ohm-cm solar cell, a blanket mass of approximately 66.6 kg (73 percent of the total system mass goal) is required to provide the necessary shielding. For similar 2 ohm-cm cells, the necessary shielding is increased so that a total blanket mass of approximately 71.7 kg (79 percent of the total system mass goal) is required to limit the solar cell radiation degradation to 20 percent.

Thus, unless it is necessary to restrict the allowable maximum power degradation, it would be advantageous from a weight standpoint to allow a greater percentage loss over the 3-year mission duration. The parametric analysis of the solar cell blanket contained in Section 3.4.1 shows that an allowable maximum power degradation, due to particle radiation damage to the solar cells, of about 28 percent will allow the use of either 100 or 125  $\mu\text{m}$  thick, 10 ohm-cm solar cells with a minimum front and back shield of 0.008  $\text{gm}/\text{cm}^2$ . The total blanket mass under these conditions is 48.2 and

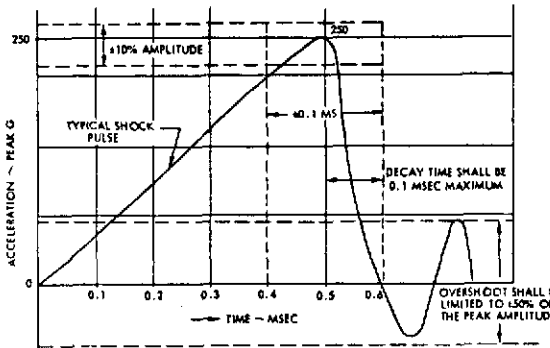


Table 3-2. Summary of Design Requirements for the Interplanetary Mission from JPL Specification ES506080B

Specification Paragraph Number	Title	Definition of Requirement																																														
3.2.2	Power requirement	<ul style="list-style-type: none"><li>10 kW at spacecraft interface at 1 AU and at the predicted solar array temperature</li></ul>																																														
3.2.3	Lifetime	<ul style="list-style-type: none"><li>3 years with no greater than a 20-percent loss of power</li></ul>																																														
3.2.4	Solar panel operating temperature	<ul style="list-style-type: none"><li>Maintain cell temperature between 50 and 70°C at 1 AU</li></ul>																																														
3.2.5	Solar panel weight	<ul style="list-style-type: none"><li>Power-to-weight ratio &gt; 110 watt/kg at 1 AU</li><li>Weight not to include panel gimbaling mechanisms</li></ul>																																														
3.2.6	Packaging volume envelope	<ul style="list-style-type: none"><li>Maximize adaptability to various spacecraft configurations</li><li>Assume Titan-Centaur launch vehicle with 907 kg spacecraft which uses two 10 kW solar panels</li></ul>																																														
3.2.7	Structural interfaces	<ul style="list-style-type: none"><li>Ease of gimbaling is important</li><li>Consider requirements imposed on spacecraft structure</li></ul>																																														
3.2.8	Structural rigidity	<ul style="list-style-type: none"><li>Deployed natural frequency <math>\geq 0.04</math> Hz</li></ul>																																														
3.2.9	Mass center location	<ul style="list-style-type: none"><li>Minimize displacement of vehicle mass center and center of solar pressure caused by thermal gradients and solar panel temperatures</li></ul>																																														
3.2.10	Flatness	<ul style="list-style-type: none"><li>Maximum out-of-plane deflection <math>\pm 10</math> degrees including that caused by thermal gradients when operating from 0.5 to 5.0 AU</li></ul>																																														
3.3.2	Launch environment																																															
3.3.2.1	Sinusoidal vibration	 <p>ACCELERATION (G O-P)</p> <p>FREQUENCY (HZ)</p> <p>SWEEP RATE=2 OCT. MIN</p> <p>0.13+ MM D.A.</p>																																														
3.3.2.2	Acoustic	<ul style="list-style-type: none"><li>At interface between solar panel assembly and the spacecraft in each of three axes</li></ul> <table><thead><tr><th>1/3 Octave Band Center Frequency (Hz)</th><th>Sound Pressure Level in 1/3 Octave Bands (db ref <math>2 \times 10^{-4}</math> dynes/cm<sup>2</sup>)</th></tr></thead><tbody><tr><td>80</td><td>132.5</td></tr><tr><td>100</td><td>136.0</td></tr><tr><td>125</td><td>138.0</td></tr><tr><td>160</td><td>140.0</td></tr><tr><td>200</td><td>142.0</td></tr><tr><td>250</td><td>142.5</td></tr><tr><td>315</td><td>143.0</td></tr><tr><td>400</td><td>142.5</td></tr><tr><td>500</td><td>141.5</td></tr><tr><td>630</td><td>140.0</td></tr><tr><td>800</td><td>138.0</td></tr><tr><td>1000</td><td>136.0</td></tr><tr><td>1250</td><td>135.0</td></tr><tr><td>1600</td><td>133.0</td></tr><tr><td>2000</td><td>132.0</td></tr><tr><td>2500</td><td>130.0</td></tr><tr><td>3150</td><td>128.5</td></tr><tr><td>4000</td><td>127.0</td></tr><tr><td>5000</td><td>125.5</td></tr><tr><td>6300</td><td>124.0</td></tr><tr><td>8000</td><td>122.5</td></tr><tr><td>10,000</td><td>120.0</td></tr></tbody></table>	1/3 Octave Band Center Frequency (Hz)	Sound Pressure Level in 1/3 Octave Bands (db ref $2 \times 10^{-4}$ dynes/cm <sup>2</sup> )	80	132.5	100	136.0	125	138.0	160	140.0	200	142.0	250	142.5	315	143.0	400	142.5	500	141.5	630	140.0	800	138.0	1000	136.0	1250	135.0	1600	133.0	2000	132.0	2500	130.0	3150	128.5	4000	127.0	5000	125.5	6300	124.0	8000	122.5	10,000	120.0
1/3 Octave Band Center Frequency (Hz)	Sound Pressure Level in 1/3 Octave Bands (db ref $2 \times 10^{-4}$ dynes/cm <sup>2</sup> )																																															
80	132.5																																															
100	136.0																																															
125	138.0																																															
160	140.0																																															
200	142.0																																															
250	142.5																																															
315	143.0																																															
400	142.5																																															
500	141.5																																															
630	140.0																																															
800	138.0																																															
1000	136.0																																															
1250	135.0																																															
1600	133.0																																															
2000	132.0																																															
2500	130.0																																															
3150	128.5																																															
4000	127.0																																															
5000	125.5																																															
6300	124.0																																															
8000	122.5																																															
10,000	120.0																																															

NOT REPRODUCIBLE

Table 3-2. Summary of Design Requirements for the Interplanetary Mission from JPL Specification ES506080B (Cont'd)

Specification Paragraph Number	Title	Definition of Requirement										
3.3.2.3	Shock											
3.3.2.4	Static acceleration	<ul style="list-style-type: none"><li>9 g's at mass center in three mutually perpendicular axes</li></ul>										
3.3.2.5	Launch pressure profile	<ul style="list-style-type: none"><li>Maximum rate of change at pressure = <math>116 \pm 8</math> torr/sec</li></ul>										
3.3.2.6	Aerodynamic heating	<ul style="list-style-type: none"><li><math>+30^{\circ}\text{C/minute}</math> for 200 seconds</li></ul>										
3.3.3	Space flight environment											
3.3.3.1	Steady state thermal/vacuum	<ul style="list-style-type: none"><li><math>-130</math> to <math>+140^{\circ}\text{C}</math> at <math>10^{-5}</math> torr or less</li></ul>										
3.3.3.2	Thermal shock	<ul style="list-style-type: none"><li><math>-190</math> to <math>+140^{\circ}\text{C}</math> at <math>10^{-5}</math> torr or less</li><li>Natural cooling and heating rates</li><li>1000 cycles</li></ul>										
3.3.3.3	Solar flare proton radiation	<table border="1" data-bbox="794 1076 1317 1274"><thead><tr><th>Proton Energy-E (MeV)</th><th>Total Fluence <math>\phi &gt; E</math> (p/cm<sup>2</sup>)</th></tr></thead><tbody><tr><td>1</td><td><math>2.0 \times 10^{12}</math></td></tr><tr><td>10</td><td><math>4.0 \times 10^{10}</math></td></tr><tr><td>30</td><td><math>9.0 \times 10^9</math></td></tr><tr><td>100</td><td><math>1.0 \times 10^9</math></td></tr></tbody></table>	Proton Energy-E (MeV)	Total Fluence $\phi > E$ (p/cm <sup>2</sup> )	1	$2.0 \times 10^{12}$	10	$4.0 \times 10^{10}$	30	$9.0 \times 10^9$	100	$1.0 \times 10^9$
Proton Energy-E (MeV)	Total Fluence $\phi > E$ (p/cm <sup>2</sup> )											
1	$2.0 \times 10^{12}$											
10	$4.0 \times 10^{10}$											
30	$9.0 \times 10^9$											
100	$1.0 \times 10^9$											
3.3.3.4	Pyrotechnic shock	<ul style="list-style-type: none"><li>Withstand shock environment from firing any pyrotechnic device on the assembly</li></ul>										

50.2 kg for 100 and 125  $\mu\text{m}$  solar cell thicknesses, respectively. These blanket masses represent 53 and 55 percent of the total system mass goal, respectively. Thus, a total degradation of 30 percent will permit an additional 3 percent allowance for other degradation sources such as ultraviolet and particle radiation damage to the coverglass material and thermal cycling induced damage. A lighter weight 10,000 watt array could be achieved by the use of higher efficiency 2 ohm-cm cells, but the degradation would be increased to about 37 percent for the same  $0.008 \text{ gm/cm}^2$  of front and back shielding.

Another philosophy which might be used in place of the specified beginning-of-life power and allowable degradation constraints is a specified end-of-mission power output with no restrictions on beginning-of-life power.

Section 3.3.3 of the specification specifies that the space flight environments are applicable for both the stowed and deployed configurations. However, it may not be realistic to expect the stowed solar array to withstand the specified thermal shock environment.

#### 3.1.1.2.2 Derived Requirements

The emission of propellant particles as well as particles of thruster material from electrostatic rockets (ion engines) must be considered in the design of the solar array system. In particular the deleterious effects of Hg and  $\text{Hg}^+$  particles must be considered in the selection of materials and construction approaches. Figure 3-1 shows the various kinds of contamination particles associated with ion engine operation. Propellant (mercury) ions and atoms, and atoms of thruster material (molybdenum or aluminum) are emitted into the exhaust hemisphere (as defined by the engine exit phase) as indicated in the figure. In addition, the primary thrust beam is a source of high angle thruster material and propellant ions which may even escape the exhaust hemisphere. If a spacecraft surface is located within the exhaust hemisphere, as shown in Figure 3-1, the surface can become a secondary source of contaminants which can then impinge on other spacecraft surfaces.

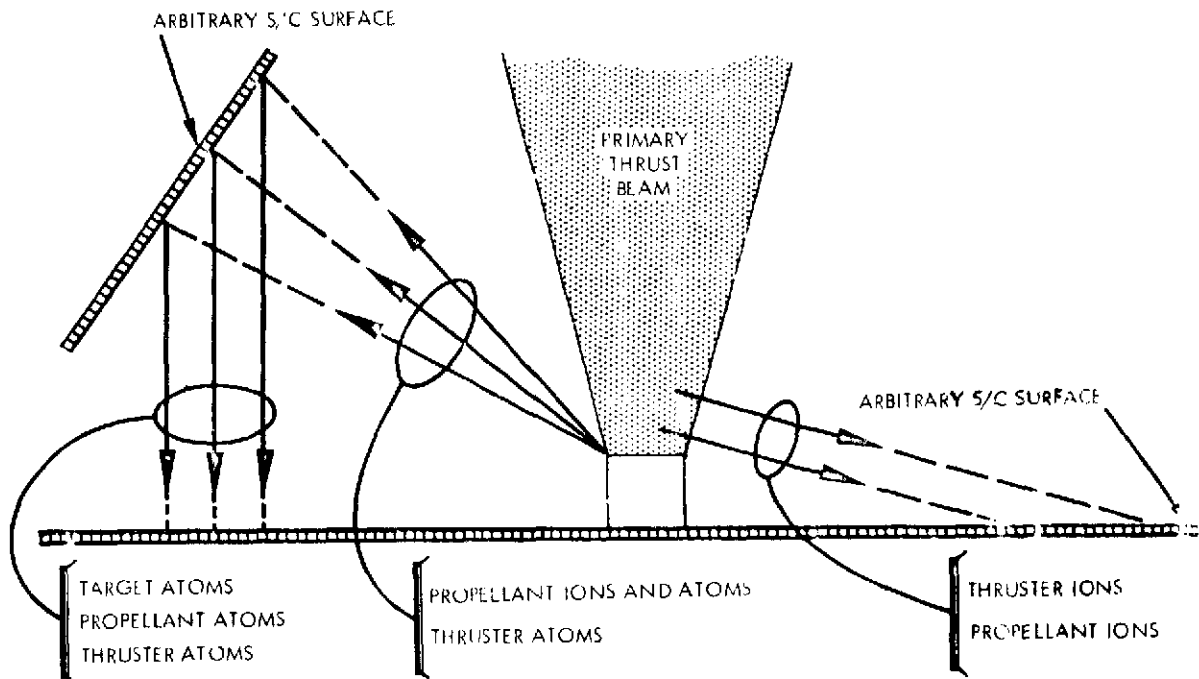


Figure 3-1. Schematic of the Classes of Particulate Contaminants Associated with Ion Engines (from reference 1)

### 3.1.1.3 Geosynchronous Mission

#### 3.1.1.3.1 Power Output Requirement

The solar panel shall have a beginning-of-life output power of 10,000 watts, measured at the panel interface, when corrected for normal solar incidence at the nominal intensity of  $135.3 \text{ mw/cm}^2$ . Figure 3-2 shows the variation in earth-sun distance, apparent solar declination and eclipse duration for a geosynchronous orbit. It was assumed that the solar array is oriented by rotation about an axis parallel to the earth's N-S axis. Therefore, the declination of the sun is reflected as an angle of incidence on the solar array surface. This angle reaches a maximum of about 23.5 degrees at the solstice times of year. If the solar array drive axis is not parallel to the earth's N-S axis by some pointing error, this angular error must be added to the angle of incidence due to the solar declination.

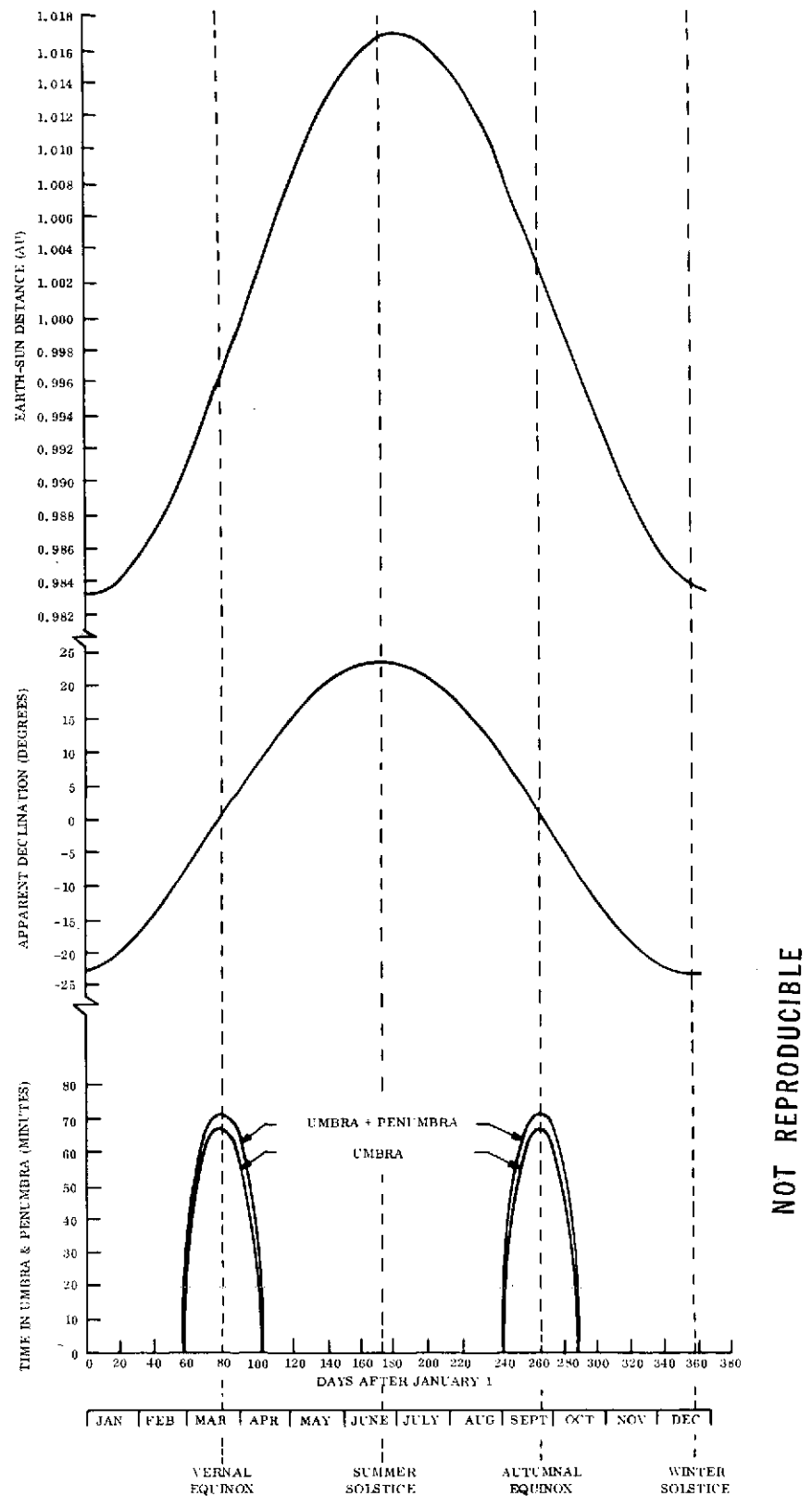


Figure 3-2. Variation in Earth-Sun Distance, Apparent Solar Declination and Eclipse Duration for a Geosynchronous Orbit

#### 3.1.1.3.2 Mission Lifetime

The solar panel shall be designed to perform over a period of five years with no failures which would prevent the panel from performing successfully in both mechanical and electrical modes. The degradation in solar array maximum power output shall not exceed 32 percent over this period.

#### 3.1.1.3.3 Thermal Shock Environment

The thermal shock environment is essentially the same as specified in Appendix A for the interplanetary mission except that the upper temperature limit of  $+140^{\circ}\text{C}$  is higher than required for this application. An upper limit of  $+70^{\circ}\text{C}$  might be more reasonable as a test extreme in this application.

#### 3.1.1.3.4 Quasi-Static Loads

Based on ATS F/G data, it is expected that the station keeping thrusters will produce vehicle accelerations of  $10^{-4}\text{g}$ . The attitude control thrusters could produce vehicle angular accelerations of about  $0.0143\text{ deg/sec}^2$ .

#### 3.1.1.3.5 Particle Radiation Environment

The particle radiation environment in geosynchronous orbit is similar to interplanetary space except for the addition of trapped electron and proton radiation. The interplanetary space components consist of galactic cosmic radiation, solar wind, and solar flare particle events. Galactic cosmic radiation consists of low intensity, extremely high-energy charged particles which are about 85 percent protons, 13 percent alphas, and the remainder heavier nuclei. These particles have energies from  $10^8$  to  $10^{19}$  electron volts (eV) per particle and an intensity of 0.2 to 0.4 particles per  $\text{cm}^2$  per steradian per sec outside the influence of the earth's magnetic field (Reference 2). The solar wind consists of very low energy protons and electrons that are continually emitted by the sun. The mean velocity of the solar wind at a distance of approximately 1.0 AU is 450 to 500 km/sec. The solar particle events are the emission of charged particles from distributed regions on the sun during solar flares. These events are composed of energetic protons and alpha particles that occur sporadically and last for several days.

The solar flare proton energy spectra for the five-year duration geosynchronous mission is assumed to be the same as that specified for the three-year duration interplanetary mission. This energy spectra is given in JPL Specification ES506080B and is shown graphically in Figure 3-3. In comparison with this solar flare proton spectra, the other constituents of the interplanetary particle environment have only a negligible effect on solar cell bulk damage.

The time-averaged trapped electron environment from Reference 3 is shown graphically in Figure 3-4. The trapped proton environment, shown in Figure 3-5 is derived from Reference 4 which is extrapolated from the AP5 model.

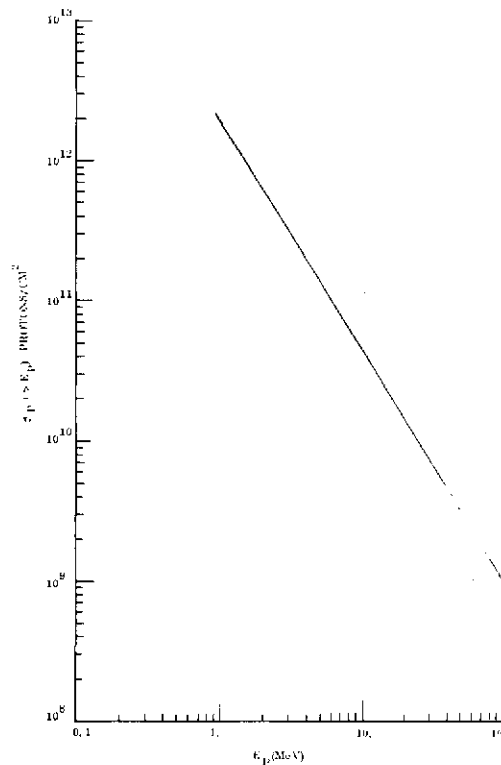


Figure 3-3. Solar Flare Omnidirectional Proton Integral Energy Spectra for Interplanetary and Geosynchronous Missions

#### 3.1.1.4 Manned Space Station Mission

##### 3.1.1.4.1 Power Output Requirement

The solar panel shall have a beginning-of-life output power of 10,000 watts, measured at the panel interface, under conditions of normal incidence at the nominal intensity ( $135.3 \text{ mw/cm}^2$ ), and at the subsolar point with a  $\beta$  angle of zero degrees (where  $\beta$  is defined as the smallest angle between the orbit plane and the sun line).

##### 3.1.1.4.2 Mission Lifetime

The solar panel shall be designed to perform over a period of 10 years with no failures which would prevent the panel from performing successfully in both mechanical and electrical modes. The degradation in maximum power over this period shall not exceed 20 percent. The solar array shall be designed to permit the in-orbit replacement of the complete panel.

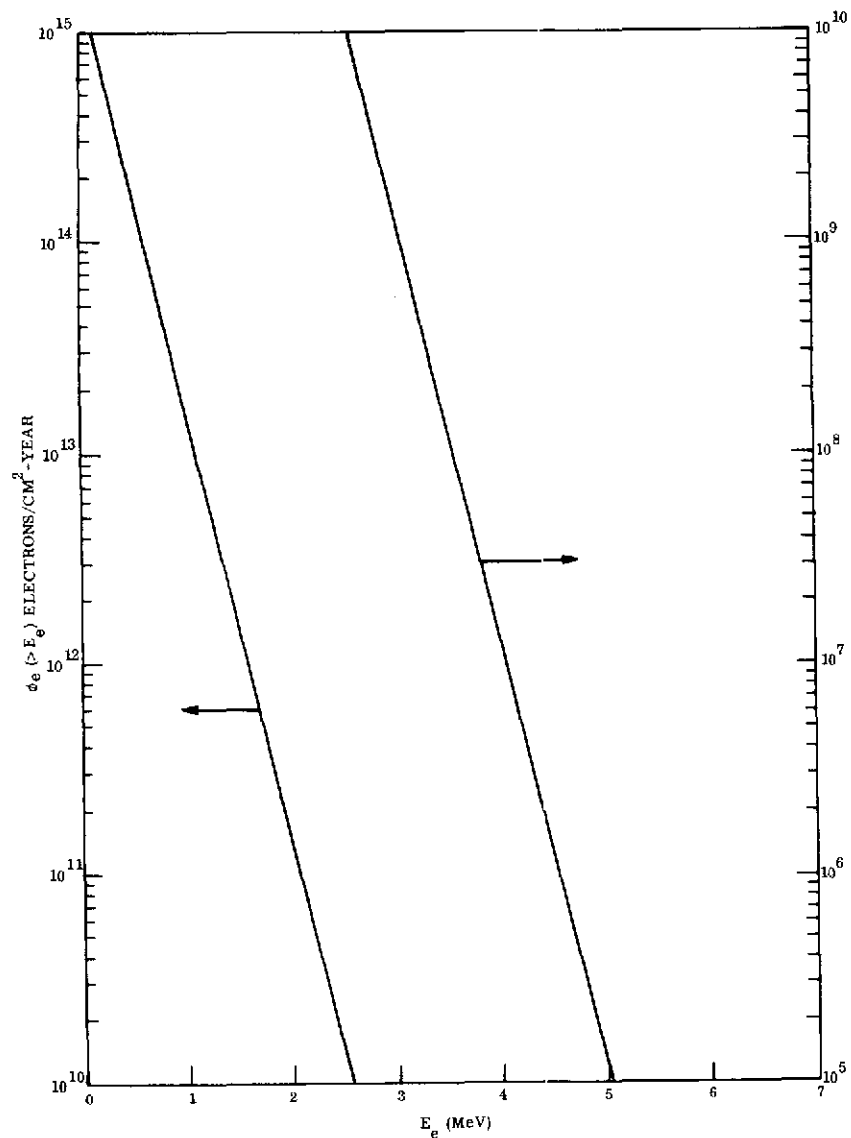


Figure 3-4. Omnidirectional Trapped Electron Integral Energy Spectra for Geosynchronous Orbit

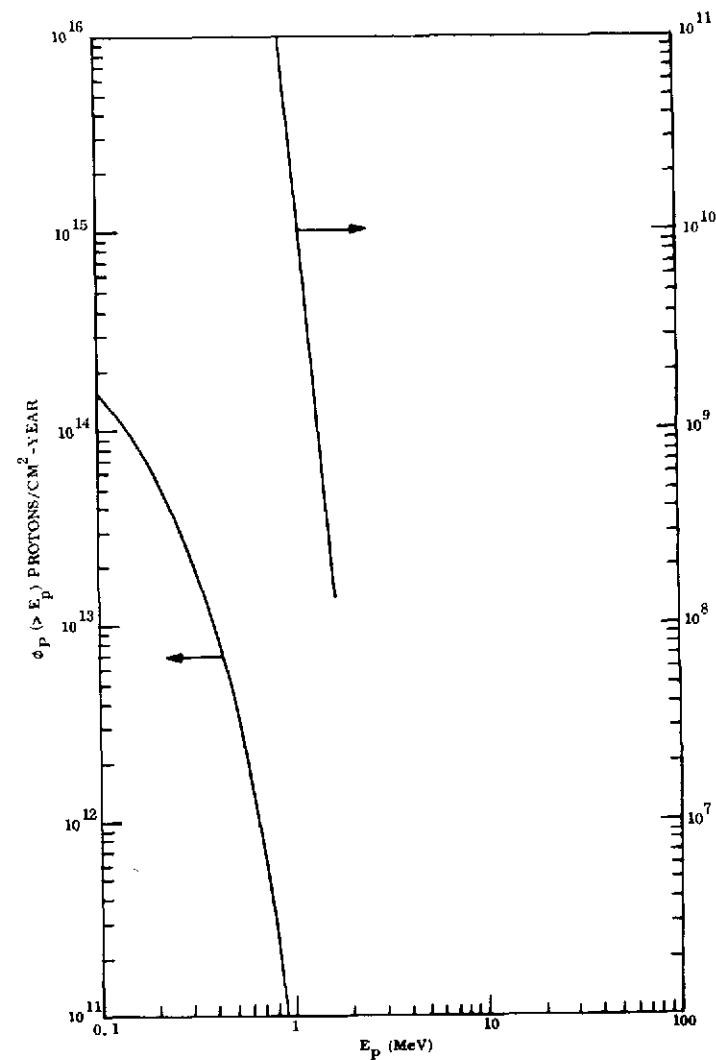


Figure 3-5. Omnidirectional Trapped Proton Integral Energy Spectra for Geosynchronous Orbit



#### 3.1.1.4.3 Thermal Shock Environment

The thermal shock temperature extremes on the deployed solar array shall be considered to be  $-91^{\circ}\text{C}$  to  $+80^{\circ}\text{C}$  at a pressure of  $10^{-5}$  torr or less. The temperature time rates of change during thermal shock shall be at the natural cooling rate of the solar panel in a simulated passage through the earth's shadow, and at the natural heating rate of the solar panel in a normally incident solar flux environment. The heat rates for this mission are given in Figure 3-6 for the  $\beta = 0$  orbit case. The total thermal shock environment shall consist of 60,000 complete cooling and heating cycles.

#### 3.1.1.4.4 Quasi-static Loads

During the loads analyses, consideration shall be given to loads induced by the solar panel's elastic and rigid body response to the following excitations which were obtained from References 5 and 6:

Due to docking: 0.035 g's for 0.3 seconds in any of three perpendicular axes.

Due to maneuvers:  $7 \times 10^{-4}$  g's for 3 seconds in any of three perpendicular axes.

Due to array orientation:  $0.137 \text{ deg/sec}^2$  for 2 seconds about each solar array orientation drive axis.

The aerodynamic drag force on a  $100 \text{ m}^2$  surface area which is normal to the velocity vector is shown in Figure 3-7. The effects of this uniformly distributed force should be checked by analysis.

The solar array shall not be required to sustain loading due to an artificial G mode of operation. In the stowed configuration, the static acceleration environment shall be 5 g's at the approximate center of mass of the solar panel. This environment shall be considered equal for each of three mutually perpendicular axes.

#### 3.1.1.4.5 Packaging Volume Envelope

The volume and shape of the shuttle cargo compartment available to the solar array panels (2 required) is a cylinder 4.27 m in diameter by 11.6 m long.

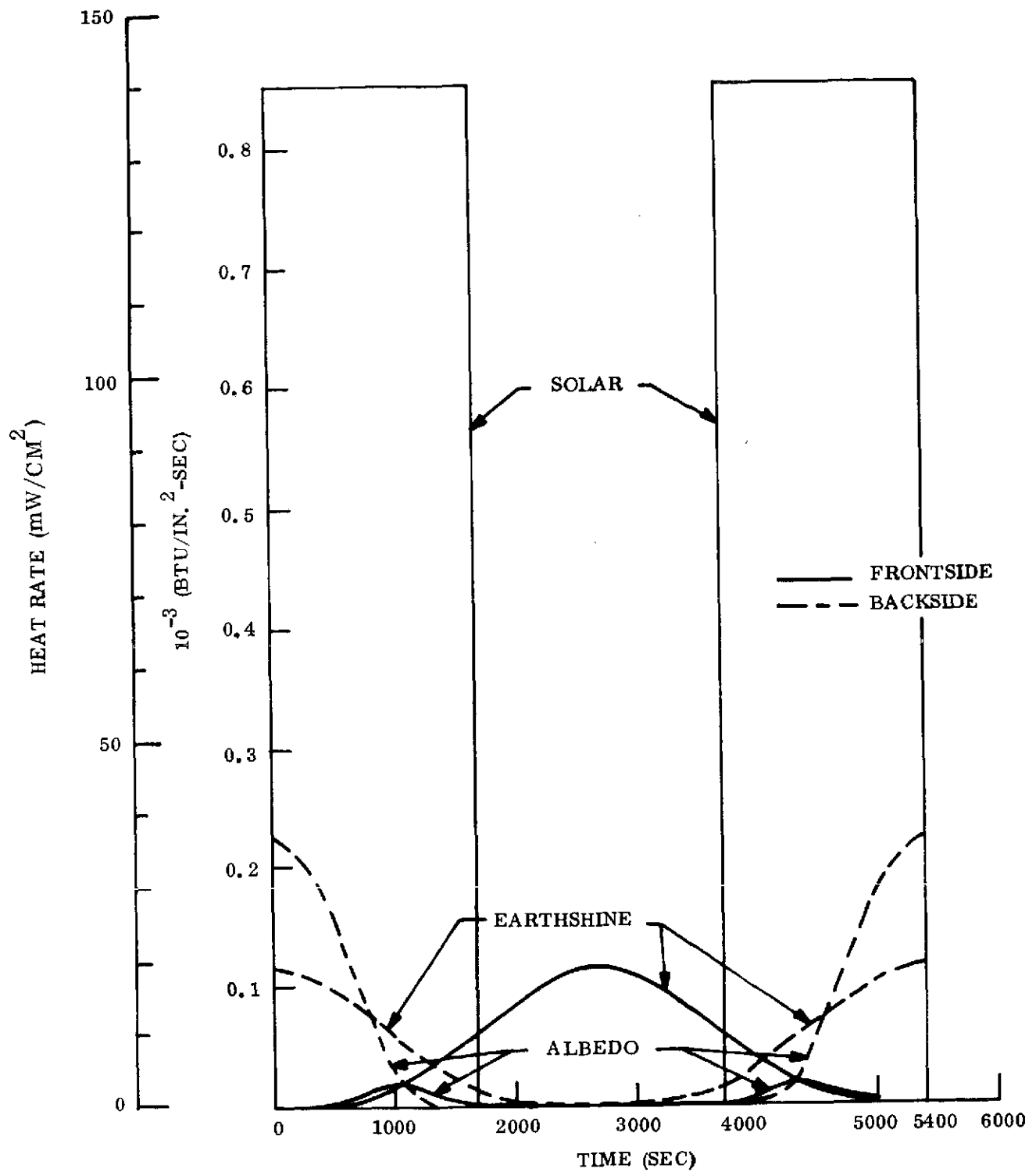


Figure 3-6. Transient Heat Rates for  $\beta=0^\circ$  Orbit  
(from Reference 5)

#### 3.1.1.4.6 Particle Radiation Environment

The trapped proton environment is of primary importance for this mission. Figure 3-8 shows the trapped proton omnidirectional integral energy spectra for an orbit which is conservatively close to the one of interest. These spectra are based on environment models developed by Vette and his collaborators and reported in Reference 7, 8 and 9. These models which cover the proton energy ( $E_p$ ) ranges of interest are:

$$\text{AP5 } (0.4 < E_p < 4 \text{ MeV})$$

$$\text{AP6 } (4 < E_p < 30 \text{ MeV})$$

$$\text{AP7 } (E_p > 50 \text{ MeV})$$

Figure 3-9 shows the omnidirectional integral energy spectra for the trapped electrons in this same orbit based on data from Reference 10 for the projected 1968 electron environment.

The solar flare proton environment in the 500 km, 55 degree inclination orbit is shown in Figure 3-10 based on data from Reference 11. This environment represents an integration of all particle events observed over the six peak years of the 19th solar cycle. It has been reduced from the free space spectra to account for the shielding of the geomagnetic field. For this mission duration of 10 years, it is assumed that this spectra, based on solar cycle 19, is applicable with no further modification and can be combined with the corresponding quantities for the trapped radiation environment to arrive at the worst case particle environment.

#### 3.1.1.5 Comparison of Requirements

Table 3-3 summarizes the significant design requirements for the three mission applications. These requirements on the solar array system design are similar for the interplanetary and geosynchronous missions, but a vast difference exists with the manned space station mission. Generally speaking, the manned space station mission imposes more severe requirements on the solar array design. The deployed array loads induced

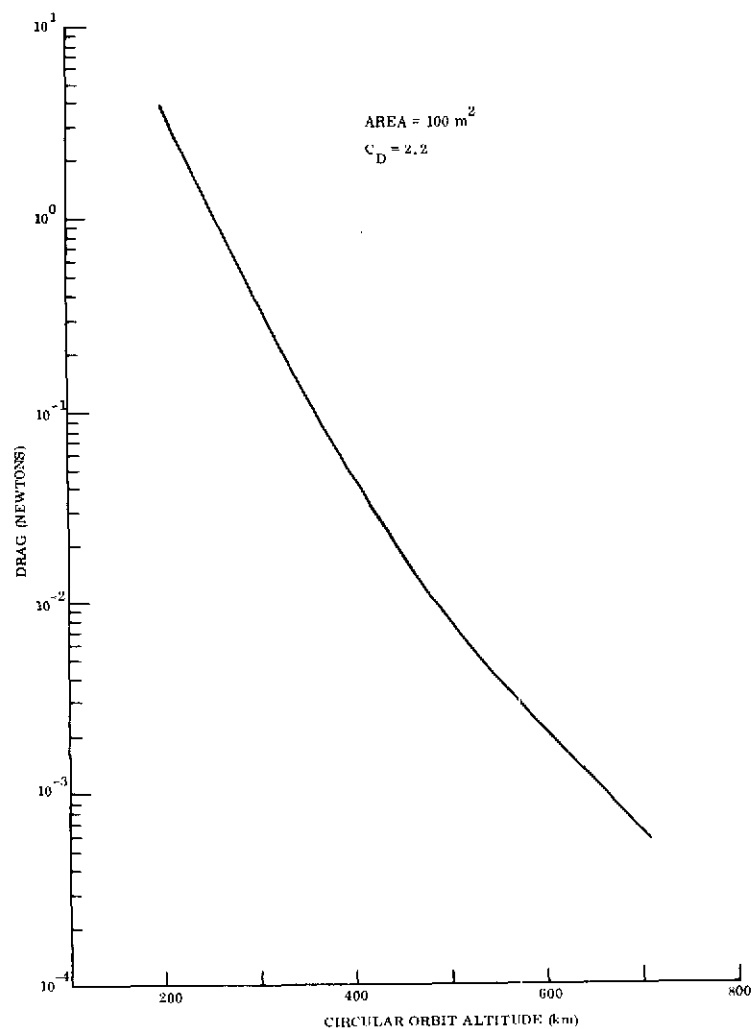


Figure 3-7. Drag Force with Normal Incidence on 100 m<sup>2</sup> Surface Area

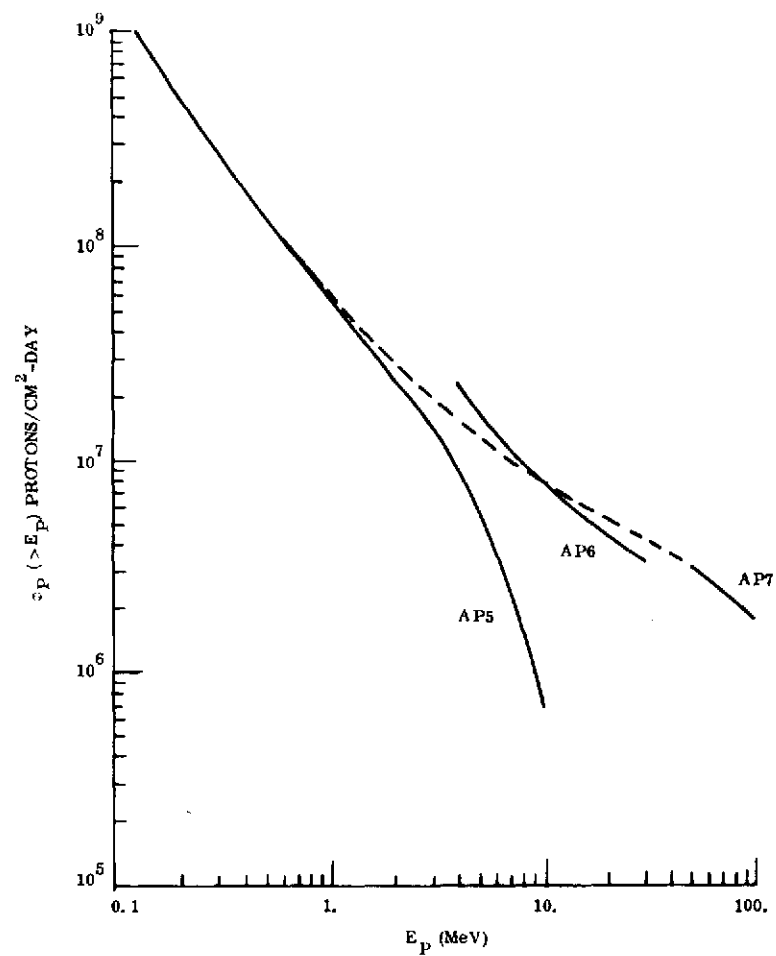


Figure 3-8. Omnidirectional Trapped Proton Integral Energy Spectra for 555 km,  $i=60^\circ$  Orbit

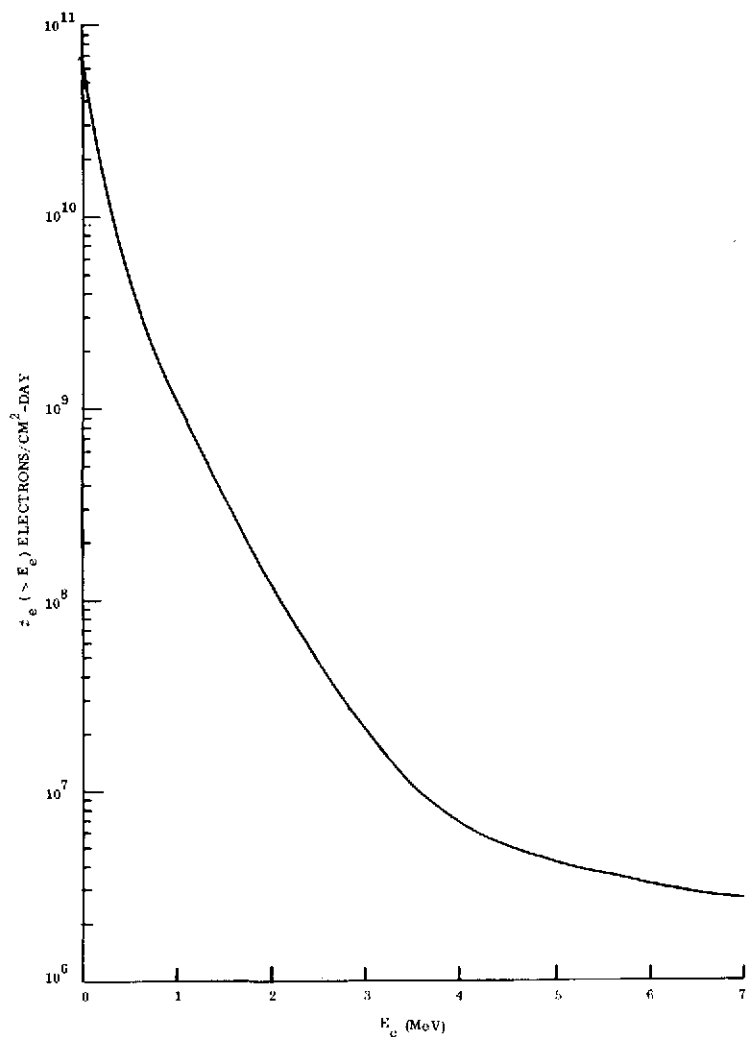


Figure 3-9. Omnidirectional Trapped Electron Integral Energy Spectra for 555 km,  $i=60^\circ$  Orbit

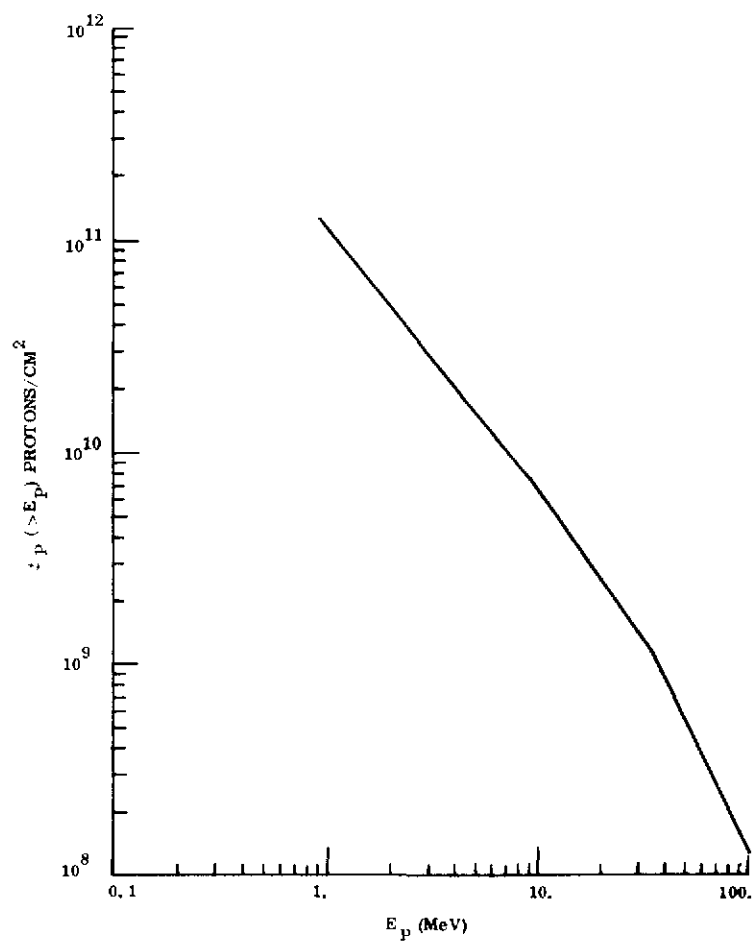


Figure 3-10. Solar Flare Omnidirectional Proton Integral Energy Spectra for 500 km,  $i=55^\circ$  Orbit

Table 3-3. Comparison of Key Design Requirements

Design Requirement	Definition of Requirement		
	Interplanetary Mission	Geosynchronous Mission	Manned Space Station Mission
Power Output	10 kW at beginning-of-life and at 1 AU		
Lifetime	3 years with loss of power $\leq 20\%$ *	5 years with loss of power $\leq 32\%$	10 years with loss of power $\leq 20\%$
Particle Radiation Environment	Solar flare protons per Figure 3-3	Solar flare protons per Figure 3-3. Trapped electrons per Figure 3-4. Trapped protons per Figure 3-5.	Solar flare protons per Figure 3-10. Trapped electrons per Figure 3-9. Trapped protons per Figure 3-8.
Quasi-Static Load (Deployed configuration)	Not specified	$10^{-4}$ g's 0.0143 deg/sec <sup>2</sup>	0.035 g's for 0.3 sec $7 \times 10^{-4}$ g's for 3 sec 0.137 deg/sec <sup>2</sup> for 2 sec
Launch Dynamic Loads (stowed configuration)	As specified in JPL Specification ES506080B Assumed to be the same for all mission applications		
Static Launch Acceleration (stowed configuration)	9 g's	9 g's	5 g's
Thermal Vacuum/Thermal Shock Environment	-190 to +140°C 1000 cycles	-190 to +70°C 1000 cycles	-91°C to +80°C 60,000 cycles
Structural Rigidity (deployed configuration)	$f_n \geq 0.04$ Hz	$f_n \geq 0.04$ Hz	$f_n \geq 0.04$ Hz or as determined by deployed loads.

\* Analysis has shown that this value should be increased to about 30 percent to allow the use of lightly shielded 10 ohm-cm cells (see Section 3.4.1)

by maneuvers and dockings are much greater than the loads which occur due to thruster firings on the other two missions. The other significant difference is in the thermal shock requirement. Both the interplanetary and geosynchronous missions require a relatively few number of cycles over a wide temperature range while the low orbiting manned space station application, with its 10-year duration, requires approximately 60,000 cycles over a smaller temperature range.

In-orbit solar array retraction capability is a logical requirement for the manned space station mission. Full or partial retraction may be required to allow for vehicle docking. In-orbit replacement of a solar array wing will require the full retraction of that wing. The other two reference missions do not have an obvious requirement for retraction based on presently defined mission guidelines.

The detailed requirements for the solar array interface with the spacecraft are not specified. Such details are impossible to define for a general feasibility study of this type. However, it is possible to establish a set of constraints which will determine the philosophy to be used in the definition of the structure required to support the solar array system in the stowed configuration. These constraints, as defined below, will be applied to all mission applications:

1. The solar array panel shall be adaptable to a gimbaling system which will provide solar orientation.
2. The solar array panel structure shall be designed to accommodate the specified input sinusoidal vibration levels at all support points when such input is applied simultaneously at all points with the worst case phase relationship assumed for motion perpendicular to the line joining the supports.

### 3.1.2 STATE-OF-THE-ART PHILOSOPHY

It was a goal of the study to base the design of the system upon the performance of components or devices which are commercially available with a delivery time of less than six months. With this approach there is a high confidence in achieving predicted system performance without the need for projections into the future. This definition of

state-of-the-art rules out the improved COMSAT violet cell performance as a basis for the prediction of system performance against the power-to-mass ratio goal. The improved performance which this cell promises is treated as a future increase in the power-to-mass ratio beyond the 110 watt/kg minimum which is achieved with current available technology.

The same argument applies to deployable boom technology. Advances which may result from the application of composite materials are not considered in assessing the performance of the baseline configuration.

Section 3.3.2 discusses advances in the state-of-the-art and assesses the performance pay-offs which result from these improvements. Approximately a 5 year program is involved in reaching the point of committing this technology to a flight hardware program. This 5 year time period includes a one year feasibility study, one year for concept development, and one year for engineering design and development testing. The remainder of the time is involved with evaluation and planning periods between these discrete program elements.

## 3.2 CONFIGURATION STUDY RESULTS

### 3.2.1 RECOMMENDED DESIGN BASELINE APPROACH FOR INTERPLANETARY MISSION

#### 3.2.1.1 Description

##### 3.2.1.1.1 General

The baseline configuration for a solar array panel which meets the 110 watt/kg goal is shown in Figure 3-11 and has the design features summarized in Table 3-4. The concept consists



Page intentionally left blank

Table 3-4. Significant Design Features of the  
Baseline Solar Array Panel  
Configuration

Parameter	Value
1. Deployed length (L')	18.565 m
2. Total width (W)	5.915 m
3. Blanket width (w)	2.830 m
4. System aspect ratio (L'/W)	3.14
5. Total gross blanket area	105.08 m <sup>2</sup>
6. Total number of solar cells (2 x 2 cm)	226,800
7. Lowest deployed natural frequency	0.04 Hz
8. Electrical power output at $V_{mp} = 193$ vdc	9860 watts
<ul style="list-style-type: none"> <li>• Beginning-of-life (BOL)</li> <li>• 57 °C</li> <li>• 1 AU, AMO illumination</li> <li>• Measured at panel interface connector</li> </ul>	
9. Expected maximum power degradation after 3 year interplanetary mission	30%
10. Total system mass	87.5 kg
11. BOL power-to-mass ratio	112.7 watt/kg
12. EOM power-to-mass ratio	78.9 watt/kg

Preceding page blank

of a single, central deployable mast which supports two flexible solar cell blankets. Tension in the solar cell blanket substrates maintains the deployed natural frequency above the minimum specified value of 0.04 Hz. The flexible solar cell blankets are stowed for launch by folding into a flat-pack package which is retained in compression between a bottom honeycomb panel and spring driven hinged honeycomb panel doors on the top. These doors are held closed during launch by the tubular leading edge member (LEM) which is attached to the deployable boom at the center and retained at each end by a launch retention cable mechanism. Solar array deployment is accomplished by firing redundant cable cutters at each end of the array which releases the end of the LEM and the restraint at each end of the supporting truss work. Application of power to the deployable boom actuator will cause the LEM to move off the door panels allowing them to swing open. Continued deployment of the boom will cause the LEM to pull each fold of the blankets from the stowed package. Interlayer cushions of Kapton H film are retained by the bottom panel. At the end of the deployment travel, the further deployment of the blankets applies the required tension load by extending a spring mechanism at the base of each blanket.

#### 3.2.1.1.2 Solar Cell Blanket Construction

Each solar cell blanket consists of an interconnection of 30 identical strips as shown in Figure 3-12. Each strip consists of two series connected solar cell modules, with each module being composed of 1890 2 x 2 cm solar cells which are interconnected 135 in series by 14 in parallel as shown in Figure 3-12. The two modules on one strip are connected in electrical series with the two modules on an adjacent strip to form a complete electrical circuit. Thus each electrical circuit is composed of 7560 cells connected 540 in series by 14 in parallel. Each circuit has a calculated 335 watt maximum power output at 196 vdc measured at the circuit terminals. If a 2-percent bus strip distribution loss is accounted for, the total calculated panel output is 9860 watts measured at the panel interface connector. Table 3-5 is a summary of the component quantities as related to the level of assembly of the panel.

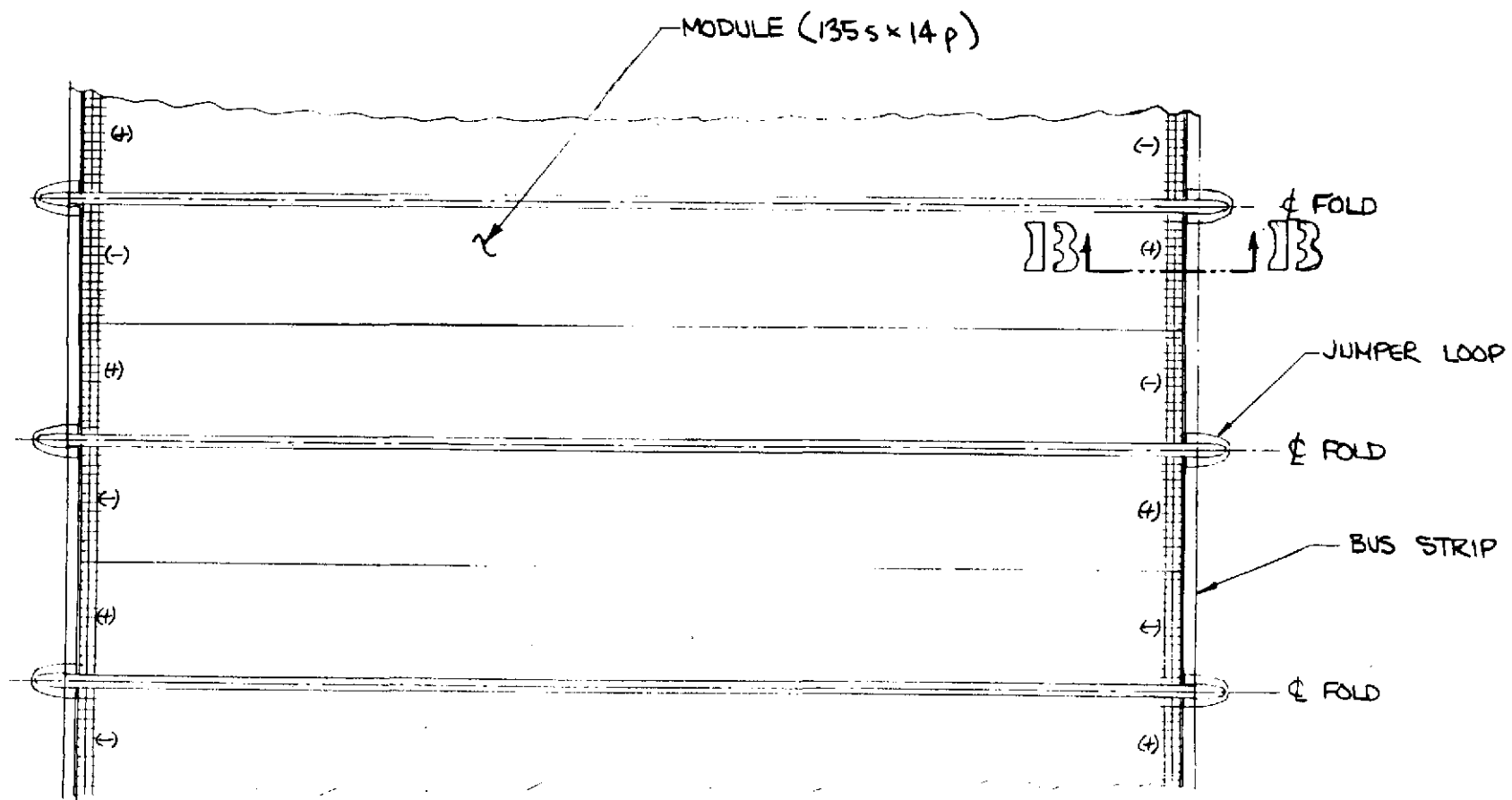


Figure 3-12. Detail of Module Arrangement on Solar Cell Blankets

Table 3-5. Component Quantity Related to Level of Assembly

	Cell	Module	Strip	Circuit	Blanket	Panel
Cell	1					
Module	1890	1				
Strip	3780	2	1			
Circuit	7560	4	2	1		
Blanket	113,400	60	30	15	1	
Panel	226,800	120	60	30	2	1

The solar cells are nominal 125  $\mu\text{m}$  thick, 2 x 2 cm, N/P silicon with a nominal base resistivity of 10 ohm-cm. Table 3-6 summarizes the significant characteristics of this cell. The solar cells are shielded from the damaging effects of low energy protons by the deposition of an integral cover of Corning 7070 glass. A nominal integral coverglass thickness of 37  $\mu\text{m}$  should provide the necessary protection within the weight constraints of this program.

Figure 3-13 shows an enlarged rear view of the substrate. The aluminum wire interconnectors are ultrasonically bonded to the gold solar cell contacts through slotted holes in the Kapton film. The wire is pinched flat in the bond areas to allow several bonds to be made at the one attachment point. Between these attachment points, the wire follows a curved path to accommodate the differential expansions and contractions which occur when the array is thermal cycled between  $-190^{\circ}\text{C}$  and  $+140^{\circ}\text{C}$ . Holes have been cut in the Kapton-H film substrate to allow the rear of the solar cells to radiate directly to space. The rear of the solar cell which is under the hole is coated with Dow Corning

Table 3-6. Design Characteristics of Ferranti 125  $\mu\text{m}$  Thick Solar Cells  
(Ferranti Cell Type MS36)

Feature	Description
Thickness	$125 \pm 25 \mu\text{m}$
Size	$20 \pm 0.15 \times 20 \pm 0.15 \text{ mm}$
Resistivity	7 to 12 ohm-cm Float zone silicon
Contact Configuration	Bottom wrap-around 24 finger grid geometry
Contact Material	Plated - nickel, copper, nickel, gold
Anti-reflective Coating	$\text{TiO}_x$
Minimum Lot Average Electrical Performance (covered)	123 ma at 0.445 volts  (equivalent AMO, 1 A. U. illumination at $25 \pm 2^\circ\text{C}$ )
Maximum Lot Average Cell Mass	0.129 gm/cell

93-500 adhesive to provide the necessary low energy proton protection. To further reduce the solar cell temperature, a high emissivity coating is applied over the entire rear solar cell contact surface except at the points of interconnector attachment.

The bus strips, which run on the sun side of the substrate along each edge, consist of flat copper conductors with Kapton-H film used as the insulator. The electrical connections between blanket strips are made by jumper loops which attach one bus strip segment to the adjacent bus strip segment. The installation of these jumper loops is shown in Figure 3-12. The fold hinge between blanket strips consists of a strip of FEP-Teflon which is heat sealed to the Kapton substrate to form a lap joint along the width of the blanket.

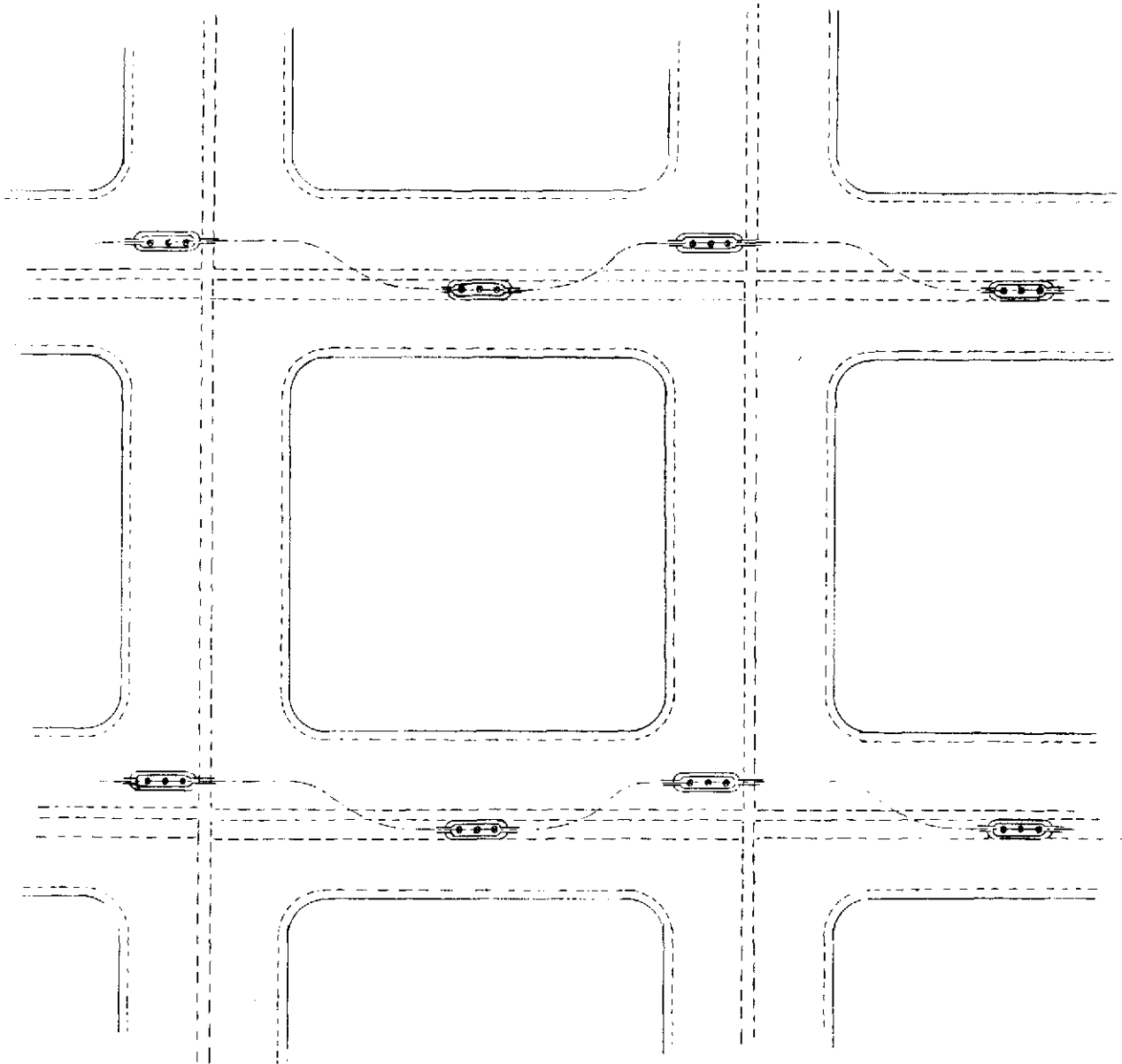


Figure 3-13. Rear View of Solar Cell Blanket

A detailed mass breakdown for the solar cell blanket is given in Table 3-7.

Table 3-7. Mass Breakdown for Solar Cell Blanket  
(Total for Both Blankets)

Items	Mass (kg)
Solar Cells (.129 gm each)	29.26
Integral Coverglass	7.26
Interconnectors	1.81
Substrate	4.04
Adhesive (rear contact low energy proton protection)	3.50
Bus Strips and Insulators	1.50
Inboard and Outboard Leaders	0.27
Circuit Terminations	0.15
Strip Hinge Joints and Bus Strip Jumpers	<u>0.71</u>
	48.50

#### 3.2.1.1.3 Alternative Blanket Folding Approach

Presently conceived light weight flatpack solar arrays consist of accordion pleated panels which, in the stowed position, require interleaved protective blankets to prevent cell to cell contact of adjacent panels. As shown in Figure 3-14, upon deployment each interleaf is released and retained at the stowage compartment. Retraction is impractical for this flatpack approach.

A flatpack concept not requiring interleaving which is also retractable is illustrated on Figure 3-15. A series of solar panels, each approximating the width and length of the stowage compartment, are joined at their ends to a scissors assembly which in essence duplicates the action of a lazy tongs mechanism. Instead of using pinned joints, the



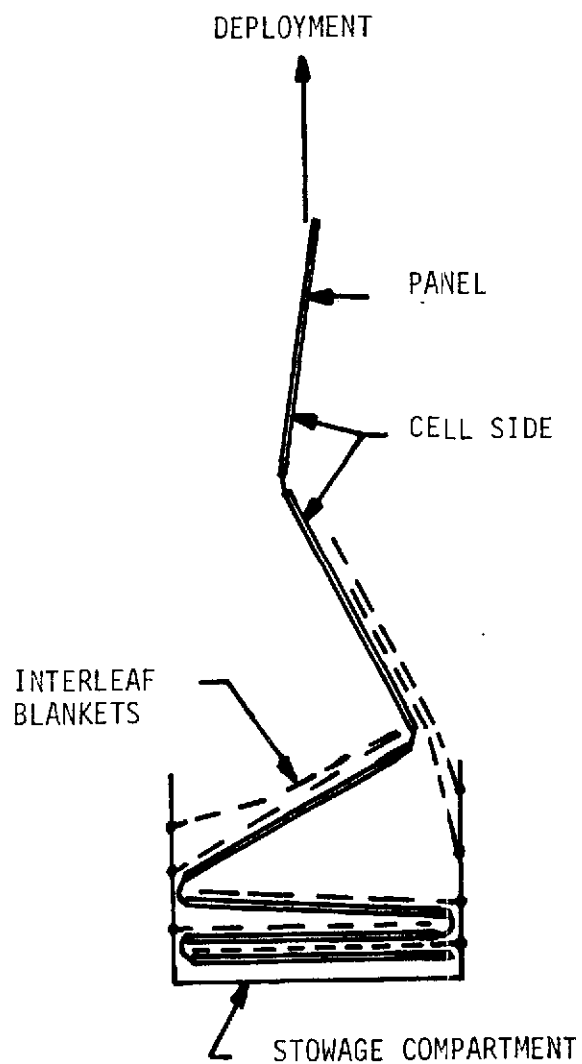


Figure 3-14. Flatpack Solar Array with Protective Interleaves

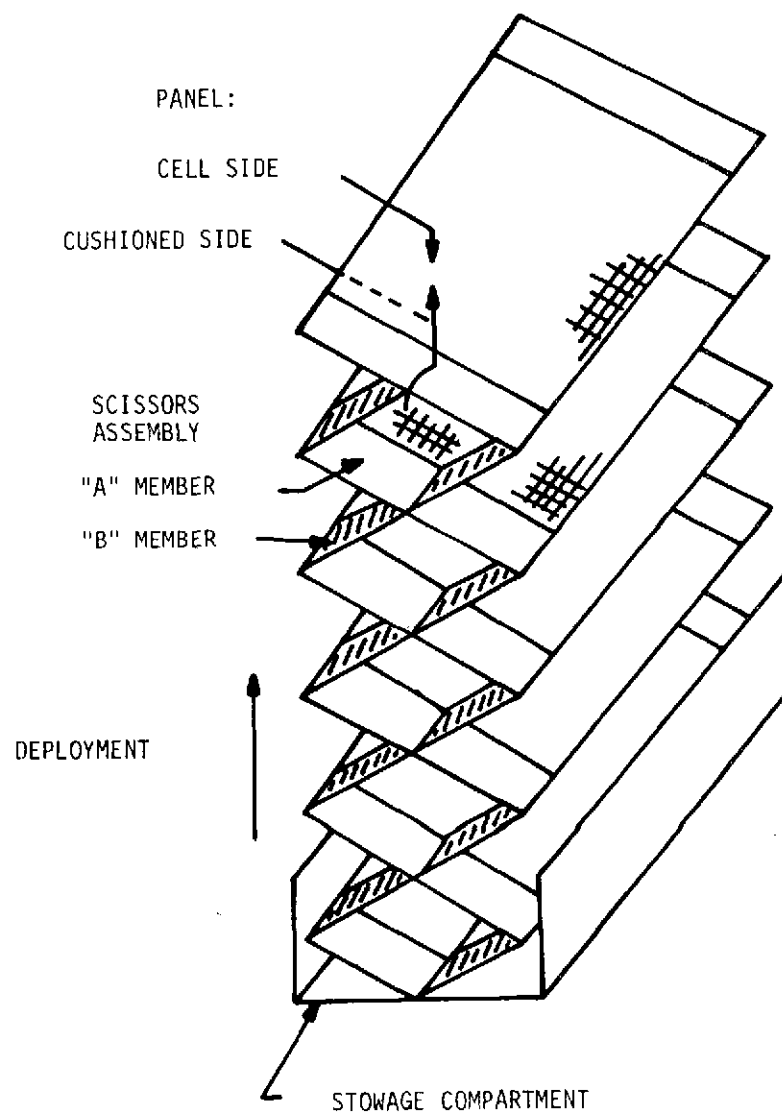


Figure 3-15. Retractable Flatpack Concept

hinges are formed by notching thin flat crossmembers and assembling them to form a collapsible egg-crate configuration. As shown the panel ends are joined only to the "A" members. In the retracted position this results in the cell side of one panel being in contact with the cushioned rear side of the adjacent panel. In the extended position all panels are coplanar with their cells facing in one direction.

For the retractable version described here, each blanket section would use two scissors assemblies, one located near the extendable boom and the other at the extreme end of the array assembly as shown on Figure 3-16.

By means of a simple leaf spring arrangement, the scissors assemblies are designed to assume a collapsed position. This permits overall retraction to be accomplished by only retracting the extendible boom. The details of this feature are described below with the aid of Figure 3-17.

Each scissors assembly actually consists of two leaf-spring subassemblies, one of which is shown in Figure 3-17(a). As presently visualized, the subassembly consists of a folded strip of beryllium copper with the integrity of the folds maintained by welding or brazing the crease a small distance of about 6 mm. Bonded to the inner surface of each crease is a short web of Kapton tape which has the function of limiting the amount of extension possible. As tension is applied at the ends the subassembly will stretch to a point limited by the bonded tapes as shown on the sketch. The tension is taken up by the straight section of the beryllium-copper strip and by the bonded tape in the other sections where the strip curves out to the crease. Since the strip in this region can be easily designed so its stresses due to the curvature are well within the elastic limit, it follows that the subassembly will return completely to its collapsed position upon the release of tension.

As mentioned earlier two copper strip subassemblies make up one scissors assemblies. Figure 3-17(b) shows how each subassembly is notched to permit interlocking to form the assembly. The notching is located identically on the "A" members of both subassemblies

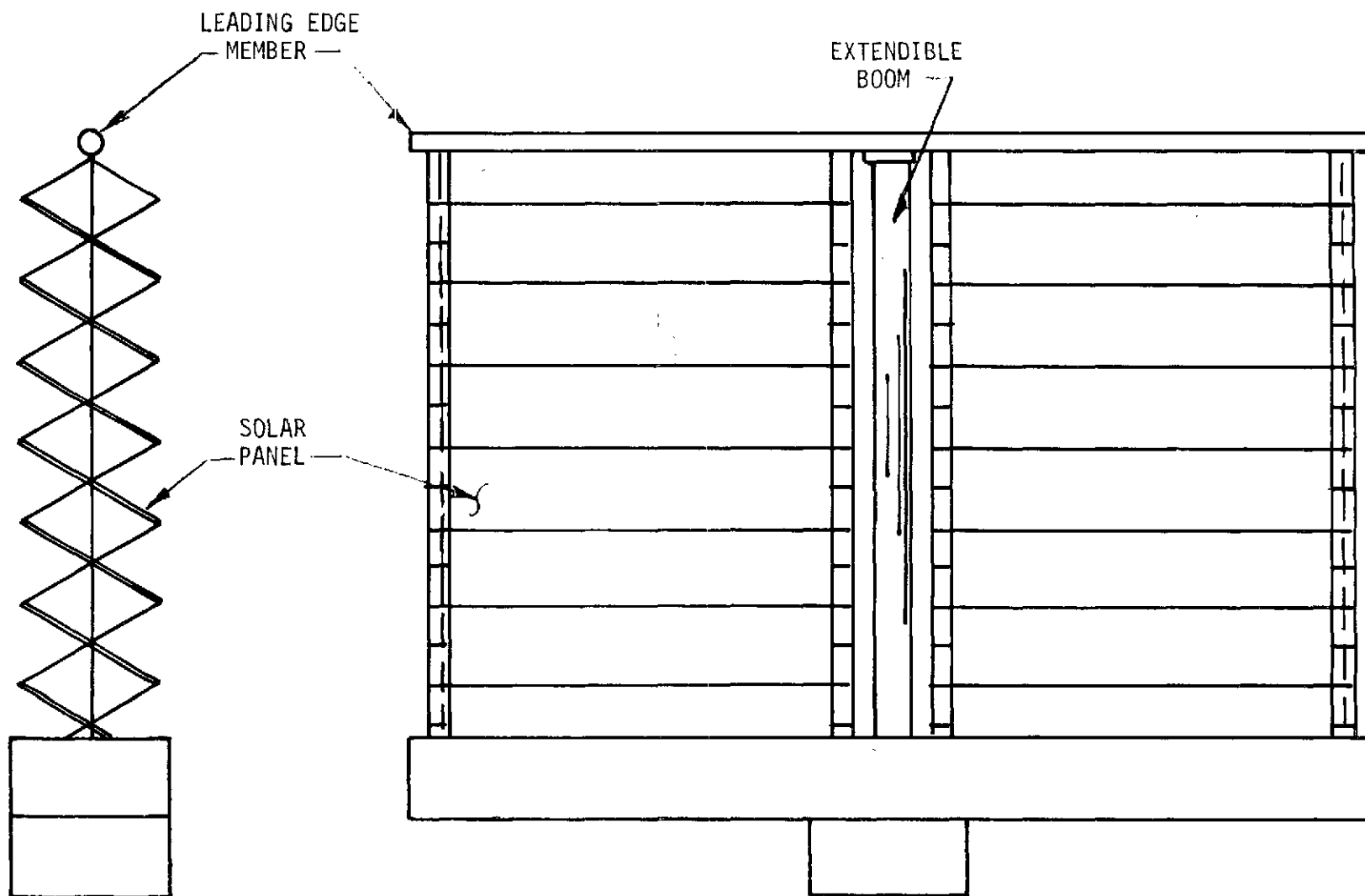
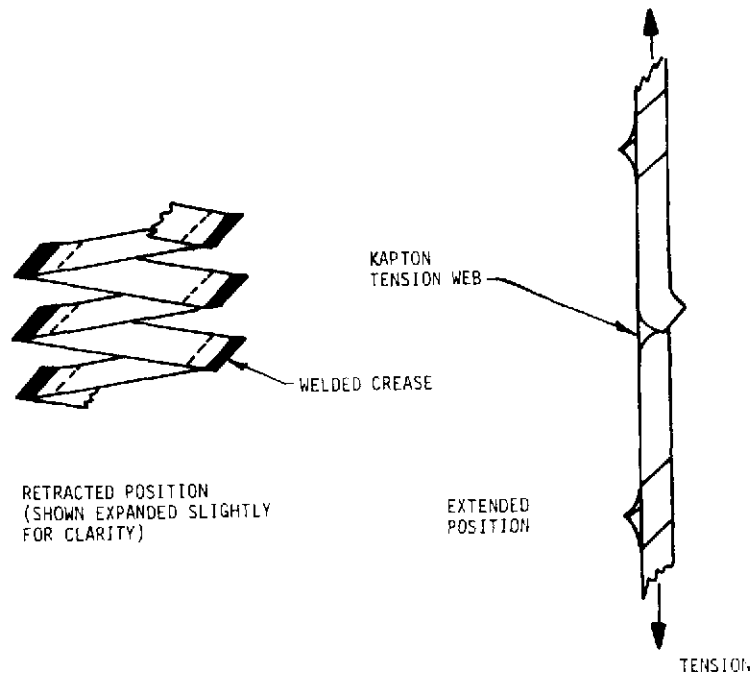
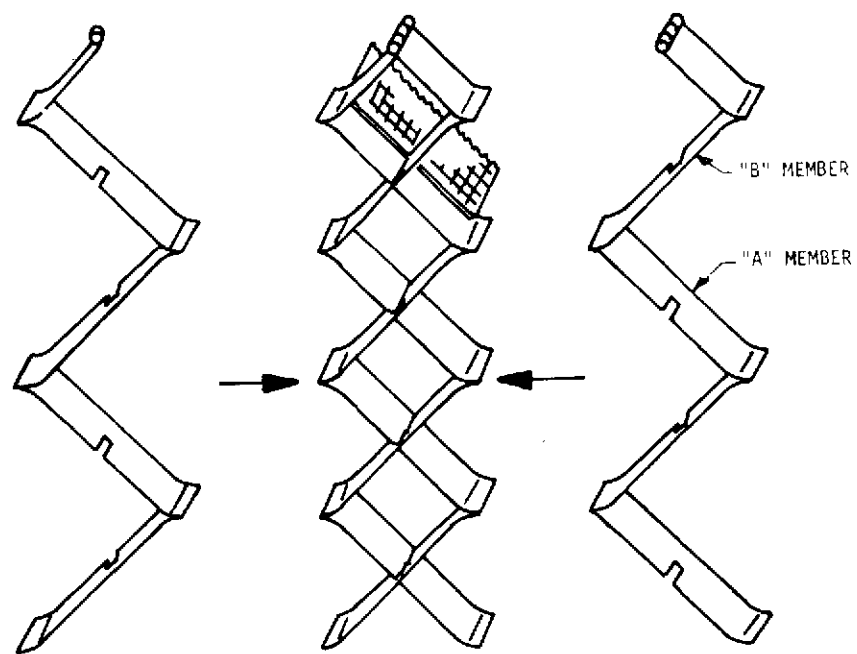


Figure 3-16. Flatpack Solar Array Configuration



(a) Leaf Spring Subassembly



(b) Scissors Assembly

Figure 3-17. Diagram of Retractable Scissors Assembly

and identically on the "B" members so that the resulting assembly has the "A" legs with their unnotched edges facing in the same direction. These are the edges to which the solar cell panels are joined as indicated by the phantom view for one panel. By this arrangement the scissors assemblies serve as the positive and negative electrical conductors for all of the panels.

It is visualized that each solar cell panel will consist of a Kapton blanket to which are bonded the solar cells with their necessary electrical interconnections. A light frame serves to stabilize the blanket edges as indicated on Figure 3-18. The short edges are lap joined to the "A" member of the scissors assembly at both ends. The lap joint stiffens the "A" member and would tend to reduce the "S" curvature during deployment. The long edges are formed into L sections to increase stiffness in the transverse direction. The L sections are formed in opposite directions so that interlocking and hence greater stiffness is achieved upon full deployment. As indicated in the sketch, no significant penalty in stacking volume is incurred because of the "L" sections.

One final feature of the concept is worth noting. With partial retraction all of the panels will tilt practically the same amount as established by the elastic properties of the beryllium copper strip. In other words, as long as the properties are identical at any section of the scissors assembly then the tension-deflection characteristics will be identical. Since the tension under weightless conditions is that due to reaction of the extendible boom only, then the deflection should be essentially equal allowing for normal tolerance differences. This characteristic is useful for modulating the power output or possibly for limiting array temperatures during near-sun mission.

In summary the described concepts have the following features:

- Compact flat-pack stowage.
- No interleaving protective blankets required.
- Full retraction capability.

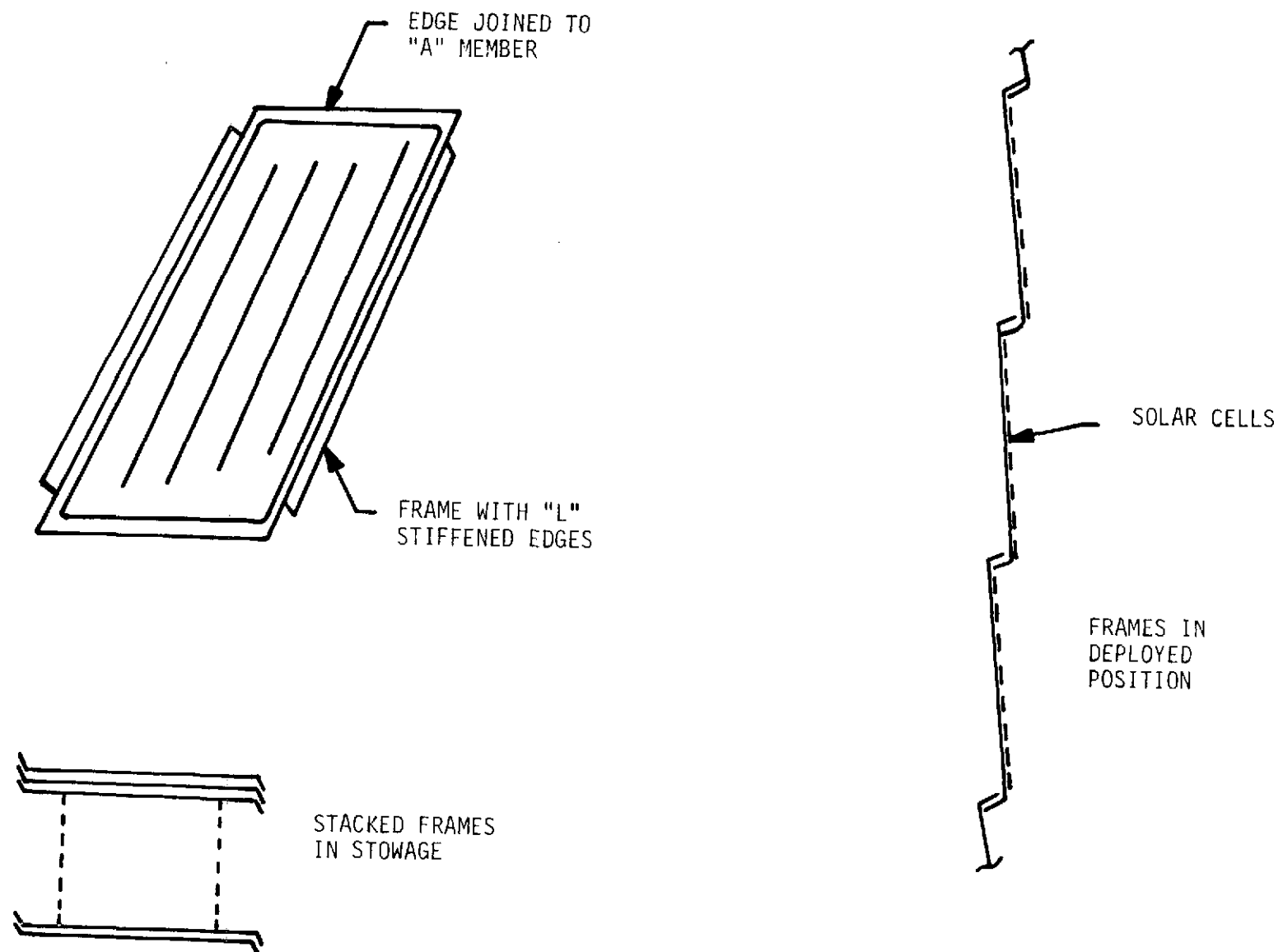


Figure 3-18. Solar Panel Frames

- o Partial retraction capability for power modulation and/or temperature control.
- o Electrical conductors combined with tensioning concept.
- o Aside from extendible boom no cables, pulleys or other mechanisms required.
- o Inherent modular panel construction.
- o Adaptable to "V" stiffening concept.

#### 3.2.1.1.4 Deployable Boom

An articulated steel longeron ASTROMAST was selected for the interplanetary mission baseline configuration because of its inherent ability to function at an upper temperature extreme of +140°C. This mast is similar to the unit developed for use on the Lockheed space station solar array program. Table 3-8 gives the size and weight of the mast and canister required for this application.

Table 3-8. Design Characteristics of  
Articulated Steel Longeron ASTROMAST

Parameter	Value
Bending stiffness	3440 N-m <sup>2</sup> (1.2x10 <sup>6</sup> lb-in <sup>2</sup> )
Diameter*	190 mm
Fully deployed length	18.6 m
Canister height	670 mm
Canister diameter	228 mm
Mast mass	3.1 kg
Canister mass	5.3 kg
Total component mass	8.4 kg

\* Diameter of circle through longeron centers.

### 3.2.1.1.5 Structural Design

3.2.1.1.5.1 Frame. The frame is a 5.9 m x 0.63 m x 0.31 m welded truss constructed from 25 mm and 19 mm O.D. by 1.3 mm wall thickness magnesium tubing. The members are sized to resist buckling under a 6.5 g load in the direction of deployment.

3.2.1.1.5.2 Blanket Stowage. The blanket is stowed in the upper end of the 0.31 m deep frame between the floor and the covers. The floor consists of a 19 mm thick, lightweight honeycomb which is supported by 13 mm O.D. by 1.3 mm wall thickness magnesium tubing.

3.2.1.1.5.3 Covers. The two covers extend the full length of the frame, are hinged at one side, and have a small gap between them at the other side. They are fabricated from 6 mm thick, lightweight honeycomb which is stiffened by five, equally spaced, magnesium channels. The covers are held in the closed position by means of a leading edge member which meets within cut-outs in the five channels. Springs at the hinge axes open the covers when the leading edge member is deployed.

3.2.1.1.5.4 Leading Edge Member. The leading edge member is a 44 mm x 76 mm x 1 mm rectangular, beryllium tube that extends the full length of the frame. The leading edge member provides the dual functions of retaining the covers and blanket in the stowed configuration and of providing the required stiffness for blanket support in the deployed configuration. The member is attached to the boom at its center by means of a bearing support and to the retention cables by means of grooved fittings at both ends.

3.2.1.1.5.5 Center Fitting. The center fitting is a welded and machined magnesium member that provides a mounting location for the boom and an interface with the vehicle solar array drive.

3.2.1.1.5.6 End Retention. In addition to the center fitting, the frame is retained to the vehicle at its four corners. Two cables, one at each end, preload the frame against four pins attached to the vehicle. One of these pins is tapered and engages a tapered hole to



take out lateral loads in both directions. A second, tapered pin engages a tapered slot to take out lateral loads in one direction only. The remaining two pins bear against the frame, but do not take lateral loads. The frame is released by cutting the cables with redundant cable cutters. Cutting the cables releases the leading edge member and allows the four pins to retract thereby releasing the frame.

3.2.1.1.5.7 Tension Device. The lower end of each blanket is fastened to a tension tube which is fabricated from 19 mm O.D. x 0.8 mm wall beryllium tubing. Each tension tube provides tension to the blanket by means of two relatively constant force springs. The tubes are constrained to move in a linear motion by means of ball bushings at both ends of each tube.

### 3.2.1.2 Performance

The baseline solar array configuration for the interplanetary mission application has a total mass of 87.5 kg as shown by the breakdown in Table 3-9. The beginning-of-life electrical

Table 3-9. Total System Mass Summary  
(Baseline Configuration for Interplanetary Mission)

Item		Mass (kg)
Solar Cell Blankets (see Table 3-7 for detail breakdown)		48.5
Stowage and Support Structure		30.6
Frame	11.0	
Container Bottom	3.6	
Container Cover	4.0	
Container Mechanisms	0.1	
Center Fitting	0.8	
Leading Edge Member	3.1	
End Retention Fittings	1.0	
End Retention Cable Cutters	0.9	
End Retention Mechanisms	0.4	
Blanket Tension Mechanisms	1.2	
Interlayer Cushioning	2.5	
Container Foam	1.8	
Coatings	0.1	
Fasteners	0.1	
Deployment Mechanism		
Mast	3.1	8.4
Canister	5.3	
Total		87.5

output of the panel is 9860 watts at the maximum power point, as shown in Figure 3-19. Thus, the resulting system power-to-mass ratio is 112.7 watt/kg.

### 3.2.1.3 Critical Technical Problems

The critical technical problems associated with a solar array of this type are in the form of uncertainties or unanswered questions concerning the solar cell blanket. These concerns stem from the ultralightweight blanket construction approach which is necessary to meet the power-to-mass ratio goal. In the area of solar cell/cover technology it remains to be seen if a 37  $\mu\text{m}$  thick integral cover can be sputtered onto a 125  $\mu\text{m}$  thick solar cell with the mechanical integrity necessary to survive the specified thermal shock environment. The welding (or bonding) of interconnectors to ultrathin solar cells is untried and thus subject to a large uncertainty. The effects of particulate contamination from the ion engines on the solar array remains an area of concern. The amalgamation of gold and mercury is a known effect which must be prevented in a solar array design which uses gold plated solar cell contacts. Also, the deposition of thin metallic films on the solar cell coverglass can have a serious effect on solar array output. A film of this type can occur in three ways: (1) condensation of propellant particles, (2) deposition of thruster material, and (3) deposition of material sputtered from other spacecraft surfaces. The first of these processes is not of great concern since mercury has a sufficiently high vapor pressure. Figure 3-20 shows the neutral arrival rate necessary to have bulk accumulation as a function of  $1000/T$ , where  $T$  is the surface temperature. Above this line there will be bulk accumulation of mercury while below the line the condensed layer thickness will decrease until approximately one monolayer or less remains. Generally the neutral flux will be less than  $10^{12}$  atoms/cm<sup>2</sup>-sec so that accumulation of mercury will not occur for surface temperatures greater than  $-75^{\circ}\text{C}$ .

The second deposition process is of greater concern since the ion engine acceleration grid is usually a metal like molybdenum or aluminum which have very low vapor pressures and thus will not evaporate from spacecraft surfaces. Figure 3-21 shows the effects of uniform molybdenum films on the front surface of a solar array panel. These curves show that films only a few monolayers thick can seriously degrade solar cell output.

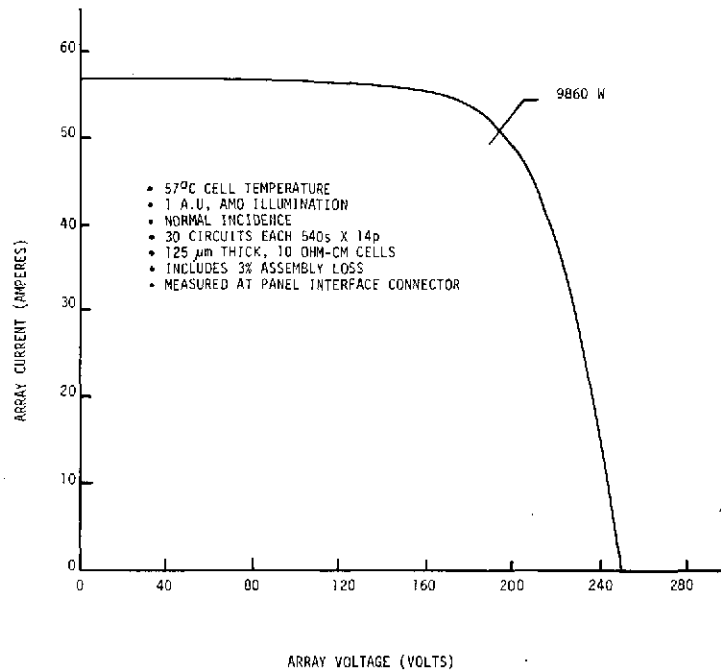


Figure 3-19. Beginning-of-Life Solar Array I-V Characteristic

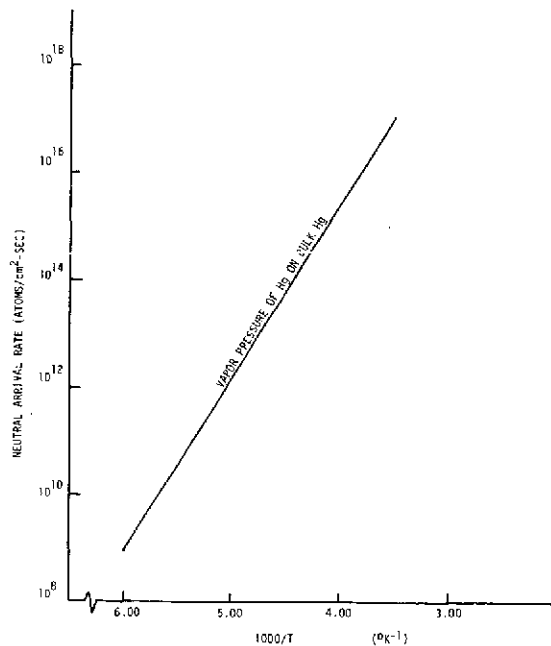


Figure 3-20. Bulk Accumulation Regions for Mercury Atoms on Surfaces Where Absorbed Monolayers Already Exist  
(From Reference 1)

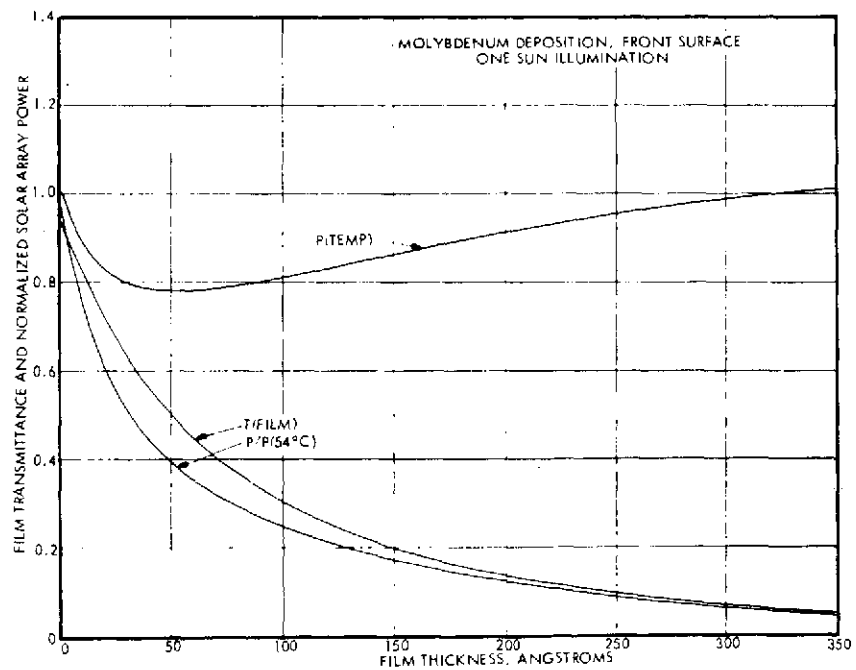
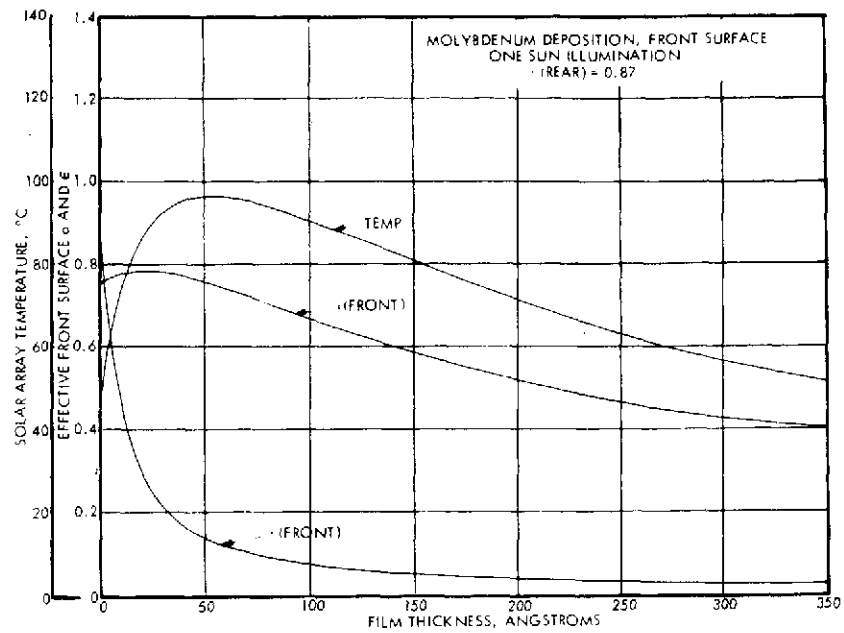


Figure 3-21. Effects of Uniform Molybdenum Film on Illuminated (Front) Surface of Solar-Cell Panel (From Reference 1)

The third source of film deposition from material sputtered from other spacecraft surfaces is very spacecraft design-dependent and should be considered.

A comparison of theoretical predictions with flight data from the SERT II spacecraft is shown in Figure 3-22. This spacecraft carried two mercury electron-bombardment thrusters. Two small arrays of solar cells were mounted with each thruster at about 4 thruster radii from each beam-axis and about 2 radii downstream. For each thruster, one array was maintained at about  $-40^{\circ}\text{C}$  (so called Lo-temp sensor) and the other at about  $+60^{\circ}\text{C}$  (so called Hi-temp sensor). Short-circuit currents of the four arrays were measured as functions of time and were seen to drop to about 50 percent of the initial value in 6 to 12 hours of thruster operation.

### 3.2.2 CHANGES TO BASELINE REQUIRED FOR GEOSYNCHRONOUS MISSION

#### 3.2.2.1 Description

The requirements on the solar array design for the geosynchronous mission are very similar to those for the baseline interplanetary mission. The following differences influence the design approach selection:

1. The maximum solar array temperature in geosynchronous orbit will be about  $70^{\circ}\text{C}$  as compared to the  $140^{\circ}\text{C}$  specified for the interplanetary mission.
2. The trapped electron environment will cause more maximum power degradation for the same solar cell blanket configuration.

The lower upper temperature extreme in geosynchronous orbit will allow the use of the continuous fiberglass longeron ASTROMAST in place of the articulated steel longeron ASTROMAST with a corresponding reduction in total system mass of about 0.7 kg. Table 3-10 gives the size and weight of the mast and canister required for this application. The trapped electron environment at geosynchronous altitude influences the total system weight only if it is required to have the same maximum power degradation at the end-of-mission. In this case, it would be necessary to increase the solar cell shielding with a corresponding increase in total system mass of about 4.0 kg.

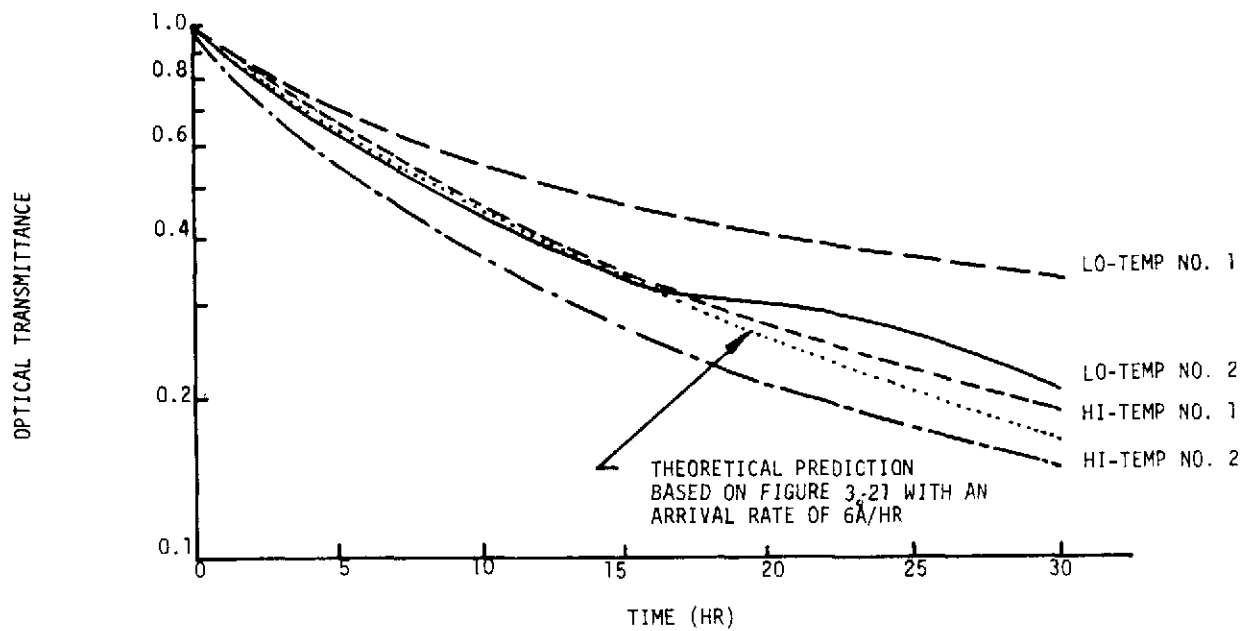


Figure 3-22. Comparison of SERT II Results with Theoretical Predictions  
(Data from Reference 1)

Table 3-10. Design Characteristics of Continuous Fiberglass Longerons ASTROMAST

<u>Parameter</u>	<u>Value</u>
Bending stiffness	3440 N - m <sup>2</sup> (1.2 x 10 <sup>6</sup> lb <sub>f</sub> - in <sup>2</sup> )
Diameter*	190. mm
Fully deployed length	18.6 m
Canister height	670. mm
Canister diameter	228. mm
Mast Mass	1.8 kg
Canister Mass	5.9 kg
Total component Mass	7.7 kg

\*Diameter of circle through longeron centers

### 3.2.2.2 Performance

The total system mass breakdown for the geosynchronous application is identical to that given in Table 3-9 except that the deployment mechanism mass changes from 8.4 kg to 7.7 kg to reflect the change from an articulated steel longeron ASTROMAST to a continuous fiber-glass longeron ASTROMAST. The corresponding total system mass of 86.8 kg yields a beginning-of-life power-to-mass ratio of 113.6 watt/kg based on the solar array output at 1 AU and normal incidence. Figure 3-23 shows the calculated beginning-of-life solar array output in a geosynchronous orbit at two seasons of the year. These curves assume that the solar array is driven about the North-South spacecraft axis by a single axis orientation mechanism.

### 3.2.3 CHANGES TO BASELINE REQUIRED FOR MANNED SPACE STATION MISSION

#### 3.2.3.1 Description

The requirement for in-orbit retraction capability for the manned space station mission can be accommodated by providing a roll-up drum stowage arrangement or by using the

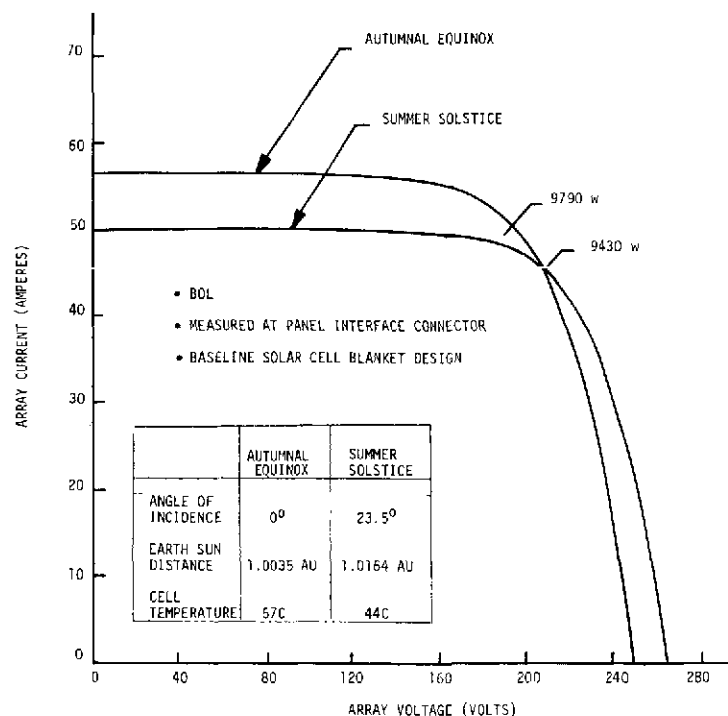


Figure 3-23. Solar Array I-V Characteristic in Geosynchronous Orbit at Two Seasons of the Year

new retractable flatpack concept described in Section 3.2.1.1.3. The weight associated with the roll-up approach was used to assess the performance for this mission, but it is expected that the retractable flatpack concept will be slightly lighter.

The solar cell base resistivity was also changed from a nominal 10 ohm-cm to 2 ohm-cm in line with the trade-off study results reported in Section 3.4.1. This change results in about the same solar array output power and maximum power voltage at the higher operating temperature without requiring a change in circuit arrangement.

A preliminary dynamic analysis was performed to evaluate the adequacy of the 190 mm diameter continuous fiberglass longeron ASTROMAST for the acceleration pulses specified in Section 3.1.1.4.4. This analysis considered the following square-wave accelerator pulses:

1. 0.035g translational acceleration for 0.3 seconds.
2. 0.137 degrees/sec<sup>2</sup> rotational acceleration for 2 seconds.
3.  $7 \times 10^{-4}$ g translational acceleration for 3 seconds.

In order to obtain a qualitative assessment of the effects of the pulses on the deployed array, the pulses were treated as an impulse function. Because the period of the array in its fundamental mode is relatively large compared to the pulse duration (25 seconds compared to 3 seconds), a reasonable estimate of the dynamic loading of the boom can be obtained from an estimate that treats the pulse effect as a velocity change to the array. This does, however, neglect the dynamic magnifications that will be obtained in the higher array modes.

The bending moment at the root of the deployed boom resulting from these pulses was calculated to be 11.7 N-m (104 in-lb), 2.34 N-m (20.7 in-lb) and 5.1 N-m (45 in-lb) for the respective acceleration pulses described above. From these results, the moment resulting from the 0.035g, 0.3 second pulse appears to be the most critical. The critical bending moment for this mast is approximately 13.6 N-m (120 in-lb) using the data given



in Reference 67. Since the calculated moment due to the pulse does not include the loads induced by thermal distortion, initial out-of-straightness and aerodynamic drag it can be concluded that this mast design is at best marginal under these loading conditions. However, no change in mast diameter has been made at this time because of the uncertainties associated with the definition of these acceleration pulses. If it is desired to explore this mission application in greater depth, it will be necessary to perform a dynamic analysis treating the response of the various deployed array modes.

### 3.2.3.2 Performance

The solar array panel for the manned space station mission application has a total mass of 95.1 kg as shown by the breakdown in Table 3-11. Note that the solar cell blanket weight has increased to account for the addition of cushioning buttons on the rear of the substrate. The beginning-of-life electrical output of the panel is 10060 watts at the maximum power point as shown in Figure 3-24. Thus, the resulting system power-to-mass ratio is 105.8 watt/kg.

Table 3-11. Total System Mass Summary for Manned Space Station Application

Item		Mass (kg)
1.	Solar Cell Blankets	50.6
2.	Stowage and Support Structure	36.8
	Center Support	1.35
	Leading Edge Member	3.10
	Outboard End Supports (2)	3.90
	Drum Shells (2)	12.70
	Inboard End Caps (2)	14.64
	Outboard End Caps (2)	0.94
	Coatings	0.10
	Fasteners	0.10
3.	Deployment Mechanism	7.7
	Mast	1.8
	Canister	5.9
TOTAL		95.1

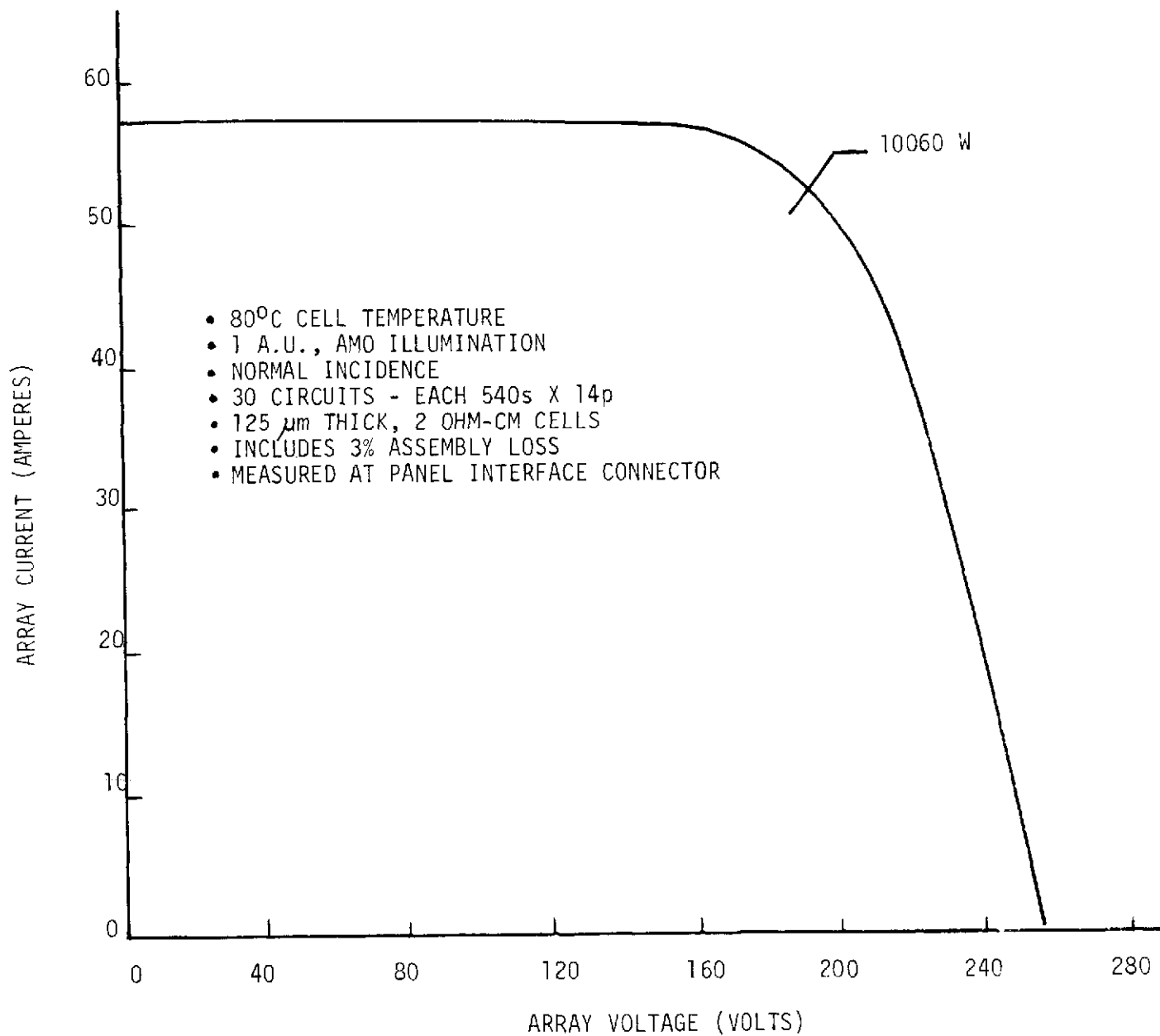


Figure 3-24. Beginning-of-life Solar Array I-V Characteristic

### 3.3 STATE-OF-THE-ART DISCUSSION

#### 3.3.1 STATE-OF-THE-ART BASELINE

##### 3.3.1.1 Solar Array System Designs

A number of lightweight solar array system concepts have been developed to the extent that working models have been built and subjected to environmental and functional performance testing. One such system has been flown as an experiment. In this section, each of these systems will be described. No attempt is made to describe all previously proposed lightweight solar array systems since some configurations are similar to existing developed concepts and do not offer any particular advantage from a power-to-weight ratio standpoint.

In general, these existing concepts can be categorized as shown in Table 3-12.

Table 3-12. Existing Lightweight Solar Array Types

Solar Array Type	Existing Solar Array Concepts
1. Roll-up	
a. Single boom, two blanket	GE/JPL 30 watt/lb
b. Two boom, single blanket	Hughes/AF
2. Flat-pack	RAE
	CTS
	Lockheed Space Station
3. "Rigid" Folding Panel	Boeing/JPL
	EOS Hollowcore

#### 3.3.1.1.1 GE/JPL 30 Watt/Lb Roll-Up Solar Array

This roll-up solar array, shown in Figure 3-25, and referred to as the RA250, was designed, fabricated and tested by the General Electric Company under contract to JPL (Contract No.'s 951970 and 952314). This array provides  $23.2 \text{ m}^2$  of deployed solar cell module area which is stored on cylindrical drums during launch (see Reference 12). These storage drums are mounted on a center support structure. Each drum has a bearing system, a slip ring assembly for the transfer of power and signals, and a Negator spring motor that provides a constant tension in the solar array blanket. A BI-STEM deployable boom is mounted on the center support and is attached to a leading edge member. The solar array blankets consist of an interconnected assembly of 55,176,  $180\mu\text{m}$  thick,  $2 \times 2 \text{ cm}$  solar cells mounted on a flexible Kapton-H film substrate. A blanket is rolled onto each drum, with the outboard edge attached to the leading edge member. The system is deployed by extending the boom. The deployed boom and the leading edge member comprise the primary structure. Each blanket is under tension from the Negator springs. Outboard end supports are provided in the launch configuration and are pyrotechnically released before deployment.

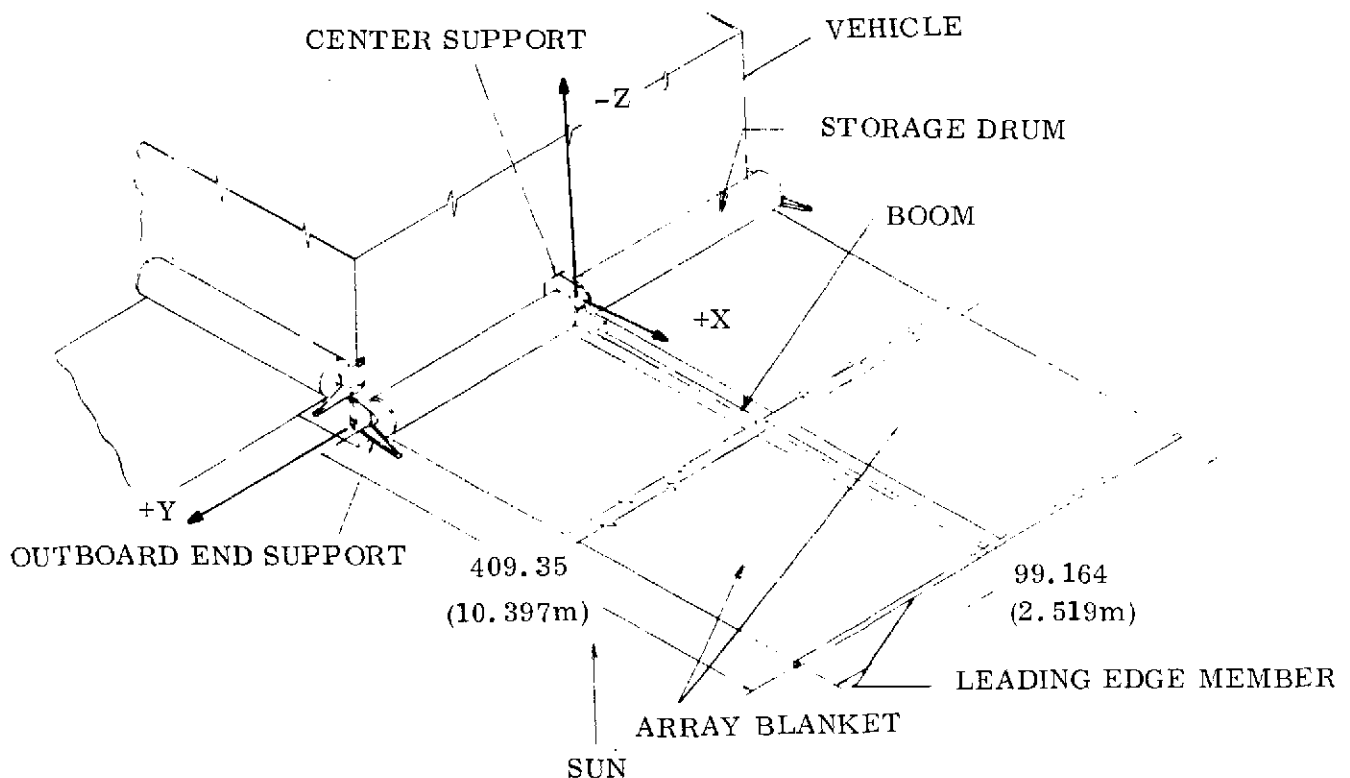


Figure 3-25. GE/JPL 30 Watt/Lb Roll-up Solar Array

The total system mass, including all the structural weight associated with stowage and deployment, is 37.4 kg. Using a specified unit electrical output of  $107.6 \text{ watt/m}^2$ , the system power-to-mass ratio is 66.8 watt/kg. The total blanket mass-to-area ratio is  $0.91 \text{ kg/m}^2$  of module area.

#### 3.3.1.1.2 Hughes/AF Roll-Up Solar Array

The roll-up array developed by Hughes Aircraft Company under Air Force Contract F33615-68-C-1676, is shown in Figure 3-26. This system was launched as a flight experiment on October 17, 1971, and the array itself has performed satisfactorily in-orbit since that time (References 13 and 14). This system uses two solar cell blankets which are rolled-up on a single storage drum. An embossed  $50 \mu\text{m}$  thick Kapton cushion protects the solar cells in the launch stowed configuration. During extension, this cushion is rolled-up on an auxiliary take-up roller. The two flexible substrates, which are a laminate of Kapton-H film and fiberglass, are mounted with a total of 34,500  $180 \mu\text{m}$  thick,  $2 \times 2 \text{ cm}$ , 2 ohm-cm cells which are covered with  $150 \mu\text{m}$  thick Microsheet. The solar cell blankets are deployed from the common drum by a pair of extendible boom actuator units. Each unit houses two 2.18 cm diameter BI-STEM booms. The total solar array system mass is given as 32.0 kg with 15.8 kg of this associated with the flexible blankets.

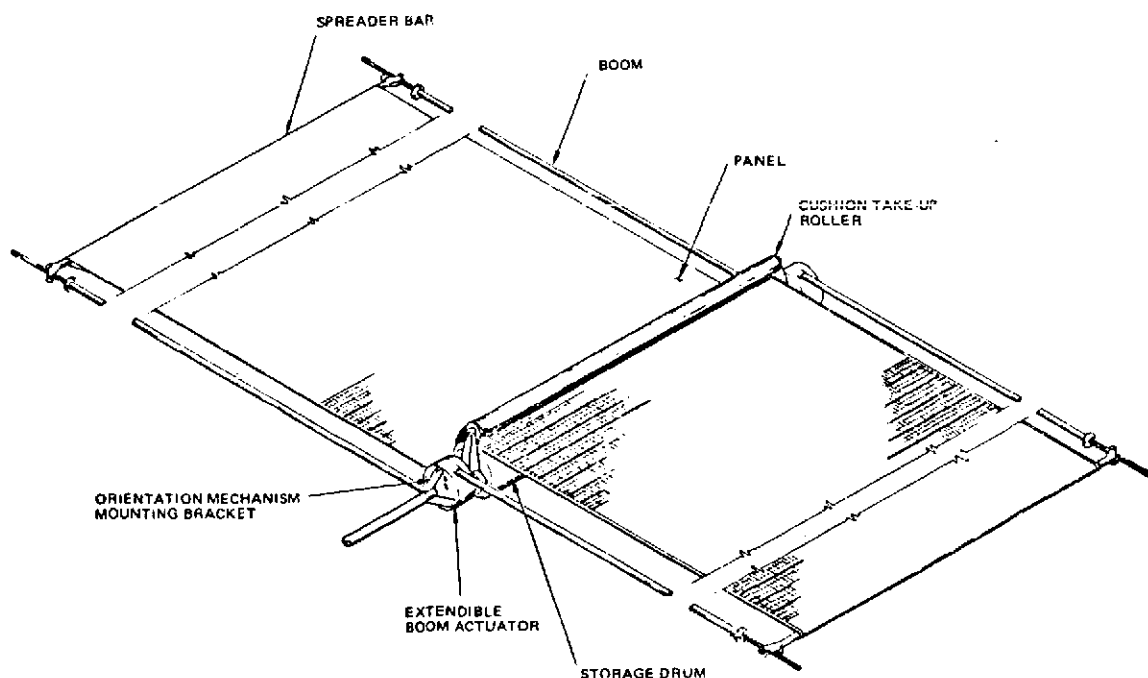


Figure 3-26. Hughes/AF Roll-Up Solar Array

### 3.3.1.1.3 RAE Flat-Pack Solar Array

The lightweight solar array concept, shown in Figure 3-27 is presently under development at the Royal Aircraft Establishment (see References 15 and 16). This design employs flexible substrates which are folded, accordion fashion, for stowage during launch. The

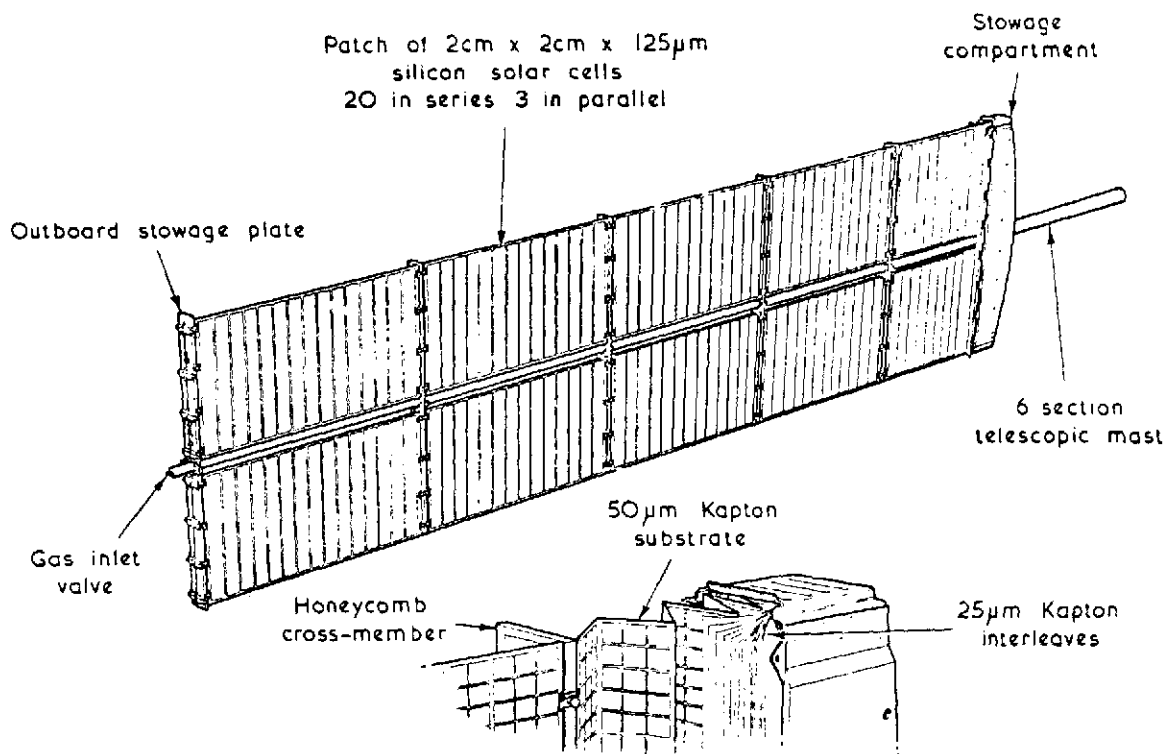


Figure 3-27. RAE Flat-Pack Solar Array

Kapton-H film substrates are mounted with a total of 7440, 125  $\mu$ m thick, 2x2 cm, 10 ohm-cm, bottom wrap-around contact Ferranti cells which are covered with PPE, 100  $\mu$ m thick, ceria stabilized glass. The solar array is deployed pneumatically through a six section, aluminum telescopic mast. Each section is mechanically latched when fully deployed. Aluminum honeycomb cross members are attached to the tube sections to function as support for the array blanket segments. The total system mass for this model is 5.35 kg. The beginning-of-life power-to-mass ratio is  $280/5.35 = 52.4$  watt/kg. The

solar cell blankets have a total mass of 2.28 kg which yields a unit blanket mass of  $0.634 \text{ kg/m}^2$  of total blanket area.

#### 3.3.1.1.4 Lockheed Space Station Solar Array

A solar array system for manned space station application is being developed by Lockheed under contract to MSC (Contract No. NAS9-11039). This system, shown in Figure 3-28, consists of two array wings per station (Reference 5). A total of 470,000 solar cells are mounted on ten strip assemblies per wing. Each strip consists of 42 modules each with 1,120 solar cells. These cells are  $2 \times 4 \text{ cm}$ , bottom wrap-around contact configuration with a base resistivity of  $2 \text{ ohm-cm}$  and a thickness of  $300 \mu\text{m}$ . The cells are covered with  $300 \mu\text{m}$  thick fused silica with no blue-reflecting filter. The solar cell copper interconnectors are integral with the substrate and are sandwiched between layers of Kapton-H film with FEP-Teflon used as an adhesive. The solar array strips on a wing are deployed by a single articulated lattice boom which is manufactured by Astro Research Corporation. Each of these strips is stowed by folding it on itself, in flat-pack fashion, within a container which is mounted on the inboard support assembly as shown in Figure 3-28.

The structural capability of this system is based on an artificial "g" requirement which imposes severe quasi-static loads on the deployed array structure. This requirement has a major influence on the total system mass which is 1341 kg for one wing.

#### 3.3.1.1.5 CTS Flat-Pack Solar Array

A flat-pack solar array is presently under development for the Communications Technology Satellite (CTS). This solar array, shown in Figure 3-29, consists of a single blanket which is deployed by a single  $3.5 \text{ cm}$  diameter BI-STEM boom (Reference 17). The boom is located behind and on the shadowed side of the blanket. Each blanket is  $6.2 \text{ m}$  long by  $1.25 \text{ m}$  wide and is mounted with 13,125  $200 \mu\text{m}$  thick,  $2 \text{ ohm-cm}$ ,  $2 \times 2 \text{ cm}$  cells which are covered with  $100 \mu\text{m}$  thick ceria-stabilized coverglass. A welded interconnection system is utilized and the solar cell modules are mounted on a Kapton-H film substrate. Each blanket is subdivided into 27 active and 3 blank panels which are folded accordion

NOT REPRODUCIBLE

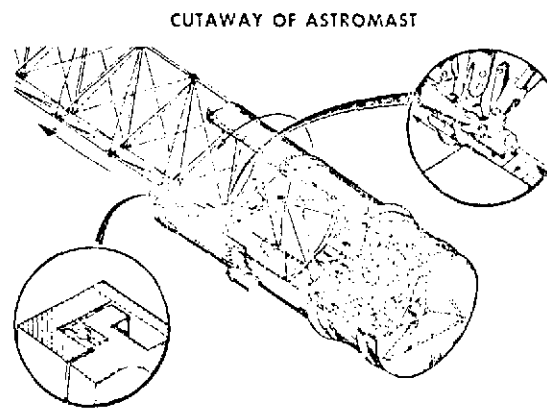
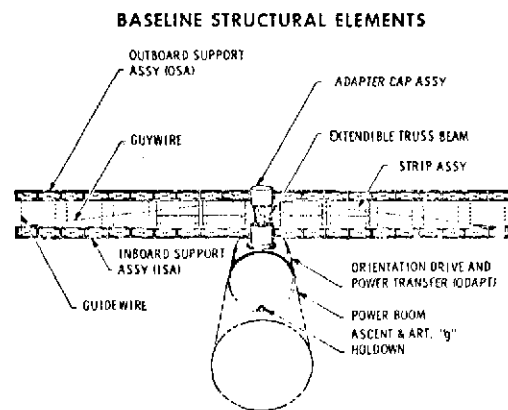
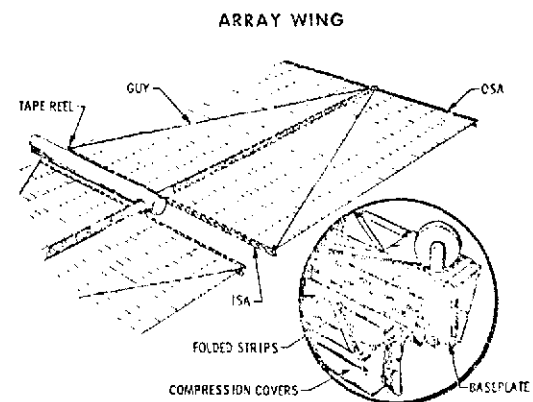
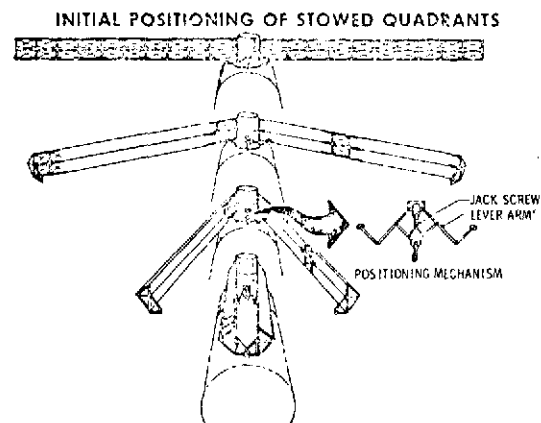


Figure 3-28. Lockheed Space Station Solar Array



NOT REPRODUCIBLE

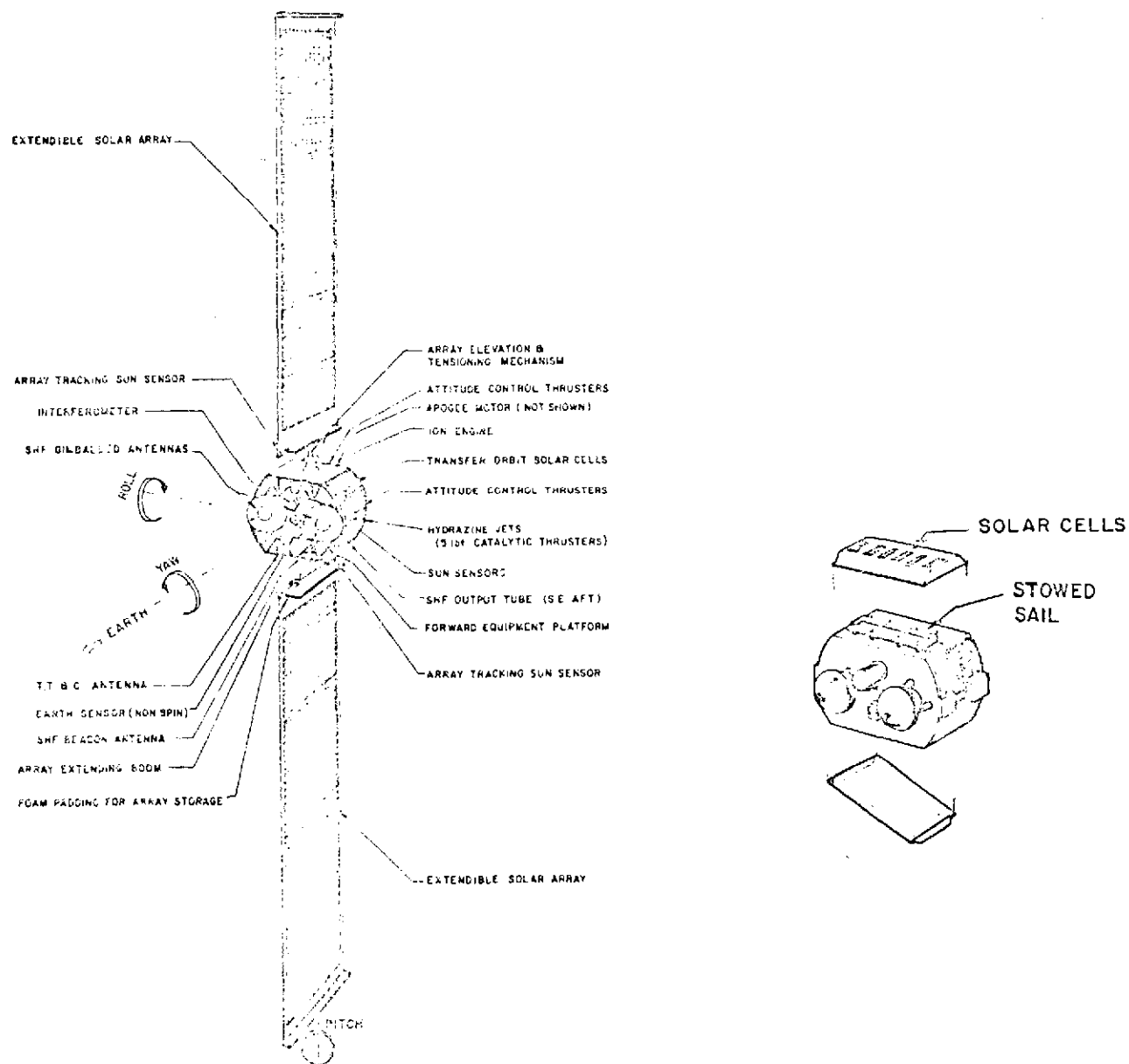


Figure 3-29. CTS Flat-Pack Solar Array

fashion in the packaged configuration. The total system mass is given as 25.29 kg for one of the solar panels. This mass includes the slip rings and orientation drive mechanism associated with one of the panels. The mass of the BI-STEM boom and deployer is 4.08 kg and the mass of each flexible blanket is 6.80 kg.

#### 3.3.1.1.6 Boeing/JPL Folding Panel Solar Array

The lightweight folding panel solar array shown in Figure 3-30 was developed by the Boeing Company under contract to JPL (Contract Nos. 951653 and 951934). This solar array panel consists of 13 panels connected by hinges and locked in a common plane when fully deployed (Reference 18). Each subpanel consists of a pretensioned fiberglass tape substrate which is sandwiched between beryllium frames. The solar cell modules, which utilize 180  $\mu\text{m}$  thick, 2 ohm-cm, 2 x 2 cm cells with 75  $\mu\text{m}$  thick Microsheet coverglass, are mounted directly to the stretched fiberglass tape substrate. A total of 256,592 cells are mounted on each panel. The total mass of the panel is 244 kg.

#### 3.3.1.1.7 EOS Hollowcore Folding Panel Solar Array

This lightweight "rigid" panel concept, shown in Figure 3-31, was developed by Electro-Optical Systems (EOS) under NASA Contract NAS7-428 (Reference 19). This design employs an electroformed biconvex aluminum hollowcore substrate which is supported in a tubular beryllium frame. The substrate is formed into the surface of a spherical segment with a radius of 414.66 cm. A total of 5040, 100  $\mu\text{m}$  thick, 2 x 2 cm solar cells with 25  $\mu\text{m}$  integral covers are bonded to an intermediate layer of 25  $\mu\text{m}$  thick Kapton-H film. The total panel mass is given as 2.330 kg with 1.435 kg of this associated with the solar cell stack and supporting substrate.

#### 3.3.1.1.8 Comparison of Existing System Concepts

A comparison of these existing lightweight solar array concepts is presented in Table 3-13. For each system, the total solar cell area per panel is given in Column 4 of the table. This area is computed by multiplying the total number of solar cells by  $4 \times 10^{-4} \text{ m}^2$  for 2 x 2 cm cells (or  $8 \times 10^{-4} \text{ m}^2$  for 2 x 4 cm cells). A range of over two orders of magnitude in size is reflected by areas which range from the RAE flat-pack at  $2.98 \text{ m}^2$  to the Lockheed Space

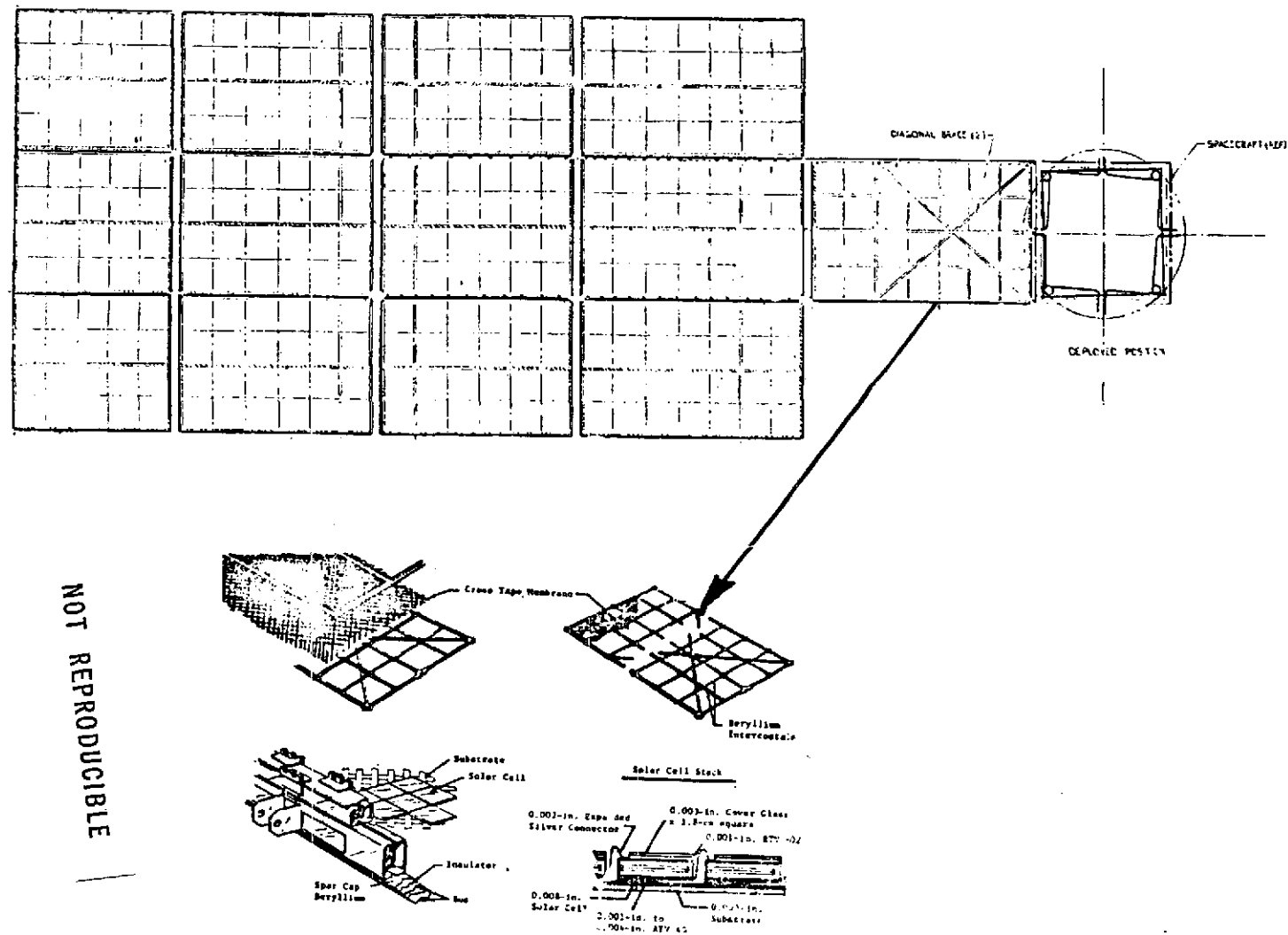


Figure 3-30. Boeing/JPL Fold-out Solar Array

This page is reproduced at the back of the report by a different reproduction method to provide better detail.

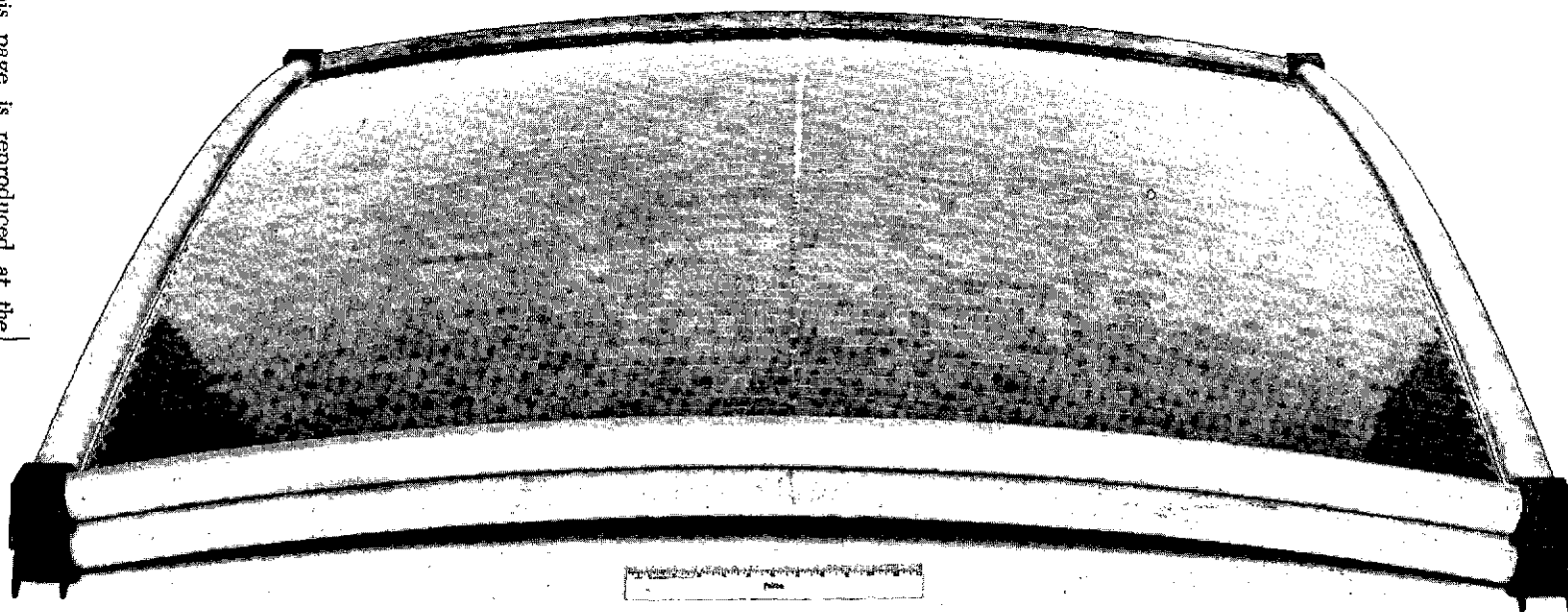


Figure 3-31. EOS Hollowcore Folding Solar Array (Phase II Demonstration Panels)

Table 3-13. Comparison of Existing Lightweight Solar Array Designs

No.	Solar Array Configuration Identification	Illustration Figure No.	Total Solar Cell Area Per Panel (m <sup>2</sup> )	Lowest Deployed Natural Frequency (Hz)	Total System Mass (kg)	Mass-to-Area Ratio (kg/m <sup>2</sup> )					Reference
						Total System	Blanket (or substrate)	Total Structure	Deployment Structure and Mechanisms	Stowage Structure and Mechanisms	
1	GE/JPL 30 Watt/lb Roll-up	3-25	22.07	0.07	37.4	1.696	0.958	0.738	0.258	0.480	12
2	Hughes/AF Roll-up	3-26	13.8	0.25	32.0	2.320	1.141	1.179	0.632	0.547	13
3	RAE Flat-pack	3-27	2.98	0.78	5.35	1.797	0.766	1.037	0.518	0.513	16
		3-27	13.5	(1)	17.25	1.279	0.718	0.561	0.262	0.299	15
4	Lockheed Space Station	3-28	376.3	0.062	1341.	3.570	2.258	1.312	(1)	(1)	5
5	CTS	3-29	5.25	(1)	25.29 <sup>(2)</sup>	4.817 <sup>(2)</sup>	1.295	3.522 <sup>(2)</sup>	0.777	(1)	17, 20
6	Boeing/JPL Fold-out	3-30	102.6	0.068	244.	2.380	0.894	1.486	(3)	(3)	18
7	EOS Hollowcore	3-31	2.016	(1)	2.33 <sup>(4)</sup>	1.156 <sup>(4)</sup>	0.712	0.444 <sup>(4)</sup>	(3)	(3)	19

## NOTES:

- (1) Information not available in the references  
 (2) Includes solar array orientation drive mass  
 (3) No attempt was made to separate stowage and deployment structural mass for the folding panel configurations  
 (4) Does not include mass required to stow and deploy a multiple panel system

NOT REPRODUCIBLE

Station at  $376.3 \text{ m}^2$ . The lowest deployed natural frequency of the solar array system is given in Column 5. For a given system area, a reduction in the deployed natural frequency requirement will result in lower total system mass. The total system mass is given in Column 6. Note that, for the CTS array, the mass includes the orientation drive which cannot be separated out to yield the mass of the solar array. The mass of the EOS Hollow-core concept does not include the mass required for stowage and deployment of a multiple panel system. Column 7 of the table give the total mass per unit area of the system. These total mass-to-area ratios range from  $1.279 \text{ kg/m}^2$  for the large RAE flat-pack to  $3.570 \text{ kg/m}^2$  for the Lockheed space station solar array. Note that the CTS array and the EOS Hollowcore have been disregarded because of the uncertainties associated with the weight numbers. In the remaining mass-to-area ratio columns, the total system mass has been broken down into the contribution due to the flexible blankets and the structure. Where possible, this structural mass has been further divided into the mass associated with: (1) deployment and deployed array support structure and mechanisms, and (2) stowage structure and mechanisms. For example, with the GE/JPL 30 watt/lb roll-up solar array, the total system mass-to-area ratio is  $1.696 \text{ kg/m}^2$  which is further divided into  $0.958 \text{ kg/m}^2$  for the flexible blankets and  $0.738 \text{ kg/m}^2$  for all associated structure. This total structural mass can be further broken down into  $0.258 \text{ kg/m}^2$  for deployment and deployed array support structures and mechanisms and  $0.480 \text{ kg/m}^2$  for structure associated with stowage. The BI-STEM boom and actuator along with the leading edge member are considered as deployment related structures while the storage drums, center support and out-board end supports are considered part of the stowage related structure. This division of structural mass applies fairly well for the flexible substrate solar arrays, but cannot be applied to the "rigid" folding panel configurations since it is difficult to allocate structural mass between stowage and deployment functions.

### 3.3.1.2 Components

This section contains a review of the existing technology base in the areas of solar cells, solar cell covers, interconnects and substrates, and deployable booms with particular emphasis on the applicability to this study.

#### 3.3.1.2.1 Solar Cells

This feasibility study was based on the use of currently available N on P silicon solar cells. It was not intended to rule out the potential offered by future developments in solar cell technology. For example, the 20 to 30% increase in output power associated with the COMSAT violet cell (Reference 21) will be considered as a potential for improving the solar array system power-to-mass ratio beyond the minimum 110 watt/kg goal. In other words, the feasibility of the 110 watt/kg goal will not be linked to projected improvements in solar cell technology.

Nominal solar cell thickness from 200 to 100  $\mu\text{m}$  were considered as having possible application on this program. Two nominal base resistivities, 2 and 10 ohm-cm, were also considered. In addition to thickness and base resistivity, the solar cells were considered to be of the basic 2 x 2 cm size with a bottom wraparound contact configuration. The bottom wraparound contact configuration, shown in Figure 3-32 was selected because of the improved reliability for lightweight solar arrays which results from reduced interconnector stresses. This was a conclusion reported by Heliotek, in Reference 22, after

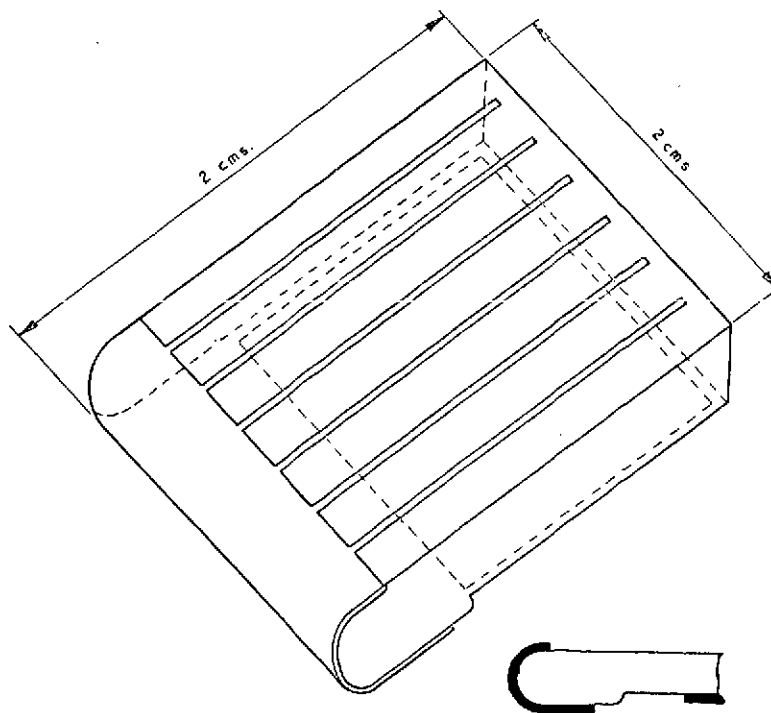


Figure 3-32. Bottom Wraparound Contact Configuration  
(from Reference 23)

performing an extensive study of the stress in conventional Z tab configuration interconnectors. In the bottom wraparound contact configuration shown in Figure 3-32, the N contact is wrapped around the edge for the full width of the cell.

The width of the N contact on the front is about 100  $\mu\text{m}$  so that increased active area is available. With this contact geometry, it is possible to make both cell connections with a flat interconnector instead of the out-of-plane Z tab. This leads to the integration of the interconnector pattern with the substrate to provide a weight effective, low stress module configuration.

A cell anti-reflective coating of  $\text{TiO}_x$  was selected over the commonly used  $\text{SiO}$  because of the demonstrated improvement in covered cell output. The use of a titanium oxide ( $\text{TiO}_x$ ) anti-reflective coating has demonstrated gains of up to 4 percent in short-circuit current of covered cells when compared to similarly covered cells with  $\text{SiO}$  anti-reflective coating (Reference 24). Some of this potential output power improvement is offset by a slight increase in the solar absorptance of the covered  $\text{TiO}_x$  cells which results in an increased in-space operating temperature when compared to covered  $\text{SiO}$  cells. The net result is a worthwhile improvement in covered cell output with the  $\text{TiO}_x$  anti-reflective coating.

The electrical performance of solar cells of this type is shown in Figure 3-33 expressed in terms of unirradiated covered cell maximum power output as a function of nominal cell thickness. This baseline performance is intended to reflect the best obtainable minimum lot average output with an economical yield using 1972 production technology. The maximum lot average cell weight associated with the nominal thickness is shown on the abscissa of the curve. The basis for these curves is data from References 15, 16, 23, 25 and 26 for a 125  $\mu\text{m}$  thick, 10 ohm-cm cell manufactured by Ferranti, Ltd. The design characteristics of this cell are summarized in Table 3-6. Figure 3-34 is the I-V characteristic which represents the minimum lot average performance of this cell at two operating temperatures, 25 and 55°C. Based on this one performance data point, the curves on Figure 3-33 were constructed using normalized data from Reference 27.



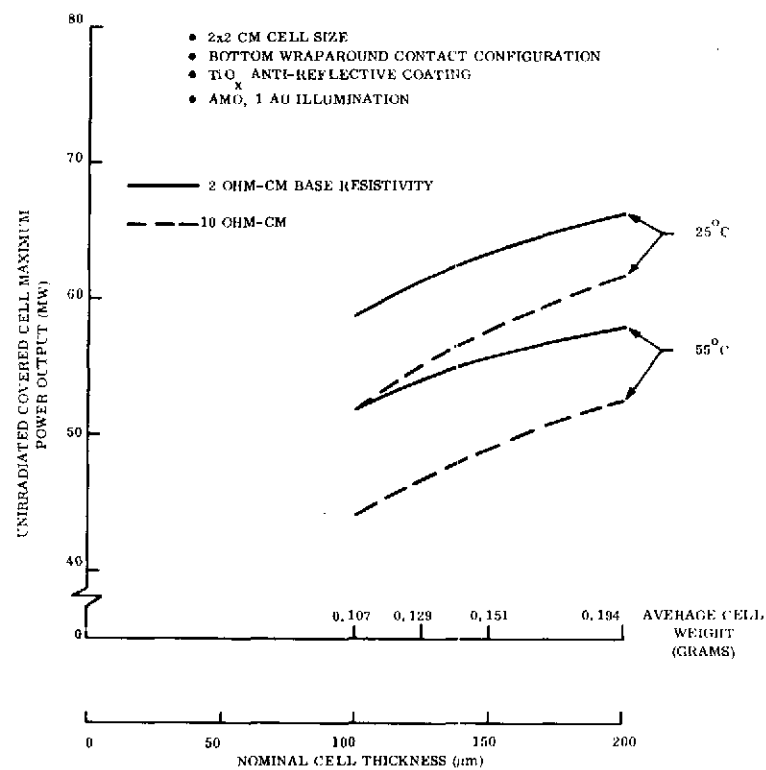
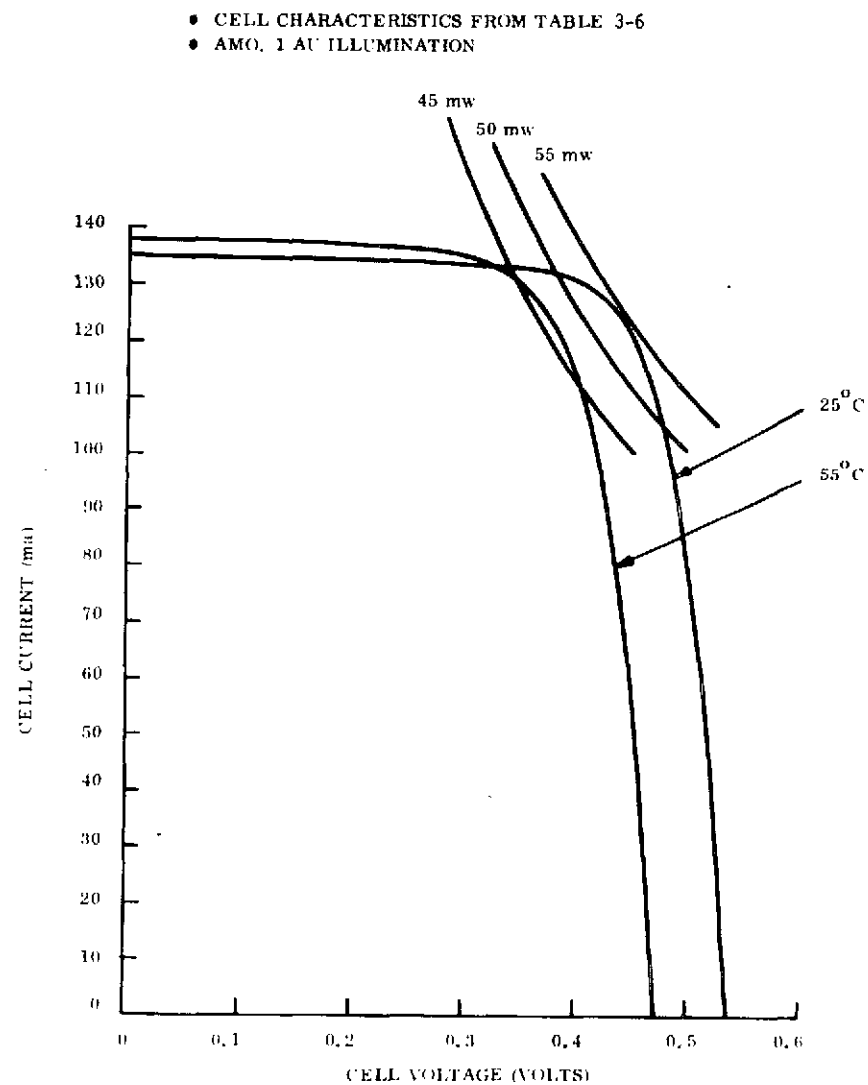


Figure 3-33. Baseline Solar Cell Electrical Performance

Figure 3-34. I-V Characteristic for 125  $\mu\text{m}$  Thick, 10 Ohm-cm Covered Ferranti Cell

### 3.3.1.2.2 Solar Cell Covers

The conventional method of protecting the active solar cell surface from the damaging effects of particle irradiation entails the application of discrete coverglass (either fused silica or Microsheet) by bonding with a silicone adhesive. Discrete coverglass thicknesses from 75 to 500  $\mu\text{m}$  have been used. A mass of 0.23  $\text{kg}/\text{m}^2$  of cell area is associated with the application of 75  $\mu\text{m}$  thick Microsheet with a 25  $\mu\text{m}$  adhesive bond line. This represents approximately 24 percent of the allowable total system mass and is prohibitively high for this application. Two promising approaches are available to provide the coverglass function at significantly reduced mass. The first of these is the integral glass cover which entails the direct deposition of glass onto the cell surface. The second method consists of the direct heat-sealing of FEP-Teflon film to the cell surface.

3.3.1.2.2.1 Integral Coverglass. The deposition of glass onto the active surface of a silicon solar cell without the use of an intermediate layer of bonding adhesive has been investigated by a number of workers as reported in References 28 through 34. The following methods for deposition of solar cell integral covers are represented by this work:

1. High Vacuum Ion Beam Sputtering (HVIBS)
2. Electron beam evaporation
3. Radio frequency sputtering
4. Fusion

The following is a brief discussion of each of these processes with comments concerning the applicability to the 110 watt/kg solar array feasibility study.

High Vacuum Ion Beam Sputtering (HVIBS). This method is a proprietary process developed by Ion Physics Corporation, Burlington, Massachusetts. The development of integral covers using this technique was performed under contract to Goddard Space Flight Center and is reported in References 30 and 32.

This process utilizes a focused ion beam propagating through a high vacuum region to sputter from a target onto substrates located in a line-of-sight position relative to the target. The Ion Physics HVIBS facility consists of a 20 kV, 250 ma argon ion beam impacting upon a target area of roughly 260 cm<sup>2</sup>. The deposition rate with this facility is 1.2  $\mu\text{m/hr}$ . Table 3-14 lists the integral cover materials which were evaluated on this program. Corning 7940 fused silica, deposited by HVIBS, produces a cover with excellent physical and performance characteristics. The only drawback is the high intrinsic stress condition which is sufficient to cause cell fragility when coating thickness exceeds 50  $\mu\text{m}$ . Figure 3-35 shows this stress expressed in terms of cover/cell bow as a function of coating thickness. The  $\text{SiO}_2/\text{Si}_3\text{N}_4$  oxynitride material yielded extreme stress levels which resulted in incidence of cover delamination. The deposited integral cover was brown in color and exhibited strong optical absorption. Corning 7740 and 7070 borosilicate glasses, best known as Pyrex, were selected for their good expansion coefficient match to that of silicon, as shown in Table 3-15. Corning 0211 Microsheet was investigated because of its known performance characteristics as a conventional cover material. The radiation darkening characteristics of 7740 and 0211 are only marginally acceptable, but this property can be improved through the introduction of  $\text{CeO}_2$ .

Table 3-14. Summary of Integral Cover Materials Deposited by HVIBS  
(From Reference 32)

Material	Deposited Stress	Integral Coating Physical Quality	Integral Coating Optical Quality
7940 fused silica	high	excellent	excellent
$\text{SiO}_2/\text{Si}_3\text{N}_4$	very high	poor	poor
7740	moderate	excellent	excellent
7740 + $\text{CeO}_2$ doping	low	excellent	good
0211 + $\text{CeO}_2$ doping	very low	excellent	good
7070	low	initially fair/ improved to excellent	excellent

Table 3-15. Comparison of Integral Cover Materials  
(From Reference 32)

Material	Thermal Expansion Coefficient ( $^{\circ}\text{C}^{-1}$ )	Annealing Point ( $^{\circ}\text{C}$ )	Relative Radiation Resistance	Constituents (weight percent)	
7070	$32 \times 10^{-7}$	495	good	$\text{SiO}_2$	70.0
				$\text{B}_2\text{O}_3$	28.0
				$\text{Li}_2\text{O}$	1.2
				$\text{Al}_2\text{O}_3$	1.1
				$\text{K}_2\text{O}$	0.5
				$\text{MgO}$	0.2
				$\text{CaO}$	0.1
7740	$33 \times 10^{-7}$	565	fair	$\text{SiO}_2$	80.5
				$\text{B}_2\text{O}_3$	12.9
				$\text{Na}_2\text{O}$	3.8
				$\text{Al}_2\text{O}_3$	2.2
				$\text{K}_2\text{O}$	0.4
0211	$72 \times 10^{-7}$	539	fair	$\text{SiO}_2$	65.5
				$\text{B}_2\text{O}_3$	10.0
				$\text{Na}_2\text{O}$	7.1
				$\text{K}_2\text{O}$	7.1
				$\text{ZnO}$	5.1
				$\text{TiO}_2$	2.7
				$\text{Al}_2\text{O}_3$	2.3
Silicon	$10-30 \times 10^{-7}$				

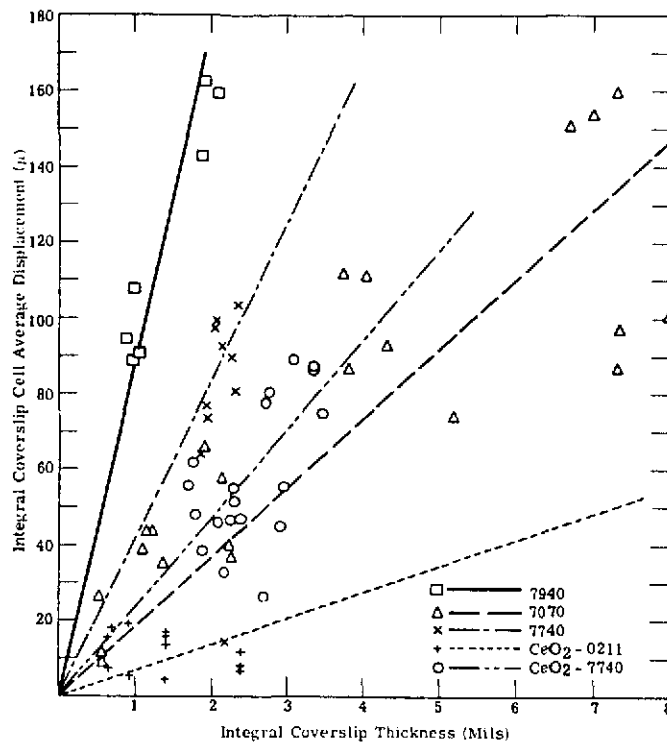


Figure 3-35. Integral Coverslip Cell Bow Versus Integral Coverslip Thickness  
(From Reference 32)

In order to evaluate darkening under electron irradiation, 150  $\mu\text{m}$  thick, unfiltered slides of 7070, 7740, 0211, 7940, and 1723 glasses were subjected to 1-MeV electron fluences of  $2.5 \times 10^{14}$  and then  $5 \times 10^{15}$  electrons/ $\text{cm}^2$  with the results shown in Figures 3-36 and 3-37. It is evident from these results that severe darkening occurred in the 0211, 7740, and 1723 glasses while much smaller losses resulted in 7070 glass and virtually no loss was incurred in the 7940 fused silica.

Solar cell samples which were covered with 50  $\mu\text{m}$  or less of 7940 fused silica have been subjected to 400 keV proton irradiation without evidence of degradation except when solderless contact bars or unprotected gaps were left exposed during irradiation. The results of irradiation with 1-MeV protons are tabulated in Table 3-16. No integrally covered cell has been observed to have sustained damage due to proton irradiation at an energy which is insufficient to penetrate the coverglass.

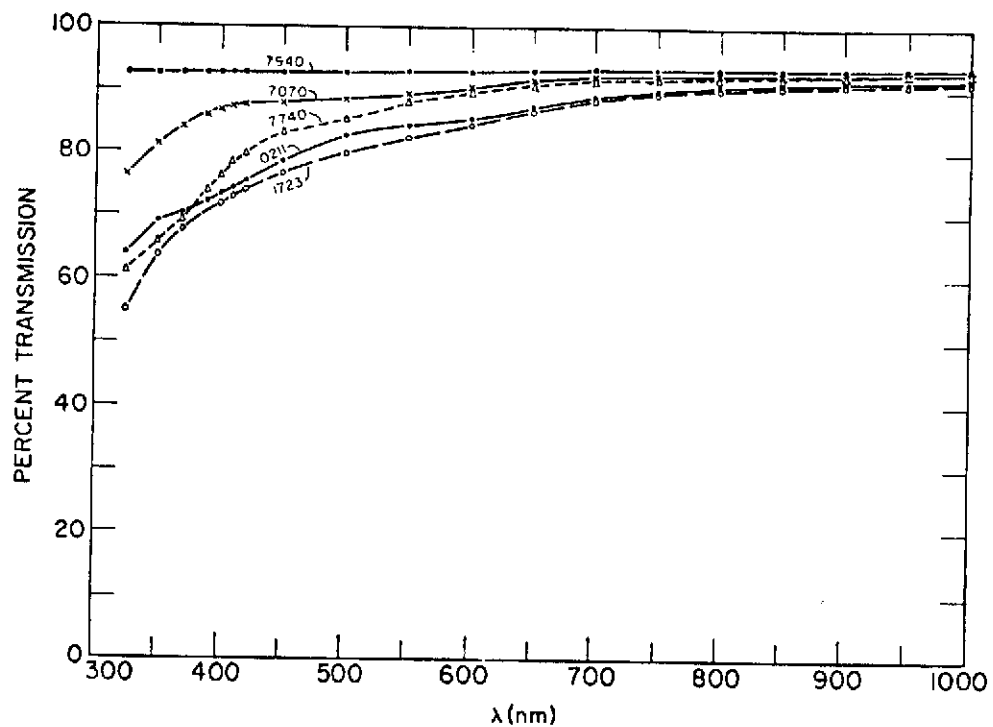


Figure 3-36. Transmission of 150  $\mu\text{m}$  Slides After  $2.5 \times 10^{14}$  1 MeV Electrons/cm<sup>2</sup> (from Reference 32)

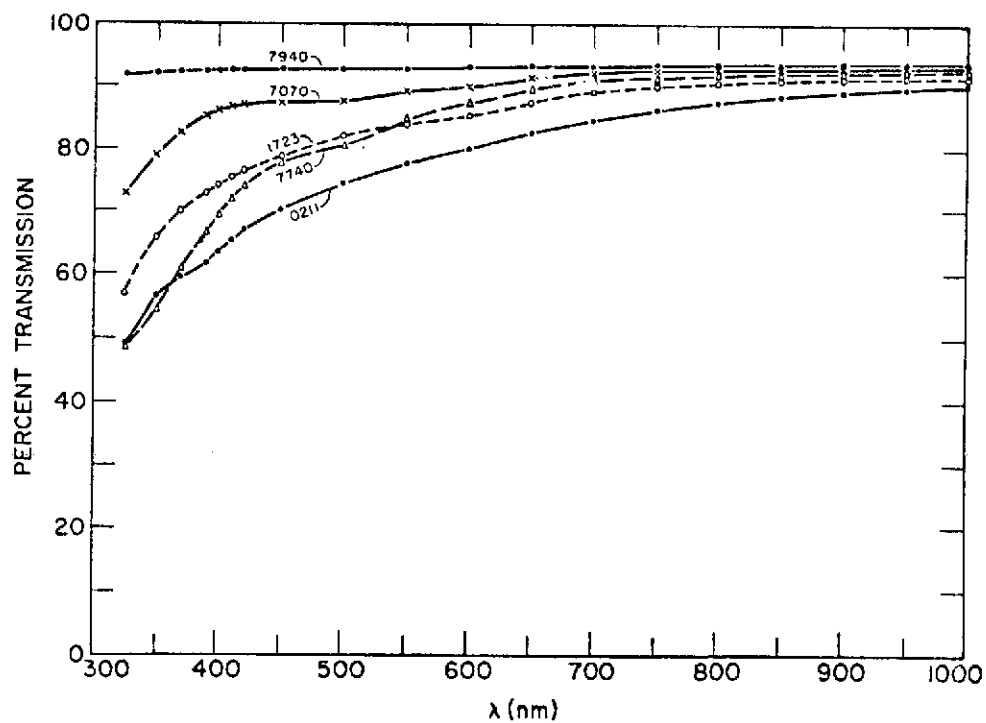


Figure 3-37. Transmission of 150  $\mu\text{m}$  Slides After  $5 \times 10^{15}$  1 MeV Electrons/cm<sup>2</sup> (from Reference 32)

Table 3-16. 1-MeV Proton Irradiation Data  
(from Reference 32)

Cell	Integral Cover Material	Nominal Thickness (mils)	Initial Performance			Change After $10^{14}$ 1 MeV p/cm <sup>2</sup>		
			I <sub>sc</sub> mA	I <sub>0.43</sub> mA	V <sub>oc</sub> V	I <sub>sc</sub> mA	I <sub>0.43</sub> mA	V <sub>oc</sub> V
FS155	7070	2	135	128	0.552	0	0	0
478-21	7070	2	139	133	0.560	0	0	0
478-24	7070	2	138	134	0.563	0	0	+0.005
478-22	7070	2	137	131	0.560	-1	+1	+0.005
D4	7070	2	137	133	0.562	+3	+2	0
G45	7070	2	140	135	0.562	0	0	0
G16	7070	6	139	132	0.547	+3	-2	-0.010
G27	7070	6	137	132	0.561	+3	+4	+0.005
B-12*	7940	2	140	134	0.556	-32*	-134*	-0.240
TA90	7940	1	144	138	0.570	-1	0	0
P29	7740	2	139	135	0.566	+3	0	-0.020
P9	7740	2	143	134	0.538	+1	0	0
CD10	CeO <sub>2</sub> doped 0211	2	132	127	0.552	+2	+3	+0.010
CD30	CeO <sub>2</sub> doped 0211	2	138	132	0.560	0	+1	+0.005
CD31	CeO <sub>2</sub> doped 7740	2	140	132	0.560	+1	0	-0.010
CD33	CeO <sub>2</sub> doped 7740	2	142	136	0.556	0	+1	+0.010
ET13	None	-	137	124	0.562	-101	-124	-0.200

\*Solderless contact bar mask lost during test with resulting irradiation of bar area.

Additional environmental testing, which included thermal cycling, U. V. radiation, and temperature-humidity storage, has indicated good performance with HVIBS integral covers.

Based on these results, it was concluded that Corning type 7070 glass represented an optimum choice for relatively thick, low stress integral covers which exhibit excellent radiation resistance.

Electron Beam Evaporation. Work in the area of electron beam evaporation of integral coverglass on silicon solar cells has been performed by Heliotek, Division of Textron, Inc., under contract to the Air Force Materials Laboratory, Wright-Patterson Air Force Base and is reported in References 29 and 33. The system which evolved from this investigation consists of a  $\text{TiO}_x$  cell anti-reflective coating and an electron beam evaporated integral coverglass. The parent glass was Corning type 1720, but the deposited glass was found to consist principally of  $\text{SiO}_2$  (96 percent) with the remainder being alkali oxides. Stress levels in the deposited films can be kept to levels below  $4 \times 10^8$  dynes/cm<sup>2</sup> ( $4 \times 10^7$  N/m<sup>2</sup>). Under these stress conditions, a 300  $\mu\text{m}$  thick, 2 x 2 cm cell with a 50  $\mu\text{m}$  thick integral cover will exhibit a radius of curvature of approximately 157 cm. Integral cover samples were subjected to both 1-Mev electron and ultra-violet irradiation. A coverglass darkening of 2 to 3 percent was observed following a total 1-MeV electron fluence of  $10^{15}$  electrons/cm<sup>2</sup>. Ultraviolet exposure of 120 equivalent sun hours produced a coverglass transmission degradation of 1.4 percent.

Radio Frequency Sputtering. Work in the area of radio frequency (RF) sputtering of integral solar cell coverglass is presently being performed by the Electrical Research Association (ERA), Leatherhead, Surrey, England, under sponsorship from the European Space Research Organization (ESTEC, Noordwijk). This deposition method consists of the sputtering of glass targets in an argon atmosphere with RF power of several kilowatts at a frequency of approximately 13.6 MHz and a peak-to-peak potential of two to three kilovolts. The solar cell substrate is maintained at approximately 25<sup>o</sup>C during deposition. The experimental equipment at ERA is capable of coating 70 2 x 2 cm cells with Corning 7070 glass at a sustained rate of 2.6  $\mu\text{m}$  per hour, with  $\pm$  10 percent thickness uniformity. Prototype production equipment,



with a capacity of 316 2 x 2 cm cells per loading, has been designed and built for operational use in the fall of 1972 (Reference 28).

During the course of this program at the ERA, RF sputtered covers of borosilicate glasses, notably Corning 7740 and 7070, and Schott 8330, as well as Corning 7940 fused silica have been investigated. The borosilicate glass films were found to have significantly lower stress than fused silica. In particular, the type 7070 glass showed very low values of stress as revealed in Figure 3-38. Films of 7070 glass have been deposited with an intrinsic stress below  $3 \times 10^7$  dynes/cm<sup>2</sup> ( $3 \times 10^6$  N/m<sup>2</sup>) which is the lower limit of the ERA measurement technique. Unsupported films of 7070 glass remain essentially flat. With this glass, it is possible to cover 125  $\mu$ m thick cells with scarcely any bowing of the coated cell. In addition, the 7070 glass shows superior optical and radiation resistance properties.

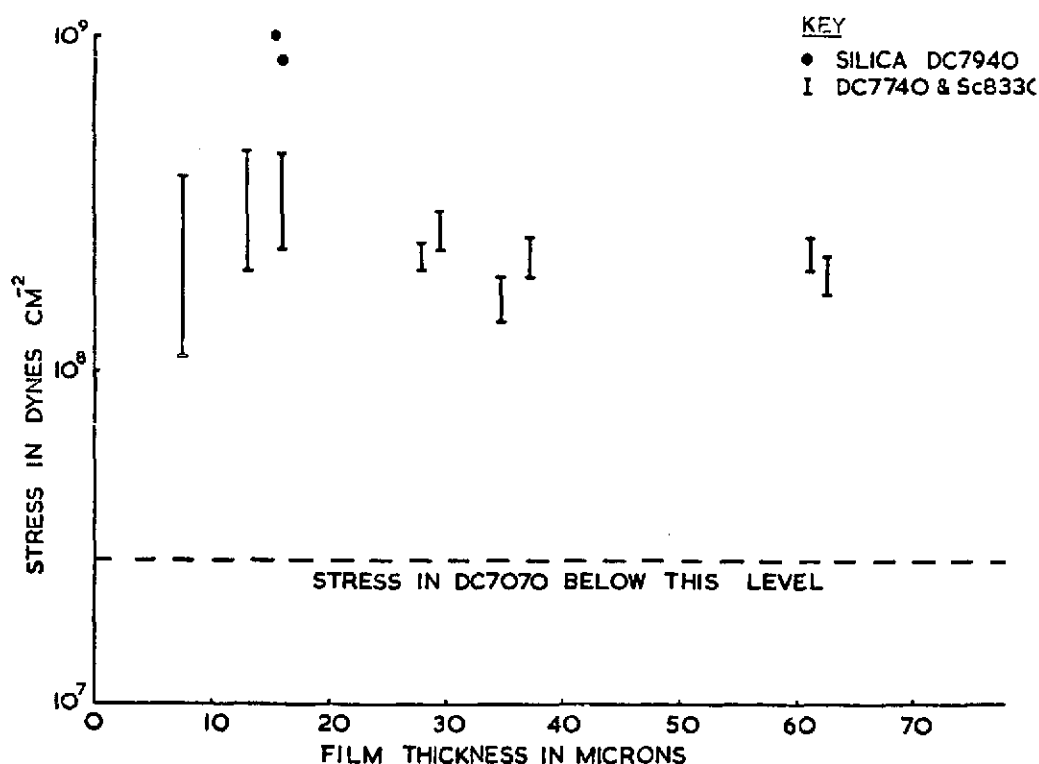


Figure 3-38. Stress in the Integral Cover as a Function of Film Thickness for Silica and Two Borosilicate Glasses (from Reference 28)

Thermal cycling tests of integrally covered solar cells have shown that  $\text{TiO}_x$  cell anti-reflective coating gives excellent resistance to delamination.

The optical transmission of 7070 glass layers of 100 to 150  $\mu\text{m}$  thickness has been measured at 99 percent between 400 and 1200 nm, falling to 95 percent at 350 nm. These transmission properties are of material without added ingredients such as cerium oxide. The addition of such modifiers, for the purpose of improving radiation resistance, will alter transmission properties.

The irradiation of 20  $\mu\text{m}$  thick films of 7070 glass (without cerium oxide) with a 1-MeV electron fluence of  $10^{15}$  electrons/ $\text{cm}^2$  has produced negligible change in transmission when compared with unirradiated control samples. This same fluence caused a 1 percent loss in transmission between 400 and 1200 nm for 50  $\mu\text{m}$  thick specimens of the same glass. The addition of cerium oxide is known to improve the radiation resistance at the expense of some loss in unirradiated transmission. Targets of 7070 glass with cerium oxide additive have been made by sintering mixed powders. Work is proceeding to determine if this additive is beneficial, and if so, to determine the optimum content.

Fusion. The fusion of fine powdered glass directly into solar cells is the subject of investigations by the General Electric Company, Space Sciences Laboratory, under contract to the Air Force Aero Propulsion Laboratory, Wright-Patterson Air Force Base (Reference 34). The objective of this program is the development of an economical, stress-free integral cover for application to large area hardened solar arrays. To date, the major effort on this program has been devoted to the formulation of glass compositions with the required fusion temperature of 500<sup>0</sup>C or less. In addition, the glasses must have the chemical, mechanical, optical and radiation resistant properties required to meet the program goals. As a test of radiation resistance, annealed glass disks of the various compositions are subjected to radiation from a  $\text{Sr}^{90}$  source. Before and after transmittance measurements are compared to determine relative radiation resistance.

Work on this contract has not, as yet, progressed to the point of producing optimized integral covers on silicon solar cells.

3.3.1.2.2.2 FEP-Teflon Covers. The application of Fluorinated Ethylene Propylene (FEP) as a cover for silicon solar cells and as a method for encapsulating cells into flexible modules is reported in References 35 through 38. Two types of FEP have been investigated: FEP-A which is untreated and FEP-C which is treated to promote cementability on one or both sides. When applied to an active surface of solar cells by a direct heat-sealing technique, this film provides protection from penetrating radiation and increases the infrared emittance. FEP-A material, which is pretreated with an adhesion promotor, had demonstrated higher bond strength and improved resistance to exposure to high temperature-humidity conditions when compared to FEP-C material. FEP covered SiO coated cells have experienced delaminations of the cover when irradiated with 1-MeV electrons at a fluence of  $10^{15}$  electrons/cm<sup>2</sup>. FEP covered Si<sub>3</sub>N<sub>4</sub> coated cells were able to withstand  $10^{16}$  electrons/cm<sup>2</sup> without delamination. Limited data indicates little or no differences between the two types of FEP under electron irradiation.

FEP-C (125  $\mu$ m thick) covered solar cells along with bare cells were subjected to 2 keV protons in a vacuum of  $7.9 \times 10^{-9}$  N/m<sup>2</sup> at an average dose rate of  $1.3 \times 10^{12}$  p/cm<sup>2</sup>-sec. Total exposures of  $1 \times 10^{13}$ ,  $1 \times 10^{15}$ ,  $1 \times 10^{17}$ , and  $2 \times 10^{17}$  p/cm<sup>2</sup> were performed. Little effect was noted on the open-circuit voltage for the FEP-covered cells. The degradation in cell short-circuit current is shown in Figure 3-39. Note that the range of 2 keV protons in FEP Teflon is approximately 2.6  $\mu$ m.

Measurements on FEP-C covered cells indicate that a decrease of about 3 percent on short-circuit current can be expected after exposure to 3600 equivalent sun hours under UV radiation. With FEP-A material, the reduction in short-circuit current will be about one-half this value.

The effects of long term exposure to high humidity and temperature were evaluated by exposing 20 FEP-C covered cells to 40°C and 95 percent relative humidity. After 160 hours of exposure, some delamination on all cells was observed.

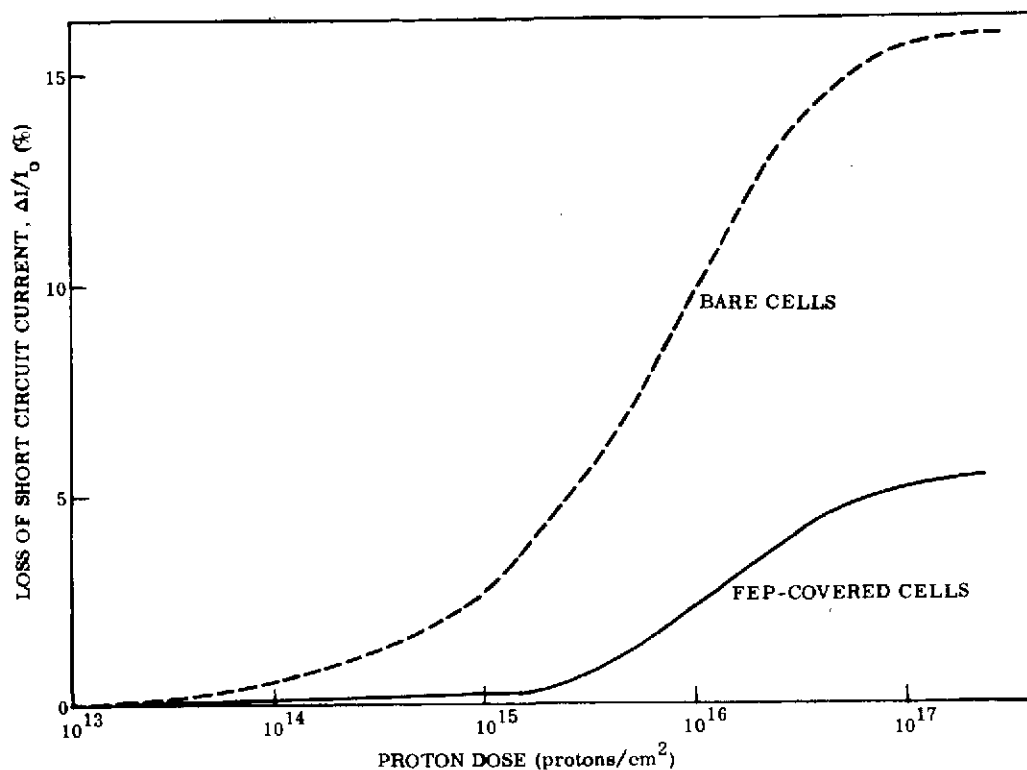
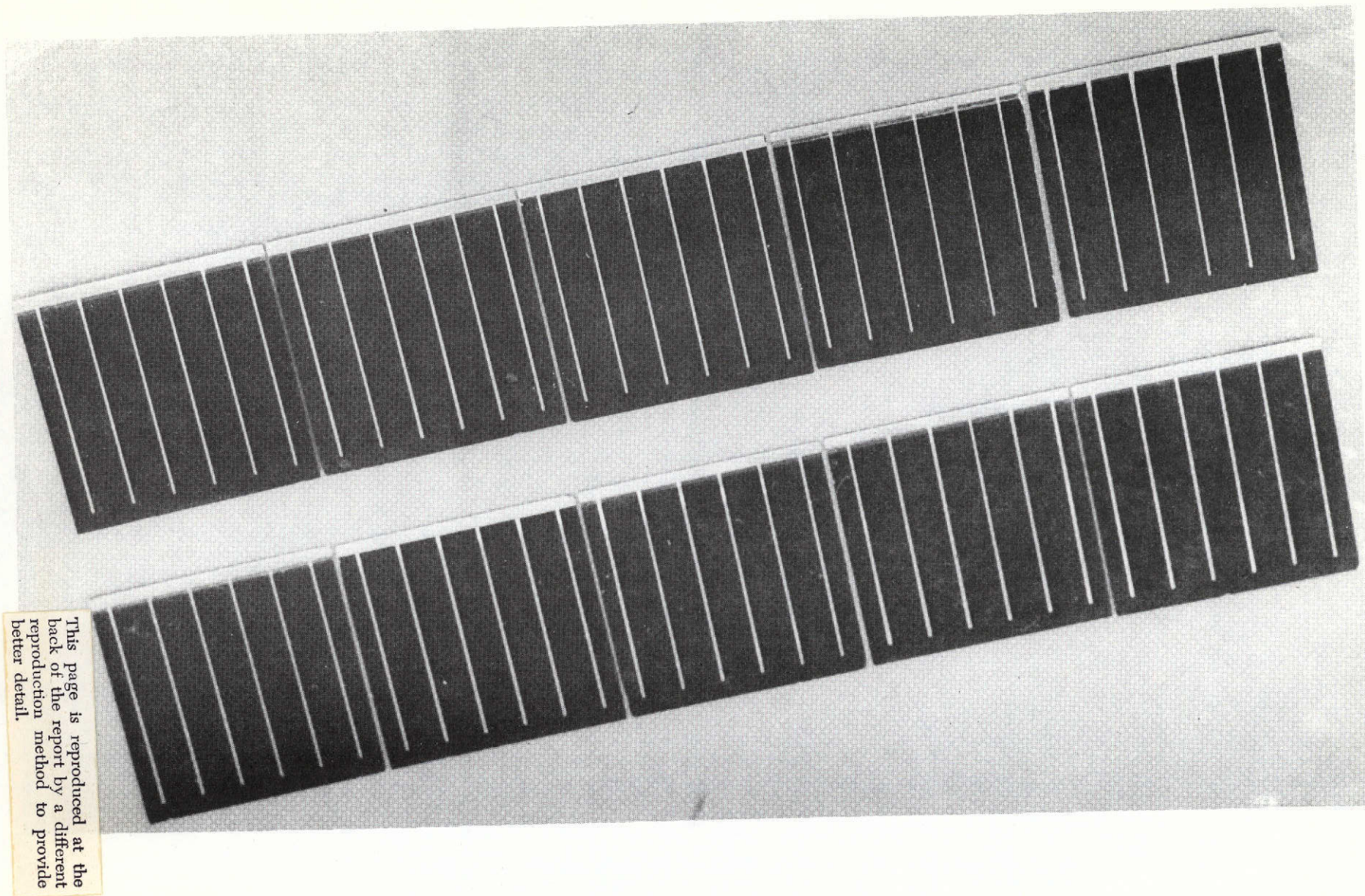


Figure 3-39. Effect of 2 keV Protons on Solar Cell Short-Circuit Current (from Reference 38)

Two kinds of multicell modules were constructed using the FEP cover technique. The first of these consisted of a 15 cell module (5 parallel x 3 series) which was made by first covering three 5 cell wide strings with 125  $\mu\text{m}$  thick FEP-C film (see Figure 3-40). The substrate was fabricated by laminating a 50  $\mu\text{m}$  thick copper foil to a 25  $\mu\text{m}$  Kapton-H film with 25  $\mu\text{m}$  FEP film used as the adhesive. The foil was then photoetched to form interconnects, soldering points for the back contacts and soldering tabs for the front contacts (see Figure 3-41). Next, another 25  $\mu\text{m}$  layer of Kapton-H film prepunched to expose soldering points and tabs, was laminated on top using 25  $\mu\text{m}$  FEP as the adhesive. The P contact soldering points and tabs were then coated with Sn62 solder. This formed the flexible substrate with integral interconnects. The five cell strings with flux-treated back surfaces were positioned on the substrate and the P contacts induction soldered. The N contact tabs were then bent in place and connected using solder preforms and reflow solder techniques. The finished 15 cell module is shown in Figure 3-42. A thermal vacuum cycling test of a module of this construction resulted in the fracture of 15 of the 15 cells when





This page is reproduced at the back of the report by a different reproduction method to provide better detail.

Figure 3-40. FEP Covered Submodules  
(from Reference 38)

the module temperature reached  $-40^{\circ}\text{C}$ . Subsequent examination revealed simple cell fracture in six cells without delamination. The remaining eight damaged cells have suffered a cleavage within the silicon. These failures were attributed to the mismatch of thermal expansion coefficients between the FEP on the front and the solder on the rear face of the cells.

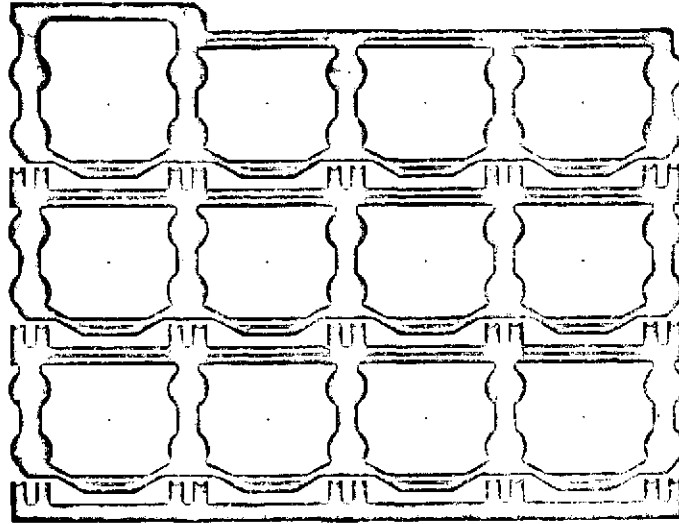


Figure 3-41. Circuit Interconnect Pattern  
(from Reference 38)

A second configuration module was fabricated using  $125\text{ }\mu\text{m}$  FEP-A as a cover and  $50\text{ }\mu\text{m}$  FEP-C20 (treated on both sides) as an adhesive to bond the cells to a  $25\text{ }\mu\text{m}$  Kapton-H film substrate. Thermocompression bonding of  $50\text{ }\mu\text{m}$  thick silver mesh was the interconnect method used. Flexible modules prepared in this manner are unaffected by thermal shock, and thermal-vacuum cycling.

Optical properties of FEP covered cells were measured with the following results (Reference 35);

$$\text{Solar absorptance } (\alpha_s) = 0.84$$

$$\text{Total hemispherical emittance } (\epsilon_h) = 0.91$$



This page is reproduced at the back of the report by a different reproduction method to provide better detail.

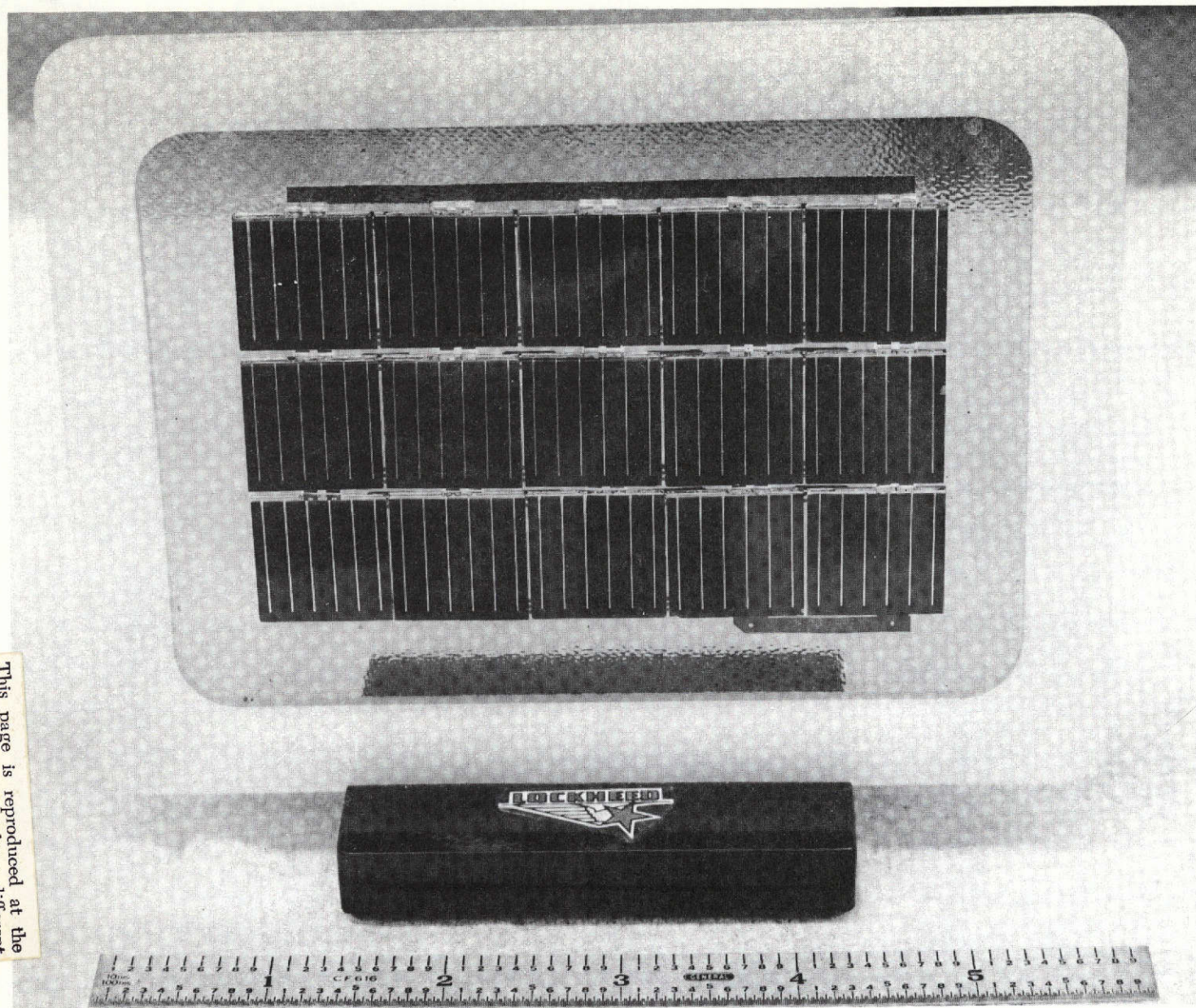


Figure 3-42. FEP Covered Module  
(from Reference 38)

### 3.3.1.2.3 Substrates

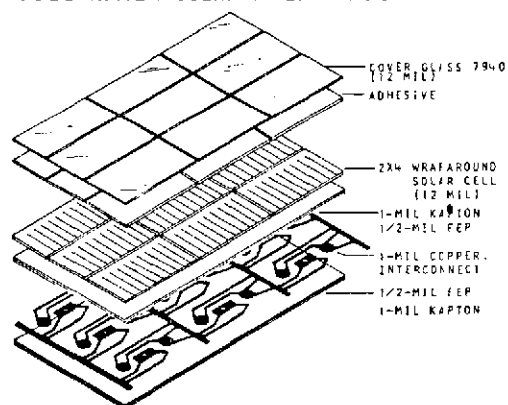
The use of bottom wraparound contact solar cells enables the use of a flat interconnector system which can be made integral with the supporting substrate. Two such substrate systems have been implemented in flexible solar array developments. The details of the Lockheed space station solar array substrate are shown in Figure 3-43. The construction of this substrate is similar to Lockheed FEP development substrate which was described in Section 3.3.1.2.2. The copper interconnection system is sandwiched between layers of Kapton-H film with FEP used as the adhesive. The solar cells are soldered to the interconnectors through holes in the upper layer of Kapton/FEP. These solder joints are the only means of attachment of the cells to the substrate. Table 3-17 gives a mass breakdown for the Lockheed space station substrate/interconnect system. This mass tabulation does not include the bus strip distribution system or the hinge joint reinforcement and locking bars between modules. The mass of the copper interconnectors was calculated based on a copper mass of  $0.305 \text{ kg/m}^2$  ( $1 \text{ oz/ft}^2$ ) and a coverage of 33 percent of the module area which was computed from a drawing of the interconnector pattern. The resulting mass of  $0.100 \text{ kg/m}^2$  of module area does not agree with the value published in Reference 5. In Section 3.2.9 of this reference, the mass of the copper interconnectors is given as  $0.0472 \text{ kg}$  ( $0.104 \text{ lb}$ ) for a module which occupies  $0.966 \text{ m}^2$  ( $10.4 \text{ ft}^2$ ) for a resultant mass-to-area ratio of  $0.049 \text{ kg/m}^2$ . A copper foil of  $0.152 \text{ kg/m}^2$  ( $1/2 \text{ oz/ft}^2$ ) would be required to achieve this mass for the interconnector pattern specified. The solder mass of  $0.031 \text{ kg/m}^2$  was calculated based on a solder coverage of 9.5 percent of the module area with an average thickness of  $37 \mu\text{m}$ .

The interconnect/substrate configuration used on the RAE flat-pack solar array is shown in Figure 3-44. This approach also consists of a cementless, soldered attachment of the solar cells to the integral substrate. The interconnectors are  $25 \mu\text{m}$  thick silver-plated molybdenum rings which are soldered to the cells through punched holes in the  $50 \mu\text{m}$  thick Kapton-H film substrate. The Kapton substrate is cut-out to reduce weight and to provide the solar cells with a direct radiating surface for more effective heat rejection. These cutout windows are triangular shaped in the current design. The black chromium emissive finish on the solar cell backs was found to provide insufficient protection from low energy

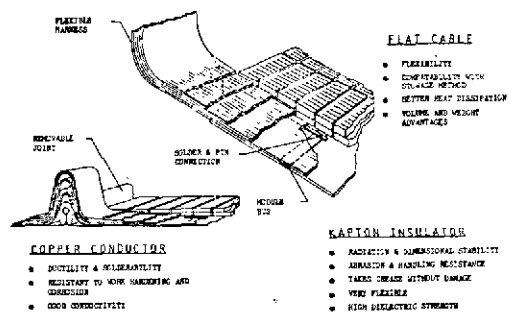


NOT REPRODUCIBLE

## SUBSTRATE ASSEMBLY EXPLODED VIEW



## FLEXIBLE FEEDER HARNESS AND CONNECTION



## HINGE JOINT

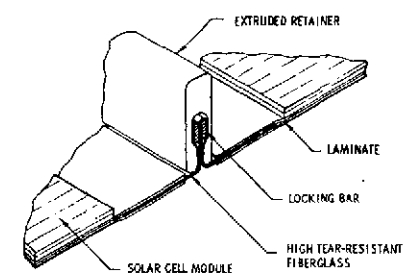


Figure 3-43. Details of Lockheed Space Station Solar Array Substrates  
(from Reference 39)

protons. To remedy this situation, the solar cell backs were coated with a 50  $\mu\text{m}$  thick layer of Midland Silicones Silastoseal B adhesive. Table 3-18 gives the mass breakdown for the REA substrate/interconnect system.

Table 3-17. Mass of Lockheed Space Station  
Solar Array Substrate

Item	Mass ( $\text{kg}/\text{m}^2$ of Module Area)
Kapton-H film (50 $\mu\text{m}$ total thickness)	0.071
FEP-Teflon (25 $\mu\text{m}$ total thickness)	0.054
Copper Interconnectors (1)	0.100
Solder	<u>0.031</u>
Total	0.256

(1) 0.305  $\text{kg}/\text{m}^2$  (1 oz/ $\text{ft}^2$ ) copper which covers 33% of the module area

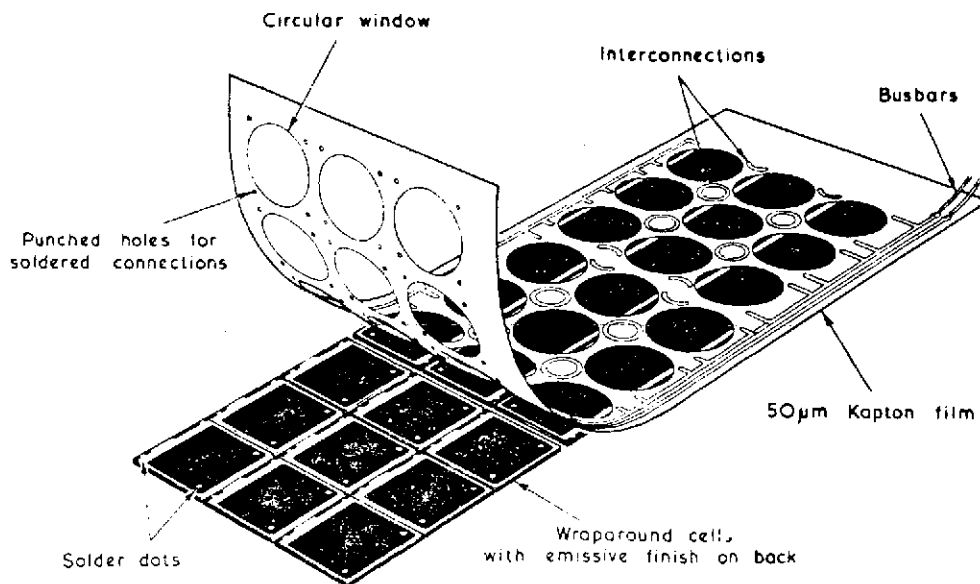


Figure 3-44. RAE Flat-pack Solar Array Substrate Configuration  
(from Reference 16)

Table 3-18. Mass of RAE Flat-Pack  
Solar Array Substrate

Item	Mass (kg/m <sup>2</sup> of Substrate Area)
Kapton-H film (perforated, 50 $\mu$ m thick) <sup>(1)</sup>	0.037
Interconnectors (Ag Plated Mo) <sup>(1)</sup>	0.022
Solder <sup>(1)</sup>	0.046
Silastoseal B Adhesive <sup>(2)</sup>	<u>0.022</u>
Total	0.127

(1) Based on data from Reference 16.

(2) For low energy proton protection, assumes an average thickness of 50  $\mu$ m covering 50% of the back of every cell, with 2060 cells per m<sup>2</sup> of substrate area.

#### 3.3.1.2.4 Interconnector Joining

The use of a welded connection between the solar cell contacts and the interconnector is a potentially attractive choice for use on the 110 watt/kg solar array system. The purpose of this section is to describe the differences and relative merits of welded vs. soldered interconnectors and to summarize the present state-of-the-art in welded solar cell interconnectors. The choice of interconnector joining method for this feasibility study is strongly influenced by the thermal shock environment. As specified in Appendix A, this shock is between the extremes of -190 and +140<sup>o</sup>C for a total of 1000 complete cooling and heating cycles.

3.3.1.2.4.1 Comparison of Welded and Soldered Interconnections. Table 3-19 summarizes the relative advantages and disadvantages of soldered and welded solar cell interconnections. Within the U. S. soldered solar cell interconnections have been exclusively used on flight solar arrays with satisfactory performance under most conditions of temperature and cycle life imposed by earth orbiting missions. The requirement for low temperature (< -120<sup>o</sup>C) and/or high temperature (> 120<sup>o</sup>C) operation raises questions concerning the applicability

Table 3-19. Comparison of Soldered and Welded Solar Cell Interconnections

METHOD	ADVANTAGES	DISADVANTAGES
Soldering	<ul style="list-style-type: none"> <li>Acceptable joints with a wide range of process parameters</li> <li>Repair easily performed to replace damaged cells</li> <li>Joint inspection criteria can be based on solder fillets</li> </ul>	<ul style="list-style-type: none"> <li>Solder joints have low peel and creep strength at high temperatures</li> <li>Solder joints may melt under "hot-spot" failure mode conditions such as partial shadowing or open circuit failures</li> <li>Solder may cause silicon flake-out at low temperatures</li> <li>Solder joint exhibits highest stresses and is the weakest link under thermal cycling</li> </ul>
Welding	<ul style="list-style-type: none"> <li>Lower weight due to the elimination of solder</li> <li>Modules can operate at higher temperatures without failures due to low peel or creep strength</li> <li>Interconnector material can be selected for a close match of the coefficient of thermal expansion to that of silicon, resulting in reduced stresses at low temperatures</li> </ul>	<ul style="list-style-type: none"> <li>Joint repair is difficult</li> <li>Visually inspection can not insure a good weld</li> <li>Process parameters must be controlled within a narrow range</li> </ul>

of the soldered interconnection. Thermal cycling to a low temperature extreme causes high stresses in the solder which results in cracks which may propagate into the silicon. The number of such solder cracks increases with decreasing low temperature extreme as shown in Figure 3-45. The stresses in the solder are greater for interconnector materials which have higher coefficients of thermal expansion than silicon and are also greater for thicker interconnectors of the same material.

At the high temperature extreme, the solder points have low contact strength and are subject to creep under sustained stress. Figure 3-46 shows the pull test tab configuration used to obtain the contact strength results shown in Figure 3-47. Figure 3-48 shows the time required for solder joint rupture versus the applied stress for two solder alloys at various temperatures.

The weight savings associated with the elimination of solder will typically amount to about 15 mg/cell or about 3.4 kg for an array of the size required for this study.

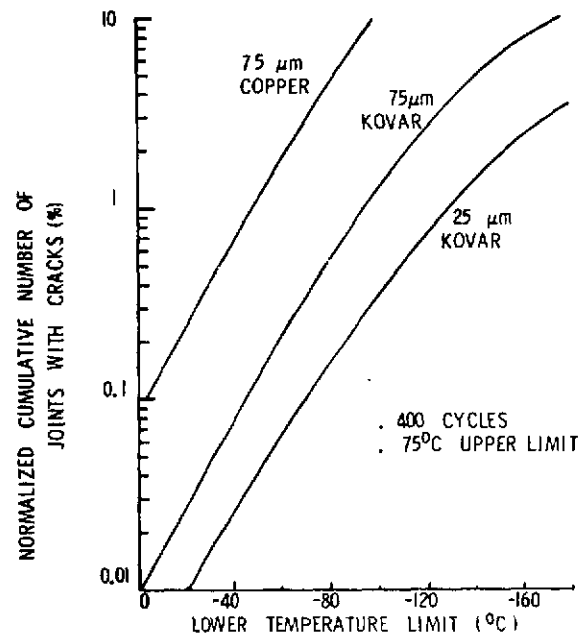


Figure 3-45. Normalized Cumulative Number of Solder Joints Showing Cracks after 400 Cycles from 75°C to the Indicated Lower Temperature Limit (from Reference 40)

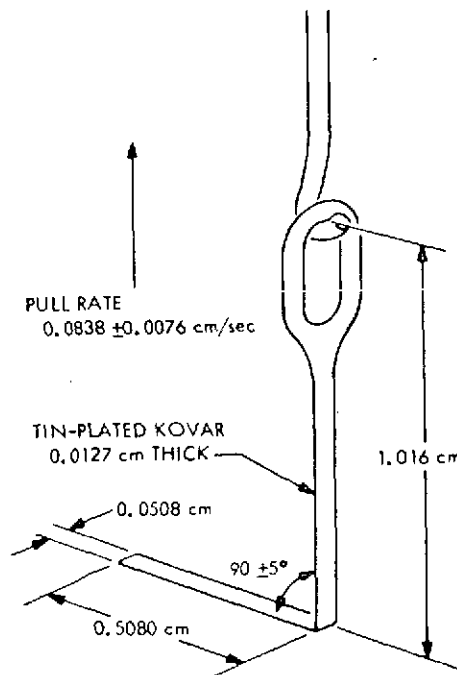


Figure 3-46. Contact Pull Strength Tab Configuration (from Reference 41)

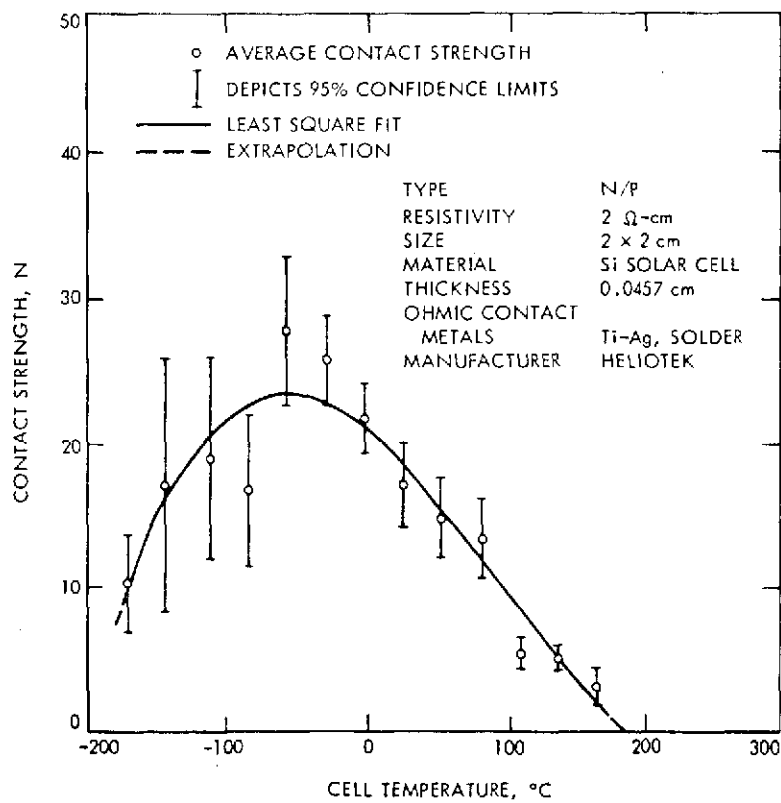


Figure 3-47. Contact Strength of Solar Cell Solder Joint (from Reference 41)

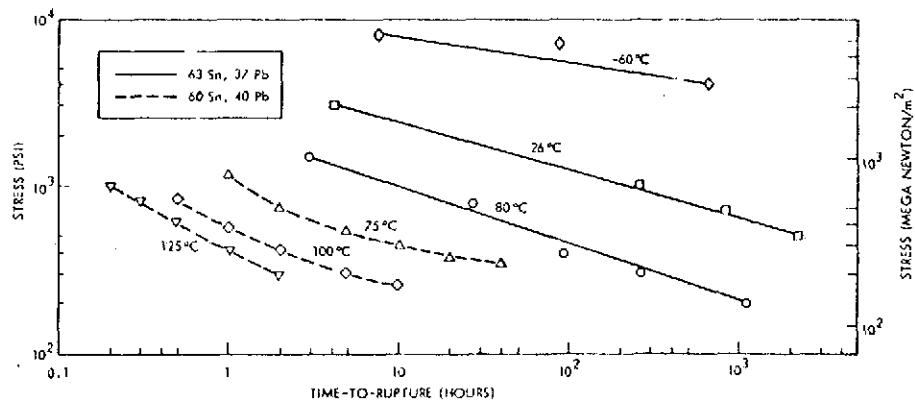


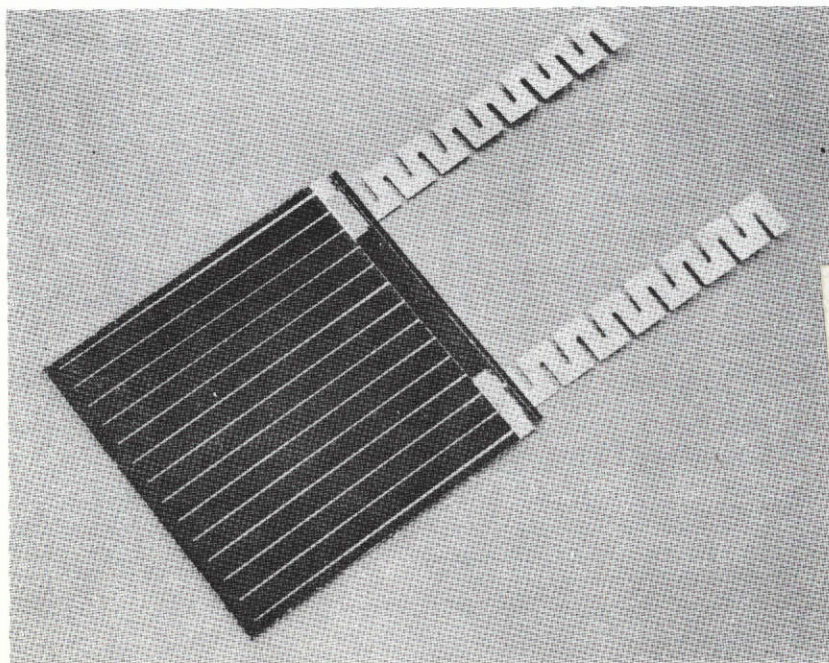
Figure 3-48. Time to Solder Joint Rupture Versus Applied Stress for Two Solder Alloys at Various Temperatures (from Reference 40)

3.3.1.2.4.2 Welded Interconnector Technology. Experience with welded solar cell interconnectors is not as extensive as with soldered joints and a large portion of the experience is European based. Four welding methods have been successfully used to join interconnectors to cell contacts. These are: (a) ultrasonic welding, (b) resistance welding (parallel gap), (c) laser welding and (d) thermal diffusion/thermal compression welding.

a. Ultrasonic Welding

Ultrasonic welding is a highly attractive approach for solar cell interconnector joining because it does not produce high temperature beyond a very shallow depth from the weld interface. The ultrasonic welding of aluminum interconnectors to aluminum contacted solar cells has been performed by TRW (Reference 42) and by Hughes (Reference 43).

The TRW interconnectors were cut from notched 1100-0 aluminum strip material which is 75  $\mu\text{m}$  thick by 3 mm wide. Welding was performed using the following welding equipment: (1) weld head, Unitek Model 1-144-01; (2) Unitek Power Supply Model 2-130-D1; and (3) Transducer Sonobond Model W-260-A. Figure 3-49 shows the two interconnector strips welded to



This page is reproduced at the back of the report by a different reproduction method to provide better detail.

Figure 3-49. TRW Welded Aluminum Interconnector Configuration (From Reference 42)

the top contacts. As shown in the figure, coverglass covers the entire top surface of the cell including the bar contact and weld joints. In addition, there is a Kapton strip which is bonded between the coverglass and the cell to function as a shield over the aluminum interconnector in the gap between cells.

The aluminum interconnector has a much higher coefficient of thermal expansion than the silicon with the result that high stresses are created in both the silicon and the aluminum at the weld joints during thermal cycling. Figure 3-50 shows the calculated stresses in the aluminum at a temperature of  $-180^{\circ}\text{C}$  normal to the cell surface acting to pull the welded joint apart. Figure 3-51 shows the calculated number of cycles of failure for the weld joint as a function of temperature extremes.

Four panel segments of this welded construction (each panel segment consisting of two 20s x 2p modules) were subjected to five temperature cycles between  $-100^{\circ}\text{C}$  and  $+100^{\circ}\text{C}$  without evidence of performance degradation.

The Hughes aluminum interconnect/aluminum contact ultrasonic welding process was developed for use on the Air Force Hardened Solar Power System (HASPS). Figure 3-52 shows a module which was interconnected using this welding process. In addition to the aluminum-to-aluminum weld, Hughes has ultrasonically welded aluminum interconnectors to solderless Ti-Ag contacted solar cells (References 43 and 44). Each weld was accomplished in a few seconds at room temperature using a Sonoweld Model W-1040 TSL weld system with a specially designed tip. Pull strength data has shown these welds to be satisfactory and comparable to the all aluminum system. Because of the concern about the aluminum-silver galvanic couple, those welded cells were subjected to extreme humidity testing which consisted of 168 hours at  $85^{\circ}\text{C}$  and approximately 95 percent relative humidity. Post test examination revealed no visible discoloration or corrosion of the weld area or interconnect and electrical testing showed no measurable effect.



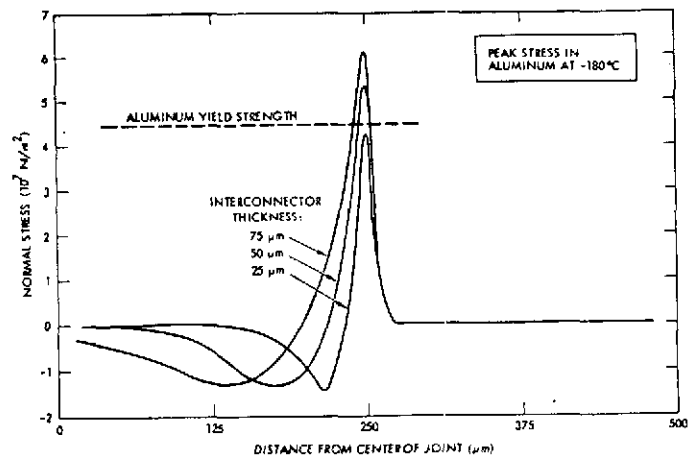


Figure 3-50. Thermal Stress in Welded Joints  
(From Reference 42)

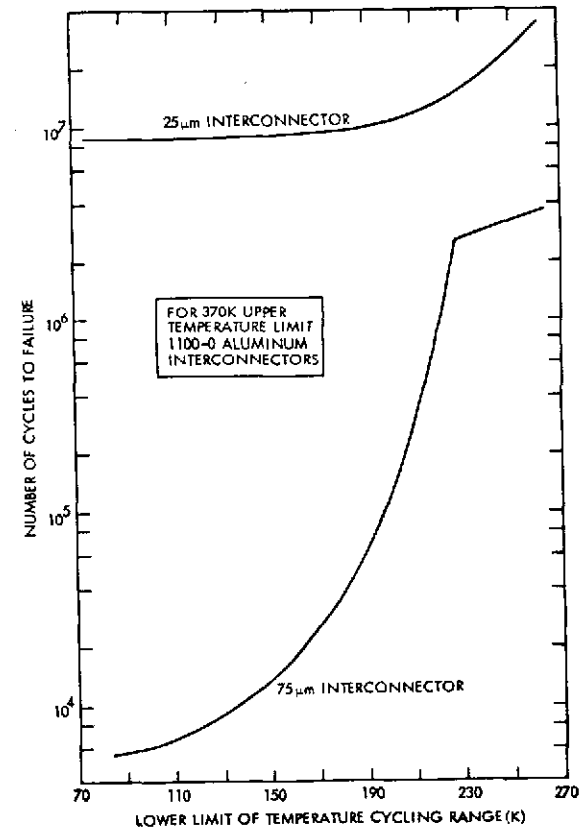


Figure 3-51. Cycles to Failure versus Temperature Range  
(From Reference 42)

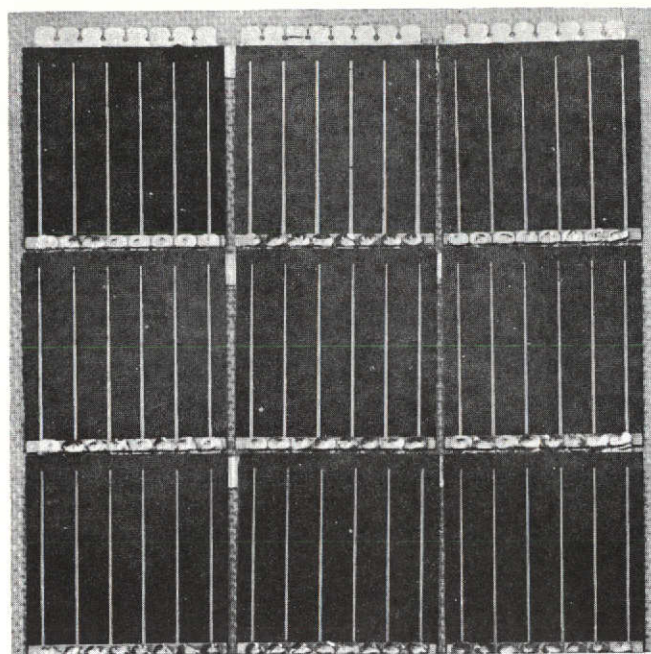


Figure 3-52. Hughes Aluminum Cell/Aluminum Interconnector Ultrasonically Welded Module (From Reference 43)

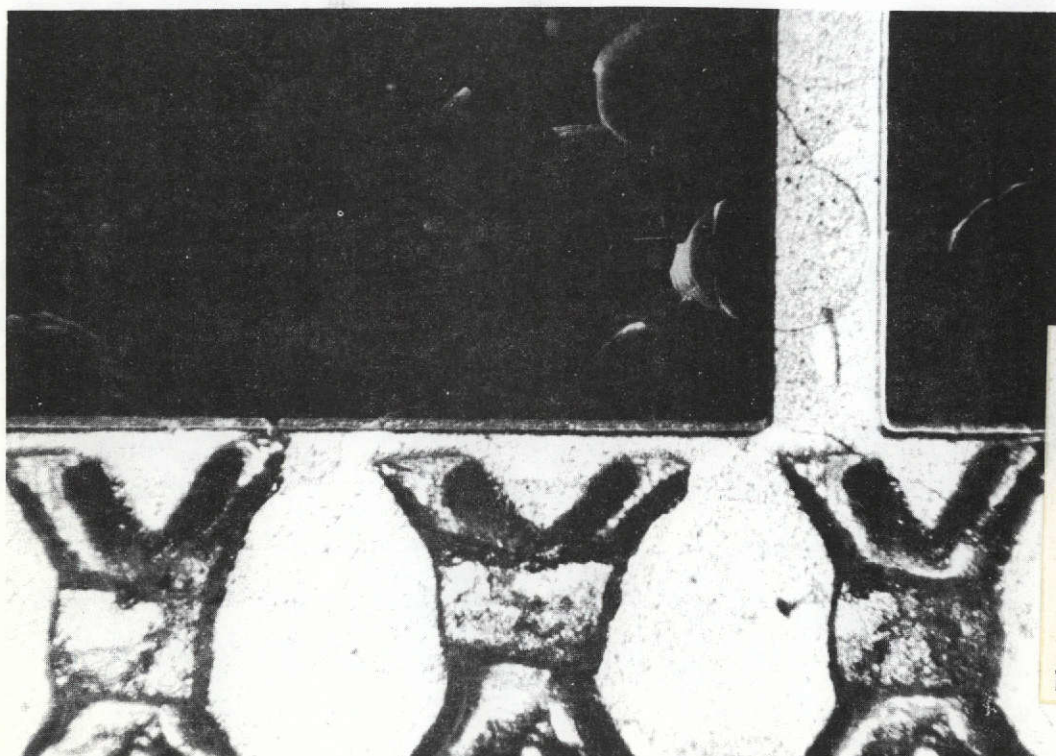
b. Resistance Welding (Parallel Gap)

Resistance welding uses the heat generated by an electric current passing through the work-piece in the space between two closely spaced electrodes which are pressed against the piece. The resulting melting in the current path can produce a weld between the interconnect material and the solar cell contact metallization.

Resistance welding of solar cell interconnectors has been performed by Messerschmitt-Bölkow-Blohm (MBB)/Siemens AG., AEG-Telefunken, and BAC/Turner. A summary of this technology which is supported by ESRO is contained in Reference 45. Resistance welding was selected over the other two methods because it gave more reproducible bonds than ultrasonic welding and did not require heating the whole solar cell to a high temperature as in thermal diffusion bonding. A potential problem with resistance welding is a degradation of the shallow junction during welding since a typical weld pulse releases 10 joules in 10 msec over an area of  $0.3 \text{ mm}^2$ . In the ESRO sponsored work, it was possible to determine a range of welding parameters when high bond strength could be obtained without junction damage.

Figure 3-53 shows a resistance welded connection between Ag expanded metal and a Ti (Pd) Ag solar cell front contact. Figure 3-54 shows a photomicrograph of the joint. These welds were obtained using a Hughes impulse welder model MCW-550 with a parallel gap bonding head VTA-66MV. Symmetrical molybdenum carbide electrodes with rectangular tips were used. This machine, shown in Figure 3-55, provides electronic control of the weld voltage and pulse duration.

AEG Telefunken has resistance welded silver plated molybdenum interconnectors to Ti (Pd) Ag cell contacts. The molybdenum thickness was 30  $\mu\text{m}$  and the optimum silver coating thickness was found to be 5  $\mu\text{m}$ . A pulse duration of 100 msec at a voltage of 0.65 v was found to give strong, reliable bonds with no obvious damage to the silicon. At the end of the optimization study, the shear strength of the welded tabs exceeded 30 N and in a series of successive welds, the shear strength did not vary more than 25 percent.



This page is reproduced at the back of the report by a different reproduction method to provide better detail.

Figure 3-53. Welded Ag Mesh Interconnector (From Reference 46)



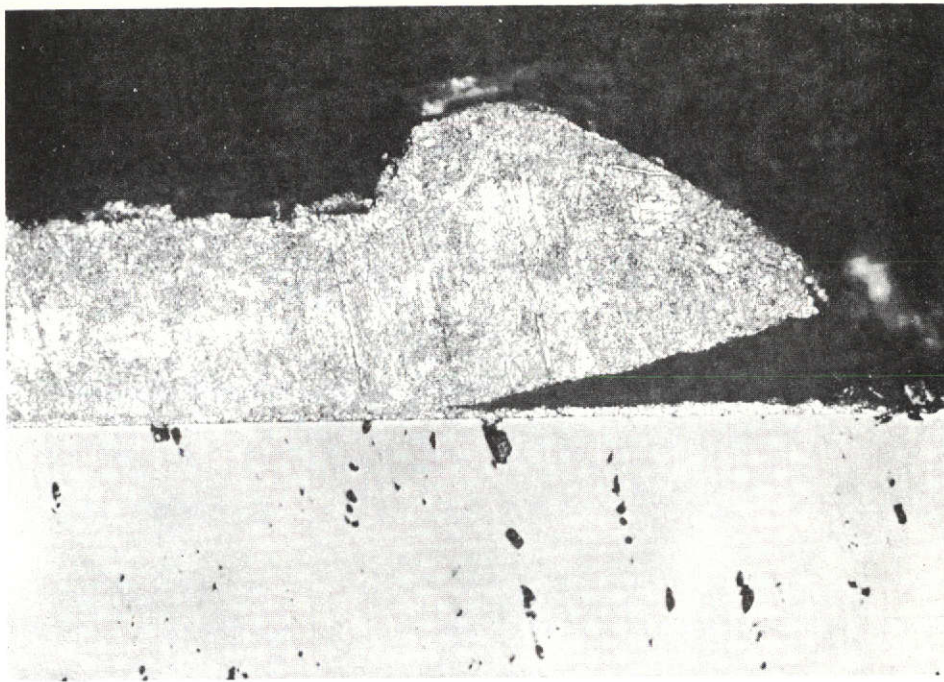


Figure 3-54. Photomicrograph of Welded Joint (From Reference 46)

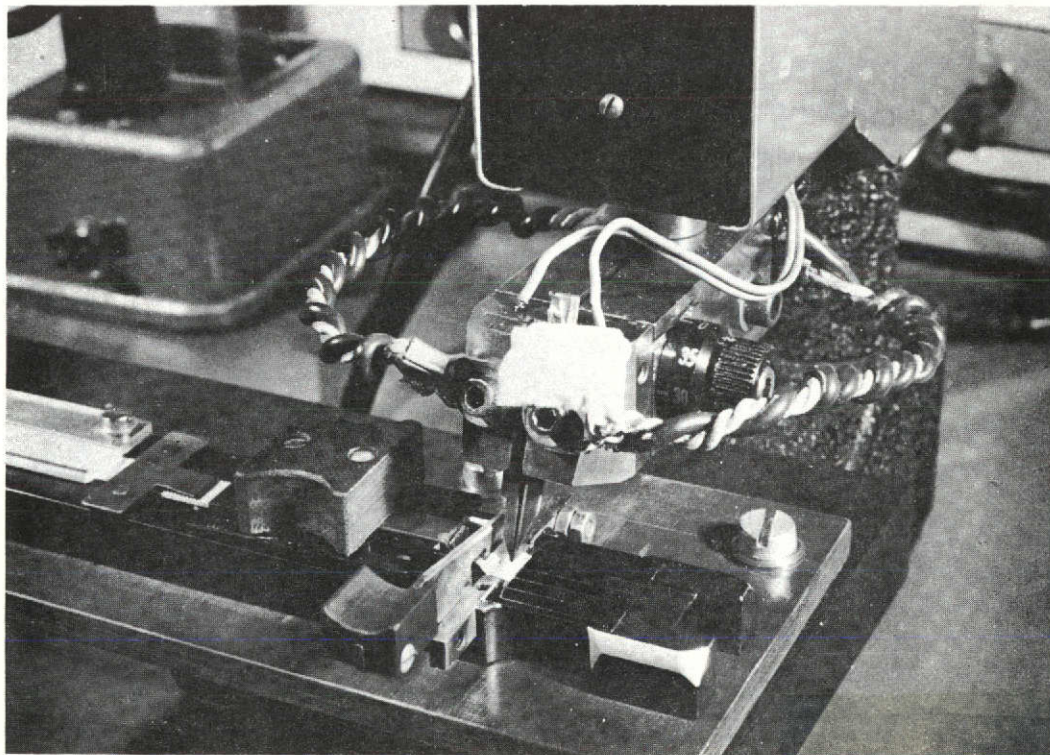


Figure 3-55. Hughes MCW-550 Impulse Welder (From Reference 46)

The solar cell interconnections for the Helios satellite are also resistance welded silver plated molybdenum. The nominal molybdenum thickness is 20  $\mu\text{m}$  with 5  $\mu\text{m}$  of silver plating on each side using a thin platinum interlayer for improved adherence (Reference 47). The selection of weld parameters was based on the mechanical strength of the weld and the electrical degradation of the cell. Figure 3-56 shows these two measures of performance as a function of welding voltage. Pull strength increases with increasing voltage.

The electrical degradation, which results from diffusion of contact material through the p-n junction, occurs at higher voltages. The final welding voltage range was selected so that the pull strength is sufficiently high with negligible electrical degradation. The silver metallization on the cell contact was chosen to be  $10 \pm 3 \mu\text{m}$  thick and the optimum weld pulse duration was found to be 200 msec. As a qualification test, the solar cell modules were subjected to a temperature cycling test which consisted of 4 days at  $-85^{\circ}\text{C}$  followed by 10 days at  $+200^{\circ}\text{C}$ . This cycle was repeated for a total test duration of 6 weeks.

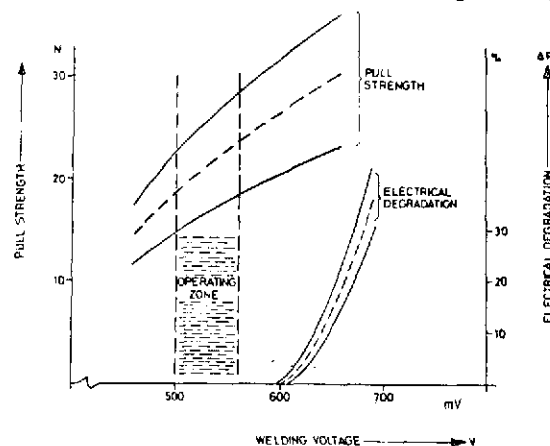


Figure 3-56. Mechanical Strength of Weld and Electrical Degradation versus Welding Voltages (From Reference 47)

A limited number of welds have been made on solar cells with plated Ni/Cu/Ni/Au contacts. Interconnectors of pure gold and gold plated molybdenum were used. The welds had a good shear strength and did not fail in thermal cycling and humidity storage (Reference 45).

### c. Laser Welding

The use of a pulsed ruby laser welder to join silver and silver plated molybdenum interconnectors to Ti-Ag solar cells has been implemented by Hughes as reported in Reference 43. The laser welder, shown in Figure 3-57 uses an optically focused beam of pulsed coherent radiation, such as red light (0.6943  $\mu\text{m}$ ). This method of welding offers flexibility



in spot size and shape control as well as control over the amount of heating at the cell junction. The molybdenum interconnector material was found to be well suited to laser welding with the best results achieved when the molybdenum was plated on only one side thereby letting the laser impinge on the exposed molybdenum. Micro-sections of laser welds revealed adequate welding, but voids were often present, possibly due to the fact that the pulse duration was too short to permit venting of absorbed or trapped gas at the weld interface.

#### d. Thermal Diffusion/Thermal Compression Welding

The Boeing Company has utilized this method to join expanded silver mesh interconnectors to solderless Ti-Ag contacted solar cells (Reference 48). The process has yielded acceptable joints with peel strengths as shown in Figure 3-58. Test samples have been subjected to 10 rapid temperature changes from  $+100$  to  $-190^{\circ}\text{C}$  with no apparent degradation in electrical or mechanical integrity.

The application of this process on a production basis is limited by the following drawbacks: (1) bonding must be accomplished in a vacuum, (2) the long time required to form the joints, and (3) the number of cells that can be interconnected at the same time is limited by the tooling and vacuum facility.

In Reference 43, Eakins reports that Hughes has experienced good results using the thermal compression method to weld silver interconnectors-to-silver contacted cells. Measurements of the dark reverse leakage current to a  $-10$  volt reverse bias have shown that no junction shunt resistance degradation occurred due to the welds.

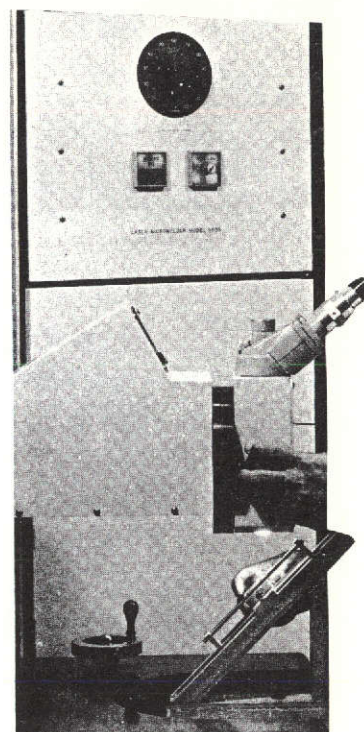


Figure 3-57. Laser Microwelder (From Reference 43)

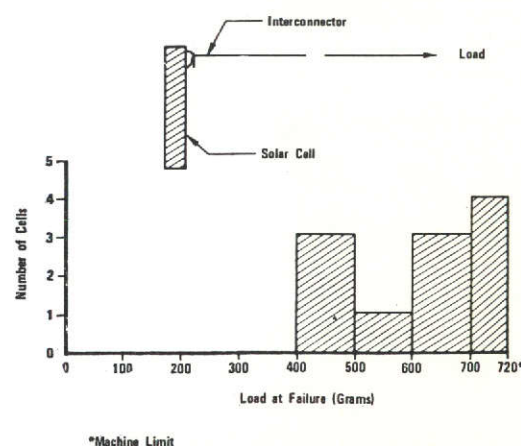


Figure 3-58. Results of Peel Tests on Thermal-Diffusion Bonded Solar Joints (From Reference 48)

### 3.3.1.2.5 Deployable Booms

An extensive summary of the deployable boom component technology as it might apply to large flexible solar arrays is contained in Section 4.1.2.2 of Reference 49. This reference lists 20 different types of deployable boom structures which have been developed. Many of these such as telescoping tubes and folding beams are obviously impractical for this application because of the large undeplied volume and relatively high weight. However, several of these boom types have shown the potentials needed for the deployable boom of a large flexible solar array. These boom categories are discussed below.

**3.3.1.2.5.1 Cylindrical Booms.** This category of deployable booms includes those with cross sections which are formed by one or more cylindrical shells. Stowage is generally by elastically flattening the element and reeling onto a spool or within a cassette. A typical example of this boom type is the STEM manufactured by SPAR Aerospace Products, Ltd. This boom, shown in Figure 3-59, is a circular, cylindrical tube formed from a single strip of material. The edges of the deployed strip overlap as shown in the figure. Booms of this type have been fabricated of beryllium copper, stainless steel, titanium and molybdenum. A variation of this basic type, which consists of an interlocked joint between the two edges of the deployed strip and thereby provides greater torsional stiffness, has been fabricated by several organizations.

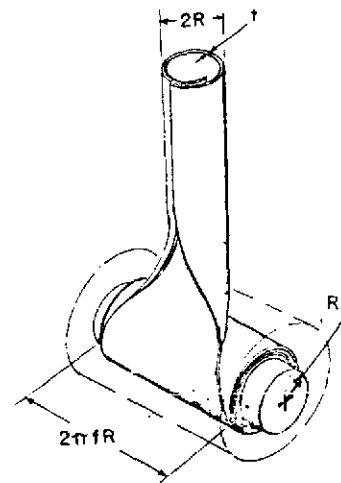


Figure 3-59. Schematic of STEM Boom  
(From Reference 50)

The BI-STEM, also manufactured by SPAR Aerospace Products, Ltd., is formed by nesting two circular, cylindrical strips as shown in Figure 3-60. These strips can be retracted and stowed on two separate reels, or on a single reel or cassette as shown in Figure 3-61. The BI-STEM has been used on the Hughes/AF roll-up solar array, the GE/JPL 30 watt/lb roll-up solar array and is planned for the CTS solar array.

The quasi-biconvex boom type shown in Figure 3-62 has been manufactured by Ryan Aeronautical, ASTRO Research and Celesco Industries. The boom is a closed section made by welding two metallic strips together along the two longitudinal edges. Thus, this section has good torsional properties and it develops buckling strength similar to that exhibited by closed, circular cylindrical shells. However, stowage of the boom presents problems with buckling of the inner compressed element. Also, buckling can occur in the transition region when this is kept small.

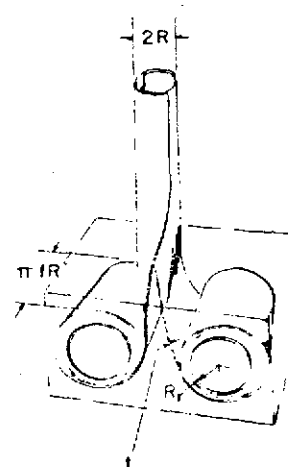


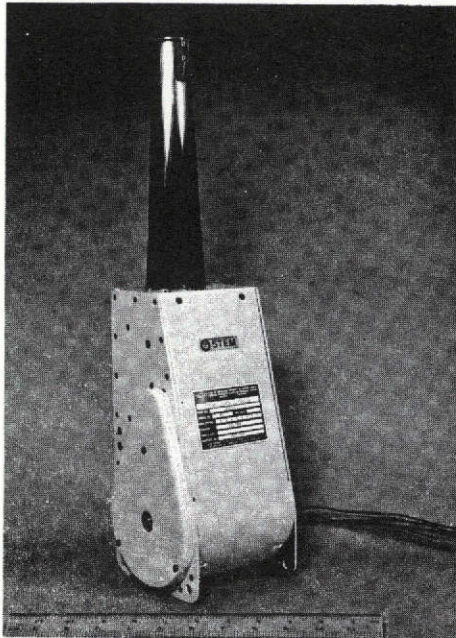
Figure 3-60. Schematic of BI-STEM Boom (From Reference 50)

#### 3.3.1.2.5.2 Coilable Lattice (or Continuous

Longeron) Booms. Coilable lattice booms, of the type manufactured by ASTRO Research, consist of a lattice structure of fiberglass rods which is shear-stiffened by diagonal cables. The boom is retracted by forcibly twisting it about its axis, thereby causing the horizontal "batten" members to buckle. The continuous longerons are thus coiled to provide a compact retracted configuration. Figure 3-63 shows the 25.4 cm diameter by 30.5 m long lunar antenna mast which is capable of withstanding an eight degree tilt from its vertical in lunar gravity when cantilevered at its base. The primary limitation of this boom type is the fact that the longerons must remain elastic when bent in the retracted portion. Therefore, the maximum thickness allowable for the longerons depends on the mast radius and the elastic strain limit of the longeron material. Thus, the overall bending strength and stiffness of the mast is limited by the radius of the mast and by the longeron material.

3.3.1.2.5.3 Articulated Longeron Booms. If high stiffness and strength is required of a small radius ASTROMAST, it is necessary to segment and articulate the longerons instead of elastically coiling them into the retracted position. Because there is no distortion of the longerons and battens in the stowed configuration, these members may be as large in cross section as the application requires.





This page is reproduced at the back of the report by a different reproduction method to provide better detail.

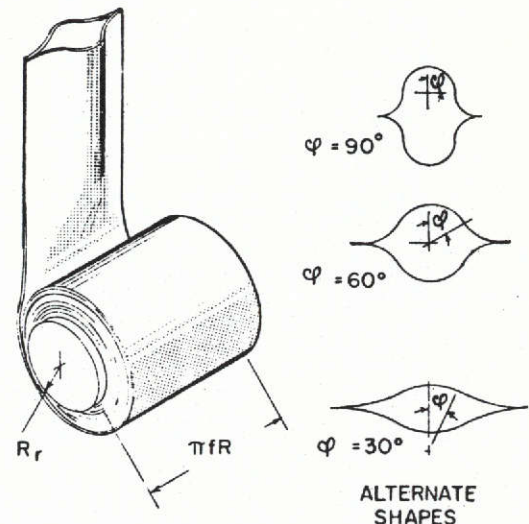


Figure 3-61. BI-STEM Deployable Boom and Actuator

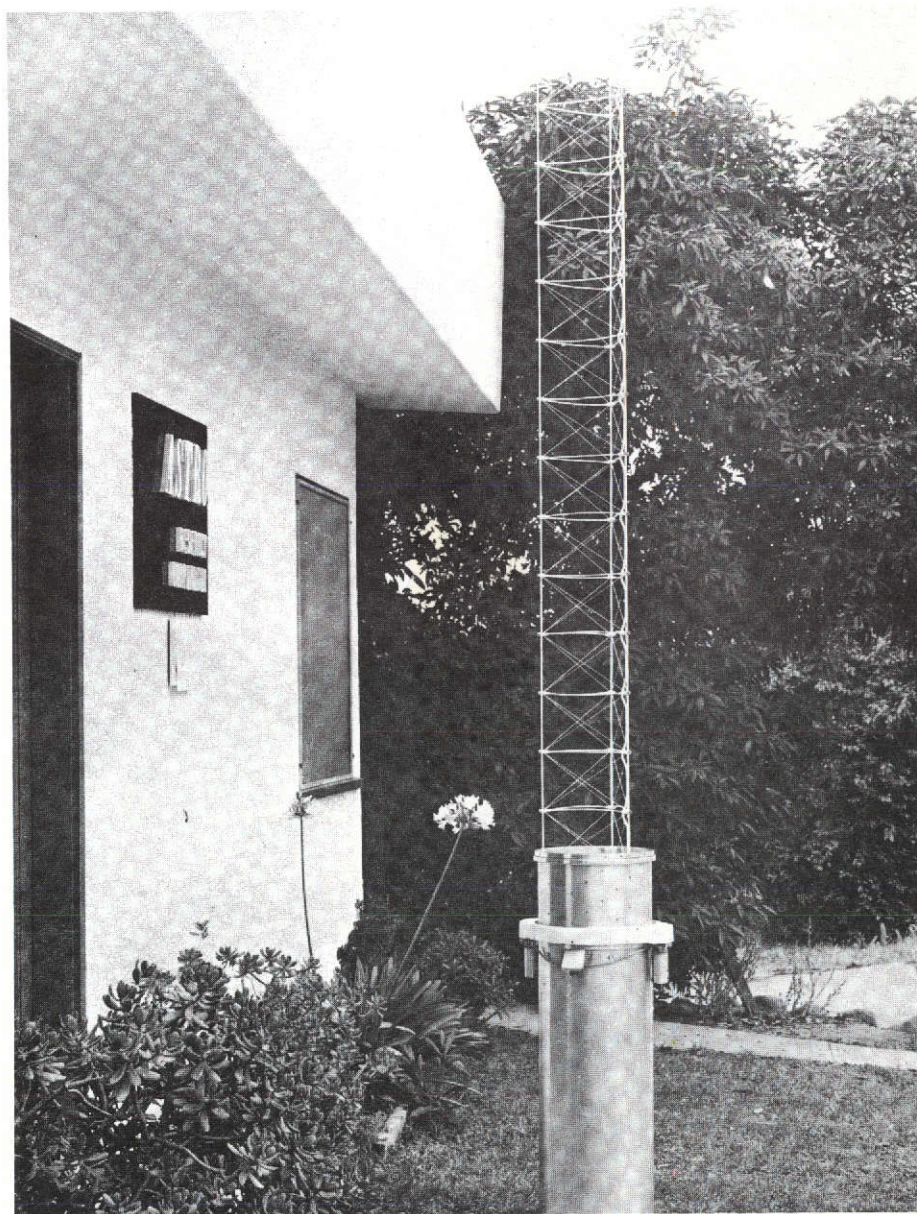
Figure 3-62. Schematic of Quasi-Biconvex Boom (from Reference 50)

Figure 3-64 shows the articulated lattice boom which is used on the Lockheed space station solar array development program.

3.3.1.2.5.4 Comparison of Deployable Boom Types. A comparison of the deployable boom types described above was performed with the aid of the formulas contained in References 50 and 51 for the BI-STEM and ASTROMAST type booms, respectively. The properties of the BI-STEM boom type are given by:

$$W = 2 \rho \gamma \pi D t L \quad (3.3-1)$$

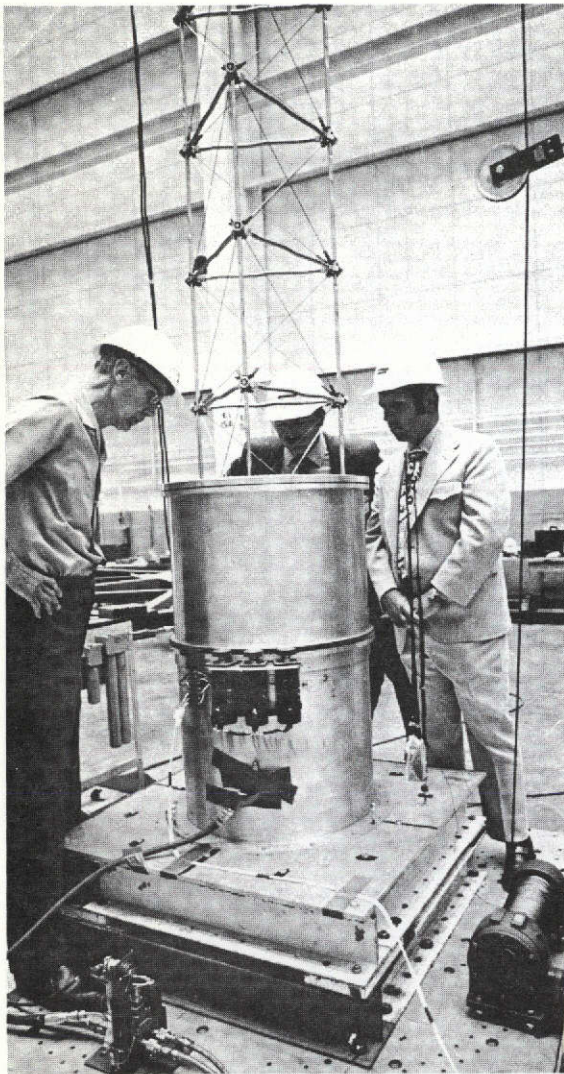
$$EI_{\min} = \frac{D^3 t}{8} \left[ \alpha + \sin \alpha \cos \alpha - \frac{2 \sin^2 \alpha}{\alpha} \right] \quad (3.3-2)$$



This page is reproduced at the back of the report by a different reproduction method to provide better detail.

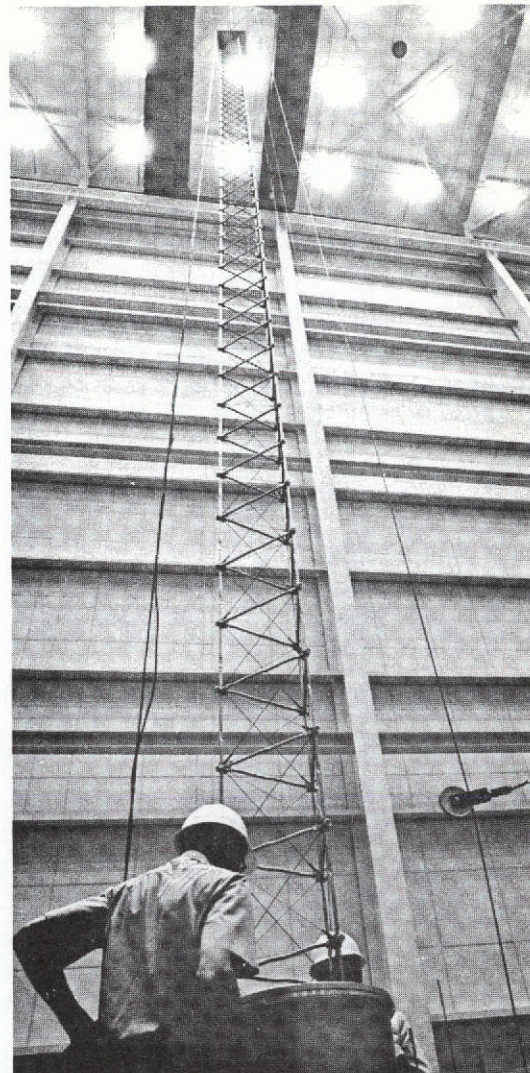
Figure 3-63. ASTROMAST Coilable Lattice Boom - Lunar Antenna Mast



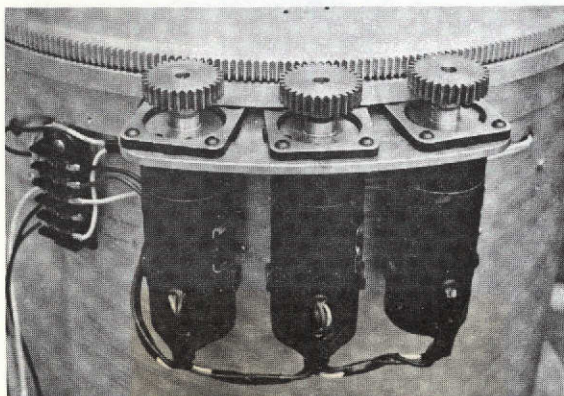


Astromast Deploying  
Automatically

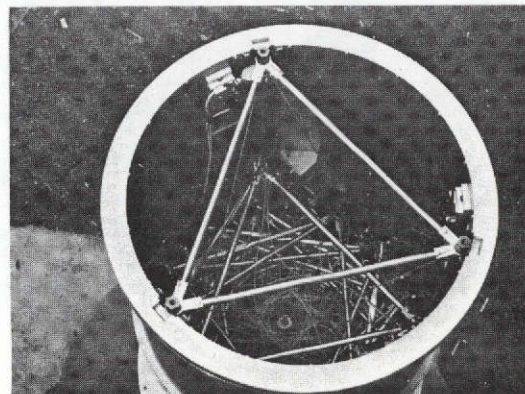
This page is reproduced at the back of the report by a different reproduction method to provide better detail.



Fully Extended Mast



Deployment Motors



Retracted Configuration

Figure 3-64. ASTROMAST Articulated Lattice Boom  
for Lockheed Space Station Solar Array

where

$W$  = mass of boom (kg)

$\rho$  = density of boom material ( $\text{kg/m}^3$ )

$\gamma$  = overlap factor =  $\frac{w}{\pi D}$

$w$  = width of strip

$E$  = modulus of elasticity of boom material ( $\text{N/m}^2$ )

$t$  = thickness of strip element (m)

$D$  = boom diameter (m)

$L$  = boom length (m)

$EI_{\min}$  = minimum boom bending stiffness ( $\text{N-m}^2$ )

$\alpha$  = overlap angle as defined in Figure 3-65

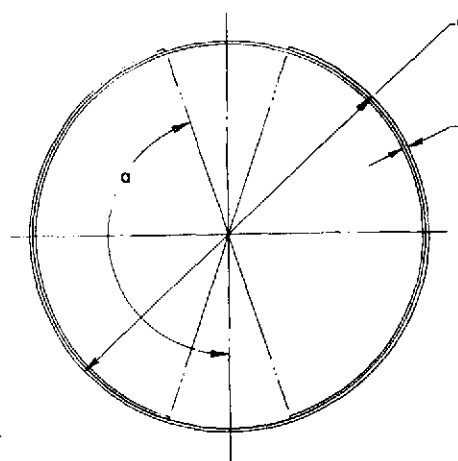


Figure 3-65. BI-STEM Section

The mass of the actuator required to deploy the BI-STEM type booms is given in Figure 3-66 as a function of boom diameter. The curve is based on limited data for existing BI-STEM designs where the largest size is 50.8 mm in diameter.

The properties of the continuous longeron ASTROMAST are given by:

$$W = 3f \rho A_{\ell} L \quad (3.3-3)$$

$$EI = 1.5 EA_{\ell} R^2 \quad (3.3-4)$$

$$H = 0.575 \frac{Ld}{R} + 2.5 R \quad (3.3-5)$$

$$W_{CAN} = 10 \left( \frac{H-2R}{21} \right) \left( \frac{R}{5} \right) + 15 \left( \frac{R}{5} \right)^2 \quad (3.3-6)$$

where

- W = mass of mast (kg)
- $\rho$  = density of longeron material ( $\text{kg/m}^3$ )
- $A_\ell$  = cross-section area of longeron ( $\text{m}^2$ )
- L = mast length (m)
- f = empirically derived factor  
= 3.4 for existing continuous lattice booms
- EI = mast bending stiffness ( $\text{N-m}^2$ )
- E = modulus of elasticity of longeron material ( $\text{N/m}^2$ )
- R = radius of a circle through the longeron centers (m)
- H = height of deployment canister (m)
- d = diameter of solid circular longeron (m)
- $W_{\text{CAN}}$  = mass of deployment canister (kg)

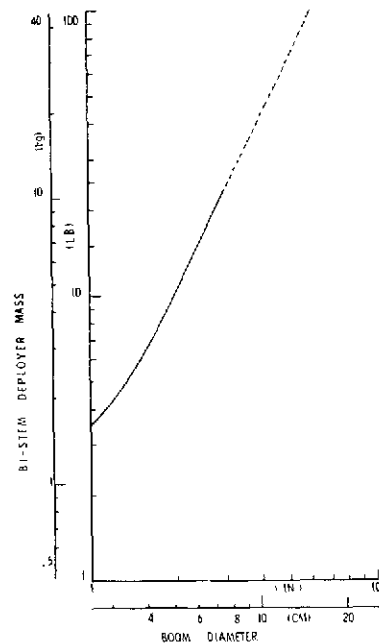


Figure 3-66. BI-STEM Deployer Mass vs. Boom Diameter

In addition, for elastic stowage the longeron diameter,  $d$ , must be

$$d \leq \frac{2S F R}{E} \quad (3, 3-7)$$

where

$$\begin{aligned} F_y &= \text{working strength of longeron material} \\ &= 10.34 \times 10^8 \text{ N/m}^2 \text{ (from Reference 50)} \end{aligned}$$

$$\begin{aligned} S &= \text{safety factor on working stress} \\ &= 0.667 \text{ (from Reference 50)} \end{aligned}$$

For the articulated longeron ASTROMAST, the appropriate formulas are:

$$W = 3f_{\rho} A_{\ell} L \quad (3.3-8)$$

$$EI = 1.5 E A_{\ell} R^2 \quad (3.3-9)$$

$$H = \frac{1.2 Ld}{\sqrt{3} R} + 3R \quad (3.3-10)$$

$$W_{CAN} = 10 \left( \frac{H-3R}{21} \right) \left( \frac{R}{5} \right) + 15 \left( \frac{R}{5} \right)^2 \quad (3.3-11)$$

where the definition of symbols is the same as previously given for the continuous longeron ASTROMAST.

Figure 3-67 shows the boom mass vs bending stiffness for the types of booms discussed above. The same curve results for a stainless steel or molybdenum BI-STEM element, however the molybdenum element will have a smaller diameter than a stainless steel element with the same EI. The articulated steel longeron ASTROMAST curve has been drawn for EI values which reflect a factor of two reduction in the theoretical stiffness given by equation (3.3-9) to account for the flexibility on the hinge joints. This is the approximate reduction measured for the space station mast (Reference 52). The f factor of 2.6 also correlates well with the space station mast. The curve for the steel Celesco bi-convex boom is based on the two data points shown on the figure, where the EI values represent the minimum for each section. The continuous fiberglass longeron ASTROMAST has the lowest mass for a given bending stiffness requirement.



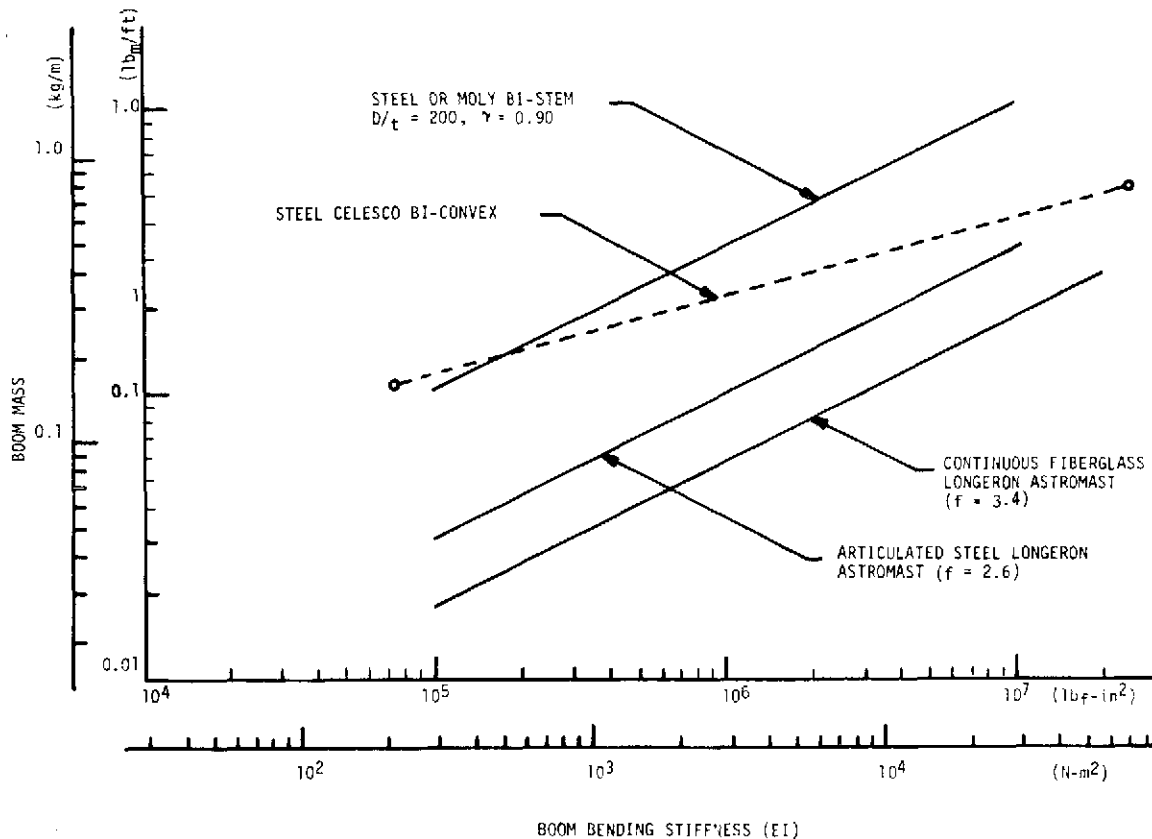


Figure 3-67. Deployable Boom Mass vs. Bending Stiffness

Figure 3-68 shows the total mass of the boom element plus deployment actuator or canister vs. bending stiffness for a boom length of 18.565 m. The slight difference between the steel and molybdenum BI-STEM booms is due to the lower actuator mass associated with the smaller diameter molybdenum element. Again these curves show that the continuous fiberglass longeron ASTROMAST is superior from an overall weight standpoint. However, the fiberglass longeron material limits the useable upper temperature extreme to about 120°C. Even at this temperature the flexural modulus of materials of this type will be significantly reduced from the room temperature value as shown in Figure 3-69. The JPL specification for the interplanetary mission (reference Appendix A) requires that the solar array be operated to a perihelion of 0.5 AU where the solar intensity is 542 mw/cm<sup>2</sup>. In addition, the upper temperature limit during thermal vacuum testing is specified as 140°C. Thus, it is necessary to select another longeron material for use on the interplanetary mission application as presently defined. The articulated steel longeron ASTROMAST is a logical choice for this application since it adds only about 1.5 kg of mass to the system weight for the EI

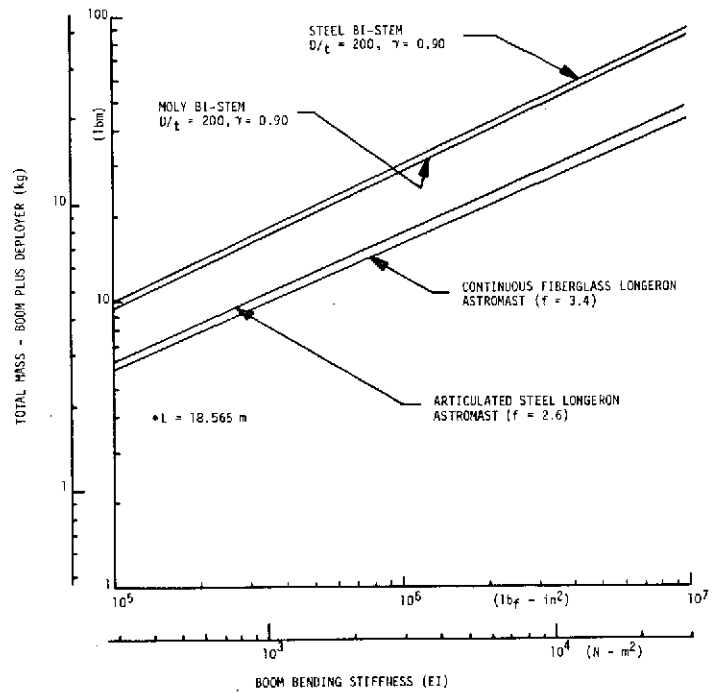


Figure 3-68. Total Mass of Boom Plus Deployer vs. Bending Stiffness

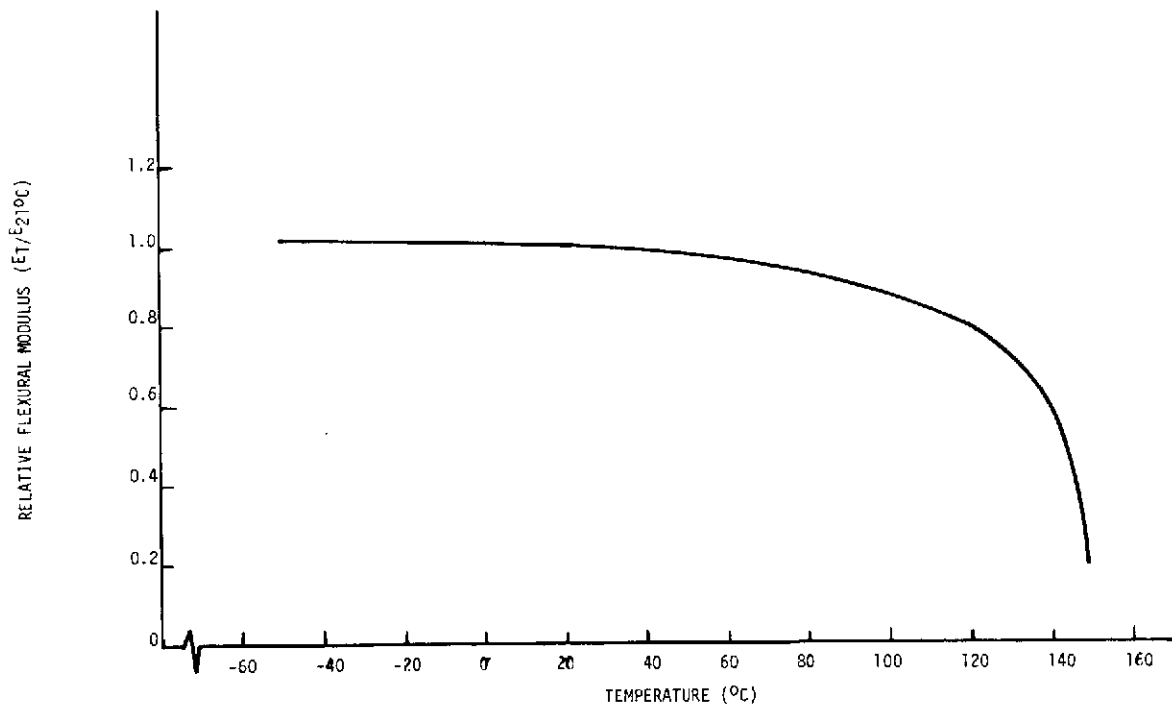


Figure 3-69. Relative Flexural Modulus vs. Temperature for "Scotchply" Type 1002 Unidirectional Fiberglass/Epoxy Composite



required. The articulated steel longeron curve on Figure 3-68 represents the minimum total component mass as shown by the curves in Figure 3-70. For a given EI requirement there is an optimum mast diameter which results in the minimum total component mass. At mast diameters which are smaller than this optimum value the total mass is dominated by the mast element whereas at the larger mast diameters the canister mass is the dominant influence.

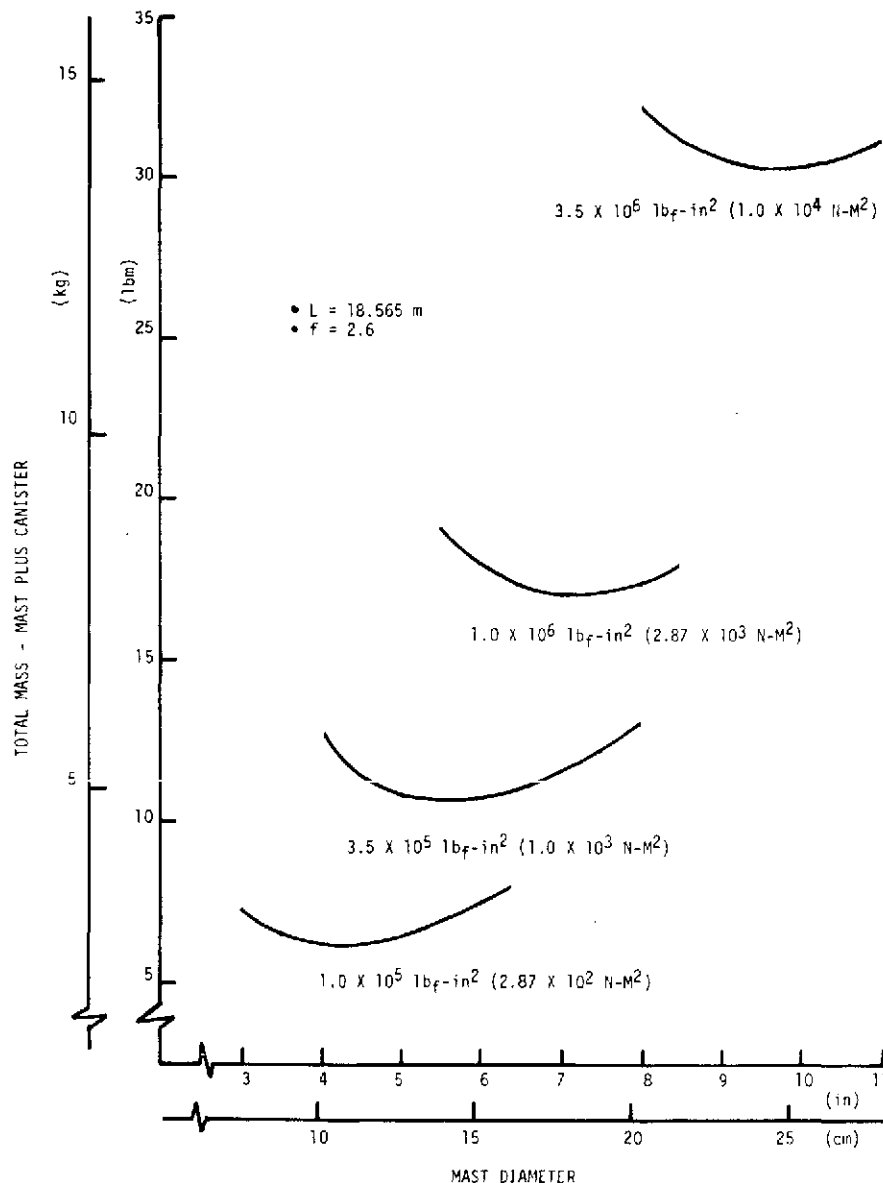


Figure 3-70. Total Mass of an Articulated ASTROMAST with Steel Longerons vs. Mast Diameter

### 3.3.2 STATE-OF-THE-ART ADVANCES

Possible advances in component technology that may influence the future development of lightweight solar arrays are discussed in this section. Improvements in solar cell conversion efficiency have the most significant impact on the ability to produce an ultra-lightweight solar array. Such an improvement has been recently demonstrated by a solar cell developed by COMSAT Laboratories. Advances in deployable boom technology through the utilization of component materials also promises to improve the solar array power-to-mass ratio.

#### 3.3.2.1 COMSAT Violet Solar Cell

The COMSAT violet solar cell has recently been licensed to Centralab for manufacture and sale (Reference 53). This improved silicon solar cell has demonstrated an increase in average conversion efficiency of approximately 30 percent when compared to current production solar cells. This improvement is achieved by the enhancement of the short wavelength response, resulting from the near elimination of the highly damaged "dead layer" which occurs in conventional cells (Reference 21). The resulting loss of lateral conductivity requires a very fine collection grid geometry. With this fine geometry it was possible to reduce the series resistance resulting in increased I-V curve fill factor. The improvements in current and curve fill factor are highly resistant to penetrating ionizing radiation as shown in Figure 3-71.

#### 3.3.2.2 Boron/Aluminum BI-STEM

The boron/aluminum matrix composite system has potential as a reduced weight alternate to conventional metals in the fabrication of a BI-STEM type deployable boom element. In the reinforced direction, this composite system has a strength-to-density and modulus-to-density ratio which is superior to any engineering alloy which is commonly used for BI-STEM elements.

This approach appears to be feasible if the monolayer tape material can be obtained with high enough matrix transverse mechanical properties to allow fabrication with a reasonable low boom D/t ratio.

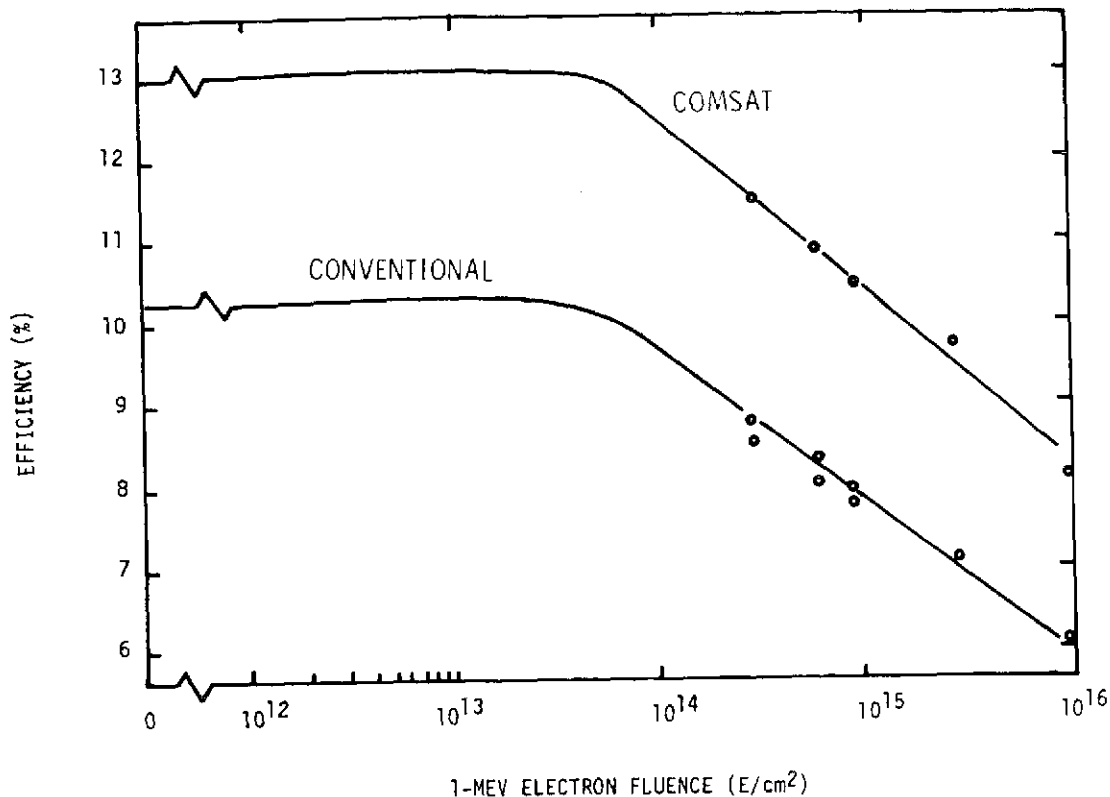


Figure 3-71. 1-MeV Electron Radiation Damage of COMSAT Violet Cells Compared with Conventional Cells (from Reference 21)

### 3.3.2.2.1 Existing B/Al Composite Technology

**3.3.2.2.1.1 Fibers.** The composites are fabricated using boron or BORSIC\* fibers. A 102  $\mu\text{m}$  diameter boron fiber has an axial modulus of  $3.86 - 3.93 \times 10^{11} \text{ N/m}^2$  ( $56-57 \times 10^6$  psi) and has an ultimate tensile strength of about  $3.1 \times 10^9 \text{ N/m}^2$  (450,000 psi). The BORSIC fiber permits fabrication at higher temperatures and has superior oxidation resistance. BORSIC fibers, in diameters of 107 and 142  $\mu\text{m}$ , have ultimate tensile strengths which are approximately 10 percent lower than uncoated boron fiber as it is currently produced. The fibers are produced by depositing boron onto a 12  $\mu\text{m}$  diameter tungsten substrate. The BORSIC fibers have an additional 3  $\mu\text{m}$  thick coating of SiC on the outside of the boron fiber.

**3.3.2.2.1.2 Matrix Material.** Aluminum alloys 2024, 6061, 5052, SAP, 713 1100 and 1145 have been used as the matrix, including both foil and plasma sprayed prealloyed powder. The properties of the matrix alloy have a strong influence on the transverse properties of the composite.

\*United Aircraft Corporation trade name for a silicon carbide coated boron fiber.

3.3.2.2.1.3 Processing. The formation of the composite by placing the fibers in the aluminum matrix alloy can be accomplished by several processes which include: hot pressure bonding, step pressing, roll bonding, plasma spraying and liquid infiltration (Reference 54).

(a) Hot Pressure Bonding

In this process, the fibers are precollimated, usually by winding onto a large diameter mandrel, to provide the desired spacing. An organic binder (acrylic, or polystyrene), which is subsequently removed by volatilization during the hot pressing cycle, is used to hold the fibers together. The collimated filament mat is sandwiched between two wrought foil layers which are forced to flow between the filaments by the application of heat and pressure. If the foil surfaces are clean and oxide free, diffusion bonding will occur. The step pressing and roll bonding processes utilize the same principles as the hot pressure bonding process to produce monolayer tape material on a semi-continuous and fully continuous basis, respectively. With the step pressing process, diffusion bonded monolayer tape is produced by a continuous series of overlapping flat die bonding cycles. Typical consolidation parameters for a boron/aluminum composite with 50 v/o filaments are 1 hour at  $48.3 \times 10^6$  N/m<sup>2</sup> (7,000 psi) and 480°C (900°F).

(b) Plasma Spraying

In this process, the filaments are wound onto a large diameter mandrel over a foil layer. The mandrel is rotated and traversed before the plasma arc. The diameter of this mandrel restricts the length of tape that can be produced by the plasma spraying process. At United Aircraft, the existing equipment restricts this length to approximately 3.65 m (12-ft). Aluminum alloy powder, which is injected into the hot gas of the plasma arc, is melted into droplets which deposit on the foil and fiber to form the monolayer tape composite. The sprayed matrix is not fully dense and therefore must be consolidated by hot pressure bonding or braze bonding. The strength of boron fibers has been observed to degrade as a result of contact with the molten aluminum droplets. The use of BORSIC fibers overcomes this problem and BORSIC/aluminum composites with a variety of matrix alloy compositions have been produced.

(c) Liquid Infiltration

With this process, continuous filaments are passed through the molten matrix alloy into an orifice of the desired geometry to produce a continuous composite rod. Chemically inert coatings of the boron fibers are required to prevent reaction with the molten aluminum alloys. General Technologies Corporation (GTC) used BORSIC fiber to provide continuous tape material. A boron nitride coated boron fiber has been used with the liquid infiltration process to produce a monolayer tape which is marketed under the trade name NITBORAL by Monjoe Scientific. Suitable matrix

materials are limited to certain casting alloys which have the ability to wet the filaments. For this reason, it is not possible to achieve matrix strengths which are equivalent to hot pressed composites.

3.3.2.2.1.4 Sources of Supply. Boron/aluminum monolayer tape material is available from any of the following sources:

1. Hamilton Standard Division of United Aircraft Corporation  
Windsor Locks, Connecticut 06096
2. Amercom, Inc.  
9060 Winnetka Avenue  
Northridge, California 91324
3. Union Carbide Corporation  
P.O. Box 24184  
Indianapolis, Indiana 46224
4. AVCO-Systems Division  
Lowell Industrial Park  
Lowell, Massachusetts 01851
5. Martin-Marietta Aluminum  
19200 S. Western Avenue  
Torrance, California 90509

3.3.2.2.1.5 Environmental Stability

- a. Salt Exposure - Exposure of 2024 and 6061 matrix BORSIC/Aluminum composites to a salt spray at 35°C resulted in corrosion of the matrix material that was most severe with the 2024 alloy in the as-fabricated condition. All specimens were loaded in flexure in a three point bend fixture. Matrices of 6061-T6 exhibited general corrosion without preference for regions of high stress whereas the 2024 matrices displayed greater depths of attack on the tensile surfaces as compared to the compression surfaces.
- b. Thermal Cycling - Thermal cycling of 50 percent by volume 107  $\mu$ m BORSIC/6061-F aluminum composites between 21°C and 354°C can cause void formation within the matrix as a result of plastic strains caused by differences in thermal expansion among the constituents. These voids result in decreased density and reduced flexural strength which amounts to about 13 percent for unidirectional material after 5000 cycles.

3.3.2.2.1.6 Composite Material Properties. The modulus of elasticity in the longitudinal direction is strongly influenced by the fiber content as shown in Figure 3-72. Table 3-20 gives the ultimate tensile strength in the axial direction for several BORSIC/Aluminum composites.

Table 3-20. Axial Tensile Strength of 142  $\mu\text{m}$  BORSIC/Al  
(from Reference 56)

Matrix	Volume Percent Boron	Ultimate Tensile Strength ( $10^3$ psi)	Elastic Modulus ( $10^6$ psi)	Strain to Fracture (%)
2024F	45	185.7	30.4	0.765
	45	197.5	27.5	0.835
	44	177.0	30.0	0.725
	47	212.0	32.0	0.825
	47	212.0	32.6	0.820
	49	194.0	32.0	0.740
2024-T6	46	202.5	32.8	0.75
	46	213.6	31.6	0.81
	47	217.0	32.3	0.830
	48	213.0	31.3	0.845
	64	279.0	40.0	0.755
2024F	70	279.5	----	-----
	66	253.0	----	-----
	67	250.2	----	-----
6061F	48	196.3	31.8	0.710
	48	171.0	28.2	0.590
	50	204.0	33.8	0.72
	50	208.0	32.0	0.76
6061-T6	52	216.5	33.8	0.78
	51	197.0	33.4	0.69
	50	203.0	----	-----

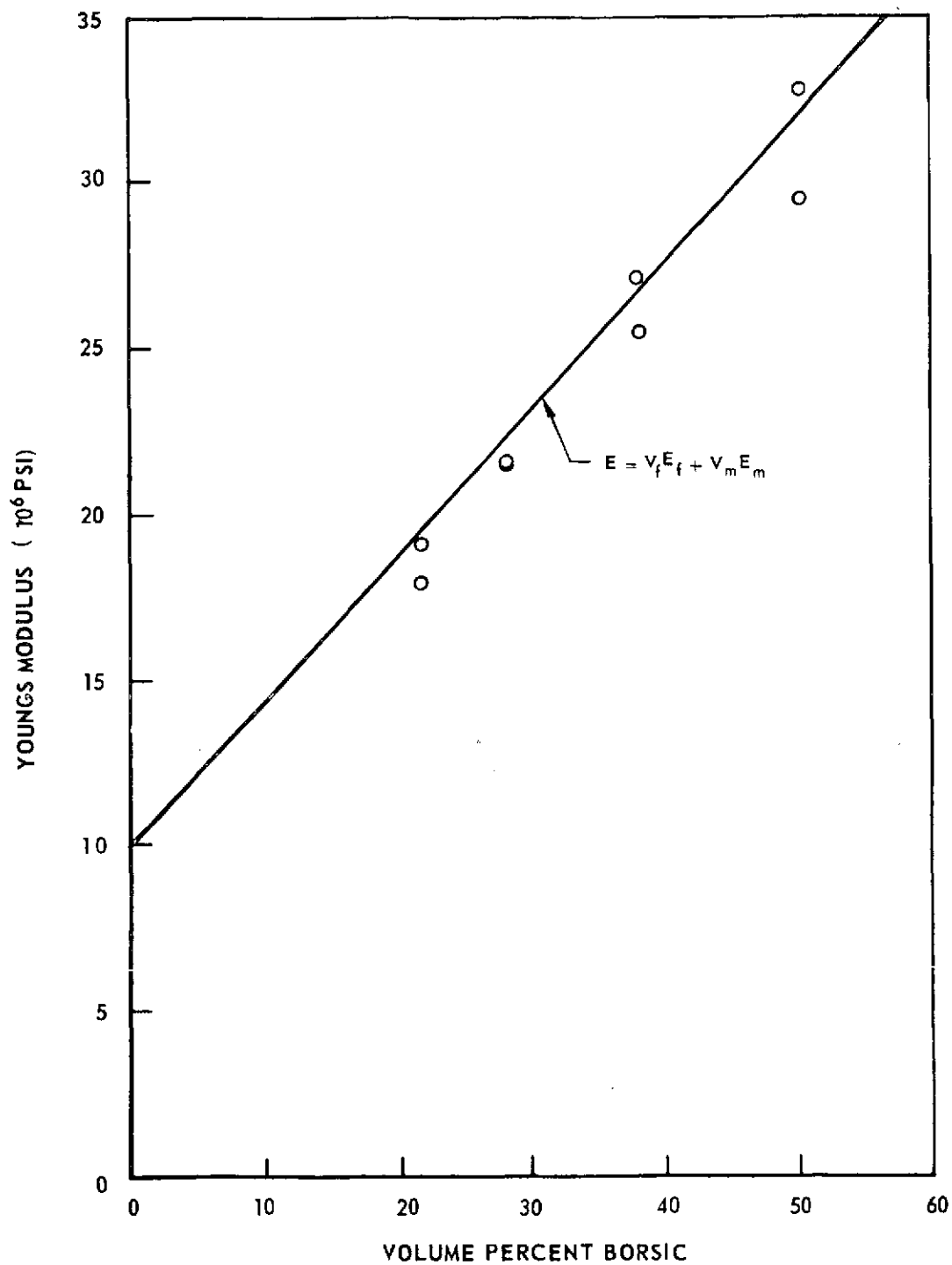


Figure 3-72. Effect of Fiber Content on Composite Modulus of Elasticity (from Reference 55)

In the transverse direction, the mechanical properties of the composite are greatly influenced by the matrix material. For the composites studied by United Aircraft, the components were BORSIC fiber and a matrix consisting of foil and plasma sprayed material. The plasma sprayed portion of the matrix can contain as much as 10 to 15 percent porosity in the as-sprayed condition. If some of this porosity is permitted to remain, the strength of the matrix will be severely reduced. The use of hot press diffusion bonding of the matrix has reduced the effect of this porosity. The transverse elastic modulus is a sensitive indicator of the degree of composite consolidation and bonding and thus can be used as a criteria for determining the integrity of the composite.

Figure 3-73 shows the transverse elastic modulus as a function of volume fraction of 107  $\mu\text{m}$  diameter BORSIC. This figure shows that the transverse elastic modulus increases with increasing volume fraction of fibers.

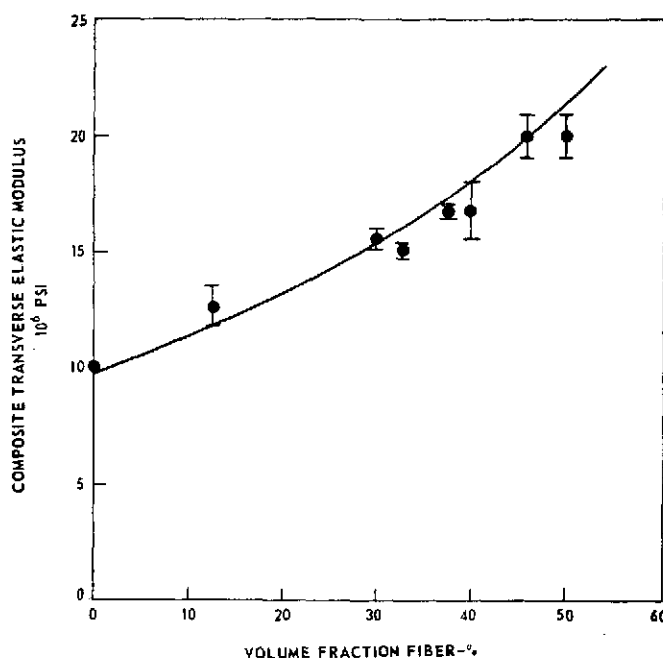


Figure 3-73. Transverse Elastic Modulus vs. Content of 107  $\mu\text{m}$  BORSIC Fibers (from Reference 56)



The transverse tensile strength of 107  $\mu\text{m}$  diameter BORSIC fiber composites as a function of matrix material tensile strength is shown in Figure 3-74. Three distinct regions of behavior are evident on this figure. In Region I, the composite strength is approximately equal to the matrix strength. In this region, the matrix fails at an applied stress below that required for fiber failure. Thus, fracture surfaces of failed composites exhibit only a small amount of split fibers. In Region II, the composite strength is relatively independent of matrix strength. Fracture surfaces exhibit a large amount of fiber splitting since the matrix strength is sufficient to cause loading of the fibers to their ultimate transverse strength prior to composite failure. This fiber failure causes an overload in the matrix material which results in composite fracture since the matrix material does not have the

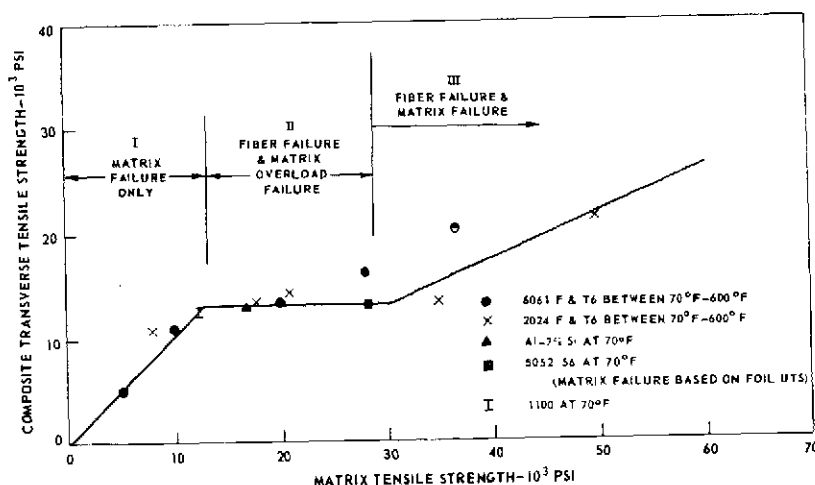


Figure 3-74. Transverse Tensile Strength of 50 Percent Volume 107  $\mu\text{m}$  BORSIC/Aluminum (from Reference 56)

necessary strength to prevent total composite failure subsequent to fiber splitting. In Region III, as in Region II, the matrix strength is sufficient to cause fiber splitting prior to composite failure. However, in Region III, the matrix strength is sufficient to prevent immediate overload failure. Thus, the composite strength is determined by the net section of load bearing matrix remaining, subsequent to fiber failure, and the strength of this matrix.

The large diameter ( $\approx 142 \mu\text{m}$ ) BORSIC fibers, which have a larger ratio of boron to tungsten core, exhibit much higher transverse fiber strengths than the smaller diameter fibers. As a result, composites fabricated with these larger diameter BORSIC fibers exhibit very little fiber splitting. The primary mode of failure is matrix rupture. Figure 3-75 shows that the composite strength is very nearly equal to the matrix strength.

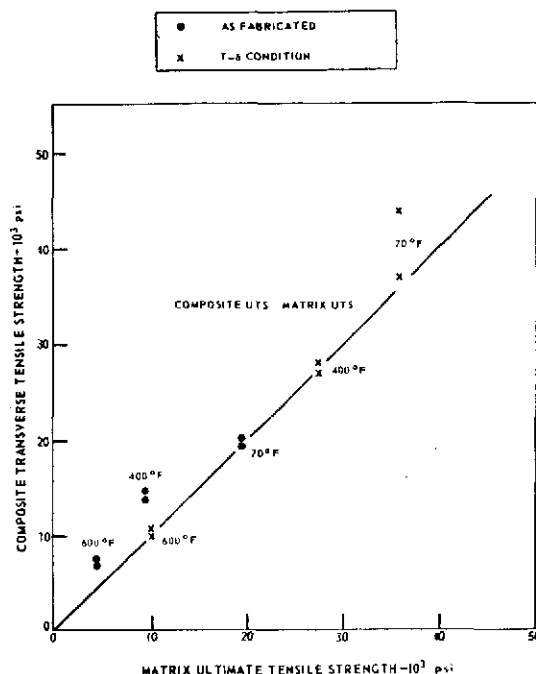


Figure 3-75. Transverse Tensile Strength of 60 Percent by Volume 154  $\mu\text{m}$  BORSIC/6061 Aluminum (from Reference 56)

### 3.3.2.2.2 Application to a BI-STEM Type Deployable Boom

The performance of a BI-STEM deployable boom element which is fabricated from B/Al composite material was analyzed. The composite tape material was postulated to be of a configuration as shown in Figure 3-76. Figure 3-77 shows some possible configurations of the monolayer tape as a function of volume percent boron fiber. Two nominal fiber diameters have been shown to illustrate the dependence of tape thickness on fiber spacing and content. For example, with a 142  $\mu\text{m}$  fiber diameter and with a 50 percent fiber content by volume, a tape thickness of 178  $\mu\text{m}$  can be achieved with a 178  $\mu\text{m}$  fiber spacing. This thickness is commonly available, with a wrought foil layer top and bottom, from the sources listed in Section 3.3.2.2.1.4. In the formation of a BI-STEM type element from this monolayer tape material, the fiber direction is along the deployment direction of the boom element. Thus,

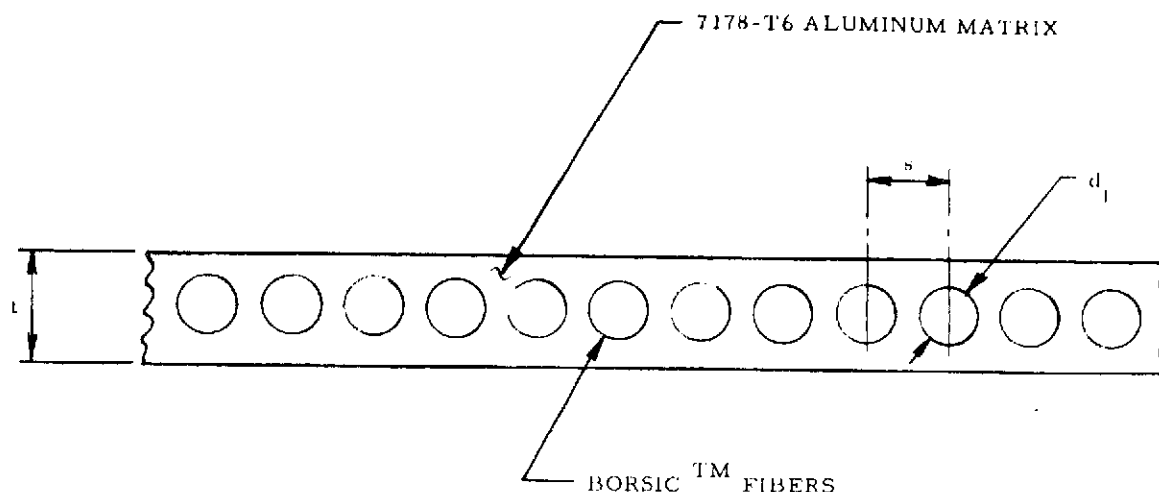


Figure 3-76. B/Al Composite Tape Material

the longitudinal modulus of elasticity of the composite is influenced by the BORSIC fiber content as shown in Figure 3-72. For a BORSIC fiber content of 50 percent by volume, the modulus of elasticity in the longitudinal direction will be about  $20.7 \times 10^{10} \text{ N/m}^2$  ( $30 \times 10^6 \text{ psi}$ ). In the transverse direction, which is the forming direction of the BI-STEM C section, it is necessary to have a matrix with a high enough tensile strength to elastically accommodate the strain associated with the flattening of the C shape. Assuming a minimum D/t ratio of 300, the aluminum alloy at the outermost fiber of the strip must be capable of elastically accommodating a strain of .0033. If a 7178 matrix alloy were used, it might be possible to achieve this low a D/t ratio. Table 3-21 lists the mechanical properties of the higher strength aluminum alloys.

For the BI-STEM type boom, the section properties are given by the formulas contained in Section 3.3.1.2.5.4. With a 50% B/Al monolayer tape strip element of  $178 \mu\text{m}$  thickness, a 53.4mm diameter BI-STEM will have a bending stiffness of  $3465 \text{ N-m}^2$  with a boom mass of 0.142 kg/m of length. When compared to a continuous fiberglass longeron ASTROMAST with the same EI, the B/Al BI-STEM element for a 18.565 m boom will have a mass which is lower by 0.4 kg.

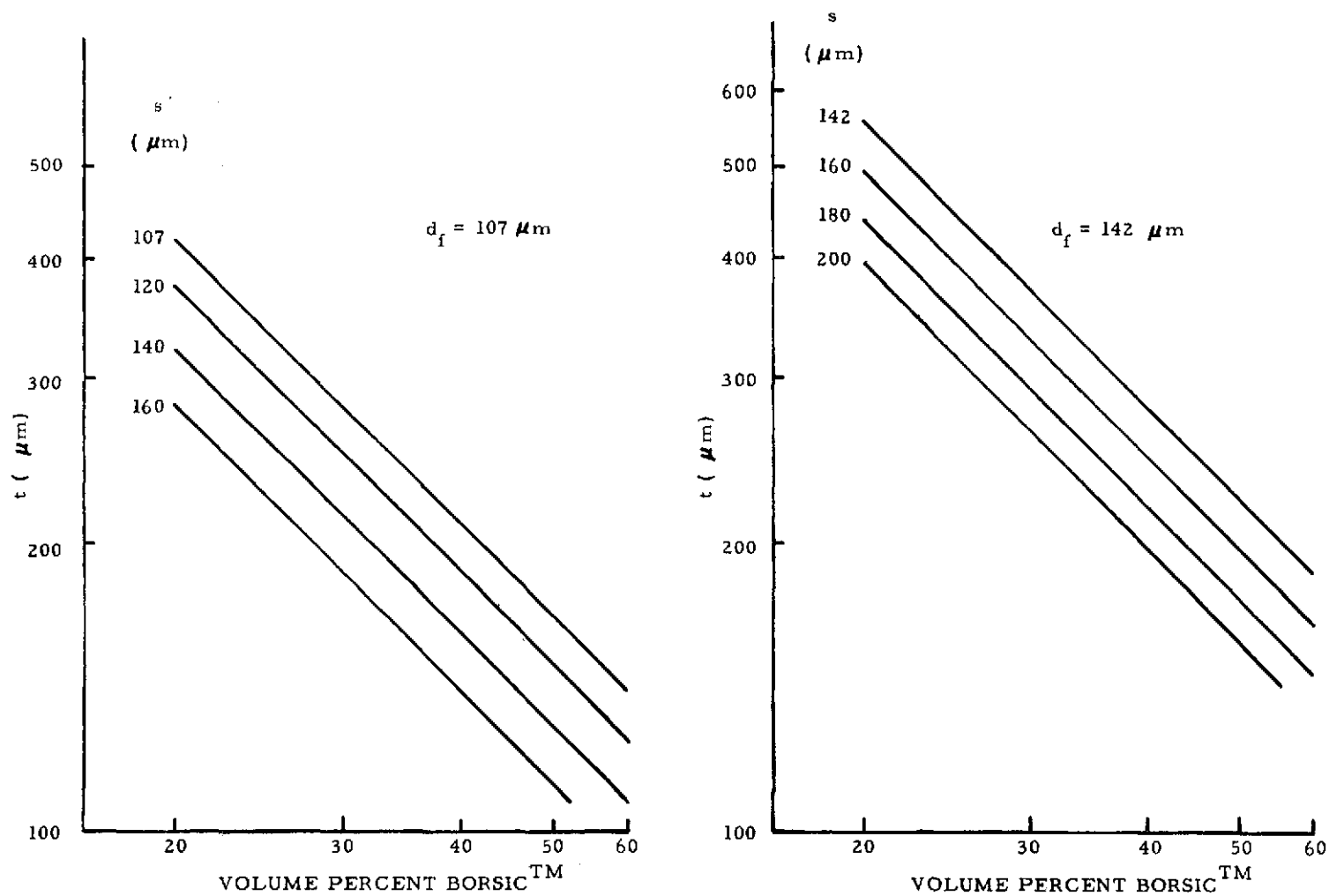


Figure 3-77. Possible Configurations of B/Al Monolayer Tape

Table 3-21. Properties of Aluminum Alloy Matrix Materials\*

ALLOY AND TEMPER	ULTIMATE TENSILE STRENGTH		TENSILE YIELD STRESS		MODULUS OF ELASTICITY		DENSITY	
	(PSI)	(N/m <sup>2</sup> )	(PSI)	(N/m <sup>2</sup> )	(PSI)	(N/m <sup>2</sup> )	(lb/in <sup>3</sup> )	(gm/cm <sup>3</sup> )
2024-T4	64,000	4.41x10 <sup>8</sup>	40,000	2.76x10 <sup>8</sup>	10.5x10 <sup>6</sup>	7.24x10 <sup>10</sup>	0.100	2.77
6061-T6	43,000	2.96x10 <sup>8</sup>	38,000	2.62x10 <sup>8</sup>	9.9x10 <sup>6</sup>	6.83x10 <sup>10</sup>	0.098	2.72
7075-T6	78,000	5.37x10 <sup>8</sup>	69,000	4.75x10 <sup>8</sup>	10.3x10 <sup>6</sup>	7.10x10 <sup>10</sup>	0.101	2.80
7178-T6	85,000	5.85x10 <sup>8</sup>	75,000	5.16x10 <sup>8</sup>	10.3x10 <sup>6</sup>	7.10x10 <sup>10</sup>	0.102	2.83

\*Values from Reference 57

### 3.3.2.3 Graphite/Epoxy Booms

The Space Division of Rockwell International Corporation (formerly North American Rockwell Corporation) has studied the application of a graphite/epoxy composite boom for the Solar Electric Propulsion Stage (SEPS) solar array configuration (Reference 58). Figure 3-78 shows the concept for this boom and actuator. The six cusp tubular boom shape consists of graphite laminated fiberglass which is flattened elastically for stowage within the actuator. The boom properties for the SEPS solar array application are summarized in Table 3-22.

The use of unidirectional graphite/epoxy composite material for the longerons in a continuous longeron ASTROMAST is another approach which is worthy of further consideration as a state-of-the-art advancement. Hercules graphite prepreg type X-3501-AS material has a 0° flexural modulus of 103. G N/m<sup>2</sup> (15 x 10<sup>6</sup> psi) and a 0° flexural strength of 1.58 G N/m<sup>2</sup> (230,000 psi) measured at 177° C (350° F) based on General Electric - Space Sciences Laboratory test data. If this material were used for the longerons in a continuous longeron ASTROMAST, a mast bending stiffness of 3440. N-m<sup>2</sup> (1.2 x 10<sup>6</sup> lb-in.<sup>2</sup>) can be achieved with a total component mass of 6.0 kg. The 18.56 m long, 183. mm (7.2 inch) diameter

mast has a mass of 0.8 kg with the remaining 5.2 kg required for the motor driven deployment canister. The calculation of these weights is based on the formulas contained in Section 3.3.1.2.5.4, using a value of 3.4 for the factor  $f$  in the mast weight formula. This factor will certainly be larger for this lightweight longeron construction. Doubling its value will still result in a net 0.9 kg mass saving when compared to the 7.7 kg allocated to the continuous fiberglass longeron ASTROMAST in the baseline design for the earth orbiting missions. The high temperature capability of this material also makes it applicable to the interplanetary mission with as much as a 1.6 kg saving when compared to the articulated steel longeron ASTROMAST.

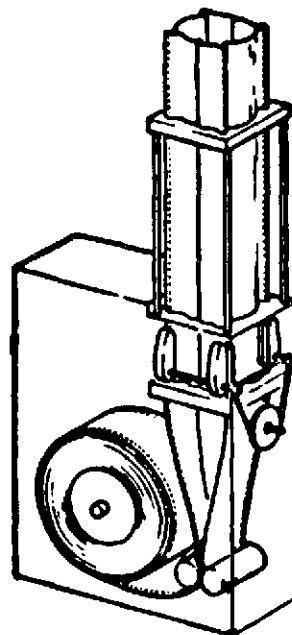


Figure 3-78. Rockwell International Corp.  
Concept for a Graphite Composite  
Deployable Boom (from Reference 58)

Table 3-22. Six-Cusp Graphite/Epoxy Tubular Boom Properties  
for SEPS Solar Array Application (from Reference 58)

Estimated Composite Material Properties

$E = 1.24 \times 10^{11} \text{ N/m}^2$	$(18 \times 10^6 \text{ psi})$
$G = 6.9 \times 10^9 \text{ N/m}^2$	$(1.0 \times 10^6 \text{ psi})$
$P = 1.63 \text{ gm/cm}^3$	$(0.059 \text{ lb/in.}^3)$

Boom Section Properties

$t = 63.5 \text{ } \mu\text{m}$	$(0.0025 \text{ in.})$
$D = 26.6 \text{ cm}$	$(10.5 \text{ in.})$
$A = 5.29 \times 10^{-5} \text{ m}^2$	$(0.082 \text{ in.}^2)$
$I = 4.7 \times 10^{-7} \text{ m}^4$	$(1.13 \text{ in.}^4)$
$J = 9.4 \times 10^{-7} \text{ m}^4$	$(2.26 \text{ in.}^4)$

### 3.3.3 VARIATIONS IN PERFORMANCE DUE TO STATE-OF-THE-ART IMPROVEMENTS

The power output improvements which will be achievable through the use of the COMSAT violet solar cell development will be reflected directly as an improvement in the solar array power-to-mass ratio. If the electrical performance of a covered 125  $\mu\text{m}$  thick COMSAT violet solar cell is improved by 30 percent compared to the baseline solar cell performance, this improvement is directly reflected as a 30 percent increase in the beginning-of-life power-to-mass ratio of an array of the same area. The end-of-mission power-to-mass ratio will be more than proportionately increased due to the inherent radiation resistance of the violet solar cells when compared to conventional solar cells of the same thickness.

If it is required to supply the same beginning-of-life electrical power output (viz., 10,000 watts), the solar array size must be decreased to account for the improved cell performance. Figure 3-79 shows the total system power-to-mass ratio as a function of average cell maximum power output (or efficiency). Cell thicknesses of 200 and 300  $\mu\text{m}$  with an associated discrete coverglass thickness of 75  $\mu\text{m}$  were selected for the presentation to show that the 110 watt/kg value can be reached with more conventional thicknesses and fabrication techniques provided that the cell performance is sufficiently high. The data for this curve was obtained by scaling the baseline design configuration for an aspect ratio of 4 and a natural frequency of 0.04 Hz. These results show that a system power-to-mass ratio of 110 watt/kg will require a cell efficiency (based on total cell area) of at least 14.6 percent for 300  $\mu\text{m}$  thick cells and 12.0 percent for 200  $\mu\text{m}$  thick cells. The reported performance of the COMSAT violet cell is about 13 percent based on total cell area (Reference 21). Thus, it would appear possible to eventually obtain 200  $\mu\text{m}$  thick cells of this type with an efficiency of 12 percent or better.

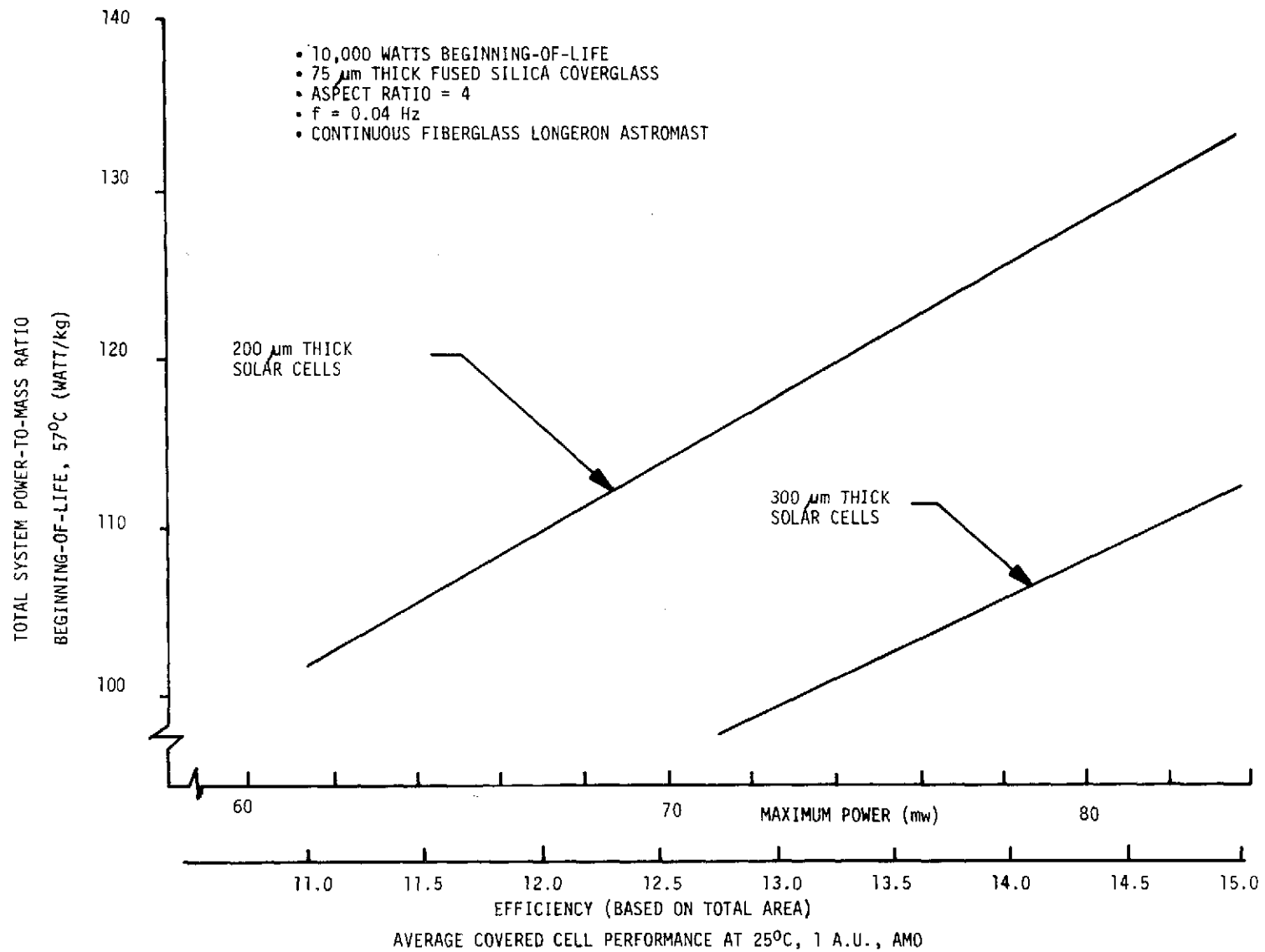


Figure 3-79. Effects of Improved Solar Cell Performance on System Power-to-Mass Ratio



### 3.4 TRADE-OFFS, ANALYSES AND STUDIES

#### 3.4.1 PARAMETRIC ANALYSIS OF SOLAR CELL BLANKET

##### 3.4.1.1 General

The selection of the solar cell/coverglass combination is an important consideration in the feasibility of the 110 watt/kg solar array system since these components, along with the supporting substrate, represent a significant fraction of the total system weight. For example, in the 30 watt/lb roll-up solar array design, the flexible solar cell blankets constituted 56.5 percent of the total system mass. Thus, for a 110 watt/kg solar array system, it is extremely important to minimize the blanket mass consistent with the other system requirements. The beginning-of-life (BOL) solar array panel output is specified as 10,000 watts at the 1 AU intensity and equilibrium temperature. In addition, the power output under these same conditions shall not decrease by more than 20 percent over the 3-year operational life. Thus, this specification defines the allowable degradation (primarily particle radiation damage) instead of specifying a desired end-of-life (EOL) power capability with no constraint on initial power (or allowable degradation).

The objective of this trade-off analysis is to assess the impact of this allowable degradation constraint and compare this result with a design which produces a specified EOL power output with no restriction on degradation.

In order to perform these trade-offs, it is first necessary to determine the effect of the particle radiation environment on the solar cell electrical characteristics. The calculation procedure employed is based on a damage equivalent 1-MeV electron fluence method which is commonly used to relate solar cell degradation to a combined electron and proton environment. This procedure involves the determination of the damage equivalency of 1-MeV electrons for each particle type and differential energy spectra. The shielding effect of the coverglass and cell backing is accounted for in the determination of this damage equivalency.

#### 3.4.1.2 Solar Cell Radiation Degradation

For each mission type, the particle radiation environment defined in Section 3.1.1 was converted into a Damage Equivalent-Normally Incident (DENI) 1-MeV electron fluence using the calculation procedure described in Reference 59. For the interplanetary mission, the DENI 1-MeV electron fluence as a function of shield density-thickness product is shown in Figure 3-80 for the specified three-year mission duration.

Figure 3-81 shows a similar curve for the geosynchronous mission. In this case, the specified three-year mission solar flare proton energy spectra was combined with the five-year trapped electron energy spectra to yield the DENI 1-MeV electron fluence.

The DENI 1-MeV electron fluence for the manned space station mission is shown in Figure 3-82. The lower curve reflects the trapped particle effect over the 10-year period. The upper curve includes the solar flare proton environment from Figure 3-10. Also shown on Figure 3-82 are comparison points from the Lockheed space station solar array study.

Table 3-23 is a reproduction of a summary table from Reference 5. The comparison data points, as indicated in Table 3-23, are from the column labeled 10 years, Trapped + Solar Flare, Webber and are for the 300 nm (555 km), 55 degree inclination orbit. There is very good agreement between these Lockheed data points and the upper curve of Figure 3-82.

The degradation of N/P silicon solar cell electrical characteristics as a function of normally incident 1-MeV electron fluence is given by the curves in Appendix B.

#### 3.4.1.3 Results of Trade Studies

The first part of this analysis consists of the evaluation of blanket mass for a solar array system which is sized to provide 10,000 watts of initial output at 1 AU and 55°C. These initial 10,000 watt systems were investigated for various allowable maximum power degradations due to the particle radiation environment associated with each mission type. Table 3-24 shows the summary of this analysis for the interplanetary mission. Solar cells with two base resistivities and with nominal thicknesses of 200, 150, 125, and 100  $\mu\text{m}$  were evaluated. Table 3-25 lists the assumed solar cell beginning-of-life (BOL) maximum power output at 1 AU, 55°C.

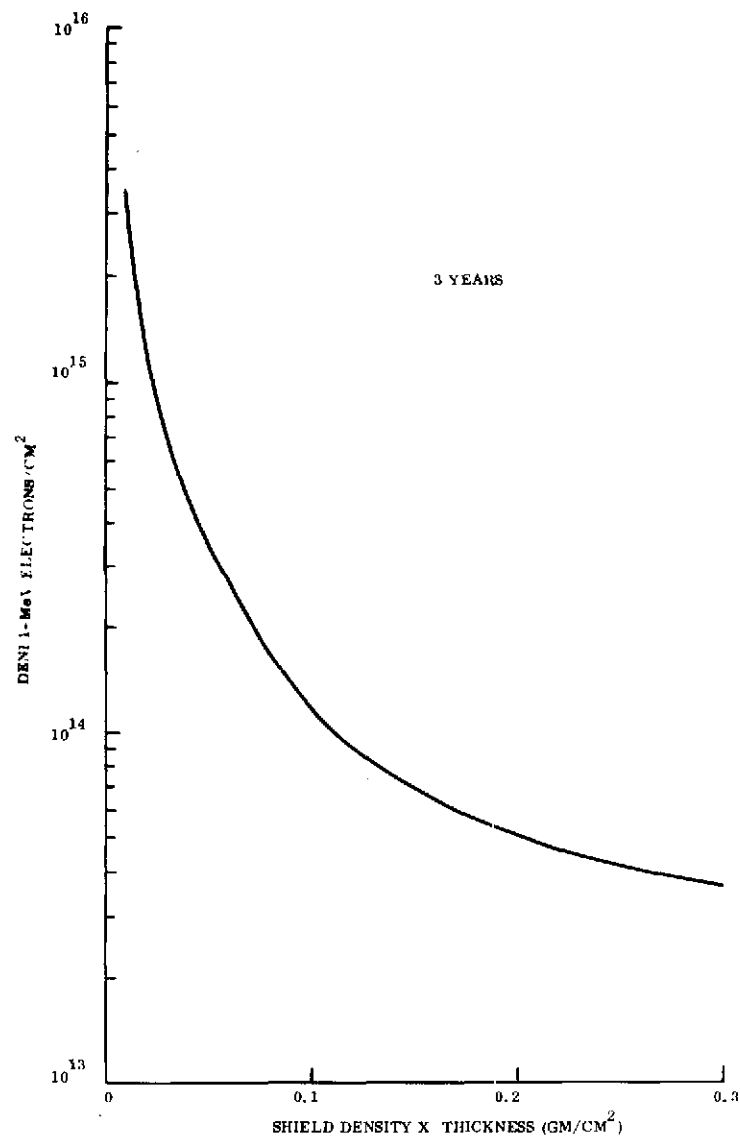


Figure 3-80. Damage Equivalent-Normally Incident (DENI) 1-MeV Electron Fluence with Infinite Backshielding for Interplanetary Mission

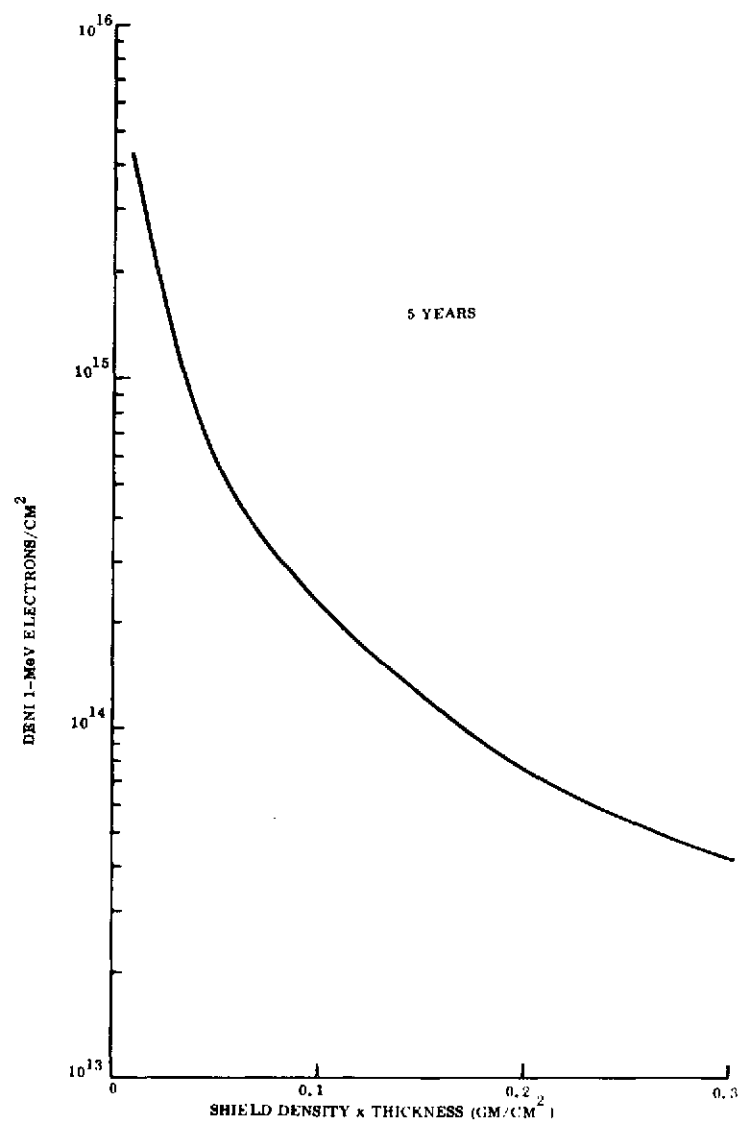


Figure 3-81. Damage Equivalent-Normally Incident (DENI) 1-MeV Electron Fluence with Infinite Backshielding for Geosynchronous Mission

Table 3-23. Equivalent 1-MeV Electron Fluences for N/P Type Silicon Solar Cells in Low Altitude Circular Orbits in the Time Period 1977 - 1990

(From Reference 5)

Mission Duration			5 years <sup>b</sup>			10 years			2.5 years <sup>b</sup>		
Inclination	Altitude	Equiv. SiO <sub>2</sub> Shield Thick. (mils)	Trapped Only	Trapped + Solar Flare		Trapped Only	Trapped + Solar Flare		Trapped Only	Trapped + Solar Flare	
				Bailey	Webber		Bailey	Webber		Bailey	Webber
			$\Phi_{eq}^a$ (e/cm <sup>2</sup> )	$\Phi_{eq}^a$ (e/cm <sup>2</sup> )	$\Phi_{eq}^a$ (e/cm <sup>2</sup> )	$\Phi_{eq}^a$ (e/cm <sup>2</sup> )	$\Phi_{eq}^a$ (e/cm <sup>2</sup> )	$\Phi_{eq}^a$ (e/cm <sup>2</sup> )	$\Phi_{eq}^a$ (e/cm <sup>2</sup> )	$\Phi_{eq}^a$ (e/cm <sup>2</sup> )	$\Phi_{eq}^a$ (e/cm <sup>2</sup> )
90	200	3	4.3	27	11	8.6	31	15	2.1	25	8.3
		6	1.9 <sup>a</sup>	13	6.2	3.8	15	8.1	.96	12	5.2
		12 <sup>d</sup>	.86	5.7	3.5	1.7	6.6	4.4	.43	5.3	3.1
		15.7 <sup>c</sup>	.64	4.1	2.7	1.3	4.7	3.4	.32	3.8	2.4
	300	3	14	37	20	28	51	31	7.1	30	13
		6	6.8	18	11	14	25	18	3.4	15	7.6
		12	3.3	8.2	5.9	6.6	11	9.2	1.6	6.5	4.3
		15.7	2.4	5.9	4.5	4.3	8.3	6.9	1.2	4.7	3.3
55 <sup>c</sup>	200	3	5.2	28	11	10	33	17	2.6	25	8.5
		6	2.6	14	6.5	5.2	17	9.4	1.3	13	5.5
		12	1.2	6.1	3.8	2.4	7.3	5	.60	5.5	3.2
		15.7	.87	4.3	3.0	1.7	5.2	3.8	.43	3.9	2.5
	300	3	18	41	24	36	59	42	9.1	32	15
		6	9.1	21	13	18	39	22	4.6	16	8.8
		12	4.4	9.3	7.0	8.8	14	11	2.2	7.1	4.8
		15.7	3.3	6.7	5.4	6.6	10	8.7	1.6	5.1	3.7
28.5	200	3	1.4	1.4	1.4	2.8	2.8	2.8	.69	.69	.69
		6	.66	.66	.66	1.3	1.3	1.3	.33	.33	.33
		12	.36	.36	.36	.72	.72	.72	.18	.18	.18
		15.7	.30	.30	.30	.30	.60	.60	.15	.15	.15
	300	3	13	13	13	25	25	25	6.3	6.3	6.3
		6	7.1	7.1	7.1	14	14	14	3.5	3.5	3.5
		12	4.0	4.0	4.0	8.1	8.1	8.1	2.0	2.0	2.0
		15.7	3.3	3.3	3.3	6.6	6.6	6.6	1.6	1.6	1.6

<sup>a</sup>Note that the values for  $\Phi_{eq}$  are in units of  $10^{13}$  1 MeV electrons/cm<sup>2</sup>.

<sup>b</sup>Solar Flare contribution for worst case 2.5 and 5 year mission beginning in 1977.

<sup>c</sup>This value is for a 12 mil cell thickness and a 3 mil equiv. thickness for the cell backing.

<sup>d</sup>This value is slightly greater than the actual (11.57) thickness for an 8 mil cell thickness.

<sup>e</sup>For this inclination orbit the solar flare contribution may be small. Values quoted are for 65° or greater inclination and are upper limits.

NOT REPRODUCIBLE

Table 3-24. Solar Cell Blanket Weight Tradeoff for Interplanetary Mission

Solar Cell Base Resistivity (ohm-cm)	Allowable Maximum Power Degradation (% of original)	Solar Cell Thickness ( $\mu\text{m}$ )	Solar Cell Area Required for 10,000 watts B.O.L., 55°C ( $\text{m}^2$ )	Total DENI 1-MeV Electron Fluence ( $\times 10^{14} \text{ e/cm}^2$ )	Front and Back Shield ( $\text{gm/cm}^2$ )	Blanket Mass (kg)
2	20	200	71.3	8.4	.044	105.0
		150	74.0	13.3	.032	82.7
		125	76.4	18.0	.026	71.7
		100	79.3	23.0	.022	63.6
	25	200	71.3	14.5	.030	84.4
		150	74.0	22.5	.023	69.0
		125	76.4	30.5	.018	59.2
		100	79.3	38.0	.016	53.8
	30	200	71.3	25.0	.020	69.8
		150	74.0	38.0	.016	58.4
		125	76.4	50.0	.013	51.3
		100	79.3	61.0	.011	45.7
	35	200	71.3	42.0	.014	61.0
		150	74.0	60.0	.011	50.8
		125	76.4	80.0	.009	45.1
		100	79.3	98.0	.007	39.2
10	20	200	78.6	13.0	.032	96.3
		150	84.2	22.0	.022	76.8
		125	88.3	33.5	.017	66.6
		100	93.8	48.0	.013	57.9
	25	200	78.6	24.5	.021	78.5
		150	84.2	43.0	.014	63.0
		125	88.3	64.0	.011	55.7
		100	93.8	90.0	.009	48.2
	30	200	78.6	45.0	.014	67.2
		150	84.2	83.0	.009	54.3
		125	88.3	120.0	.007	46.6
		100	93.8	160.0	.004	40.5
	35	200	78.6	83.0	.009	59.1
		150	84.2	150.	----	----
		125	88.3	220.	----	----
		100	93.8	290.	----	----

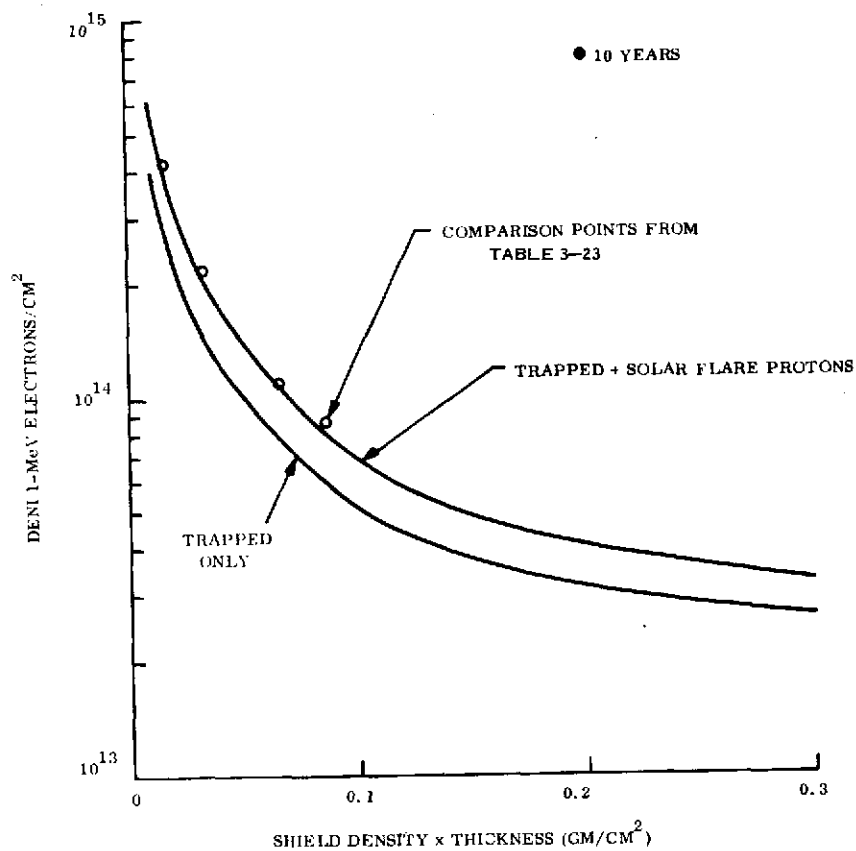


Figure 3-82. Damage Equivalent-Normally Incident (DENI) 1-MeV Electron Fluence with Infinite Backshielding for Manned Space Station Mission

Table 3-25. Baseline Solar Cell Maximum Power Output

Nominal Cell Thickness (μm)	Average Cell Mass (gm/cell)	Covered Cell Maximum Power Output @ BOL, 1 AU, 55°C (Watts/Cell)	
		2 ohm-cm	10 ohm-cm
200	0.194	0.0578	0.0525
150	0.151	0.0557	0.0490
125	0.129	0.0540	0.0467
100	0.107	0.0520	0.0440

Thus, the total solar cell area required to produce 10,000 watts at BOL is shown in Column 4 of Table 3-24. A 3 percent solar array fabrication loss, which accounts for cell mismatch and the series resistance of module interconnects, has been used. Bus strip distribution losses have not been included in this calculation so the 10,000 watt capability should be considered as measured at the module level. The total DENI 1-MeV electron fluence required to produce the allowable maximum power degradation was obtained from Figure B-3 and B-6 of Appendix B for 2 ohm-cm and 10 ohm-cm base resistivities, respectively. The shield factor ( $\text{gm}/\text{cm}^2$ ) required to limit the DENI 1-MeV electron fluence to this value is obtained from Figure 3-80 and is given in Column 5 of Table 3-24 based on the assumption that the front and back shield factors are equal. The solar cell blanket mass is calculated as follows:

$$W_b = A_c [2.5 (W_c + W_I) + 10. (1 + F_p) W_s] \quad (3.4-1)$$

where:

$$\begin{aligned} W_b &= \text{Mass of solar cell blanket (kg)} \\ W_c &= \text{Mass of solar cell (gm/cell)} \\ W_I &= \text{Mass of interconnectors and solder} = 0.033 \text{ gm/cell}^* \\ A_c &= \text{Solar cell area required from Column 4 (m}^2\text{)} \\ W_s &= \text{Front and back shield factor (gm/cm}^2\text{)} \\ F_p &= \frac{\text{Solar cell blanket module area}}{\text{Solar cell area}} = 1.055 \end{aligned}$$

This mass does not include the bus strip distribution network on the blanket and assumes that the back shield covers the complete module area of the blanket. The data contained in Table 3-24 is plotted in Figure 3-83 where the solar cell blanket mass is shown as a function of percent allowable maximum power degradation due to the particle radiation environment for

---

\*Note that solder is not used in recommended baseline design approach.

the various solar cell thicknesses and base resistivities. In the graphical presentation of the data, blanket masses for front and back shield factors of less than  $0.008 \text{ gm/cm}^2$  have been disallowed. This minimum shield factor, which is equivalent to a  $25 \mu\text{m}$  integral coverglass or  $50 \mu\text{m}$  of Kapton-H film, is considered necessary for low energy proton protection. Table 3-26 shows this minimum blanket mass for each cell type and thickness.

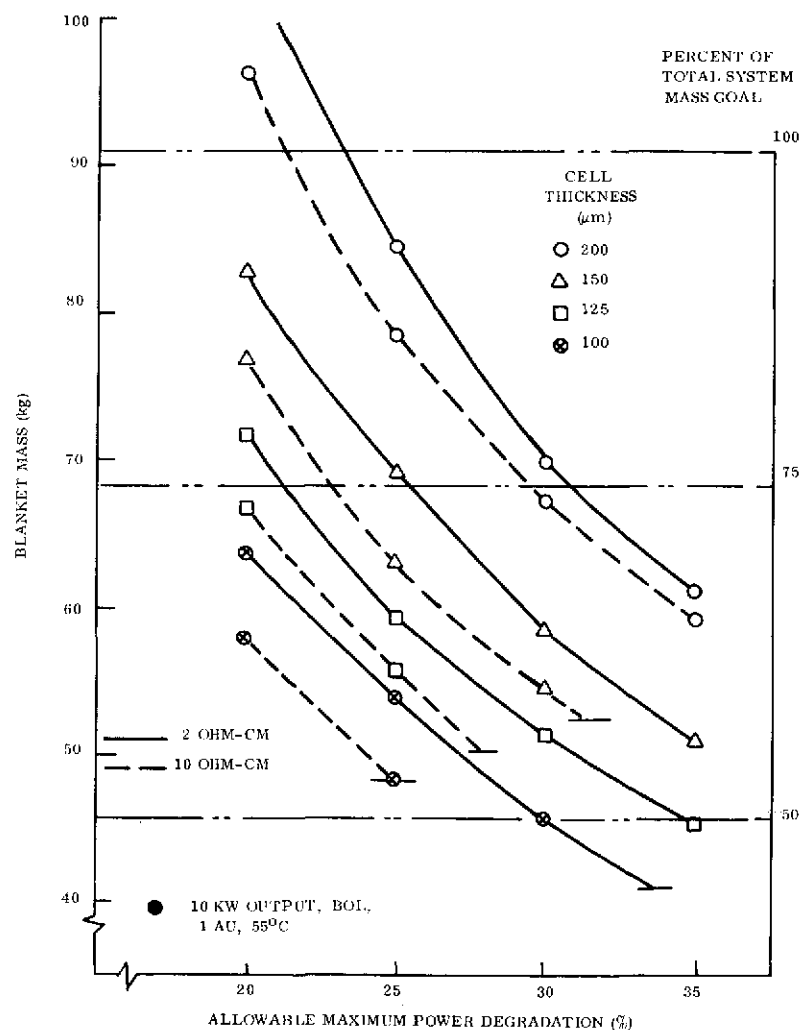


Figure 3-83. Solar Cell Blanket Mass for Interplanetary Mission (10 kW, BOL Output)



Table 3-26. Minimum Possible Blanket Mass for 10,000 Watts, BOL, 1 AU, 55°C

Solar Cell Base Resistivity (ohm-cm)	Nominal Cell Thickness ( $\mu\text{m}$ )	Cell Area Required ( $\text{m}^2$ )	*Minimum Blanket Mass-to-Area Ratio ( $\text{kg}/\text{m}^2$ )	Minimum Blanket Mass (kg)
2	200	71.3	0.732	52.2
	150	74.0	0.624	46.2
	125	76.4	0.569	43.5
	100	79.3	0.514	40.8
10	200	78.6	0.732	57.5
	150	84.2	0.624	52.5
	125	88.3	0.569	50.2
	100	93.8	0.514	48.2

\*Based on a minimum front and back shield factor of  $0.008 \text{ gm}/\text{cm}^2$

For the geosynchronous mission, the trade study results are summarized in Table 3-27 and plotted in Figure 3-84. The calculation procedure is identical to that described above for the interplanetary mission with the exception that the required front and back shield factors are obtained from Figure 3-81.

Table 3-28 summarizes the results for the manned space station mission. Note that the range of allowable maximum power degradations has been shifted to correspond to the reduced particle radiation environment for this mission. The required front and back shield factor is obtained from Figure 3-82. The results are plotted in Figure 3-85.

Table 3-27. Solar Cell Blanket Mass Tradeoff for Geosynchronous Mission

Solar Cell Base Resistivity (ohm-cm)	Allowable Maximum Power Degradation (% of original)	Solar Cell Thickness ( $\mu\text{m}$ )	Solar Cell Area Required for 10,000 watts B.O.L., 55°C ( $\text{m}^2$ )	Total DENI 1-MeV Electron Fluence ( $\times 10^{14} \text{ e/cm}^2$ )	Front and Back Shield ( $\text{gm/cm}^2$ )	Blanket Mass (kg)
2	20	200	71.3	8.4	.064	134.3
		150	74.0	13.3	.046	104.0
		125	76.4	18.0	.038	90.6
		100	79.3	23.0	.033	81.5
	25	200	71.3	14.5	.044	105.0
		150	74.0	22.5	.033	84.2
		125	76.4	30.5	.027	73.3
		100	79.3	38.0	.023	65.3
	30	200	71.3	25.0	.031	85.9
		150	74.0	38.0	.023	69.0
		125	76.4	50.0	.0185	60.0
		100	79.3	61.0	.015	52.2
	35	200	71.3	42.0	.021	71.2
		150	74.0	60.0	.016	58.4
		125	76.4	80.0	.011	48.2
		100	79.3	98.0	.009	42.4
10	20	200	78.6	13.0	.047	120.5
		150	84.2	22.0	.034	97.6
		125	88.3	33.5	.025	81.1
		100	93.8	48.0	.019	69.4
	25	200	78.6	24.5	.031	94.7
		150	84.2	43.0	.021	75.1
		125	88.3	64.0	.015	63.0
		100	93.8	90.0	.009	50.2
	30	200	78.6	45.0	.020	76.9
		150	84.2	83.0	.0105	56.9
		125	88.3	120.0	.007	48.5
		100	93.8	160.0	.005	42.5
	35	200	78.6	83.0	.011	62.4
		150	84.2	150.0	----	----
		125	88.3	220.0	----	----
		100	93.8	290.0	----	----

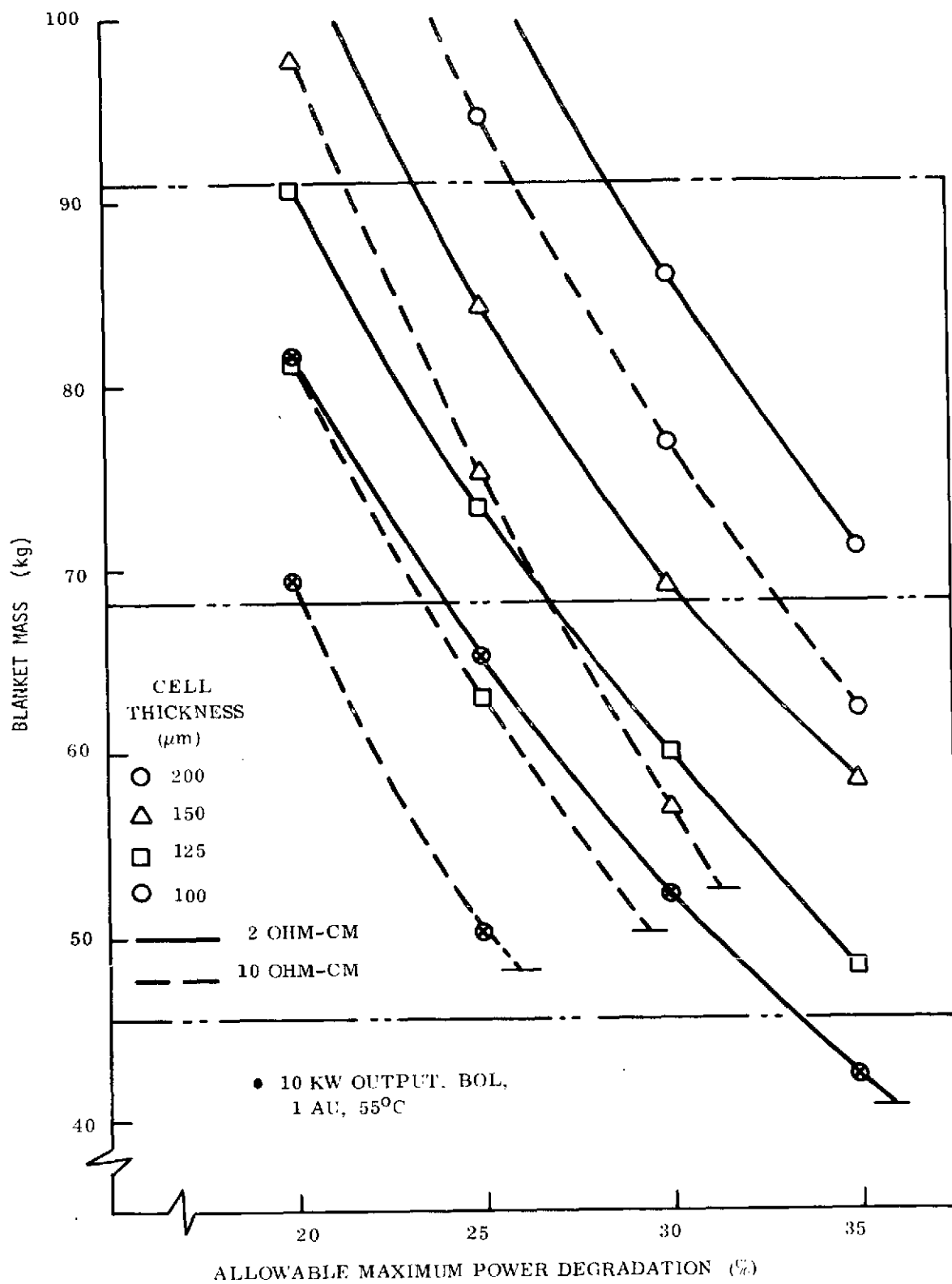


Figure 3-84. Solar Cell Blanket Mass for Geosynchronous Mission (10 kW, BOL Output)

Table 3-28. Solar Cell Blanket Mass Tradeoff for  
Manned Space Station Mission

Solar Cell Base Resistivity (ohm-cm)	Allowable Maximum Power Degradation (% of original)	Solar Cell Thickness ( $\mu\text{m}$ )	Solar Cell Area Required for 10,000 watts B.O.L., 55°C ( $\text{m}^2$ )	Total DENI 1-MeV Electron Fluence ( $\times 10^{14}$ e/cm $^2$ )	Front and Back Shield (gm/cm $^2$ )	Blanket Mass (kg)
2	5	200	71.3	0.9	.168	286.6
		150	74.0	1.8	.077	151.1
		125	76.4	2.2	.065	133.0
		100	79.3	2.8	.051	110.9
	10	200	71.3	2.3	.062	131.3
		150	74.0	4.0	.034	85.8
		125	76.4	5.4	.024	68.6
		100	79.3	6.9	.020	60.3
	15	200	71.3	4.6	.030	84.4
		150	74.0	7.7	.017	59.9
		125	76.4	10.5	.012	49.8
		100	79.3	13.1	.009	42.4
	20	200	71.3	8.4	.016	64.0
		150	74.0	13.5	.009	47.7
		125	76.4	18.0	.006	40.3
		100	79.3	23.0	----	----
10	5	200	78.6	1.35	.103	211.0
		150	84.2	2.25	.063	147.8
		125	88.3	3.7	.037	102.9
		100	93.8	6.0	.022	75.2
	10	200	78.6	3.3	.042	112.5
		150	84.2	5.3	.026	83.7
		125	88.3	8.6	.016	64.8
		100	93.8	13.0	.009	50.2
	15	200	78.6	6.8	.020	76.9
		150	84.2	11.0	.011	57.8
		125	88.3	17.5	.006	46.6
		100	93.8	26.0	.003	38.6
	20	200	78.6	13.0	.009	59.1
		150	84.2	22.0	.005	47.4
		125	88.3	33.0	----	----
		100	93.8	48.0	----	----

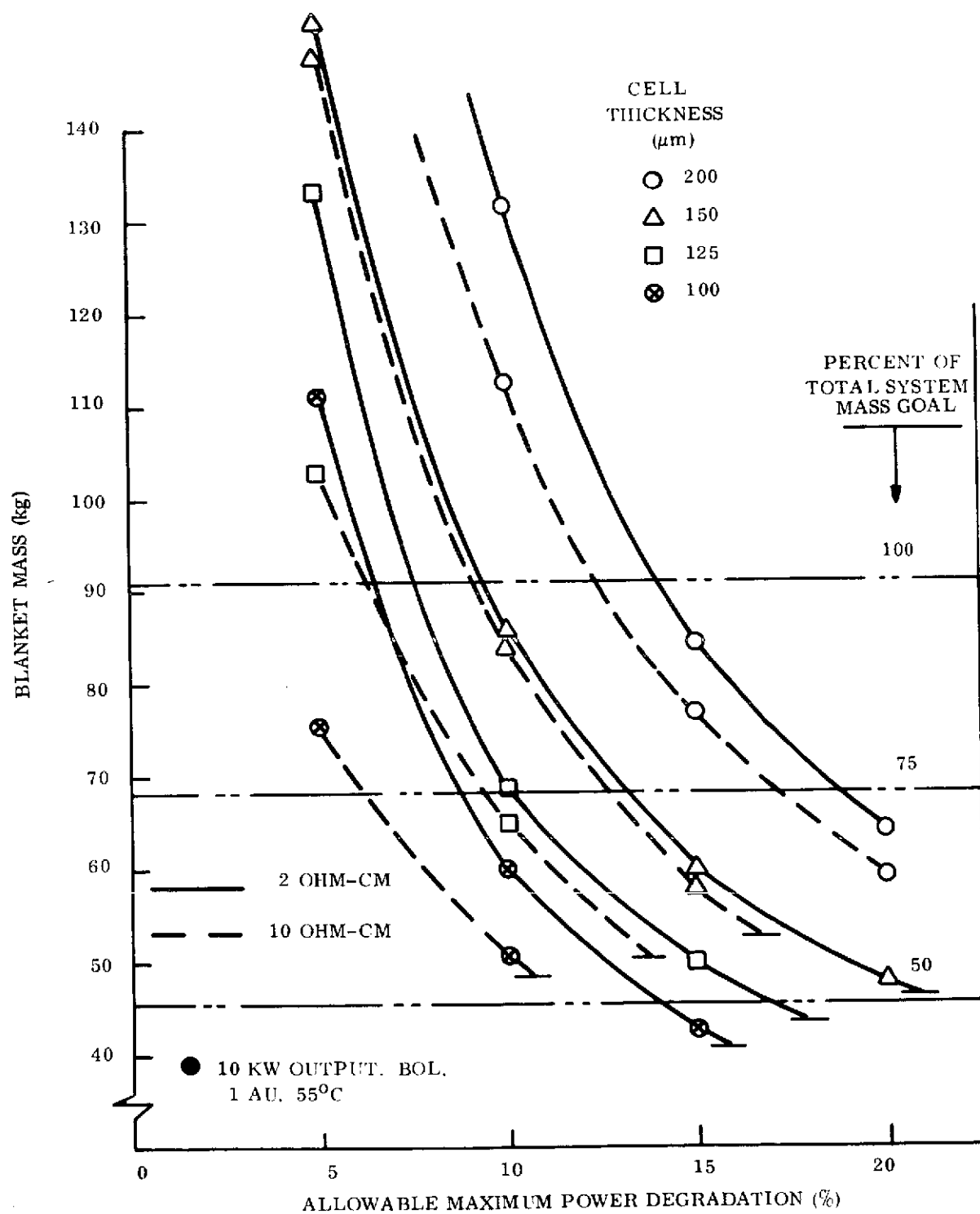


Figure 3-85. Solar Cell Blanket Mass for Manned Space Station Mission (10 kW, BOL Output)

The second part of this analysis consisted of an evaluation of the blanket mass for a specified end-of-life (EOL) power output capability with no restriction on the BOL power output (or allowable maximum power degradation). The results of this analysis are shown in Figures 3-86, 3-87, and 3-88 for the interplanetary, geosynchronous and manned space station missions, respectively. In each of these figures, the blanket mass, solar cell area, and fraction of original maximum power remaining are plotted as a function of front and back shield factor. The EOL power output is assumed to be 7,500 watts for all missions.

#### 3.4.1.4 Discussion of Results

If the initial solar array output power of 10,000 watts is coupled with an allowable maximum power degradation over the mission duration, the results of the first part of this study are as summarized in Figures 3-89 and 3-90, for 100 $\mu$ m and 125 $\mu$ m thick cells, respectively. These curves were generated from the data presented in Figures 3-83, 3-84 and 3-85. For the interplanetary mission (see Figure 3-89), the minimum blanket mass is obtained with 10 ohm-cm cells as the allowable maximum power degradation is increased from 20 percent to 25 percent. At a blanket mass of 48.2 kg, the front and back shields have reached the maximum allowable shield factor of 0.008 gm/cm<sup>2</sup>. At this point, it is not possible to reduce the blanket mass until the 2 ohm-cm base resistivity curve is reached. As the allowable maximum power degradation is increased further, the blanket mass can be decreased until the minimum mass for these 2 ohm-cm cells is reached at 40.8 kg. This is the absolute minimum blanket mass possible without considering cells thinner than 100 $\mu$ m.

The curve for the geosynchronous mission (see Figure 3-89) is basically the same as for the interplanetary mission except that the permissible maximum power degradation for a given blanket mass must be increased slightly because of the more severe particle radiation environment in the geosynchronous mission. For example, with the 100  $\mu$ m thick, 10 ohm-cm cell, a 26 percent allowable maximum power degradation is required for a 48.2 kg blanket mass. This is approximately one percentage point greater than required for the interplanetary mission. Expressed in different terms for an allowable maximum power degradation of 25 percent, the geosynchronous mission blanket would be approximately 2 kg heavier than required for the interplanetary mission using 100  $\mu$ m thick, 10 ohm-cm

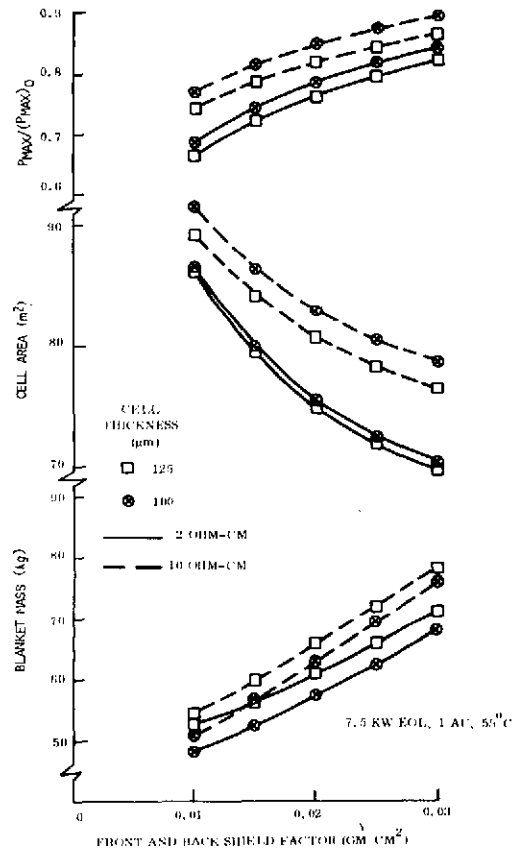


Figure 3-86. Solar Cell Blanket Trade-off for Interplanetary Mission (7.5 kW, EOL Output)

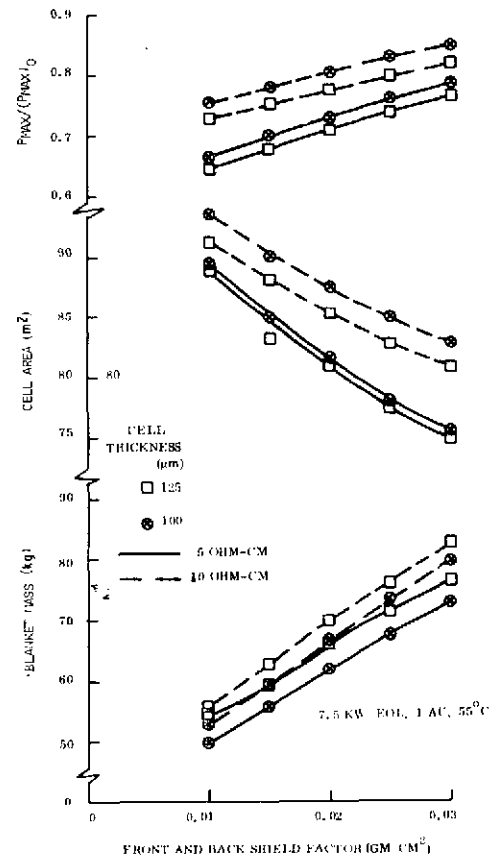


Figure 3-87. Solar Cell Blanket Trade-off for Geosynchronous Mission (7.5 kW, EOL Output)

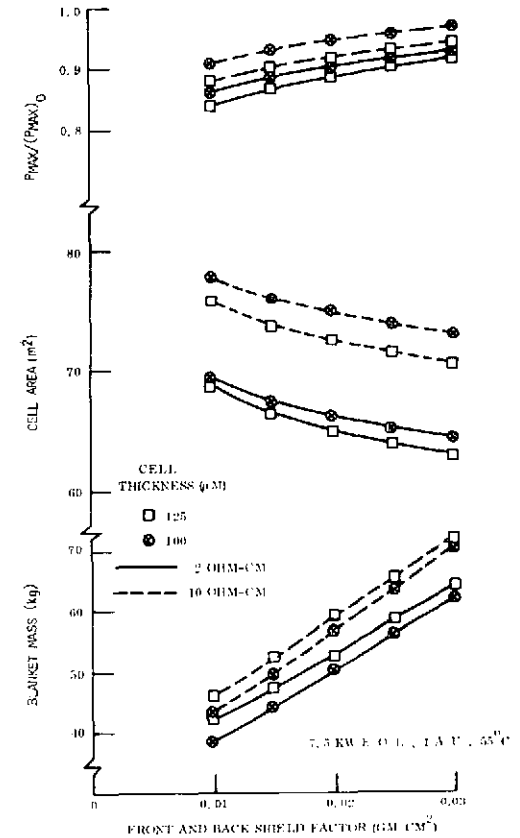


Figure 3-88. Solar Blanket Trade-off for Manned Space Station Mission (7.5 kW, EOL Output)

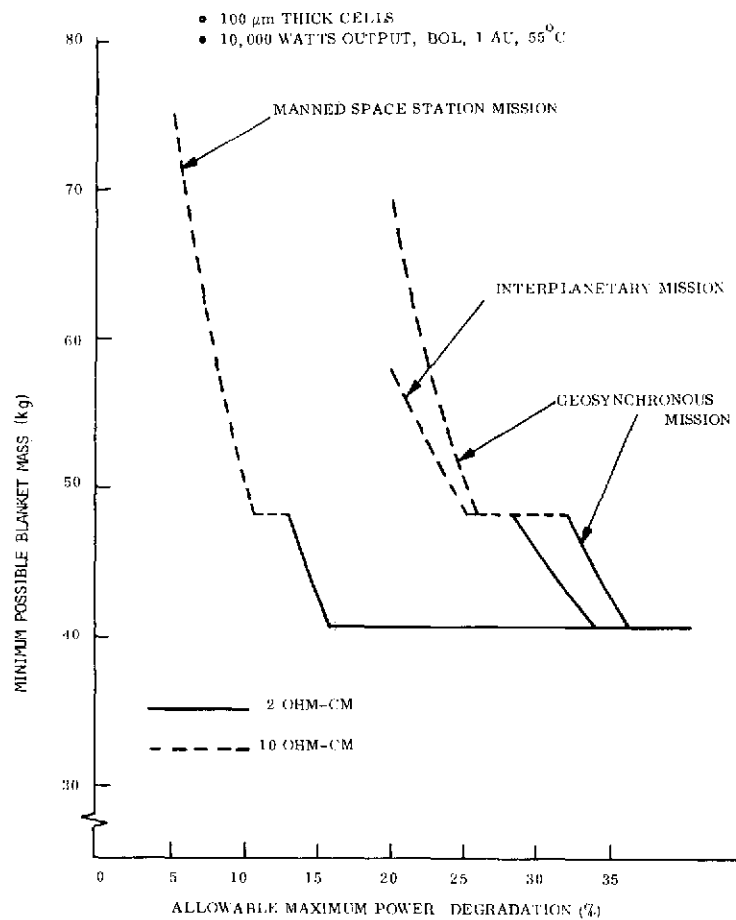


Figure 3-89. Minimum Possible Blanket Mass for 100  $\mu\text{m}$  Thick Cells

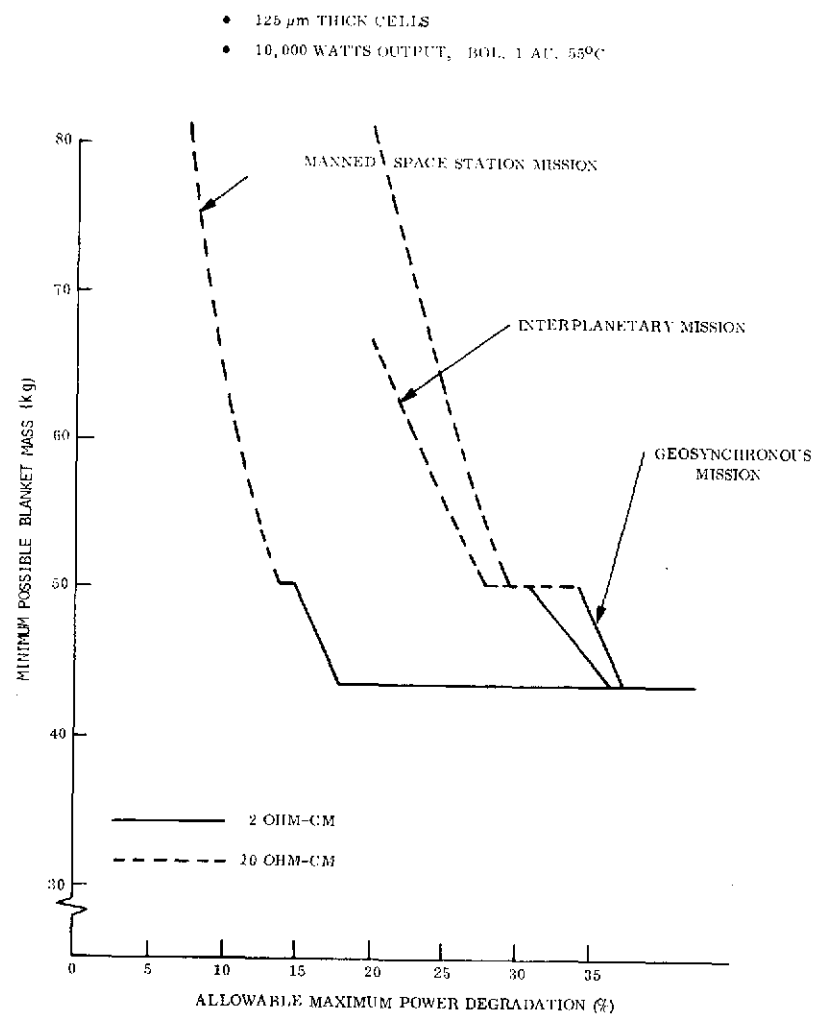


Figure 3-90. Minimum Possible Blanket Mass for 125  $\mu\text{m}$  Thick Cells



cells. For the manned space station mission, the lowest possible blanket mass of 40.8 kg can be achieved with 100  $\mu\text{m}$  thick, 2 ohm cells if the allowable maximum power degradation is specified as 16 percent or greater.

Figure 3-90 shows a similar set of curves for 125  $\mu\text{m}$  thick cells. Cell thicknesses greater than 125  $\mu\text{m}$  are not presented here because it is unlikely that the system power-to-mass goal can be realized with cells which are thicker than 125  $\mu\text{m}$ , regardless of the allowable maximum power degradation.

The second part of the trade study, which evaluated the blanket mass for a specified EOL power capability, yielded the results shown in Figures 3-86, 3-87 and 3-88. These curves show that the minimum blanket mass is achieved with 100  $\mu\text{m}$  thick, 2 ohm-cm cells. For the interplanetary and geosynchronous missions, the difference between 2 ohm-cm and 10 ohm-cm base resistivities is not great for lightly shielded, low weight blanket constructions.

Thus, the trade-off between base resistivities should be made based on other factors which depend on overall power subsystem requirements including load power demand profile. For some missions it may be desirable to limit the maximum power degradation to some upper limit. For a dissipative type shunt voltage regulator and a constant average load power demand, increased maximum power degradation results in the need for greater power dissipation capability at the beginning-of-life. On the other hand, if the load can use the integrated energy available over the life of the mission, then the selection of the lower base resistivity will give the highest integrated solar array output for a specified end-of-life power capability.

For the manned space station mission, the choice is more clearly directed toward 2 ohm-cm base resistivity.

### 3.4.2 PARAMETRIC ANALYSIS OF BUS STRIP DISTRIBUTION SYSTEM

#### 3.4.2.1 General

The mass of the bus strip network required to distribute the solar cell module current from the generation site on the blanket to the inboard end of the blanket is a significant factor which must be considered in the design of a 110 watt/kg solar array. The power dissipation in the bus strip distribution system must be compensated for by increased generating capability if a specified power output is to be delivered at the interface of the solar array with the remainder of the power subsystem. The use of low resistance conductors, with the associated mass penalty, will reduce the distribution power losses thereby reducing the extra generating capability required to supply these losses. On the other hand, higher resistance, lower mass conductors will increase the distribution power losses thereby increasing the extra generating capability required to supply these losses. Thus, an optimum power loss and associated bus strip mass should exist for a given set of design conditions.

The purpose of this analysis is to define this optimum bus strip power loss and associated bus strip mass required for solar array configurations which meet the requirements for this feasibility study and have the potential for meeting the 110 watt/kg power-to-mass ratio goal.

#### 3.4.2.2 Method of Analysis

The method of analysis follows the mathematical procedures described by J. Roger in Reference 60. A similar analysis, with specific application to the 30 watt/lb roll-up array, is discussed in Reference 66. For this analysis, it is assumed that the circuits are arranged on the two solar cell blankets as shown in Figure 3-91. All circuits ( $n$  per solar cell blanket, or  $2n$  for the total solar array panel) are identical and each supplies the full voltage,  $V$ , to the bus. Each circuit is assumed to have separate positive and negative bus strips which run down to the base of the blanket. All bus strip conductors are sized to have the same voltage drop,  $\Delta V$ . The power at the terminals of each blanket are given by:

$$n (V - \Delta V) i = (V - \Delta V) I \quad (3.4-2)$$

where  $I = ni$  is the total current from one blanket.

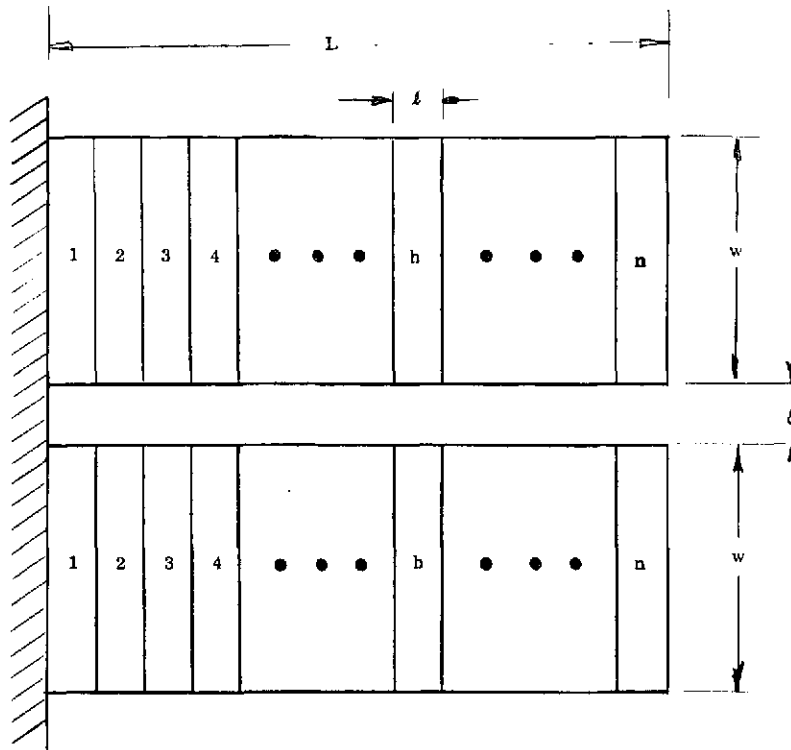


Figure 3-91. Schematic of Solar Cell Blanket Circuit Configuration

Based on the derivation in Reference 60, the total bus strip mass for the solar array panel (both solar cell blankets) is given by:

$$W_b = \frac{4\rho d \bar{w} \ell^2}{3\alpha V^2} n(n+1)(2n+1) \quad (3.4-3)$$

- where:  $\rho$  = resistivity of the bus strip conductors [ohm-m]
- $d$  = density of the bus strip conductor material including allowance for the insulation [kg/m<sup>3</sup>]
- $V$  = circuit operating voltage measured at the circuit terminals [volts]
- $\bar{w}$  = nominal power output from one circuit [watts]
- $\ell$  = dimension of one circuit along the length of the blanket [m]
- $\alpha$  = fraction of circuit voltage (or power) loss in bus strips
- =  $\frac{\Delta V}{V} = \frac{\Delta P}{P}$

The total mass of the solar array panel is given by:

$$W_t = S f_s + W_b \quad (3.4-4)$$

where

$$\begin{aligned} S &= \text{total solar array panel area [m}^2\text{]} \\ &= 2Lw \\ f_s &= \text{system mass-to-area ratio including the mass of solar cell} \\ &\quad \text{blankets, deployment and stowage mechanisms and structures} \\ &\quad \text{[kg/m}^2\text{]}. \end{aligned}$$

By defining

$$m = \frac{2\rho d\bar{w}\ell}{3V_w^2} (n+1)(2n+1) \quad (3.4-5)$$

Equation (3.4-3) becomes

$$W_b = \frac{mS}{\alpha}$$

The figure of merit of the solar array panel, in terms of power delivered to the interface per unit mass is:

$$p = \frac{(1-\alpha)P}{S f_s + \frac{mS}{\alpha}} = \frac{\alpha(1-\alpha)s}{\alpha f_s + m} \quad (3.4-6)$$

where  $s$  = system power-to-area ratio with the power measured at the circuit level [watt/m<sup>2</sup>]

The optimum value of  $\alpha$ , defined as  $\alpha_o$ , is obtained by setting the derivative of equation (3.4-6), with respect to  $\alpha$ , equal to zero. Thus, this optimum value of  $\alpha$  is given by:

$$\alpha_o = \frac{m}{f_s} \left[ \sqrt{1 + \frac{f_s}{m}} - 1 \right] \quad (3.4-7)$$

At this optimum value of voltage drop, we can write:

$$m_o = \frac{\alpha_o^2 f_s}{1 - 2\alpha_o}$$

$$W_{bo} = \frac{\alpha_o S f_s}{1 - 2\alpha_o} \quad (3.4-8)$$

$$p_o = \frac{P(1 - 2\alpha_o)}{S f_s}$$

### 3.4.2.3 Results of Analysis

The general analysis approach described above was utilized to study the bus strip mass associated with a solar array panel which produces 10,000 watts with the power-to-mass ratio of at least 110 watt/kg. For this analysis, the two solar cell blankets per panel are mounted with 100  $\mu$ m thick, 10 ohm-cm bottom wrap-around contact solar cells. The total blanket mass (not including distribution bus strips) is 48.2 kg based on the analysis in Section 3.4 1. The required area of solar cells is 93.8 m<sup>2</sup>. Assuming a packing factor of 1.055, the total blanket module area is equal to 99.0 m<sup>2</sup>. The aspect ratio of the blanket,  $R_b$ , defined as L/w, has a significant effect on the bus strip weight and will be used as a parameter in this analysis.

The bus strip conductors were assumed to be copper with a resistivity,  $\rho$ , equal to  $1.724 \times 10^{-8}$  ohm-m at 20°C. With a temperature coefficient of resistance at 20°C of 0.00393, the resistivity of the copper at 55°C is  $1.960 \times 10^{-8}$  ohm-m. The bus strips are composed of copper foil conductors with Kapton-H film insulating layers. The equivalent density of this composite was derived based on the assumption that the copper strip and the Kapton insulator are the

same width and the thickness of the copper is 1.5 times the thickness of the insulator. With those assumptions, the equivalent density,  $d$ , is given by:

$$\begin{aligned} d &= d_{\text{cu}} + 2/3 d_k \\ &= 8940 + 2/3 (1420) = 9900 \text{ kg/m}^3 \end{aligned}$$

where

$$\begin{aligned} d_{\text{cu}} &= \text{density of copper} = 8940 \text{ kg/m}^3 \\ d_k &= \text{density of Kapton-H film} = 1420 \text{ kg/m}^3 \end{aligned}$$

The system mass-to-area ratio,  $f_s$ , is assumed to be approximately given by:

$$f_s = \frac{10,000}{110 (99.0)} = 0.92 \text{ kg/m}^2$$

By substitution of appropriate values into equation (3.4-5), the parameter  $m$  is represented by:

$$m = \frac{2 (1.960 \times 10^{-8}) (9900) (5,000) L (n+1) (2n+1)}{3V^2 wn^2}$$

If the value of  $m$  is substituted into equation (3.4-7), the optimum value of power loss,  $\alpha_o$ , is as plotted in Figure 3-92 as a function of circuit voltage,  $V$ . Four different values of blanket aspect ratio, as well as three values of  $n$  have been plotted to show the affect of these variables. Figure 3-93 shows the total bus strip mass ( $W_{bo}$  from equation (3.4-8)) at the optimum power loss as a function of the circuit voltage,  $V$ . The number of circuits per blanket,  $n$ , has been selected as 10 for this presentation, but the same four blanket aspect ratios are plotted.

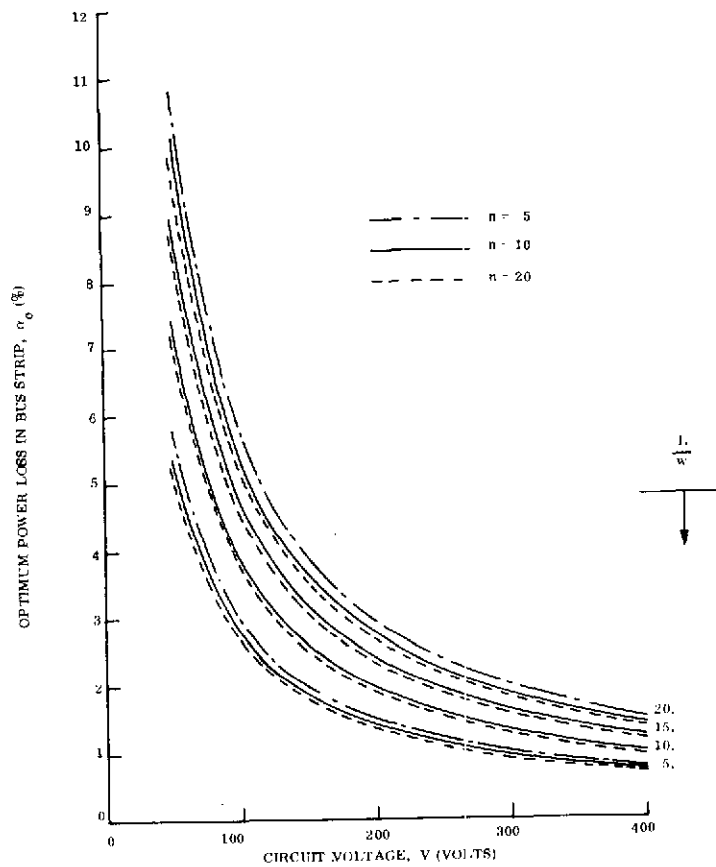


Figure 3-92. Optimum Bus Strip Power Loss vs Voltage

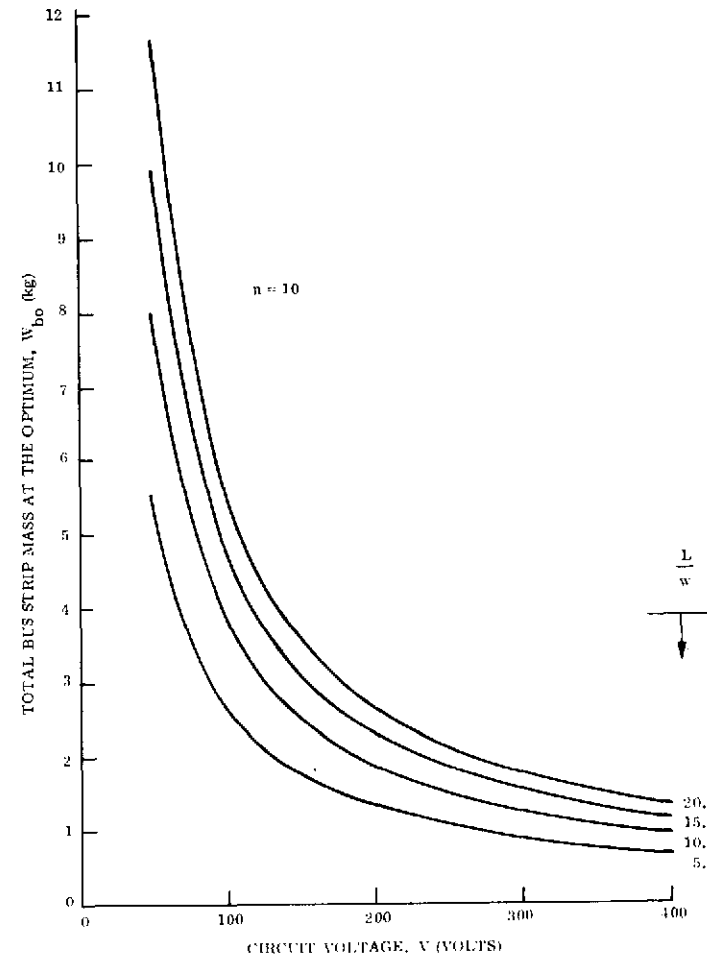


Figure 3-93. Total Bus Strip Mass at the Optimum vs Voltage

In Table 3-29, the constituents of the total blanket mass are summarized based on the previous analysis. Column 3 is the optimum power loss from Figure 3-92 for a value of  $n = 10$ . Column 4 is the solar cell area required to produce 10,000 watts output at beginning-of-life, 1 AU and  $55^{\circ}\text{C}$ . This output is measured at the interface and includes the power losses in the bus strip distribution network. The blanket mass in Column 5 is based on the use of 100  $\mu\text{m}$  thick, 10 ohm-cm bottom wraparound contact cells with a minimum front and back shielding of  $0.008 \text{ gm/cm}^2$ . The bus strip mass in Column 6 is from Figure 3-93 with a proportionate increase to reflect the increased solar cell blanket area necessary to make up for the power loss in the bus strips. The total blanket mass from Column 7 is plotted in Figure 3-94 as a function of blanket aspect ratio,  $L/w$ .

### 3.4.3 PLANAR SOLAR ARRAY ASPECT RATIO TRADE STUDY

#### 3.4.3.1 Introduction

Parametric studies which relate total system weight to aspect ratio were performed to determine the optimum solar array geometry for a specified minimum deployed frequency requirement. The first part of this task consisted of determining the minimum boom bending stiffness and blanket tension required to meet the frequency requirement.

#### 3.4.3.2 Optimum Boom and Blanket Tension Analysis

Two deployable boom configurations were considered in this trade study. The first is a continuous fiberglass longeron ASTROMAST. The second configuration uses a steel BI-STEM boom with a  $D/t$  ratio of 200 and an overlap factor of 0.90.

The dynamics analysis required to determine the optimum boom stiffness and tension was performed using a discrete parameter model used for previous RA250 analyses and verified by test. The model used a five by two discretization as shown in Figure 3-95. Because of the symmetry of the solar array configuration, only half the array was analyzed with appropriate boundary conditions to determine either the symmetric or antisymmetric array modes. Each blanket was represented by 10 rectangular elements that describe the out-of-plane stiffness caused by the blanket tension. The leading edge member (LEM) and boom were



Table 3-29. Summary of Blanket Mass vs Aspect Ratio Trade Study

V (volts)	$\frac{L}{w}$	$\alpha_o$	Cell Area Required for 10,000 watts at Interface (m <sup>2</sup> )	Blanket Mass Less Bus Strips (kg)	Bus Strip Mass (kg)	Total Blanket Mass (kg)
100	5	0.02770	96.47	49.59	2.75	52.34
	10	0.03871	97.58	50.16	3.97	54.13
	15	0.04698	98.42	50.59	4.95	55.54
	20	0.05384	99.14	50.96	5.81	56.77
200	5	0.01405	95.14	48.90	1.34	50.24
	10	0.01975	95.69	49.18	1.91	51.09
	15	0.02408	96.11	49.40	2.36	51.76
	20	0.02770	96.47	49.59	2.75	52.34
300	5	0.00941	94.69	48.67	0.88	49.55
	10	0.01325	95.06	48.86	1.26	50.12
	15	0.01618	95.34	49.00	1.54	50.54
	20	0.01864	95.58	49.13	1.79	50.92
400	5	0.00707	94.47	48.56	0.65	49.21
	10	0.00997	94.74	48.70	0.94	49.64
	15	0.01219	94.96	48.81	1.15	49.96
	20	0.01405	95.14	48.90	1.34	50.24

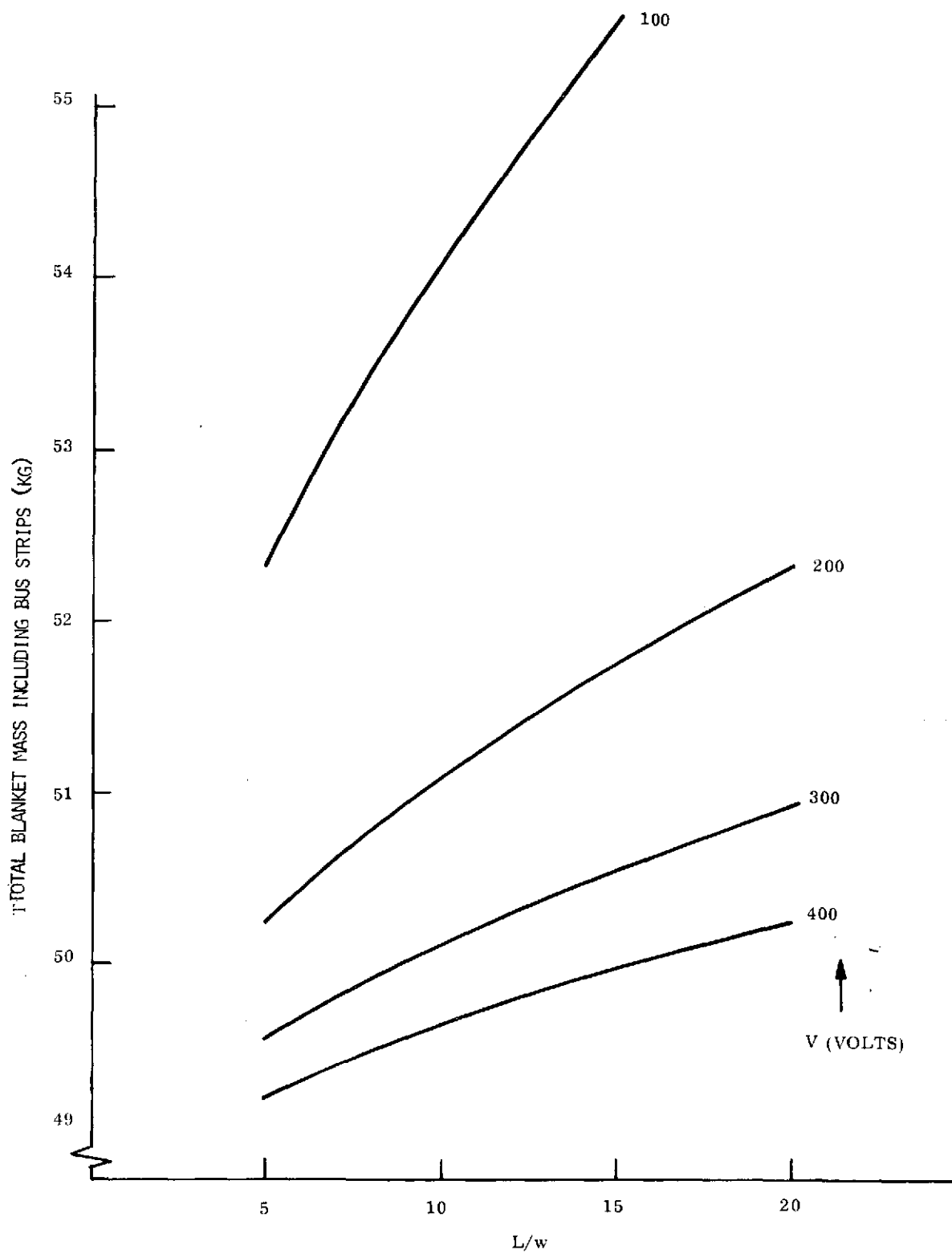
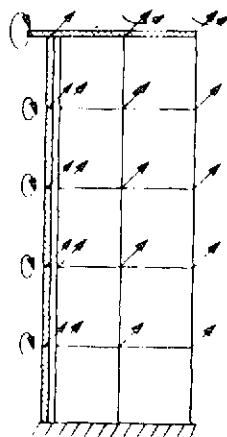
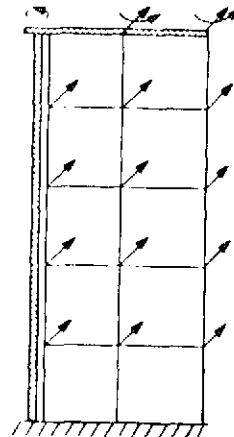


Figure 3-94. Total Blanket Mass vs Blanket Aspect Ratio



(a) Symmetric



(b) Anti-symmetric

Figure 3-95. Finite-Element Model of Two Blanket,  
Single Boom Solar Array

modeled using beam elements and included the effect of axial preload on the boom stiffness. The leading edge member was free to rotate relative to the boom about the longitudinal axis of the array. A consistent mass representation was used. The boom density was varied in accordance with the boom stiffness as shown in Figures 3-96 and 3-97 for the continuous longeron ASTROMAST and steel BI-STEM booms, respectively. The analyses were performed using the appropriate subroutines in a DYNAMO II program that enabled the parameters to be varied over the range of interest.

The optimization of the blanket tension and boom stiffness for each aspect ratio and frequency was accomplished in two steps. First, the required blanket tension to obtain a desired antisymmetric frequency was determined. Because the LEM is free to rotate about the boom axis, the boom stiffness does not affect the antisymmetric or torsional frequency of the array. Therefore, the blanket tension required for the desired torsional frequency was first determined. For the required blanket tension, a symmetric vibration analysis was

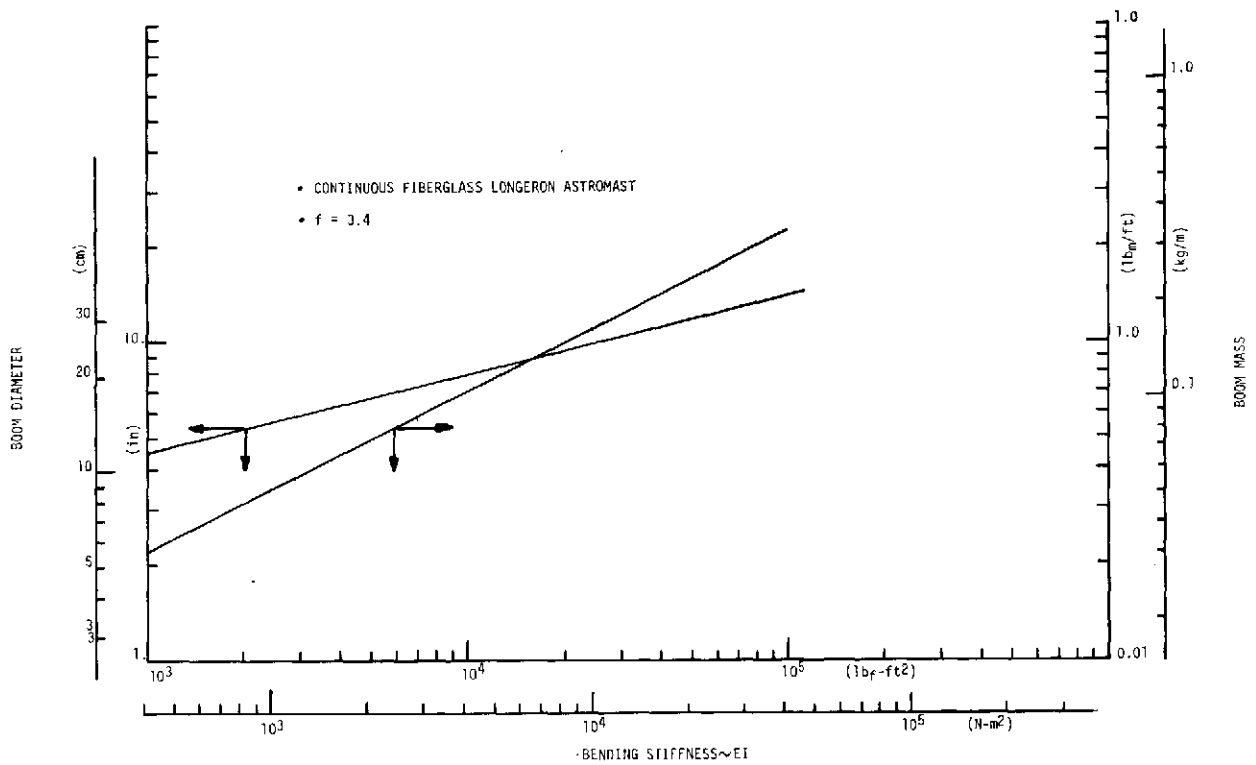


Figure 3-96. Continuous Fiberglass Longeron ASTROMAST  
Mass and Diameter as a Function of Bending Stiffness

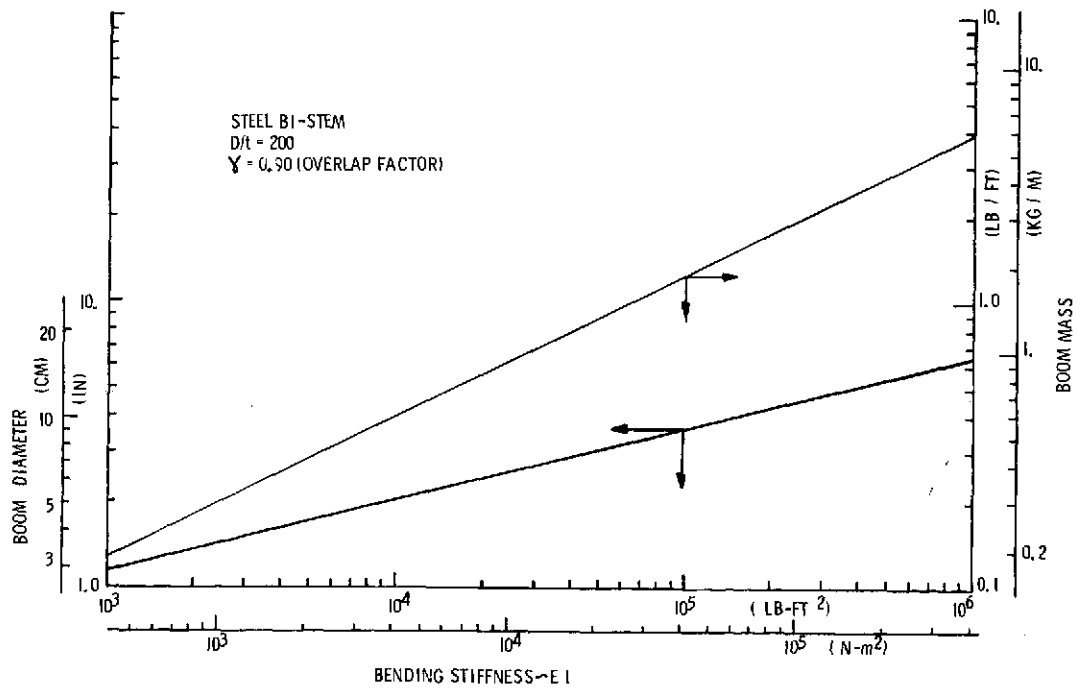


Figure 3-97. Steel BI-STEM Mass and Diameter  
as a Function of Bending Stiffness

then performed for various values of boom stiffness. Based on previous studies, it was estimated that the boom stiffness would correspond to that required to provide approximately 25 percent of critical buckling under the blanket tension load. Therefore, the symmetric array frequencies were determined for boom stiffnesses corresponding to 22 and 26 percent of critical buckling. A linear interpolation was then used to estimate the boom stiffness for the desired array frequency. The final boom stiffness was then bounded by interpolating between the third frequency and each of the other two frequencies. In general, the bounds of the boom stiffness were within a few percent. Using this approach, an array design having equal symmetric and antisymmetric frequencies was obtained as in previous optimization studies (Reference 61).

To verify that the analysis method provided the optimum design, additional analyses were performed which varied the blanket tension while holding all other array properties constant. To bracket the range of configurations analyzed in this study, these analyses were performed for aspect ratios of 2 and 10, and required array minimum frequencies of 0.02 and 0.2 Hertz. The resulting variations in the symmetric and antisymmetric frequencies with blanket tension are shown in Figures 3-98 and 3-99. These curves show that any increase in blanket tension over that required to obtain the desired antisymmetric frequency results in a reduced symmetric frequency, i. e., an increased boom axial load reduces the effective boom stiffness sufficiently to lower the symmetric (bending) frequency of the array. Although a reduction in blanket tension from that required to obtain the required antisymmetric frequency provides a slight increase in the symmetric frequency for the aspect ratio of two configurations, the antisymmetric frequency is reduced so that it no longer satisfies the minimum resonant frequency requirement. On the other hand, the aspect ratio of 10 configuration results in a symmetric frequency reduction for tensions other than that which satisfies the antisymmetric frequency requirement. For either configuration, the results of the tension variation analysis confirm that the selected approach results in an optimum design.

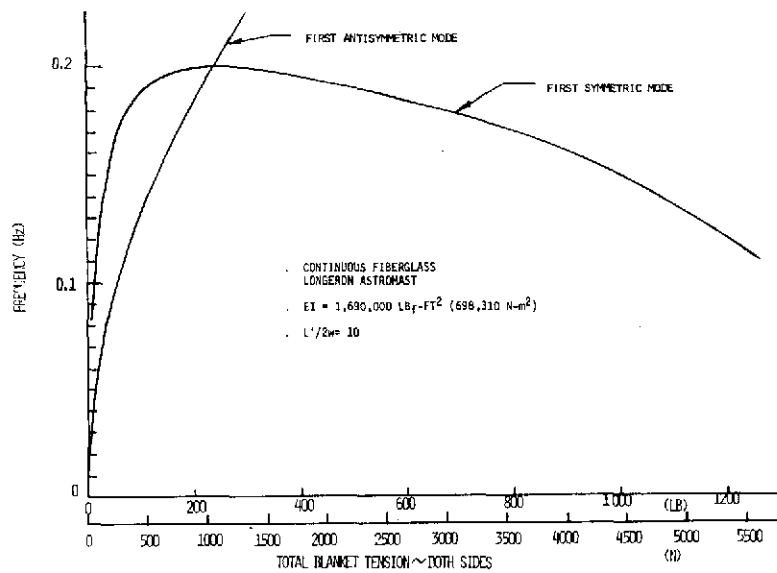


Figure 3-98. Symmetric and Antisymmetric Frequency vs Tension

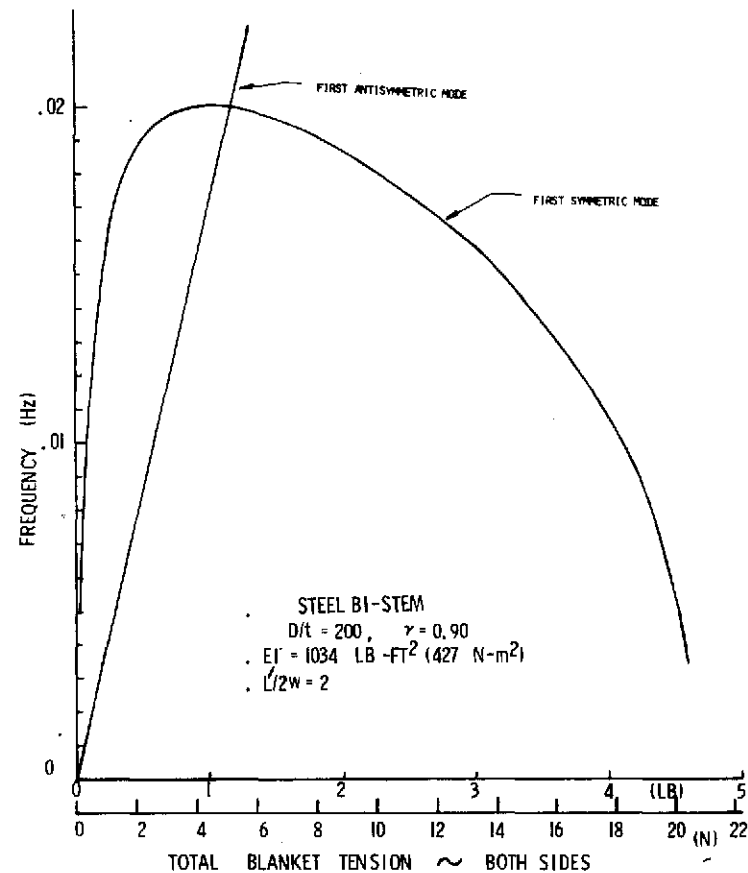


Figure 3-99. Symmetric and Antisymmetric Frequency vs Tension

For the continuous fiberglass longeron ASTROMAST configuration, Figure 3-100 shows the optimum boom stiffness and tension as a function of frequency for various values of aspect ratio ( $L'/2w$ ). The baseline design point at an  $L'/2w$  ratio of  $18.565/(2)(2.830) = 3.28$  is shown to have the required frequency of 0.04 Hz with a bending stiffness of  $3447 \text{ N-m}^2$  and a total blanket tension (both sides) of 26N. For the steel BI-STEM configuration, a similar presentation of the data are shown in Figure 3-101.

#### 3.4.3.3 Deployment and Support Structure Analysis

The total system mass consists of the sum of the masses of the three major subsystems: (1) solar cell blankets, (2) deployment structure and mechanisms, and (3) stowage structure and mechanisms. For this analysis, the solar cell blanket mass was assumed to remain constant at 48.5 kg independent of aspect ratio. This simplification ignores the variation of bus strip mass with aspect ratio which could amount to an error of about 3 kg in total blanket mass over the range of aspect ratios considered in this study.

The mass of the deployment structure and mechanisms includes the deployable boom element as well as the actuator required to deploy the element. Figure 3-96 gives the boom mass and diameter as a function of required boom bending stiffness for a continuous fiberglass longeron ASTROMAST. Note that stiffnesses of less than  $287 \text{ N-m}^2$  (mast diameter  $< 10.2 \text{ cm}$ ) are not achievable due to practical limits on element size. Figure 3-97 shows the same boom properties for a steel BI-STEM element with a  $D/t$  ratio of 200.

The mass of the actuator required to deploy the BI-STEM type elements is given in Figure 3-66 as a function of boom diameter.

The mass of the ASTROMAST deployment canister was obtained using the formula contained in Section 3.3.1.2.5.4.

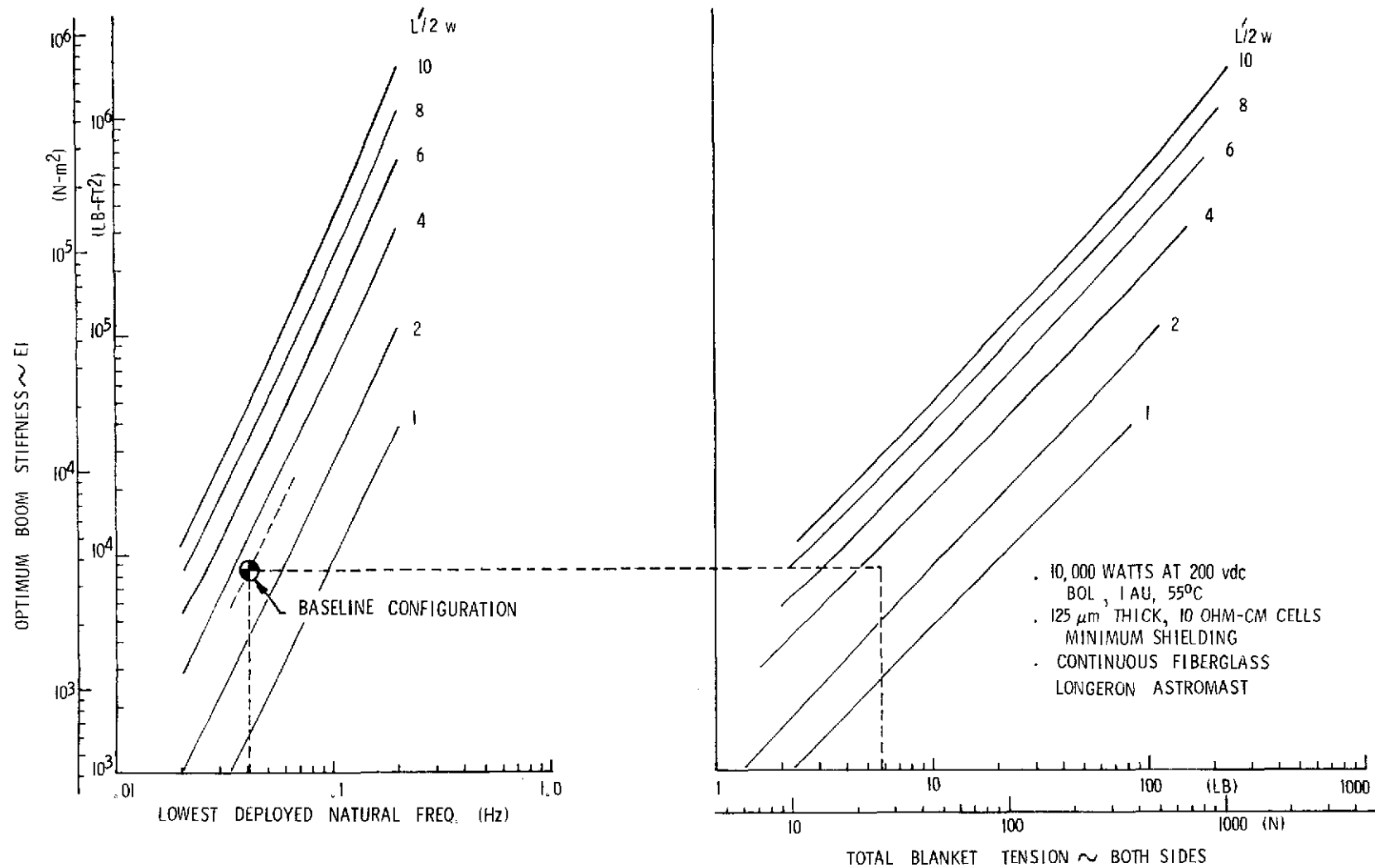


Figure 3-100. Optimum Boom Stiffness and Tension vs Frequency



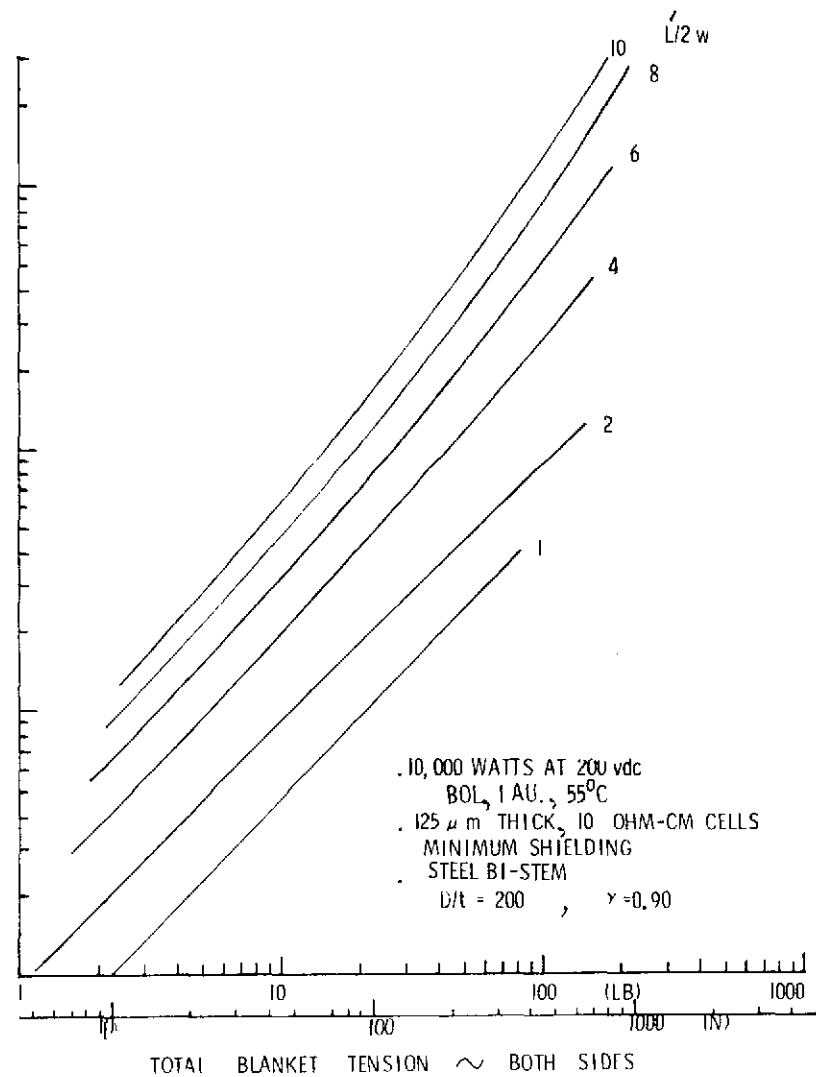
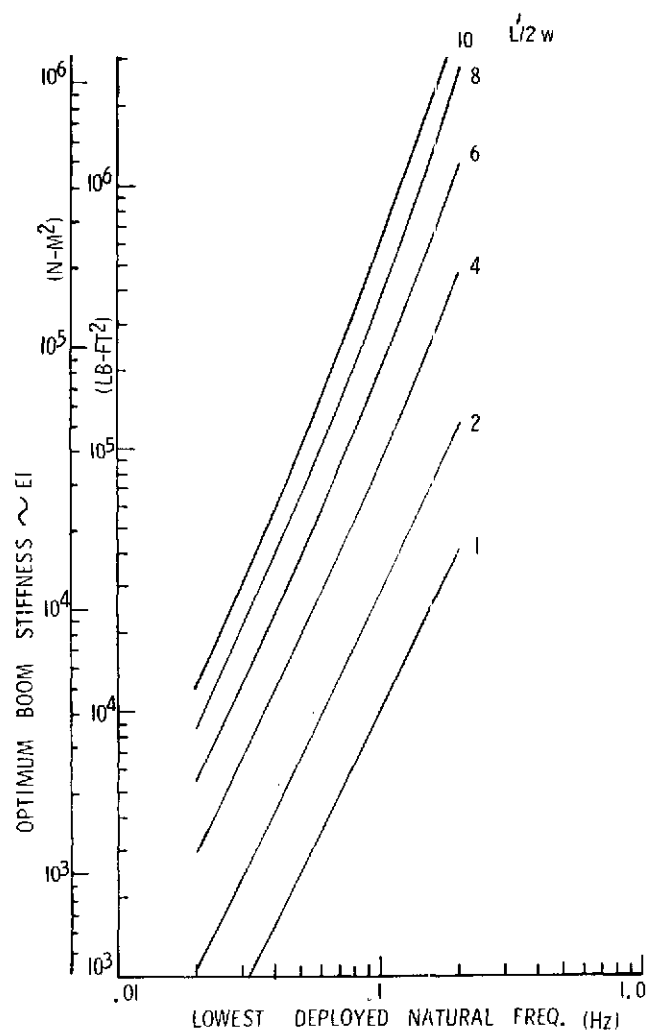


Figure 3-101. Optimum Boom Stiffness and Tension vs Frequency

The mass of the stowage structure and mechanisms was calculated based on using the same flat-pack stowage concept as shown in Figure 3-11 for the baseline configuration. Figure 3-102 shows the effects of blanket width,  $w$ , and strip length,  $\ell$ , on this total structural mass. These curves were established by calculating the mass for the baseline configuration and proportionately changing the weights as  $w$  and  $\ell$  were changed. For reasonable changes in these parameters, this proportioning assumption will yield sufficiently accurate masses since most members are sized by minimum gauges and not by stress levels.

#### 3.4.3.4 Study Results

Based on the previous analyses, it is possible to determine the total array system mass as a function of aspect ratio ( $L'/2w$ ) and deployed natural frequency. Figures 3-103 and 3-104 show the total system mass as a function of lowest deployed natural frequency for various values of  $L'/2w$  for the two boom configurations, continuous longeron ASTROMAST and steel BI-STEM, respectively. These same data are plotted in Figures 3-105 and 3-106 with aspect ratio on the abscissa.

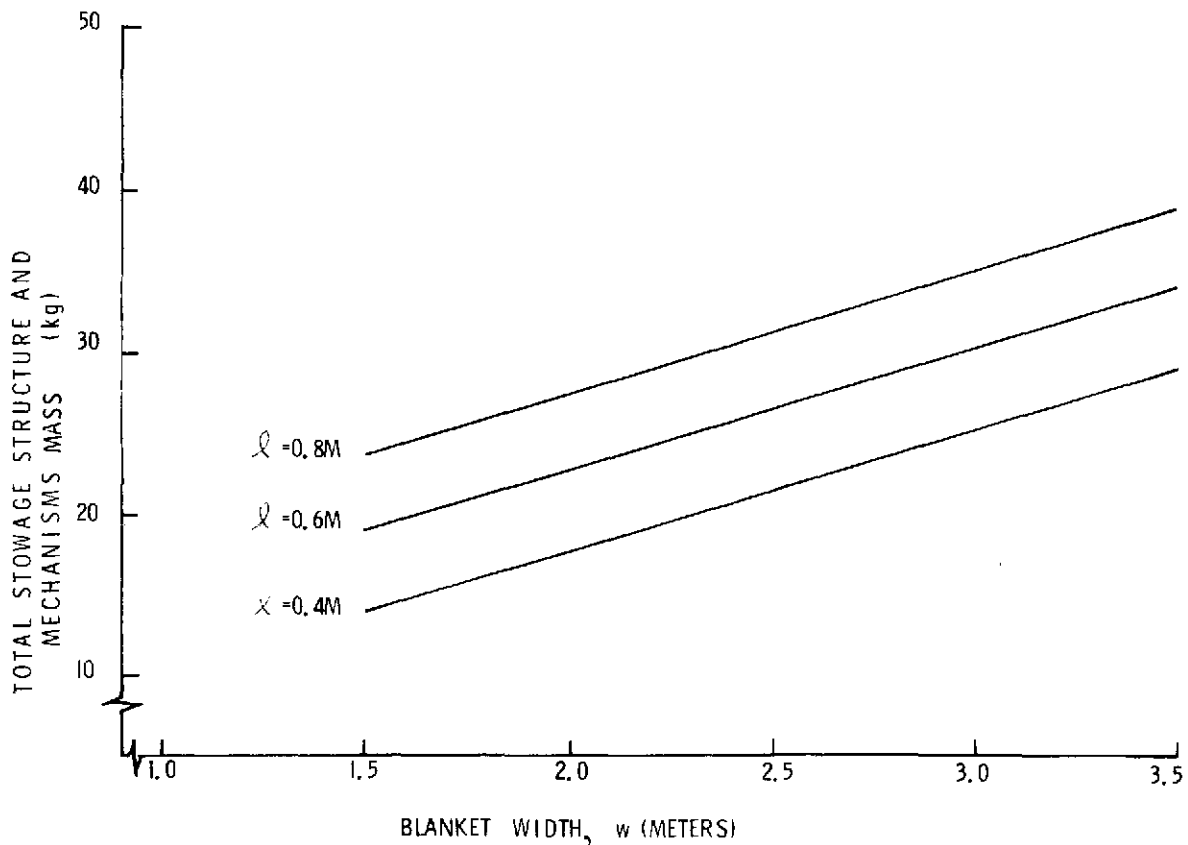


Figure 3-102. Total Structural Mass vs Blanket Width and Strip Length

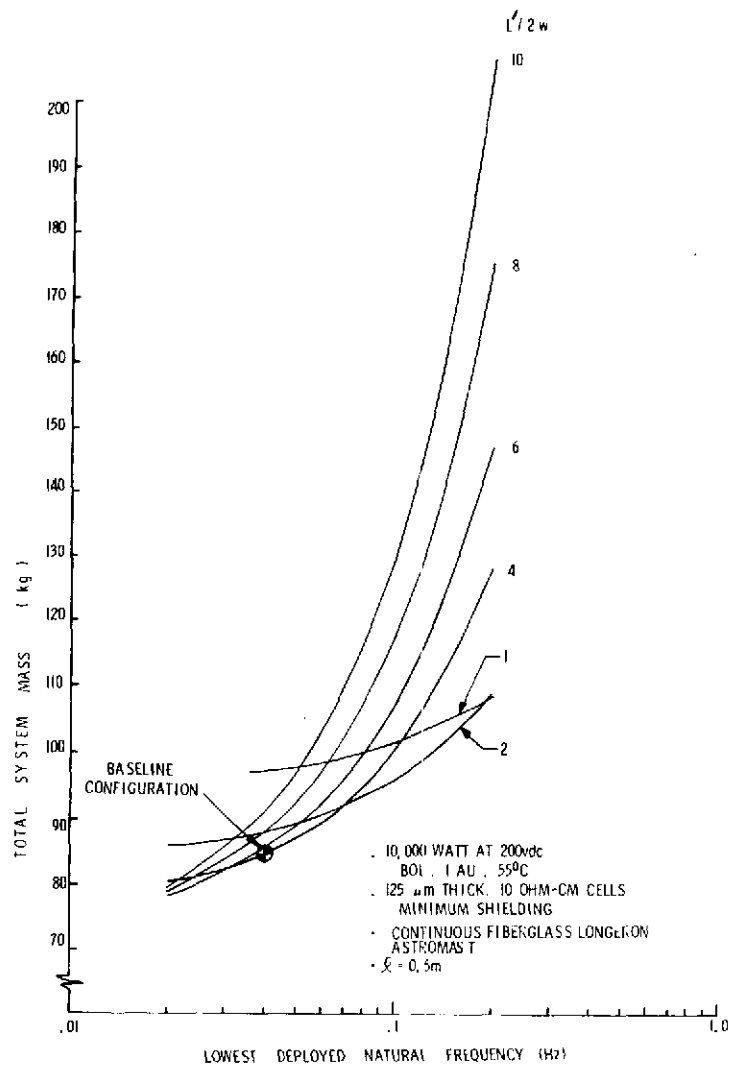


Figure 3-103. Total System Mass vs Deployed Natural Frequency

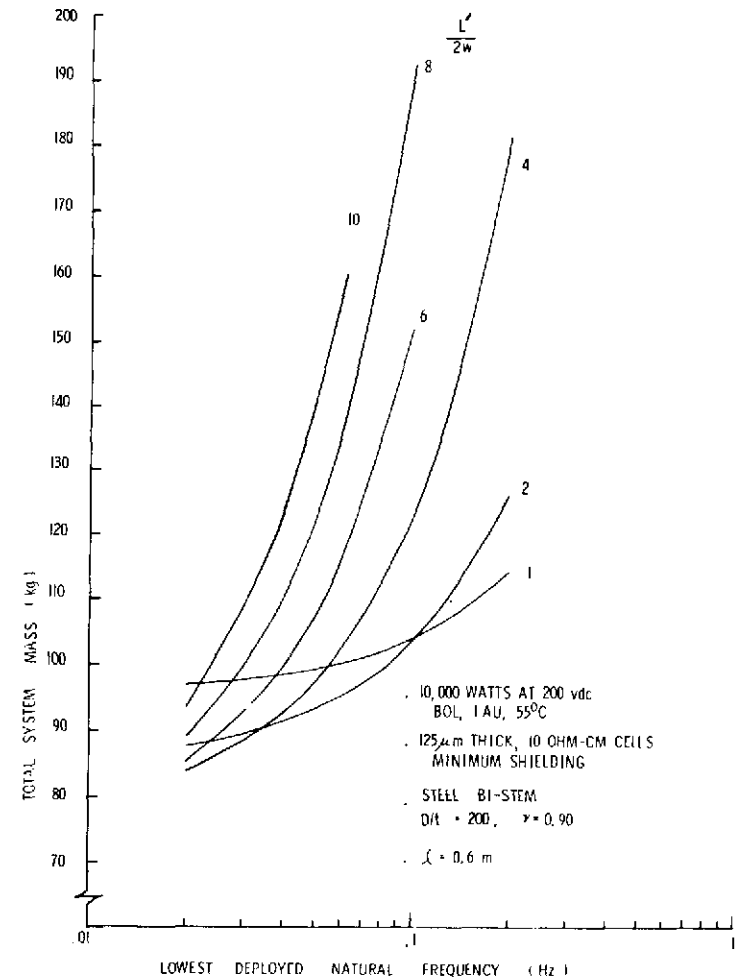


Figure 3-104. Total System Mass vs Deployed Natural Frequency

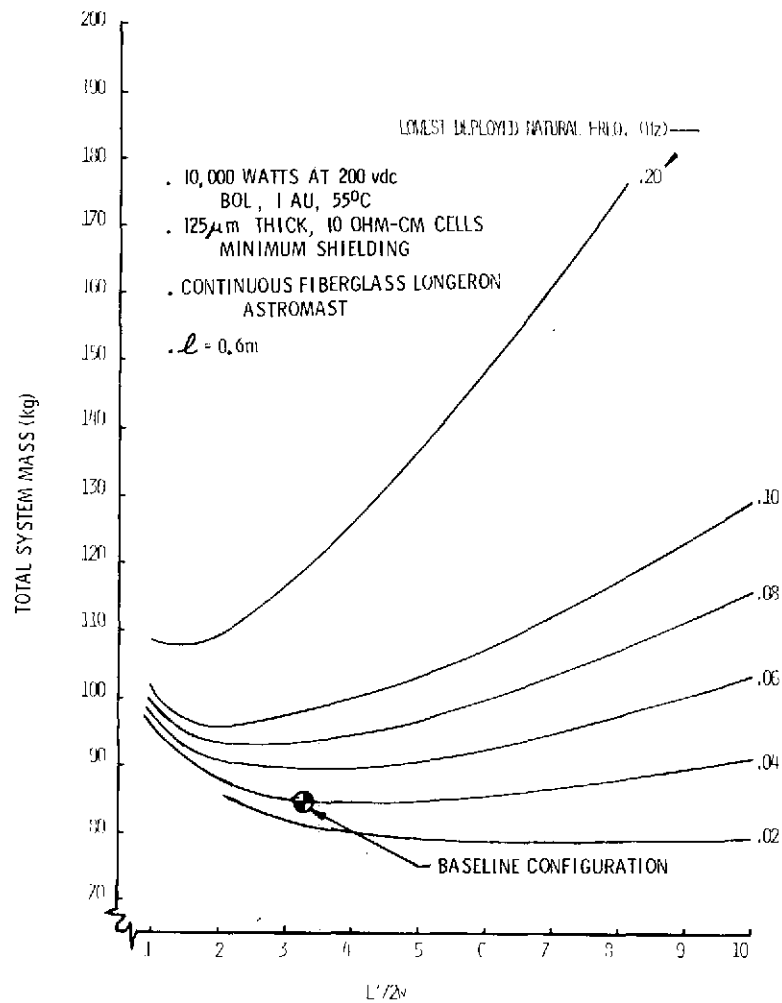


Figure 3-105. Total System Mass  
vs Aspect Ratio

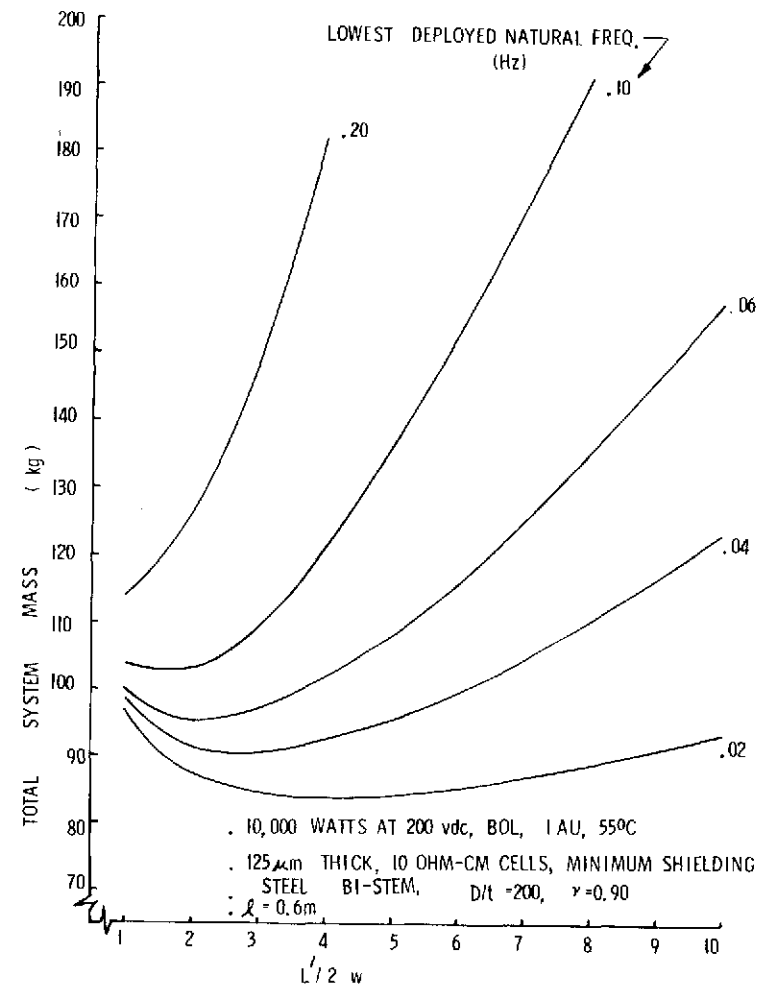


Figure 3-106. Total System Mass  
vs Aspect Ratio

### 3.4.4 SOLAR CELL BLANKET CONFIGURATION TRADE STUDY

#### 3.4.4.1 Introduction

In the preceding section, the total system mass was presented as a function of system blanket aspect ratio. The purpose of this section is to define the allowable blanket geometries in terms of solar cell circuit configurations which meet the electrical requirements. The 10 kw beginning-of-life power output requirement establishes the solar cell area on the blankets for a given selection of solar cell base resistivity and thickness. In addition, the selection of circuit operating voltage has a small effect on total solar cell area since there is an optimum bus strip distribution system power loss which is a function of this voltage (see Section 3.4.2).

#### 3.4.4.2 Definitions and Nomenclature

The basic circuit configuration to be considered is shown in Figure 3-107. In this context, a circuit is defined as a group of interconnected solar cells which supply power to the solar array bus at the full rated voltage. The solar array consists of a number of identical parallel connected circuits. Each circuit consists of a number of series connected modules. The length of the modules,  $b$ , is the width of the circuit as shown in Figure 3-107. In turn, each module is composed of a number of series connected submodules which are a parallel connection of solar cells which develop the full module short-circuit current, but only the voltage associated with a single cell. The following list of symbols and definitions will be used in connection with this description:

$N_{P/M}$	=	number of parallel cells per module (or circuit)
$N_{S/C}$	=	number of series cells per circuit
$N_{S/M}$	=	number of series cells per module
$N_{M/C}$	=	number of modules per circuit
$N_{C/B}$	=	number of circuits per blanket
$N_{B/A}$	=	number of blankets per array

- $N_{SC/A}$  = number of solar cells per array  
 $N_{SC/B}$  = number of solar cells per blanket  
 $N_{P/B}$  = number of parallel cells per blanket

Based on these definitions, the following relations are apparent:

$$N_{SC/A} = N_{SC/B} N_{B/A}$$

$$N_{SC/B} = N_{S/C} N_{P/B}$$

$$N_{SC/B} = N_{S/C} N_{P/M} N_{C/B}$$

$$N_{S/C} = N_{M/C} N_{S/M}$$

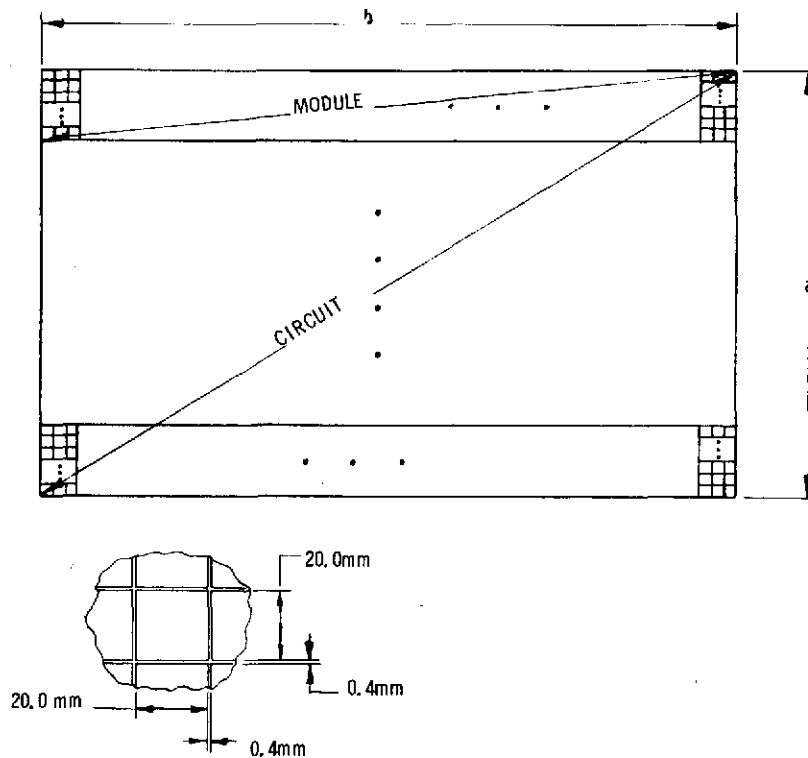


Figure 3-107. Solar Cell Circuit Configuration

The dimensions of the circuit, a and b, in meters, are given by:

$$a = .0200 N_{P/M} N_{M/C} + .0004 (N_{P/M} N_{M/C} - 1) \quad (3.4-10)$$

$$b = .0200 N_{S/M} + .0004 (N_{S/M} - 1)$$

Figure 3-108 shows the arrangements of circuits on a blanket. The module length, b, has been placed normal to the deployment direction of the solar array. The blanket width, w, is larger than b by the amount required to accommodate the bus strips on both sides. A strip, as shown on the figure, represents a separable portion of a blanket. In other words, the blanket is composed of the series mechanical connection of a number of strips. A strip may or may not contain a complete electrical circuit. Thus, the strip length, a', may or may not be equal to the circuit length, a, on Figure 3-107. For a flat-pack stowage concept, the blanket is folded at each space between strips. The length of the blanket, L, is given by:

$$L = a' N_{ST/B} + s(N_{ST/B} - 1) \quad (3.4-11)$$

where

$N_{ST/B}$  = number of strips per blanket

s = separation required between strips to accommodate fold.

Note that this length, L, does not include either an inboard or outboard leader length.

#### 3.4.4.3 Candidate Blanket Configurations

With a nominal 125  $\mu$ m thick, 10 ohm-cm solar cell, the maximum power voltage is 0.375 volts per cell at 55°C. Assuming a 1 percent voltage loss within the modules, 540 series connected cells are required to provide a 200 volt system bus voltage. The 540 series connected cell circuit arrangement is convenient because it allows for a wide choice of module lengths since the number 540 is evenly divisible by 2, 3, 4, 5, 6, 9, etc. Table 3-30 shows the possible module lengths and module maximum power voltages for 10 ohm-cm cells operating at 55°C.

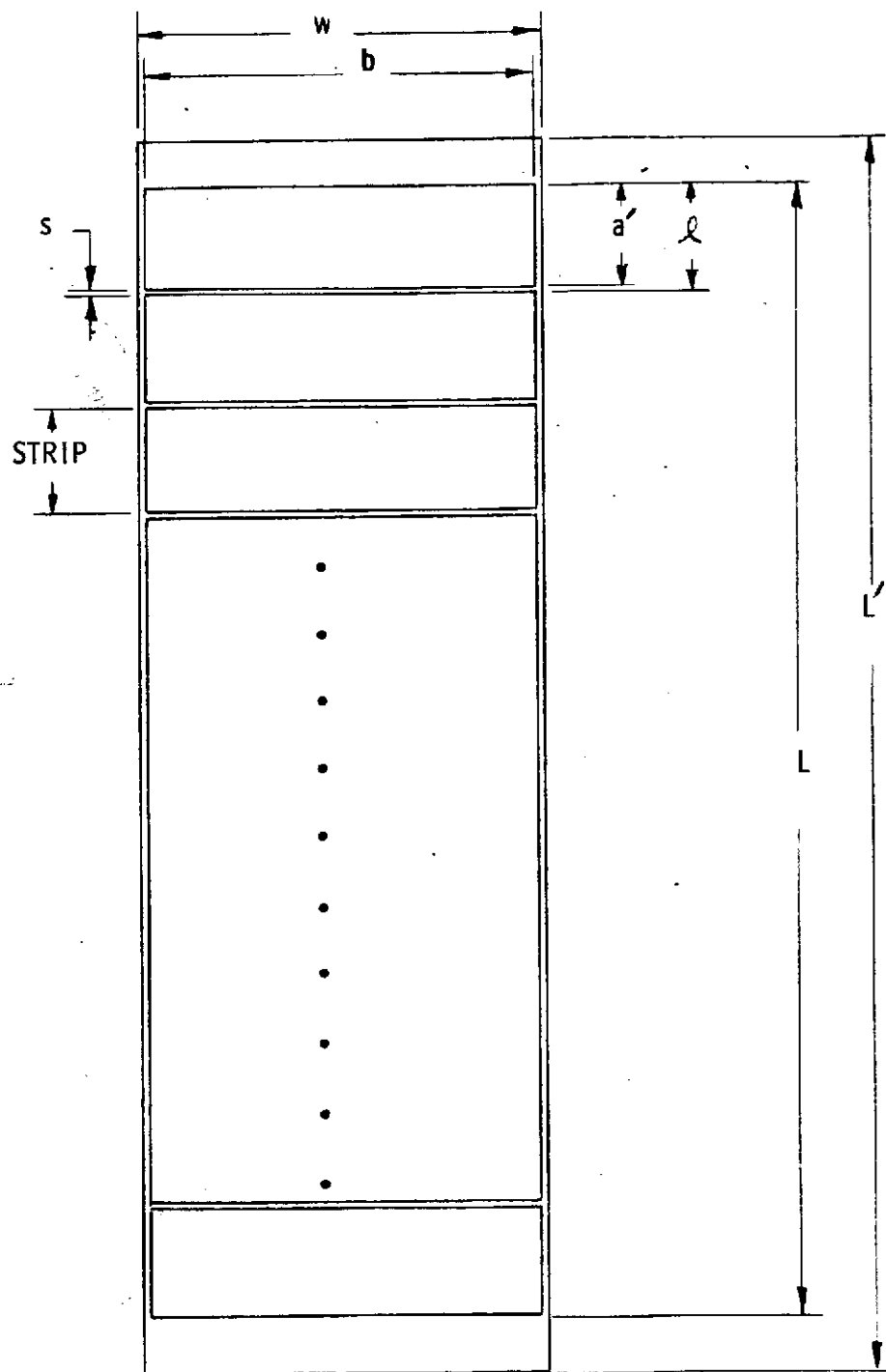


Figure 3-108. Solar Cell Blanket Configuration



Table 3-30. Possible Module Lengths

$N_{S/M}$	Module Maximum Power Voltage for 10 ohm-cm Cells Operating at 55°C (volts)	b (m)
540	200	11.0156
270	100	5.5076
180	66.7	3.6716
135	50	2.7536
108	40	2.2028
90	33.3	1.8356
60	22.2	1.2236
54	20	1.1012
45	16.7	0.9176
36	13.3	0.7340
30	11.1	0.6116
27	10	0.5504

For a total solar array power output of 10,000 watts at beginning-of-life, the number of solar cells required is given by:

$$N_{SC/A} = N_{S/C} N_{P/B} N_{B/A} = \frac{10,000}{P_{cell} (1 - \alpha_o) (1 - \gamma)} \quad (3.4-12)$$

where

$$\begin{aligned} P_{cell} &= \text{cell maximum power output at } 55^{\circ}\text{C, 1 AU} \\ &= .0464 \text{ watts for } 125 \mu\text{m thick 10 ohm-cm cells} \\ &= .0442 \text{ watts for } 100 \mu\text{m thick 10 ohm-cm cells} \\ \alpha_o &= \text{optimum bus strip power loss from Figure 3-92} \\ &= .02 \text{ for } V = 200 \text{ volts, a blanket aspect ratio of 10, and 10} \\ &\quad \text{circuits per blanket} \\ \gamma &= \text{module assembly power loss, including interconnector} \\ &\quad \text{series resistance and current mismatch} \\ &= .03 \end{aligned}$$

Therefore,  $N_{P/B} N_{B/A} = 420$  for the  $125\ \mu\text{m}$  thick cells and 442 for the  $100\ \mu\text{m}$  thickness, or for a two blanket per solar array system, the number of required parallel solar cells per blanket,  $N_{P/B}$ , is 210 and 221, respectively. For the manned space station mission where the use of 2 ohm-cm cell base resistivity is indicated (see Section 3.4.1), and the design operating temperature is about  $80^\circ\text{C}$ , the direct substitution of 2 ohm-cm cells for 10 ohm-cm cells in the same circuit configuration will yield a slightly greater output ( $< 1\%$ ) at the same maximum power voltage. This is demonstrated by the data plotted in Figure 3-109 which show that the 2 ohm-cm cells operating at  $80^\circ\text{C}$  have almost exactly the same maximum power point as 10 ohm-cm cells operating at  $55^\circ\text{C}$ .

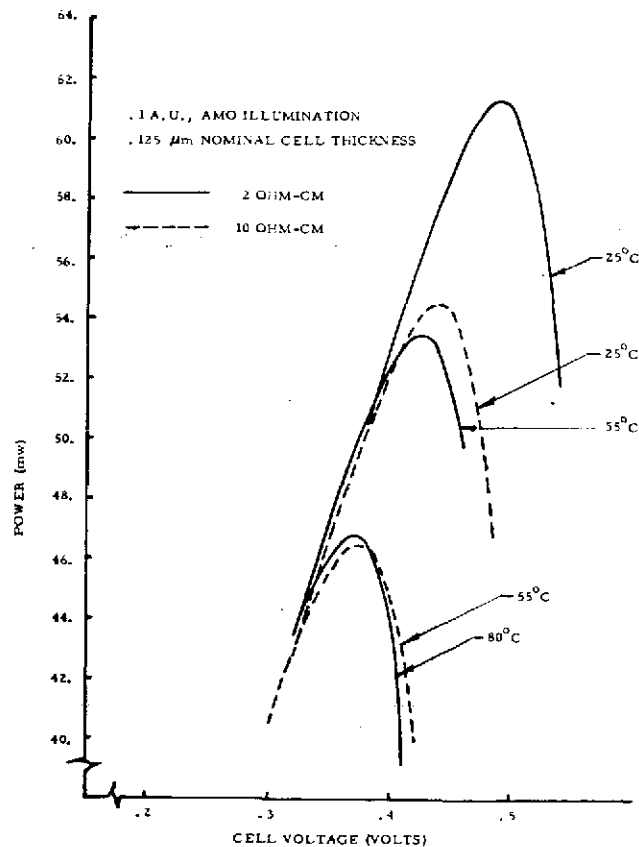


Figure 3-109. Comparison of 2 and 10 ohm-cm Cells at Various Operating Temperatures

Table 3-31 lists the possible circuit arrangements for  $N_{S/C} = 540$  and  $N_{P/M} N_{C/B} = 210$  and 221. From among these possible combinations of  $N_{P/M}$  and  $N_{C/B}$ , the most practical choices have been indicated by a box in the table. For each of these most practical circuit arrangements, it is possible to establish the associated configurations of the blanket based on the definition of terms from Figure 3-108.

Table 3-31. Possible Circuit Arrangements for  $N_{S/C} = 540$

$N_{P/M} N_{C/B}$	210		221	
$N_{S/C/A}$	226,800		238,680	
	$N_{P/M}$	$N_{C/B}$	$N_{P/M}$	$N_{C/B}$
	1	210	1	221
	2	105	13	17
	3	70	17	13
	5	42	221	1
	6	34		
	7	30		
	10	21		
	14	15		
	15	14		
	21	10		
	30	7		
	35	6		
	42	5		
	70	3		
	105	2		
	210	1		

Table 3-32 lists the possible blanket configurations for  $N_{P/M} N_{C/B} = 221$ . The strip length,  $a'$ , has been limited to about 1 meter to allow for convenient handling of individual strips. Thus, if the circuit length,  $a$ , from Figure 3-107, exceeds about 1 meter, the circuit is divided between two or more strips. For example, in row 4 of Table 3-32, the six module electrical circuit has been divided between two strips to limit the strip length. The total blanket length, as given by equation (3.4-11), is tabulated for three values of  $s$ , the separation between strips. The corresponding blanket area, for one of the two blankets, and the ratio,  $L/b$ , are given for the same three values of  $s$ .

Table 3-32. Possible Blanket Configurations for  $N_{P/M} N_{C/B} = 221$

$N_{P/M}$	$N_{C/B}$	$N_{M/C}$	(1) $N_{M/ST}$	(2) $N_{ST/B}$	b (m)	a' (m)	L(m)			Blanket Area (m <sup>2</sup> )			L/b		
							s=3 cm	s=4 cm	s=5 cm	s=3 cm	s=4 cm	s=5 cm	s=3 cm	s=4 cm	s=5 cm
13	17	2	2	17	5.5076	0.5300	9.4900	9.6500	9.8100	52.2671	53.1483	54.0296	1.7230	1.7521	1.7812
		3	3	17	3.6716	0.7952	13.9984	14.1584	14.3184	51.3965	51.9840	52.5714	3.8126	3.8562	3.8998
		4	4	17	2.7536	1.0604	18.5068	18.6668	18.8268	50.9603	51.4009	51.8415	6.7209	6.7791	6.8372
		6	3	34	1.8356	0.7952	28.0268	28.3568	28.6868	51.4460	52.0517	52.6575	15.2684	15.4482	15.6280
		9	3	51	1.2236	0.7952	42.0552	42.5552	43.0552	51.4587	52.0705	52.6823	34.3700	34.7787	35.1873
17	13	2	2	13	5.5076	0.6932	9.3716	9.4916	9.6116	51.6150	52.2759	52.9368	1.7015	1.7234	1.7452
		3	3	13	3.6716	1.0400	13.8800	14.0000	14.1200	50.9618	51.4024	51.8430	3.7803	3.8131	3.8457
		4	2	26	2.7536	0.6932	18.7732	19.0232	19.2732	51.6939	52.3823	53.0707	6.8176	6.9085	6.9993
		6	3	26	1.8356	1.0400	27.7900	28.0400	28.2900	51.0113	51.4702	51.9291	15.1394	15.2757	15.4119
		9	3	39	1.2236	1.0400	41.7000	42.0800	42.4600	51.0241	51.4891	51.9541	34.0797	34.3903	34.7009

NOTES: (1) number of modules per strip.  
(2) number of strips per blanket

A similar tabulation for  $N_{P/M} N_{C/B} = 210$  is given in Table 3-33 for a value of  $s = 3$  cm. The selected circuit arrangement and corresponding blanket configuration for the current baseline configuration have been indicated in this table.

### 3.4.5 ANALYSIS OF "V"-STIFFENED SOLAR ARRAY

#### 3.4.5.1 Introduction

A "V"-stiffened solar array configuration was conceived as a means of obtaining significant increases in the minimum array resonant frequency without added complexity. Thus, it is possible to meet a specified deployed natural frequency requirement with reduced boom stiffness (and reduced total system weight) when compared with a planar array geometry. This concept, shown in Figure 3-110, uses the slight angle of the array blankets to enable observed in-plane stiffening resulting from the redistribution of blanket tension to provide out-of-plane stiffness. Static tests and analysis of the RA250 in-plane behavior (Reference 62) showed that the array blanket tension was redistributed such that the array rotated about

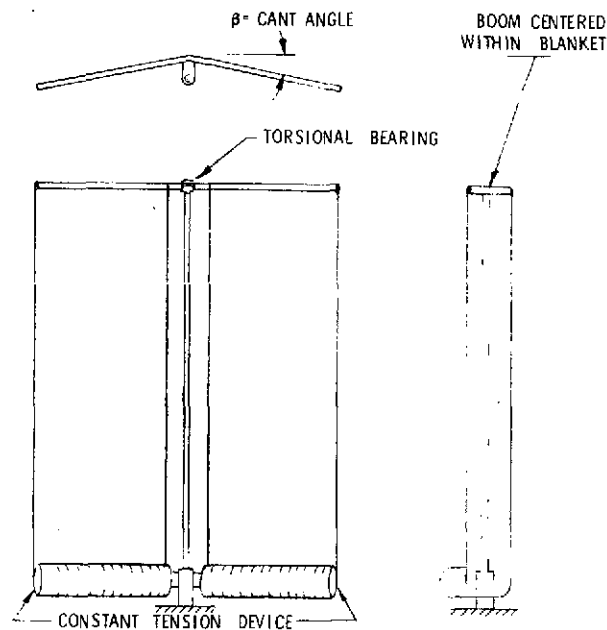


Figure 3-110. "V" Configuration, Single Boom Solar Array Concept

Table 3-33. Possible Blanket Configurations for  $N_{P/M} N_{C/B} = 210$  (with  $s = 3$  cm)

$N_{P/M}$	$N_{C/B}$	$N_{M/C}$	$N_{M/ST}$	$N_{ST/B}$	b (m)	a' (m)	L (m)	Blanket Area (m <sup>2</sup> )	L/b
10	21	2	2	21	5.5076	.4076	9.1596	50.4474	1.6630
		3	3	21	3.6716	.6116	13.4436	49.3395	3.6615
		4	4	21	2.7536	.8156	17.7276	48.8147	6.4379
		5	5	21	2.2028	1.0196	22.0116	48.4872	9.9925
		6	3	42	1.8356	.6116	26.9172	49.4092	14.6639
		9	3	63	1.2236	.6116	40.3908	49.4222	33.0098
		10	5	42	1.1012	1.0196	44.0532	48.5114	40.0047
14	15	2	2	15	5.5076	.5708	8.9820	49.4693	1.6308
		3	3	15	3.6716	.8564	13.2660	48.7074	3.6131
		4	2	30	2.7536	.5708	17.9940	49.5483	6.5347
15	14	6	3	30	1.8356	.8564	26.5620	48.7572	14.4705
		9	3	45	1.2236	.8564	39.8580	48.7702	32.5744
		2	2	14	5.5076	.6116	8.9524	49.3062	1.6255
		3	3	14	3.6716	.9176	13.2364	48.5988	3.6051
		4	2	28	2.7536	.6116	17.9348	49.3853	6.5132
		6	3	28	1.8356	.9176	26.5028	48.6485	14.4382
21	10	9	3	42	1.2236	.9176	39.7692	48.6616	32.5018
		2	2	10	5.5076	.8564	8.8340	48.6541	1.6040
		4	2	20	2.7536	.8564	17.6980	48.7332	6.4272
		6	2	30	1.8356	.8564	26.5620	48.7572	14.4705
		10	2	50	1.1012	.8564	44.2900	48.7721	40.2198

← Baseline  
Configu-  
ration

one edge. In effect, the blanket provided a moment constraint to the tip of the deployable boom until an edge tension condition was achieved after which the boom behaved as a cantilever. By canting the blankets and centering the boom within the blankets, this boom tip constraint can also be used to stiffen the array for symmetric out-of-plane motion.

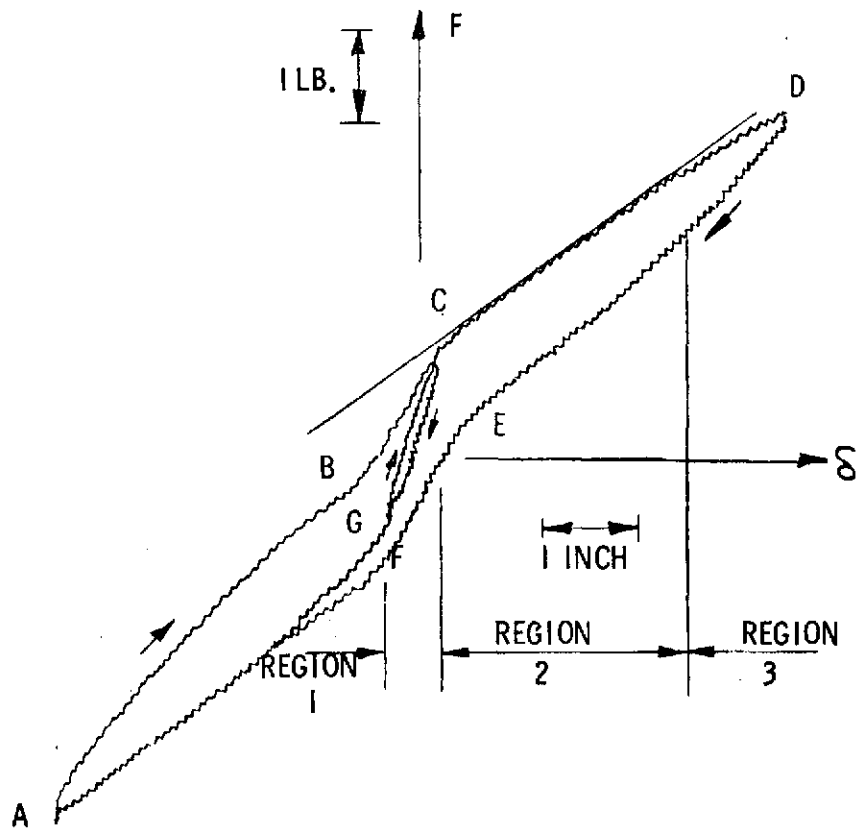
The effect of the canted blankets will also provide stiffening for torsional motion of the array. For a given boom, the tip constraint will enable greater tension to be applied without buckling the boom; hence, an increase in the torsional frequency. In addition, the boom will be required to bend during torsional vibration with some increase in the frequency. (Because of the high in-plane stiffness, the array will tend to twist about the center of the "V" causing bending of the boom.) However, this analysis is only concerned with the effects of the canted blankets on the symmetric frequency; torsional stiffening should be considered in a subsequent analysis.

The approach used in the analysis is to use the present out-of-plane analytical model of the array with linear modifications to the boom stiffness which account for the effect of the canted blankets at various amplitudes of motion. The first portion of this section reviews the in-plane analysis and test results for the RA250 which are used for modifying the boom stiffness. The symmetric analysis of the "V" Stiffened Array is then presented. Effects of the "V" configuration on the "baseline" array are then discussed.

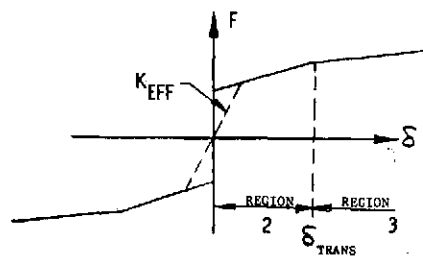
#### 3.4.5.2 RA250 In-Plane Test and Analysis

The study of the in-plane behavior of the RA250 (Reference 62) showed that the shift in the blanket tension distribution was a major factor in the observed stiffness. The tests indicated that there were three regions of different stiffnesses for in-plane deflections as shown in Figure 3-111 and described below:

Region 1: For small deflections, hysteretic behavior of the BI-STEM boom caused a relatively high stiffness. This is best predicted semi-empirically and is not predicted by simplified analytical modeling.



(a) Measured on RA250 (from Reference 62)



(b) Linearized

Figure 3-111. In-Plane Force-Deflection Characteristic



Region 2: For medium deflections, the tension distribution of the blankets changes such that the slope ( $\theta$ ) at the tip of the leading edge member is proportional to the tip deflection ( $\delta$ ) divided by the array length ( $L$ ).

$$\theta = \delta/L \quad (3.4-13)$$

This results from a constraining moment at the tip of the boom due to the blanket tension and is valid until the tension shifts to the edges of the blanket. The deflection at which this region ends is represented by

$$\delta_{\text{TRANS}} = Tw \left[ \frac{2 EI}{L^2 (1 + 4\bar{\alpha})} + \frac{T (1 + 12\bar{\alpha})}{15 (1 + 4\bar{\alpha})^2} \right]^{-1} \quad (3.4-14)$$

where

$$\begin{aligned} T &= \text{Tension per blanket} \\ EI &= \text{Boom stiffness} \\ \bar{\alpha} &= \text{Factor accounting for root flexibility} \\ &= EI/K_r L \\ w &= \text{Half width of the array} \end{aligned}$$

In Region 2, the force deflection characteristic is best represented as:

$$F = \left[ \frac{4 EI}{L^3 (1 + 4\bar{\alpha})} - \frac{4T}{15 (1 + 4\bar{\alpha})^2 L} \right] \delta + \frac{Tw}{L} \quad (3.4-15)$$

This relation has been shown to provide excellent agreement with RA250 model test results.

Region 3: For large deflections, the effect of blanket tension is no longer present and the boom behaves as a cantilever. This occurs after the transitional deflection given by Equation (3.4-14).

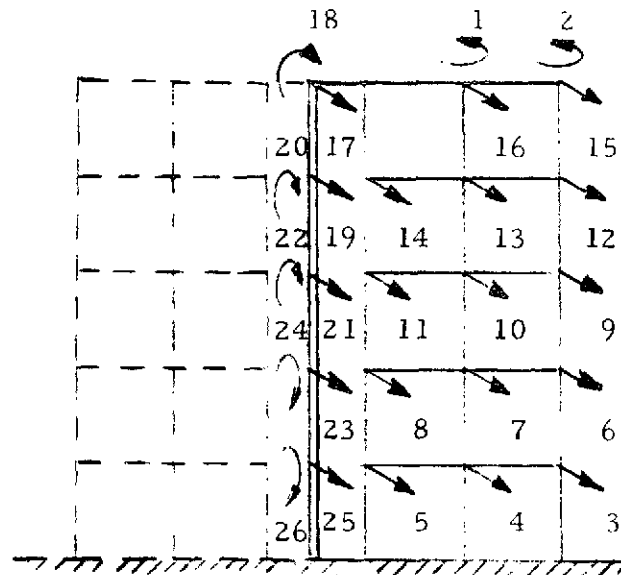
Using the idealized representation shown in Figure 3-111(b), an effective linear stiffness ( $K_{\text{eff}}$ ) can be defined for a selected amplitude of motion. Although other methods could be used to arrive at a linearized stiffness, this appears to be a reasonable estimate. It is conservative for large amplitudes in that the stiffness is higher than predicted, but may be unconservative for small amplitudes because the Region 1 stiffness is not included in the stiffness representation.

#### 3.4.5.3 Symmetric Vibration Analysis

The approach used in performing this symmetric vibration analysis of the "V" stiffened array was to use the existing model of the blankets and revise the boom stiffness representation to reflect the effect of the blanket tension redistribution. The original analytical model of the array is shown in Figure 3-112(a). The revised model of the array is shown in Figure 3-112(b) where the major modification is to replace the boom finite element model by an effective linear spring ( $K_{\text{eff}}$ ). This appears reasonable in that the cant angle of the array being considered is small (on the order of  $10^0$ ) so that significant area is not added to the array due to the change in the projected area. The resulting change in the membrane stiffness due to the small angular rotation should not be significant, but should actually increase the blanket stiffness. Therefore, the main effect seems to be the revised boom stiffness.

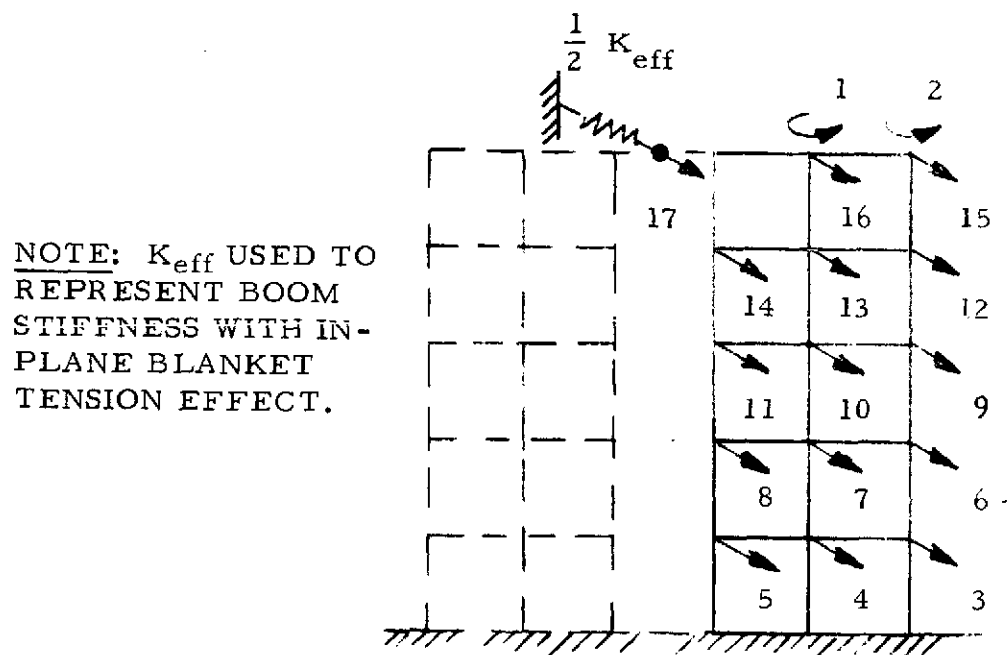
Consider the out-of-plane deflections of the "V" stiffened array shown in Figure 3-113, and the free body diagram of the Leading Edge Member (LEM) shown in Figure 3-114. These diagrams are identical to those of Reference 62 except for the modified width which now becomes the projected width; i. e.,  $w$  is replaced by  $w \sin \beta$ . The force deflection relation now becomes:

$$F = \left[ \frac{4 EI}{L^3 (1 + 4 \bar{\alpha})} - \frac{4T}{15 (1 + 4 \bar{\alpha})^2 L} \right] \delta + \frac{Tw \sin \beta}{L} \quad (3.4-16)$$



NOTE: SYMMETRY BOUNDARY CONDITIONS  
IMPOSED ALONG BOOM  $\bar{C}$

(a) Planar Solar Array



NOTE:  $K_{eff}$  USED TO  
REPRESENT BOOM  
STIFFNESS WITH IN-  
PLANE BLANKET  
TENSION EFFECT.

(b) "V" - Configuration Solar Array

Figure 3-112. Symmetric Models

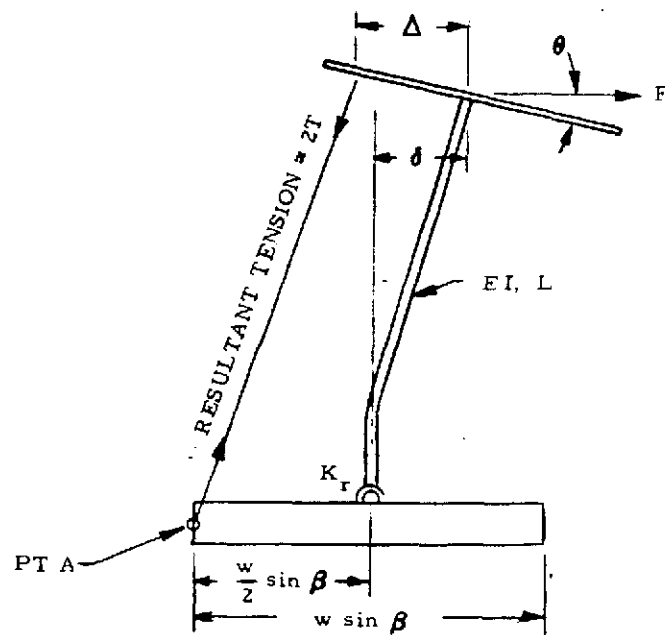


Figure 3-113. Edge View of Deflected Array

$$V = \frac{6EI\delta}{L^3(1+4\alpha)} - \left[ \frac{11+76\alpha+160\alpha^2}{5(1+4\alpha)^2} \right] \frac{T\delta}{L}$$

$$M = \frac{2EI\delta}{L^2(1+4\alpha)} + \frac{T\delta(1+12\alpha)}{15(1+4\alpha)^2}$$

Figure 3-114. Force Diagram at Outer End of Array

or, neglecting root flexibility

$$F = \left[ \frac{4 EI}{L^3} - \frac{4T}{15L} \right] \delta + \frac{Tw \sin \beta}{L} \quad (3.4-16a)$$

and the limiting deflection at which the transition from Region 2 to Region 3 now becomes:

$$\delta_{\text{TRANS}} = Tw \sin \beta \left[ \frac{2 EI}{L^2 (1 + 4 \bar{\alpha})} + \frac{T (1 + 12 \bar{\alpha})}{15 (1 + 4 \bar{\alpha})^2} \right]^{-1} \quad (3.4-17)$$

or, neglecting root flexibility,

$$\delta_{\text{TRANS}} = Tw \sin \beta \left[ \frac{2 EI}{L^2} + \frac{T}{15} \right]^{-1} \quad (3.4-17a)$$

Using  $K_{\text{eff}}$  to linearize the boom stiffness over the range of applicable deflections and neglecting root flexibility:

$$K_{\text{eff}} = \frac{F}{\delta} = \frac{4 EI}{L^3} - \frac{4T}{15L} + \frac{Tw \sin \beta}{L} \frac{1}{\delta} \quad (3.4-18)$$

where  $1/2 K_{\text{eff}}$  is added to the stiffness matrix of the analytical model at coordinate 17.

It will be noted that the tension effect on the boom stiffness is included in the linearized stiffness. As the tension is increased, the boom stiffness decreases as indicated by the first two terms of Equation 3.4-18. When  $2T = \frac{30 EI}{L^2}$ , the boom stiffness becomes zero and the  $K_{\text{eff}}$  is due only to the initial offset value. From the buckling standpoint, the critical buckling load in Region 2 is increased from  $\frac{\pi^2 EI}{L^2}$  to  $\frac{30 EI}{L^2}$ , an increase of approximately 3 to 1.

The mass of the boom is included at the boom tip coordinate using one-fourth of the boom mass.

#### 3.4.5.4 Assessment of Stiffening Effects

An evaluation of the effectiveness of the "V" stiffened configuration was performed using the basic geometry of the baseline configuration as a point of reference. This array configuration was postulated to have a cant angle, of 10 degrees. The following values were assumed for the parameters specified:

Total deployed length	=	18.565 m (60.9 ft)
Blanket width	=	2.754 m (9.0 ft)
Boom Stiffness (EI)	=	4173 N-m <sup>2</sup> (10,000 lb-ft <sup>2</sup> )
LEM Stiffness (EI)	=	2066 N-m <sup>2</sup> (5,000 lb-ft <sup>2</sup> )
Blanket Weight	=	0.135 kg/m (0.091 lb/ft)
Tension per Blanket	=	14.2 N (3.2 lb)
Boom Buckling Load	=	114.3 N (25.7 lb)

The analysis was performed for blanket tension values varying from 4.4 to 356 N (1 to 80 lb). For the baseline configuration, the optimum blanket tension was found to be approximately 14.2 N (3.2 lb) so that the tension variation encompasses the values of interest. The resulting force deflection characteristics of the boom are shown in Table 3-34 in terms of the offset force, and the deflection and force at which the transition to Region 3 occurs. It will be noted that the acceleration requirement of  $7 \times 10^{-4}$  g for the space station mission corresponds to a force of approximately 0.36 N (0.08 lbs) so that the small force values listed in the table are actually large for the quiescent environment of space. Comparison of the offset force with the force at transition indicates that the offset provides most of the total transition force for the high tensions and is a major factor in the effective stiffness at transition.

The effect of the cant angle on the array characteristics can be seen from the previous analytical expressions. The deflection at which transition occurs is directly proportional

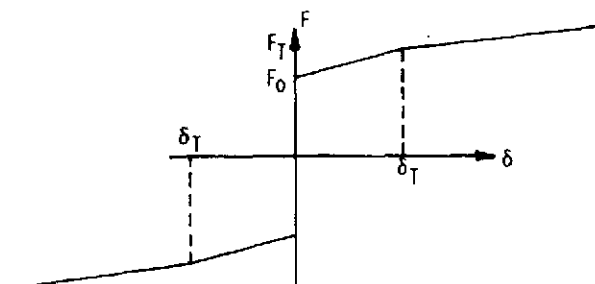
to the sine of the angle (Equation 3.4-17a) so that the transitional deflection can be increased, if necessary, by increasing the angle (e.g., a 15 degree angle would result in approximately 50 percent increase in the transition deflection). For a given deflection, the effective boom stiffness is increased significantly due to the increase in the offset force (Equation 3.4-18). On the other hand, the effective boom stiffness at the transitional deflection can be shown to be

$$K_{\text{eff}} = \frac{6 EI}{L^3} - \frac{3T}{15 L} \quad (3.4-18)$$

which is not affected by the cant angle (i.e., the increase in the transitional deflection compensates for the increase in the force deflection characteristics).

Table 3-34. Effect of Blanket Tension on Force-Deflection Characteristics of "V" Configuration Solar Array

Blanket Tension per Side (T)		Transition Deflection ( $\delta_T$ )		Symmetric Frequency at $\delta_T$	Offset Force ( $F_o$ )		Transition Force ( $F_T$ )	
(lb)	(N)	(ft)	(m)		(lb)	(N)	(lb)	(N)
40	177.9	7.70	2.347	0.1476	1.027	4.568	1.853	4.684
37	164.6	7.31	2.228	0.1429	0.950	4.226	1.071	4.764
34	151.2	6.89	2.100	0.1380	0.873	3.883	1.007	4.790
31	137.9	6.45	1.966	0.1329	0.796	3.541	1.072	4.768
28	124.5	5.98	1.823	0.1275	0.719	3.198	1.053	4.684
25	111.2	5.49	1.673	0.1220	0.642	2.856	1.021	4.541
22	97.9	4.97	1.515	0.1161	0.565	2.513	0.974	4.332
20	89.0	4.61	1.405	0.1120	0.513	2.282	0.933	4.150
14	62.3	3.43	1.046	0.0985	0.359	1.597	0.761	3.385
11	48.9	2.78	0.847	0.0909	0.282	1.254	0.644	2.865
10	44.5	2.56	0.780	0.0881	0.257	1.143	0.601	2.673
7	31.1	1.85	0.564	0.0789	0.180	0.801	0.452	2.010
4	17.8	1.09	0.332	0.0671	0.103	0.458	0.275	1.223
2.5	11.1	0.70	0.213	0.0583	0.064	0.285	0.181	0.805
1.	4.5	0.28	0.085	0.0425	0.026	0.116	0.075	0.334



The fundamental symmetric resonant frequency determined from the analytical model is shown in Figure 3-115 for the range of tension values investigated. For comparison, the symmetric and antisymmetric frequencies of the baseline planar array are also shown. The "V" array frequency is shown for oscillation amplitudes equal to the transitional deflection and one-tenth the transitional deflection. It should be noted that the small amplitude curve is questionable due to neglecting the Region 1 stiffness. The calculated "V" symmetric frequency trend does not show the flattening effect exhibited by the planar array and indicates that planar array symmetric frequency at the transitional amplitudes can be nearly tripled by increasing the blanket tension of the "V" configuration. It appears that the high blanket tension is indeed realistic since the critical buckling load for the boom for Region 2 is approximately 356 N (80 lb) (e.g., an 89 N (20 lb) blanket tension corresponds to approximately 50 percent of the Region 2 buckling load). Without considering the additional torsional stiffening derived from the "V" configuration, antisymmetric frequencies, approximately three times those of the baseline can be obtained as shown by the planar array antisymmetric frequency variation.

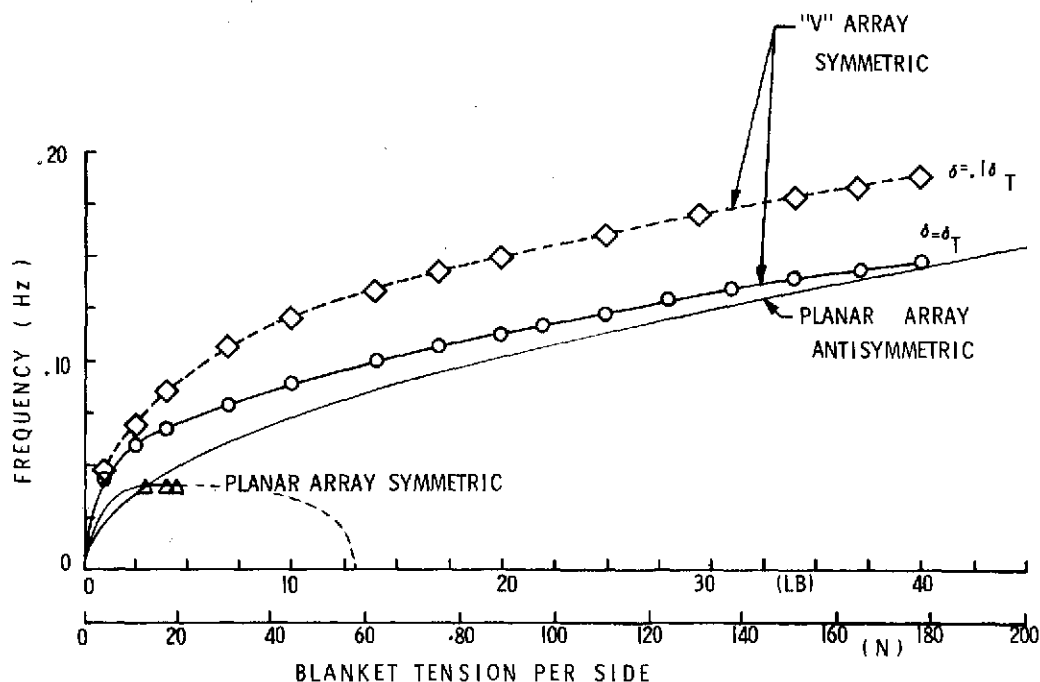


Figure 3-115. Effect of Blanket Tension on Solar Array Frequency



#### 3.4.5.5 Assessment of Reduced Stiffness

In this section, the reduction of the boom stiffness that can be obtained for the baseline configuration is examined. In the previous section, the stiffening effect of the "V" configuration was studied and shown to be highly effective. Another way of taking advantage of the stiffening would be to lower the bending stiffness of the boom while holding the blanket tension constant at a value sufficient to satisfy the 0.04 Hz frequency requirement. This was studied using a BI-STEM boom and neglecting the effect of the "V" shape on the antisymmetric frequency.

For the baseline design, the required blanket tension (per side) of a planar configuration was determined to be approximately 14.2 N (3.2 lb). The tension was set at this value and the boom stiffness varied through the range of practical interest.

The range of boom stiffness that was considered practical was based on the buckling load of the array for the required tension value. If a conservative design approach is used, a criteria that the buckling load of the cantilever boom is not exceeded could be selected. Alternately, a less conservative criteria is that the buckling load of the boom with the blanket restoring moment acting would not be exceeded. Using the first criteria, the boom could not buckle for any range of deflections whereas the second criteria would result in boom buckling if the tip deflection was greater than the transitional deflection. Using these two criteria, a boom stiffness in the range of 248 to 1240 N-m<sup>2</sup> (600 to 3000 lb-ft<sup>2</sup>) was selected as shown in Figure 3-116. This approximately spans the buckling load of the boom with and without the blanket tension constraint; i.e., an EI of 1053 N-m<sup>2</sup> (2550 lb-ft<sup>2</sup>) satisfied the first criteria and an EI of approximately 330 N-m<sup>2</sup> (800 lb-ft<sup>2</sup>) satisfies the second criteria. Force-deflection values are summarized in Table 3-35.

The calculated symmetric frequencies for this boom stiffness range satisfies the 0.04 Hz requirement for oscillations at the transitional deflection and a large margin is indicated for smaller oscillation amplitudes. Consequently, the controlling factor is boom buckling.

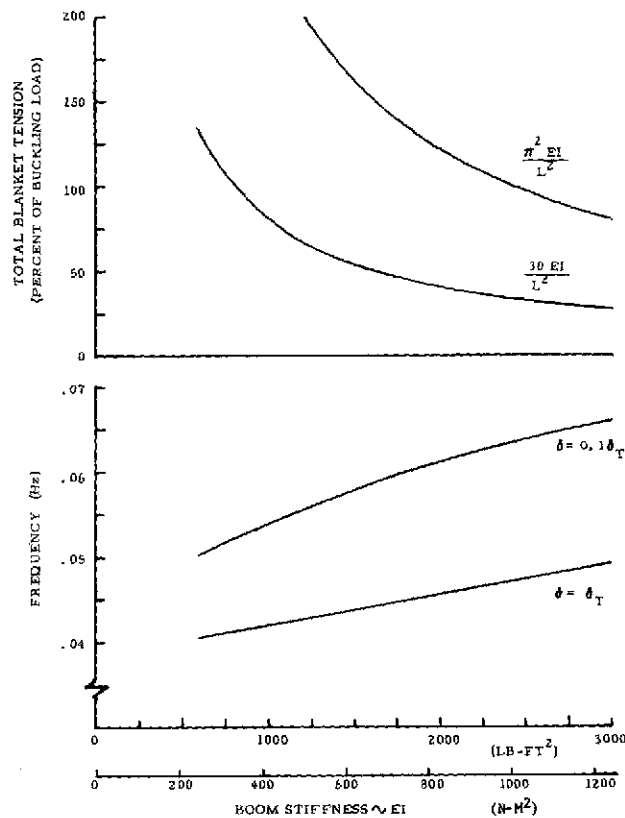


Figure 3-116. Effect of Boom Stiffness on "V" Configuration Solar Array Characteristics

Table 3-35. Effects of Boom Stiffness on Force-Deflection Characteristic of "V" Configuration Solar Array

Boom Bending Stiffness		Transitional Deflection ( $\delta_T$ )		Symmetric Frequency @ $\delta_T$	Offset Force		Transition Force	
(lb-ft <sup>2</sup> )	(N-m <sup>2</sup> )	(ft)	(m)		(lb)	(N)	(lb)	(N)
3000	1240	2.73	.832	.0486	.0822	.366	.189	.841
2700	1116	3.00	.914	.0478			.184	.818
* 2400	992	3.32	1.012	.0469			.177	.787
2100	868	3.72	1.134	.0459			.169	.752
1800	744	4.22	1.286	.0449			.158	.703
1500	620	4.89	1.490	.0439			.144	.641
1200	496	5.81	1.771	.0427			.125	.556
900	372	7.16	2.182	.0416	.0822	.366	.096	.427
** 600	248	9.31	2.838	.0404			.051	.227

\* Less than cantilever buckling load

\*\* Less than constrained buckling load

For the lowest practical value of boom stiffness considered, the transitional deflection of the boom tip is 2.2 m (7.2 ft), and the boom transitional force is 0.44 N (0.10 lbs). This transitional force appears to compare favorably with space station mission requirement of  $7 \times 10^{-4}$  g, a 0.36 N (0.08 lb) force.

### 3.4.6 THERMAL ANALYSIS OF SOLAR CELL BLANKET

#### 3.4.6.1 Introduction

A detailed thermal analysis of several possible solar cell blanket configurations was performed to determine the solar cell steady-state equilibrium temperatures. In all cases, the integrally covered, 125  $\mu\text{m}$  thick cells were assumed to have a solar absorptance ( $\alpha_s$ ) of 0.84 and a hemispherical emittance ( $\epsilon_h$ ) of 0.84.

#### 3.4.6.2 Solar Cell/Substrate Modeling

A 37 mode thermal analytical model was established for the two possible design concepts shown in Figure 3-117. System symmetry allows the model to be described in terms of one quarter of a solar cell. Concept A has a continuous sheet of Kapton behind, but not in contact with the rear surface of the solar cell. Concept B has about 50% of Kapton substrate cut away at the cell center with a silicone adhesive protective coating applied to the cell contact in the cut-out area. The back surface of the cell was assigned two values of hemispherical emissivity, 0.03 and 0.85. The thermal properties of all concept materials used in this evaluation are given in Table 3-36.

#### 3.4.6.3 Transmittance Properties of Kapton-H Film

The transmittance of the Kapton film solar cell blanket substrate is an important factor in the determination of the steady-state equilibrium temperature of the solar cells. After a review of the available properties data on this material failed to yield transmittance in the infrared portion of the spectrum, the measurement shown in Figure 3-118 was performed on a 50  $\mu\text{m}$  thick specimen using a Perkin-Elmer Model 457 Infrared Spectrophotometer. This transmittance curve was then used to determine the effective transmittance at various solar cell operating temperatures. This calculation is shown in Table 3-37 for a cell temperature of

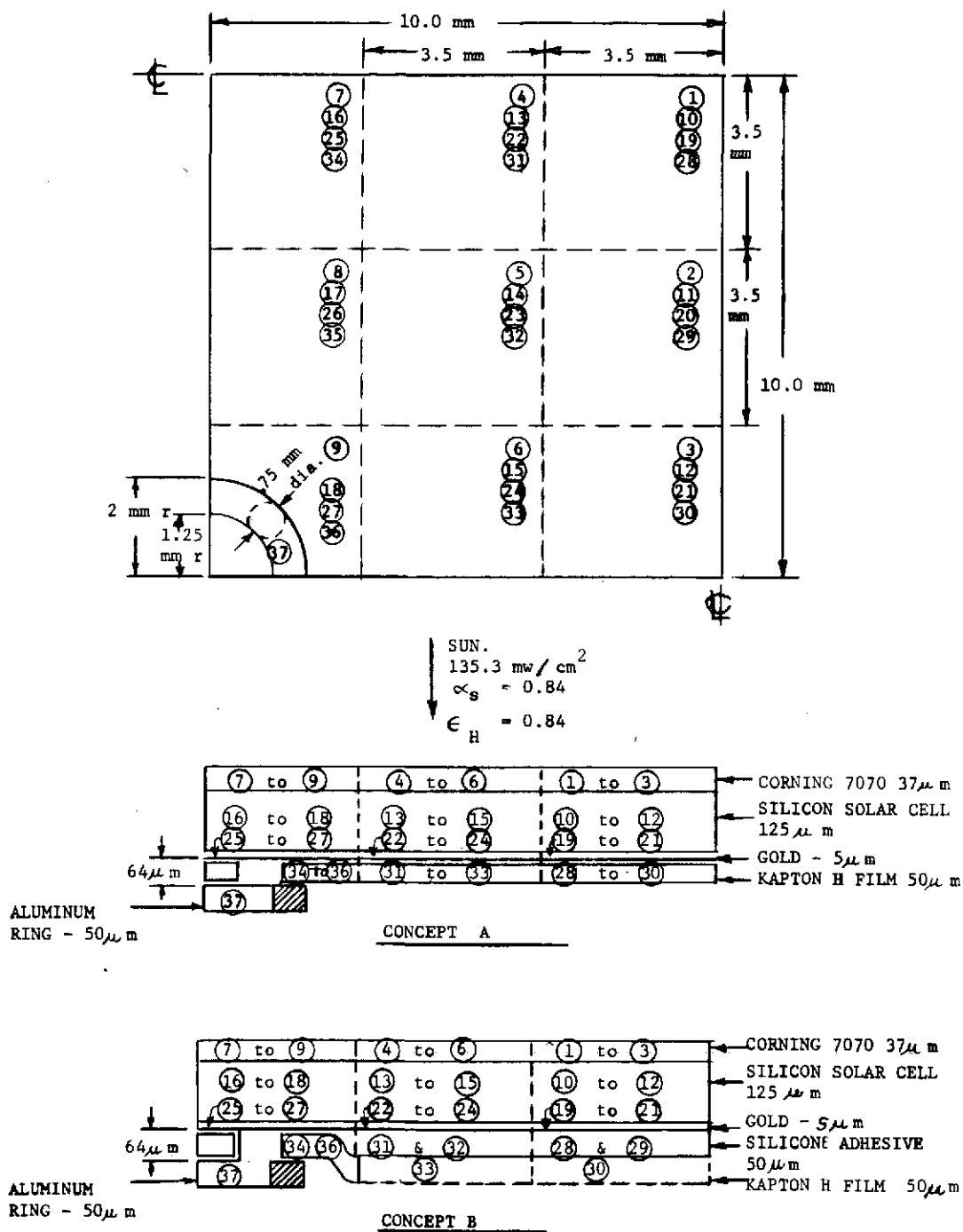


Figure 3-117. Solar Cell Thermal Model - 37 Nodes

76.7°C (170°F). The wavelength band from 2.5 to 40 μm was divided into 91 intervals as indicated by columns 1 and 2 of the table. Planck's law for the monochromatic thermal radiation intensity of a black body in the normal direction is given by

$$i_{\lambda bn} = \frac{2C_1}{\lambda^5 \left[ \exp \left( \frac{C_2}{\lambda T} \right) - 1 \right]} \quad (3.4-19)$$

where

T = absolute temperature (R)

λ = wavelength (μm)

C<sub>1</sub> = 0.18892 x 10<sup>8</sup> Btu · μm<sup>4</sup> · hr<sup>-1</sup> · ft<sup>-2</sup>

C<sub>2</sub> = 25896 μm · R

Table 3-36. Material Thermal Properties

Material	Thermal Conductivity (Btu/hr ft°F)	Density (lb/in <sup>3</sup> )	Specific Heat (Btu/lb°F)	Hemispherical Emissivity	Solar Absorptivity
Corning 7070 Glass	0.70	0.077	0.17		
Silicon (Solar Cell)	48.3	0.084	0.162	0.84	0.84
Gold (on back surface of cell)	170.0	0.698	0.031	0.03/.85**	---
Kapton H Film* (50 μm)	0.097	0.051	0.30	0.67	---
Silicone Adhesive	0.10	0.038	0.34	0.85	---
Aluminum	100.	0.100	0.23	0.34/.85**	---

\* Transmittance = 0.37 (see Section 3.4.6.3)

\*\* Maximum value assumed obtainable with surface treatment or coating

Page intentionally left blank

Table 3-37. Calculation of Kapton Transmittance for a  
76.7°C (170°F) Black Body Radiation Spectrum

WAVELENGTH INTERVAL (MICRONS)	ENERGY DENSITY (BTU/HR-FT <sup>2</sup> -°C)	FRACTION OF TOTAL ENERGY IN INTERVAL	KAPTON TRANSMISSION	ACCUM. ENERGY THRU KAPTON
2.5	2.6	0.0034914	0.96	0.0033518
2.6	2.7	0.0052579	0.98	0.0086097
2.7	2.8	0.0077183	0.95	0.0163280
2.8	2.9	0.0109078	0.75	0.0272358
2.9	3.0	0.0149565	0.82	0.0421927
3.0	3.1	0.0199866	0.88	0.0621793
3.1	3.2	0.0260666	0.78	0.0882459
3.2	3.3	0.0333333	0.40	0.1215797
3.3	3.4	0.0417834	0.70	0.1633631
3.4	3.5	0.0514726	0.08	0.2148407
3.5	3.6	0.0624144	0.03	0.2772551
3.6	3.7	0.0746092	0.70	0.3518643
3.7	3.8	0.0880006	0.80	0.4398649
3.8	3.9	0.1025668	0.82	0.5424317
3.9	4.0	0.1182328	0.75	0.6606655
4.0	4.1	0.1349176	0.66	0.7955831
4.1	4.2	0.1525277	0.67	0.9481011
4.2	4.3	0.1709631	0.76	1.1190642
4.3	4.4	0.1901044	0.82	1.3095686
4.4	4.5	0.2098456	0.79	1.5207142
4.5	4.6	0.2300668	0.80	1.7527810
4.6	4.7	0.2506478	0.80	2.0058288
4.7	4.8	0.2714744	0.84	2.2892932
4.8	4.9	0.2924323	0.80	2.6027255
4.9	5.0	0.3134124	0.73	2.9461379
5.0	5.1	0.3343187	0.65	3.3205494
5.1	5.2	0.3550296	0.71	3.7259786
5.2	5.3	0.3754785	0.65	4.1624571
5.3	5.4	0.3955738	0.58	4.6300309
5.4	5.5	0.4152396	0.56	5.1298774
5.5	5.6	0.4344877	0.54	5.6620666
5.6	5.7	0.4533174	0.38	6.2253840
5.7	5.8	0.4718158	0.30	6.8167997
5.8	5.9	0.4898359	0.21	7.4366356
5.9	6.0	0.5073021	0.02	8.0839377
6.0	6.1	0.5242195	0.01	8.7581572
6.1	6.2	0.5405833	0.05	9.4593405
6.2	6.3	0.5564738	0.14	10.1878143
6.3	6.4	0.5668768	0.28	10.9446881
6.4	6.5	0.5768832	0.10	11.7215613
6.5	6.6	0.5864884	0.20	12.5180597
6.6	6.7	0.5956924	0.25	13.3342521
6.7	6.8	0.6044965	0.12	14.1700486
6.8	6.9	0.6128138	0.03	15.0253624
6.9	7.0	0.6206483	0.04	15.8999107
7.0	7.1	0.6280149	0.04	16.7929249
7.1	7.2	0.6349182	0.08	17.7048497
7.2	7.3	0.6413629	0.07	18.6357976
7.3	7.4	0.6473533	0.01	19.5857509
7.4	7.5	0.6528933	0.05	20.5546442
7.5	7.6	0.6579878	0.03	21.5425220
7.6	7.7	0.6626409	0.01	22.5494829
7.7	7.8	0.6668576	0.01	23.5745305
7.8	7.9	0.6706429	0.01	24.6176734
7.9	8.0	0.6739999	0.02	25.6787223
8.0	8.1	0.6769315	0.02	26.7576738
8.1	8.2	0.6794417	0.02	27.8545280
8.2	8.3	0.6815345	0.02	28.9692022
8.3	8.4	0.6832138	0.02	30.0917160
8.4	8.5	0.6844835	0.02	31.2221895
8.5	8.6	0.6853486	0.02	32.3605381
8.6	8.7	0.6858131	0.02	33.5067512
8.7	8.8	0.6858822	0.02	34.6608294
8.8	8.9	0.6855511	0.02	35.8227725
8.9	9.0	0.6848244	0.02	36.9925969
9.0	9.1	0.6837087	0.02	38.1703056
9.1	9.2	0.6822071	0.02	39.3559137
9.2	9.3	0.6803255	0.02	40.5493292
9.3	9.4	0.6780688	0.02	41.7505530
9.4	9.5	0.6754321	0.02	42.9595851
9.5	9.6	0.6724204	0.02	44.1764155
9.6	9.7	0.6690387	0.02	45.4009542
9.7	9.8	0.6652919	0.02	46.6331961
9.8	9.9	0.6611851	0.02	47.8730422
9.9	10.0	0.6567244	0.02	49.1194926
10.0	10.1	0.6519159	0.02	50.3725485
10.1	10.2	0.6467655	0.02	51.6322100
10.2	10.3	0.6412791	0.02	52.8984791
10.3	10.4	0.6354626	0.02	54.1703567
10.4	10.5	0.6293229	0.02	55.4478436
10.5	10.6	0.6228660	0.02	56.7309406
10.6	10.7	0.6160988	0.02	58.0196384
10.7	10.8	0.6090282	0.02	59.3139370
10.8	10.9	0.6016611	0.02	60.6138361
10.9	11.0	0.5940045	0.02	61.9193356
11.0	11.1	0.5860654	0.02	63.2304364
11.1	11.2	0.5778408	0.02	64.5471384
11.2	11.3	0.5693377	0.02	65.8694516
11.3	11.4	0.5605631	0.02	67.1973760
11.4	11.5	0.5515250	0.02	68.5309120
11.5	11.6	0.5422414	0.02	69.8699604
11.6	11.7	0.5327203	0.02	71.2145212
11.7	11.8	0.5229707	0.02	72.5645919
11.8	11.9	0.5129916	0.02	73.9199635
11.9	12.0	0.5027831	0.02	75.2805360
12.0	12.1	0.4923452	0.02	76.6463092
12.1	12.2	0.4816779	0.02	78.0172821
12.2	12.3	0.4707812	0.02	79.3934547
12.3	12.4	0.4596550	0.02	80.7748269
12.4	12.5	0.4482992	0.02	82.1613987
12.5	12.6	0.4367137	0.02	83.5531702
12.6	12.7	0.4248984	0.02	84.9501414
12.7	12.8	0.4128532	0.02	86.3523126
12.8	12.9	0.4005780	0.02	87.7596846
12.9	13.0	0.3880728	0.02	89.1722574
13.0	13.1	0.3753375	0.02	90.5900299
13.1	13.2	0.3623721	0.02	92.0129920
13.2	13.3	0.3491766	0.02	93.4411436
13.3	13.4	0.3357510	0.02	94.8744946
13.4	13.5	0.3220954	0.02	96.3130450
13.5	13.6	0.3082098	0.02	97.7567958
13.6	13.7	0.2940942	0.02	99.2057469
13.7	13.8	0.2797486	0.02	100.6598983
13.8	13.9	0.2651730	0.02	102.1191497
13.9	14.0	0.2503674	0.02	103.5835011
14.0	14.1	0.2353318	0.02	105.0528525
14.1	14.2	0.2200662	0.02	106.5272039
14.2	14.3	0.2045706	0.02	108.0065553
14.3	14.4	0.1888450	0.02	109.4909067
14.4	14.5	0.1728894	0.02	110.9802581
14.5	14.6	0.1566938	0.02	112.4746095
14.6	14.7	0.1402582	0.02	113.9739609
14.7	14.8	0.1235826	0.02	115.4783123
14.8	14.9	0.1066670	0.02	116.9876637
14.9	15.0	0.0895014	0.02	118.4920151
15.0	15.1	0.0720858	0.02	120.0013665
15.1	15.2	0.0554102	0.02	121.5157179
15.2	15.3	0.0394746	0.02	123.0350693
15.3	15.4	0.0242790	0.02	124.5594207
15.4	15.5	0.0098234	0.02	126.0887721
15.5	15.6	0.0000000	0.02	127.6231235
15.6	15.7	0.0000000	0.02	129.1624749
15.7	15.8	0.0000000	0.02	130.7068263
15.8	15.9	0.0000000	0.02	132.2561777
15.9	16.0	0.0000000	0.02	133.8105291
16.0	16.1	0.0000000	0.02	135.3698805
16.1	16.2	0.0000000	0.02	136.9342319
16.2	16.3	0.0000000	0.02	138.5035833
16.3	16.4	0.0000000	0.02	140.0779347
16.4	16.5	0.0000000	0.02	141.6572861
16.5	16.6	0.0000000	0.02	143.2416375
16.6	16.7	0.0000000	0.02	144.8309889
16.7	16.8	0.0000000	0.02	146.4253403
16.8	16.9	0.0000000	0.02	148.0246917
16.9	17.0	0.0000000	0.02	149.6290431
17.0	17.1	0.0000000	0.02	151.2383945
17.1	17.2	0.0000000	0.02	152.8527459
17.2	17.3	0.0000000	0.02	154.4720973
17.3	17.4	0.0000000	0.02	156.0964487
17.4	17.5	0.0000000	0.02	157.7258001
17.5	17.6	0.0000000	0.02	159.3601515
17.6	17.7	0.0000000	0.02	161.0005029
17.7	17.8	0.0000000	0.02	162.6468543
17.8	17.9	0.0000000	0.02	164.2992057
17.9	18.0	0.0000000	0.02	165.9575571
18.0	18.1	0.0000000	0.02	167.6219085
18.1	18.2	0.0000000	0.02	169.2922599
18.2	18.3	0.0000000	0.02	170.9686113
18.3	18.4	0.0000000	0.02	172.6509627
18.4	18.5	0.0000000	0.02	174.3393141
18.5	18.6	0.0000000	0.02	176.0336655
18.6	18.7	0.0000000	0.02	177.7340169
18.7	18.8	0.0000000	0.02	179.4403683
18.8	18.9	0.0000000	0.02	181.1527197
18.9	19.0	0.0000000	0.02	182.8710711
19.0	19.1	0.0000000	0.02	184.5954225
19.1	19.2	0.0000000	0.02	186.3257739
19.2	19.3	0.0000000	0.02	188.0621253
19.3	19.4	0.0000000	0.02	189.8044767
19.4	19.5	0.0000000	0.02	191.5528281
19.5	19.6	0.0000000	0.02	193.3071795
19.6	19.7	0.0000000	0.02	195.0675309
19.7	19.8	0.0000000	0.02	196.8338823
19.8	19.9	0.0000000	0.02	198.6062337
19.9	20.0	0.0000000	0.02	200.3845851
20.0	20.1	0.0000000	0.02	202.1689365
20.1	20.2	0.0000000	0.02	203.9592879
20.2	20.3	0.0000000	0.02	205.7556393
20.3	20.4	0.0000000	0.02	207.5579907
20.4	20.5	0.0000000	0.02	209.3663421
20.5	20.6	0.0000000	0.02	211.1806935
20.6	20.7	0.0000000	0.02	213.0010449
20.7	20.8	0.0000000	0.02	214.8273963
20.8	20.9	0.0000000	0.02	216.6597477
20.9	21.0	0.0000000	0.02	218.4980991
21.0	21.1	0.0000000	0.02	220.3424505
21.1	21.2	0.0000000	0.02	222.1928019
21.2	21.3	0.0000000	0.02	224.0491533
21.3	21.4	0.0000000	0.02	225.9115047
21.4	21.5	0.0000000	0.02	227.7798561
21.5	21.6	0.0000000	0.02	229.6542075
21.6	21.7	0.0000000	0.02	231.5345589
21.7	21.8	0.0000000	0.02	233.4209103
21.8	21.9	0.0000000	0.02	235.3132617
21.9	22.0	0.0000000	0.02	237.2116131
22.0	22.1	0.0000000	0.02	239.1159645
22.1	22.2	0.0000000	0.02	241.0263159
22.2	22.3	0.0000000	0.02	242.9426673
22.3	22.4	0.0000000	0.02	244.8649187
22.4	22.5	0.0000000	0.02	246.7931701
22.5	22.6	0.0000000	0.02	248.7274215
22.6	22.7			

This equation was integrated over each energy interval to obtain the results given in column 3. Column 4 gives this energy in terms of the fraction of the total energy emitted at this temperature, where the total energy is given by:

$$i_{bn} = \frac{\sigma T^4}{\pi} \quad (3.4-20)$$

where

$$\begin{aligned} \sigma &= \text{Boltzmann constant} \\ &= 0.1714 \times 10^{-8} \text{ Btu hr}^{-1} \text{ ft}^{-2} \text{ R}^{-4} \end{aligned}$$

The average Kapton transmittance in each energy interval is given in column 5 based on the test results shown in Figure 3-118. The last column in the table gives the accumulative energy which is transmitted through the Kapton.

The total average transmittance can be obtained by dividing the transmitted energy (28.626 Btu/hr-ft<sup>2</sup>) by the total energy emitted by the solar cell (85.766 Btu/hr-ft<sup>2</sup>). The resulting average transmittance of 0.334 assumes that the transmittance above 40  $\mu\text{m}$  wavelength is zero. Table 3-38 shows the results of the average transmittance calculations for various assumptions as to the transmittance above 40  $\mu\text{m}$ . For the higher temperatures where a large fraction of the total energy is below 40  $\mu\text{m}$ , the total average transmittance can be calculated within a few percentage points.

An average Kapton transmittance of 0.37 was used to obtain the results reported in the next section.

#### 3.4.6.4 Results of Analysis

Steady-state temperature distributions by mode (as defined in Figure 3-117) are presented in Table 3-39 for the two design concepts. These results reflect the influence of the values for the emissivity of the solar cell rear surface:  $\epsilon_h = 0.03$  and 0.85. The lower value is typical for an uncoated gold surface, while the higher emissivity could be made possible through the



Table 3-38. Calculation of Total Average Kapton Transmittance

Solar Cell Temperature		Fraction of Total Energy Less than 40 $\mu\text{m}$	Total Radiated Energy (Btu/hr ft <sup>2</sup> )	Total Energy Through Kapton Less than 40 $\mu\text{m}$ (Btu/hr ft <sup>2</sup> )	Total Average Transmittance			
$^{\circ}\text{C}$	$^{\circ}\text{F}$				Zero Average Transmittance Above 40 $\mu\text{m}$	0.30 Average Transmittance Above 40 $\mu\text{m}$	0.50 Average Transmittance Above 40 $\mu\text{m}$	0.90 Average Transmittance Above 40 $\mu\text{m}$
76.7	170	0.9628	85.766	28.626	0.334	0.345	0.352	0.367
65.6	150	0.9596	75.377	25.416	0.337	0.349	0.357	0.374
54.4	130	0.9560	65.962	22.514	0.341	0.355	0.363	0.381
-101.1	-150	0.8012	5.017	2.116	0.422	0.481	0.521	0.601
-157.3	-250	0.5880	1.054	0.382	0.362	0.486	0.568	0.733

Table 3-39. Steady-State Temperature Distributions

Node No.	Nodal Temperatures ( $^{\circ}\text{F}$ )						
	Concept A			Concept B			
	$\epsilon_h = 0.03$ No Power Extraction	$\epsilon_h = 0.85$ No Power Extraction	$\epsilon_h = 0.85$ 6.0 w/ft <sup>2</sup> Power Extraction	$\epsilon_h = 0.03$ No Power Extraction	$\epsilon_h = 0.85$ No Power Extraction	$\epsilon_h = 0.03$ 6.0 w/ft <sup>2</sup> Power Extraction	$\epsilon_h = 0.85$ 6.0 w/ft <sup>2</sup> Power Extraction
1	240.33	163.82	153.65	176.17	148.07	165.72	138.27
2	240.32	163.82	153.65	176.50	148.17	166.02	138.36
3	240.31	163.82	153.64	177.16	148.37	166.63	138.54
4	240.32	163.82	153.65	176.50	148.17	166.02	138.36
5	240.30	163.82	153.63	176.77	148.26	166.26	138.43
6	240.26	163.82	153.62	177.33	148.43	166.76	138.57
7	240.31	163.82	153.64	177.16	148.38	166.63	138.54
8	240.26	163.82	153.62	177.33	148.43	166.76	138.57
9	240.16	163.82	153.55	177.51	148.51	166.87	138.59
10	240.36	163.84	153.67	176.20	148.09	165.74	138.29
11	240.35	163.84	153.67	176.52	148.19	166.04	138.37
12	240.34	163.84	153.66	177.18	148.39	166.65	138.56
13	240.35	163.84	153.67	176.52	148.19	166.04	138.37
14	240.33	163.84	153.65	176.79	148.28	166.28	138.44
15	240.30	163.84	153.63	177.35	148.45	166.78	138.59
16	240.34	163.84	153.66	177.18	148.39	166.65	138.56
17	240.29	163.84	153.63	177.35	148.45	166.78	138.59
18	240.19	163.84	153.57	177.53	148.52	166.89	138.61
19	240.36	163.84	153.67	176.20	148.09	165.74	138.28
20	240.35	163.84	153.67	176.52	148.19	166.04	138.37
21	240.34	163.84	153.66	177.18	148.39	166.65	138.56
22	240.35	163.84	153.67	176.52	148.19	166.04	138.37
23	240.33	163.84	153.65	176.79	148.27	166.28	138.44
24	240.29	163.84	153.63	177.35	148.45	166.78	138.59
25	240.34	163.84	153.66	177.18	148.39	166.65	138.56
26	240.29	163.84	153.63	177.35	148.45	166.78	138.59
27	240.19	163.84	153.57	177.53	148.52	166.89	138.61
28	-194.32	19.46	11.67	176.00	147.92	165.56	138.13
29	-191.84	19.52	11.73	176.32	148.02	165.85	138.22
30	-188.64	19.69	11.90	-199.25	7.95	-202.45	0.45
31	-191.84	19.52	11.73	176.32	148.02	165.85	138.22
32	-186.06	19.88	12.09	176.59	148.11	166.09	138.29
33	-175.49	21.51	13.70	-187.76	10.01	-191.50	2.49
34	-188.64	19.69	11.90	-199.25	7.95	-202.45	0.45
35	-175.49	21.51	13.70	-187.76	10.01	-191.50	2.49
36	-132.29	37.44	29.07	-158.25	25.00	-163.62	16.93
37	240.19	163.84	153.57	177.53	148.52	166.89	138.60

use of a black chromium coating over the gold on the rear contact surface. For Concept A, the average solar cell equilibrium temperatures are  $240.3^{\circ}\text{F}$  ( $115.7^{\circ}\text{C}$ ) and  $163.8^{\circ}\text{F}$  ( $73.2^{\circ}\text{C}$ ) for  $\epsilon_h = 0.03$  and  $0.85$  respectively, as compared to  $177.0^{\circ}\text{F}$  ( $80.6^{\circ}\text{C}$ ) and  $148.3^{\circ}\text{F}$  ( $64.6^{\circ}\text{C}$ ) for the same emissivities when used with the Concept B configuration. The influence of electrical power extraction is shown for Concept A for an end-of-mission electrical output of  $6 \text{ watt/ft}^2$  ( $64.6 \text{ watt/m}^2$ ). For this substrate configuration, the solar cell temperature with the high emissivity back is reduced from  $163.8^{\circ}\text{F}$  ( $73.2^{\circ}\text{C}$ ) with no electrical output to  $153.7^{\circ}\text{F}$  ( $67.6^{\circ}\text{C}$ ) with the  $6 \text{ watt/ft}^2$  output. The Concept A model was modified to include the conductivity coupling of the interconnector to the Kapton at the points where the interconnectors are welded to the solar cell. This model resulted in an average solar cell temperature of  $149.9^{\circ}\text{F}$  ( $65.5^{\circ}\text{C}$ ) under the conditions of  $6 \text{ watt/ft}^2$  ( $64.6 \text{ watt/m}^2$ ) electrical power extraction with the high emissivity rear coating. Based on this initial equilibrium condition, a 72 minute eclipse and subsequent heat-up transient temperature history was calculated with the resulting average solar cell temperature as given in Figure 3-119. A minimum cell temperature of  $-301^{\circ}\text{F}$  ( $-185^{\circ}\text{C}$ ) was achieved with an initial cool-down rate of  $123.2^{\circ}\text{F/minute}$ . Upon emergence from the shadow, the initial heat-up rate of the solar cell is  $139.9^{\circ}\text{F/minute}$  ( $188.8^{\circ}\text{C/minute}$ ).

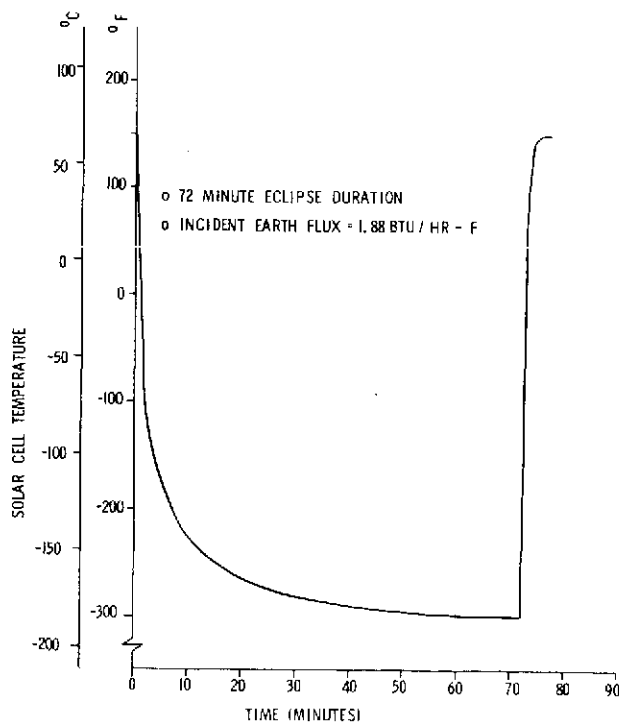


Figure 3-119. Cool-down and Heat-up Transient Temperature History in Geosynchronous Orbit

#### 3.4.6.5 Discussion of Results

The solar cell steady-state equilibrium temperatures from Table 3-39 were found to range from 240.3°F (115.7°C) to 138.5°F (59.2°C) depending on the assumed conditions of construction. The low emissivity of gold makes the use of a high emissivity coating mandatory in Concept A with a continuous Kapton sheet substrate. The lowest possible solar cell temperature with Concept A is about 150°F (65.5°C) with 6 watt/ft<sup>2</sup> (64.6 watts/m<sup>2</sup>) of electrical power extraction and with a conductivity attachment of the cell to the Kapton at the interconnector weld points. Under similar conditions, Concept B would yield a steady-state equilibrium temperature of about 135°F (57.2°C). These two extremes result in significantly different solar array outputs as shown in Figure 3-120. The continuous Kapton substrate configuration (Concept A) would produce 9.52 kw as opposed to 10.07 kw for Concept B with the cut-outs in the Kapton. Assuming no increase in blanket weight, this would be reflected as a power-to-mass ratio of 109.5 watt/kg for Concept A and 115.7 watt/kg for Concept B (see Figure 3-121). Thus, it is necessary to lower the solar cell temperature below 150°F (65.5°C) if the 110 watt/kg goal is to be achieved with the baseline configuration. The approach of cutting holes in the Kapton is an effective way to achieve this reduced temperature goal, but the cost impact of implementing this approach is significant since it is necessary to cover the exposed rear cell contact with an equivalent layer of adhesive to stop low energy protons.

#### 3.4.7 THERMAL STRESS ANALYSIS OF SOLAR CELL BLANKET

##### 3.4.7.1 Introduction

A thermal stress analysis of two possible solar cell blanket configurations was performed to evaluate the stress in the interconnectors which results when the solar array is thermal cycled in a geosynchronous orbit. The first configuration uses gold plated molybdenum circular ring interconnectors which are welded to the solar cell corners through small holes in the Kapton substrate. This configuration is similar to the RAE flat pack array. The second configuration, shown in Figure 3-13, uses wire interconnectors which are ultrasonically bonded to the solar cell through small slotted holes in the Kapton.

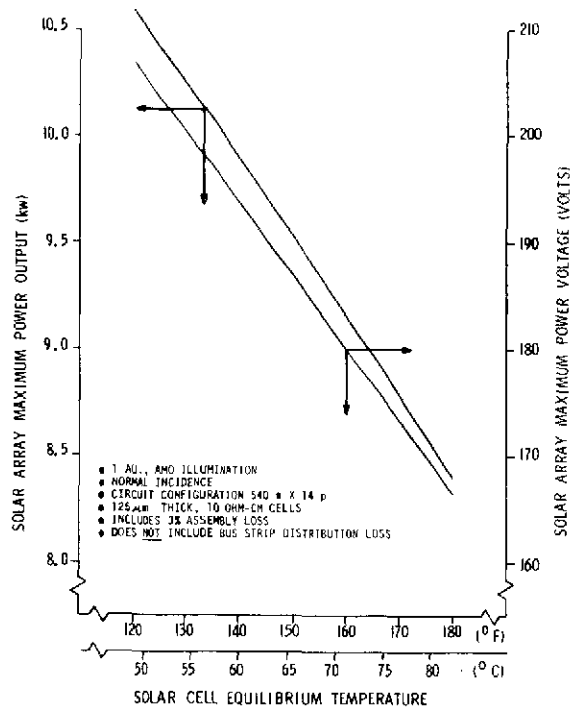


Figure 3-120. Solar Array Maximum Power Output vs Equilibrium Temperature

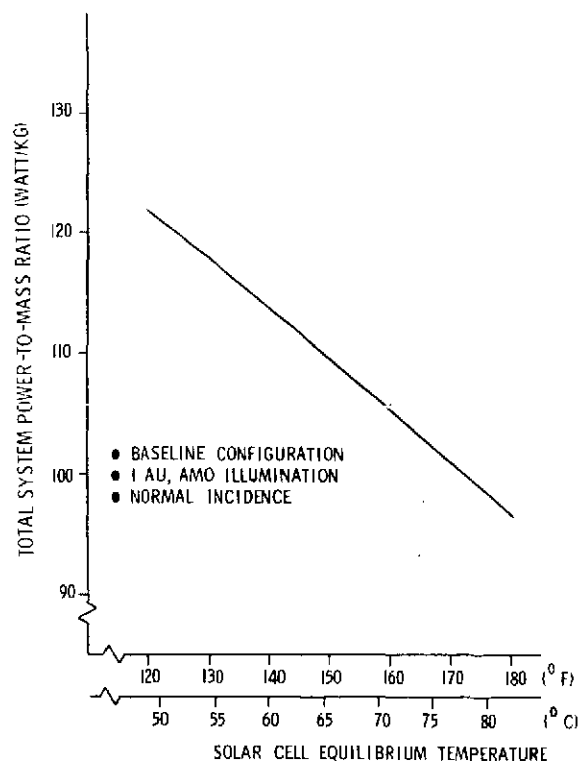


Figure 3-121. Power-to-Mass Ratio of Baseline Solar Array Panel Configuration vs Temperature

### 3.4.7.2 Material Properties

The mechanical properties of the various materials in the solar cell blanket must be established over the temperature range of interest ( $-190$  to  $+140^{\circ}\text{C}$ ). These properties include modulus of elasticity, modulus of rigidity, ultimate tensile strength, tensile yield strength, and linear thermal expansion. Table 3-40 lists the available mechanical properties data for the four materials in the solar cell blanket which interact in the mounting of the solar cells to the substrate.

The linear thermal expansion data for these materials is given in Figure 3-122 in terms of the fractional change in length  $\left( \frac{L - L_{20}}{L_{20}} \right)$  as a function of temperature. The unavailability of data for Kapton-H film at temperatures below  $20^{\circ}\text{C}$  led to the experimental determination of this data as described below.

Table 3-40. Mechanical Properties of Materials

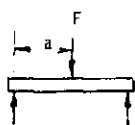
Material	Ultimate Tensile Strength			Tensile Yield Strength			Modulus of Elasticity			Reference
	T( $^{\circ}\text{C}$ )	Value (psi)	Value (GN/m $^2$ )	T( $^{\circ}\text{C}$ )	Value(1) (psi)	Value(1) (GN/m $^2$ )	T( $^{\circ}\text{C}$ )	Value (psi)	Value (GN/m $^2$ )	
Kapton-H film	-195	35,000	0.241				-195	510,000	3.52	65
	25	25,000	0.172	25	10,000	0.069	25	430,000	2.96	
	200	17,000	0.117	200	6,000	0.041	200	260,000	1.79	
Aluminum 1100-0	-195	28,000	0.193	-195	9,000	0.062	-195	$11.1 \times 10^6$	76.5	64
	25	13,000	0.090	25	7,000	0.048	25	$10.0 \times 10^6$	68.9	
Silicon Solar Cell (Heliotek, 10 $\mu$ -cm, Ag contacts, SiO coating, grid side in tension)	25	21,600 <sup>(2)</sup>	0.149 <sup>(2)</sup>	----	-----	-----	25	$6.6 \times 10^6$	45.5	41
Gold, pure, hard drawn	25	20,000	0.138	----	-----	-----	25	$11.4 \times 10^6$	78.6	

(1) At 3% elongation

(2) Average failure stress,  $\sigma^*$ , determined from three-point flexure test

$$\sigma^* = \frac{3aF}{bt^2}$$

where F = breaking force  
b = width of solar cell  
t = thickness of solar cell



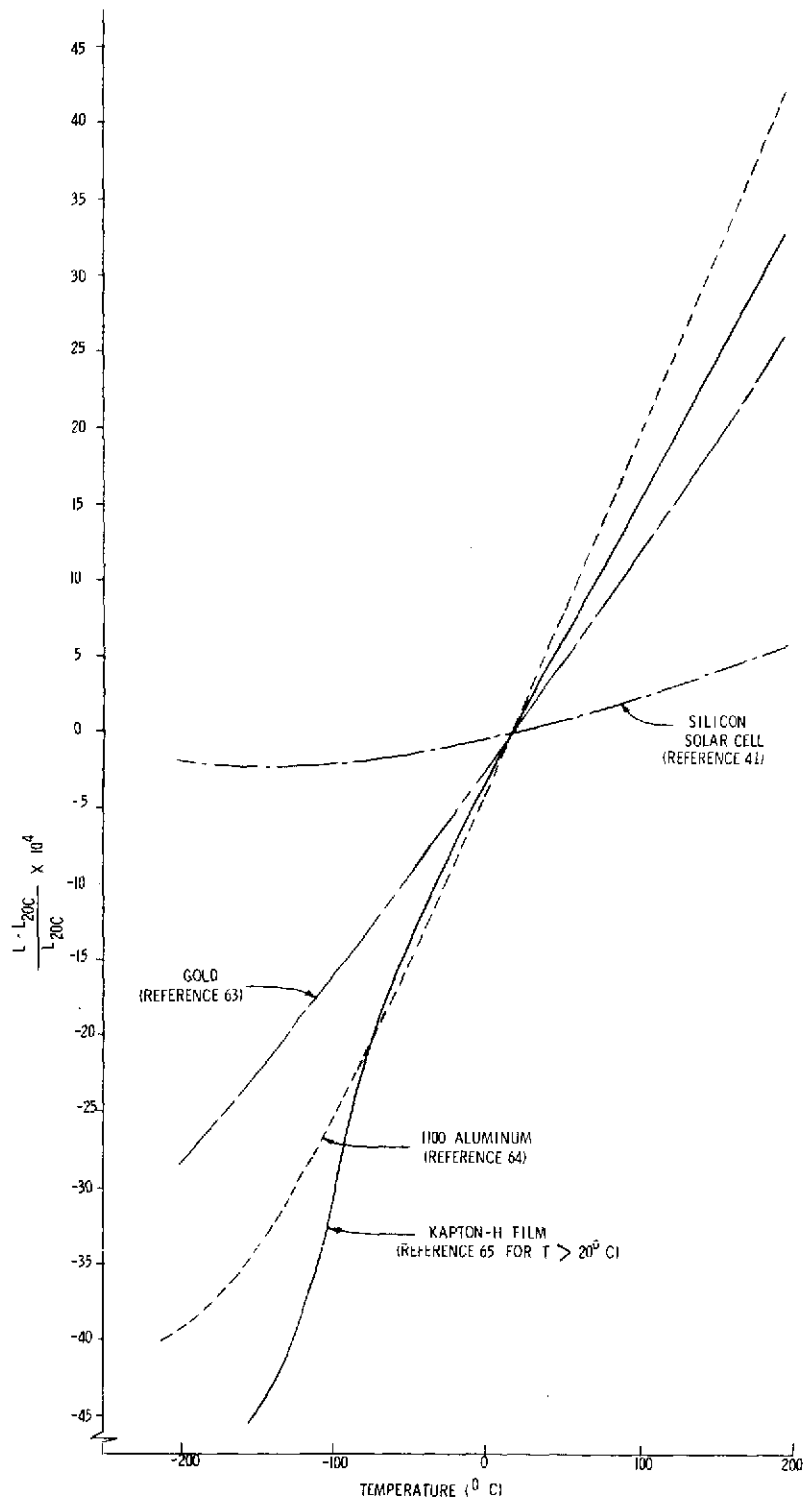


Figure 3-122. Linear Thermal Expansion of Solar Cell Blanket Materials

A 50  $\mu\text{m}$  (2 mil) thick sheet of Kapton-H film was mounted on a quartz frame to establish "fixed" points of reference for the end of the loop and the fixed part of an LVDT (Linear Variable Differential Transformer) displacement transducer. The moving part of the transducer was attached to the free end of the Kapton loop and produced a signal directly related to the position of the free end of the Kapton. The test fixture and specimen, shown in Figure 2-123, were installed in a temperature test chamber which was controlled at the discrete test temperature by the flow of liquid nitrogen into the chamber. The LVDT transducer temperature was controlled by an electric strip heater.

The LVDT transducer was calibrated by means of a micrometer over the displacement range of interest. The raw data measurements are given in Table 3-41 along with the corresponding calculated values for the specimen length which is given by:

$$\begin{aligned} L &= 2 \left[ Y - \frac{1}{2} (D_1 + D_2) \right] + \frac{\pi}{2} (D_1 + D_2) \\ &= 2Y + \left( \frac{\pi}{2} - 1 \right) (D_1 + D_2) \end{aligned} \quad (3.4-21)$$

This page is reproduced at the back of the report by a different reproduction method to provide better detail.

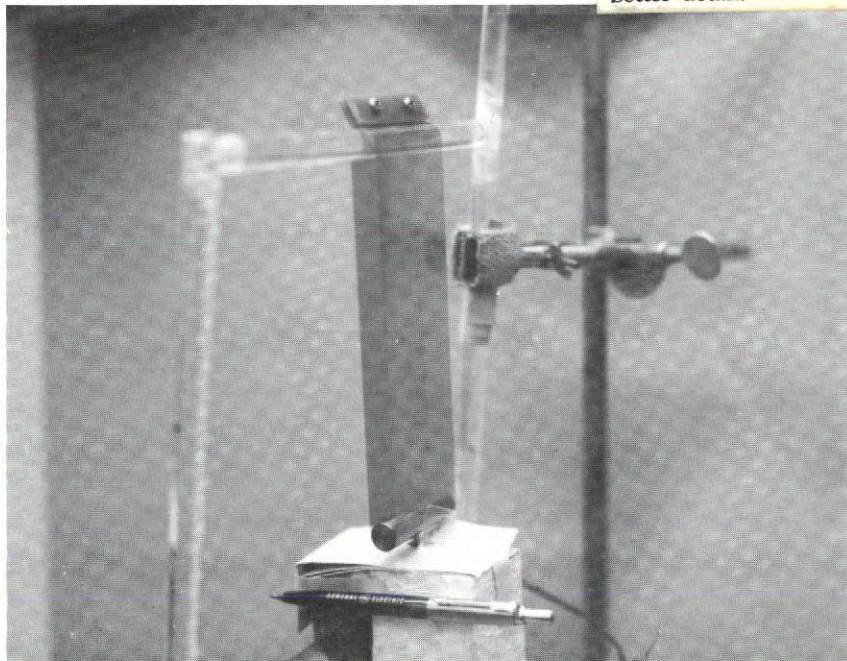
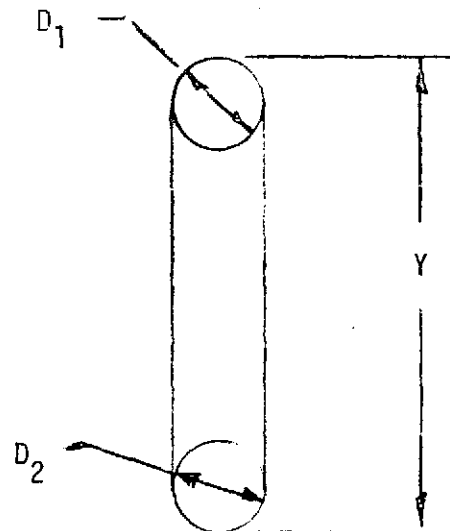


Figure 3-123. Kapton Thermal Expansion Test Set-up

Table 3-41. Raw and Reduced Data for Kapton Specimen Length

Test Temperature (°F)	LVDT Reading (volts)	Position (inches)	Specimen Length (L) (inches)
75.0	1.008	0.67200	14.55253
0.	1.560	0.67733	14.54175
-100.0	2.804	0.68647	14.52327
-200.0	4.787	0.70022	14.49559
-250.0	5.623	0.70529	14.48537
-200.0	4.621	0.69912	14.49779
-100.0	2.897	0.68716	14.52189
0.0	1.650	0.67798	14.54045
75.0	0.996	0.67184	14.55285



$$\left. \begin{array}{l} D_1 = 0.468 \text{ in} \\ D_2 = 0.500 \text{ in} \\ L = 7.000 \text{ in} \end{array} \right\} \text{ at } 75^{\circ}\text{F}$$



where

L = length of Kapton specimen (inches)

Y = distance between fixed point and LVDT reference

D<sub>1</sub>, D<sub>2</sub> = diameter of cylinders at ends of Kapton specimen

In this equation, Y and D<sub>2</sub> vary with test temperature, and D<sub>1</sub> is constant because the coefficient of fused quartz is assumed to be zero in this analysis. The room temperature value of Y is 7.00 inches as determined by measurement. The specimen length, L, given in Table 3-41 was determined by this equation with the dimension D<sub>2</sub> estimated based on published values for the coefficient of thermal expansion for steel. Based on these data, the average coefficient of linear thermal expansion is given in Table 3-42 for various temperature ranges based on the following definition:

$$\alpha = \frac{1}{L} \frac{\Delta L}{\Delta T} = \frac{1}{L_i} \left( \frac{L_f - L_i}{T_f - T_i} \right) \quad (3.4-22)$$

where

$\alpha$  = average coefficient of linear expansion (in/in<sup>°</sup>F)

L = specimen length (inches)

T = specimen temperature (°F)

and subscripts f, i refer to final and initial conditions

Inspection of these data show the reading at the 75<sup>°</sup>F end point test was not the same as it was for the 75<sup>°</sup>F beginning point of the test. Similarly, there are differences at the 0, -100, and -200 data points. It is not known if there is truly hysteresis in the specimen or if the accumulated errors in the test setup and instrumentation are the major contributor. The fact that the deviations are not consistent with respect to the largest value are considered to indicate the difference is due to errors in the data rather than hysteresis in the material. Note that the differences in specimen length are larger than the apparent hysteresis as shown by comparison of the value in Table 3-42. The maximum difference in  $\alpha$  is 0.000003 and occurs for the data at -200<sup>°</sup>F and -250<sup>°</sup>F. In most cases, the difference between comparable values is less than 10%.

Table 3-42. Linear Coefficient of Thermal Expansion  
for Kapton-H Film (50  $\mu\text{m}$  thick)

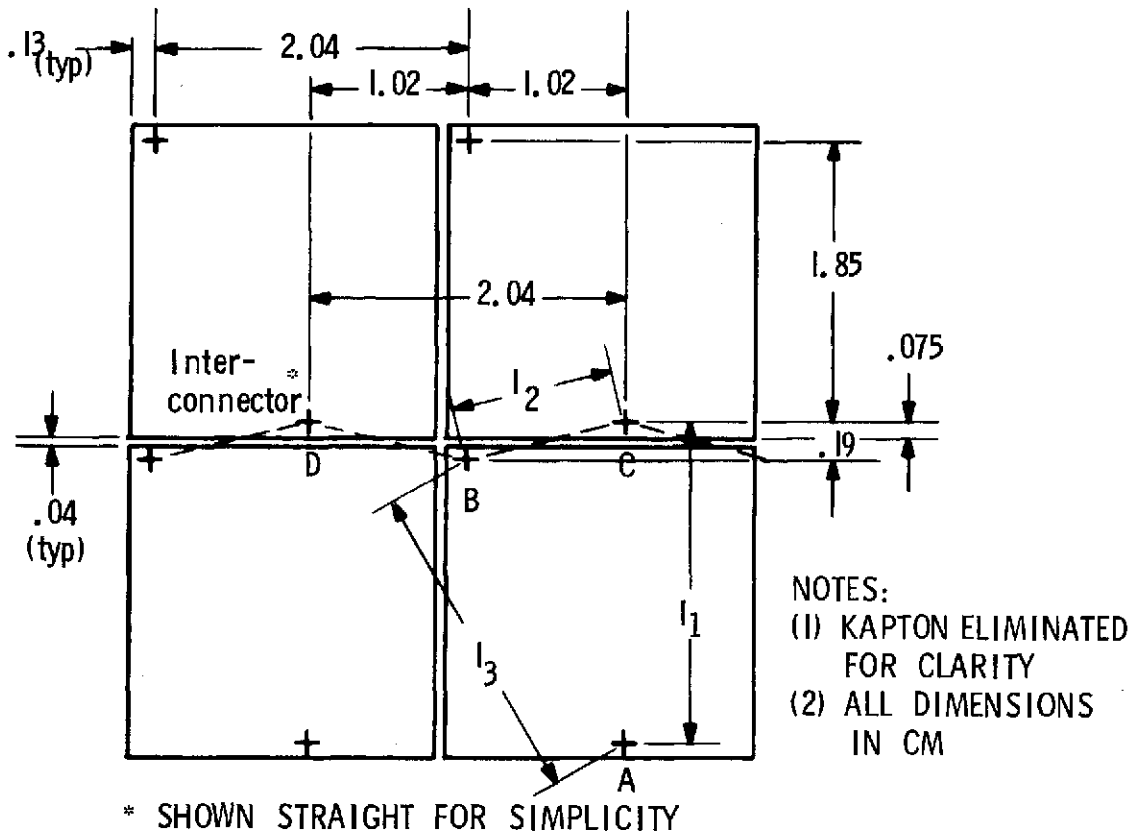
Temperature Range ( $^{\circ}\text{F}$ )		$\alpha$ (in/in- $^{\circ}\text{F}$ )
Initial	Final	
75.0	0.	0.000010
75.0	-100.0	0.000011
75.0	-200.0	0.000014
75.0	-250.0	0.000014
0.	-100.0	0.000013
0.	-200.0	0.000016
0.	-250.0	0.000016
-100.0	-200.0	0.000019
-100.0	-250.0	0.000017
-200.0	-250.0	0.000014
-250.0	-200.0	0.000017
-250.0	-100.0	0.000017
-250.0	0.	0.000015
-250.0	75.0	0.000014
-200.0	-100.0	0.000017
-200.0	0.	0.000015
-100.0	75.0	0.000014
-100.0	0.	0.000013
-100.0	75.0	0.000012
0.	75.0	0.000011

#### 3.4.7.3 Results of Analysis

A cursory examination of the first configuration revealed that the accumulative effect of the differential thermal expansions of the silicon and molybdenum compared to the Kapton were such that the holes in the Kapton would have to be over-sized to prevent the Kapton from applying excessive loads to the welds. The size of these clearance holes was such as to make this configuration impractical for this temperature range. Further investigation of this configuration was therefore abandoned.

The second configuration which uses wire loop interconnectors allows for more variation in the distance between attachment points of the interconnectors as the wire can adjust itself (by bending) to the required thermal deflection of the silicon and Kapton. As the silicon solar cells are not rigidly connected to each other as in the first configuration, the cumulative effect of the thermal expansion of the silicon and Kapton is not a problem. The room temperature geometry of the wire interconnectors are shown in Figure 3-124. Under the influence of temperature changes, the geometry of the solar cell/interconnector/substrate changes in accordance with the thermal expansion/contraction properties of the various materials.

Figure 3-125 shows a diagram of the deflected positions with an assumed solar cell temperature of  $73.2^{\circ}\text{C}$  ( $163.8^{\circ}\text{F}$ ) and with aluminum used as the interconnector wire material. Under this steady-state equilibrium condition, the Kapton substrate will operate at approximately  $-6.8^{\circ}\text{C}$  ( $19.7^{\circ}\text{F}$ ) (see Section 3.4.6.4). This distortion diagram was established based on the following assumptions:



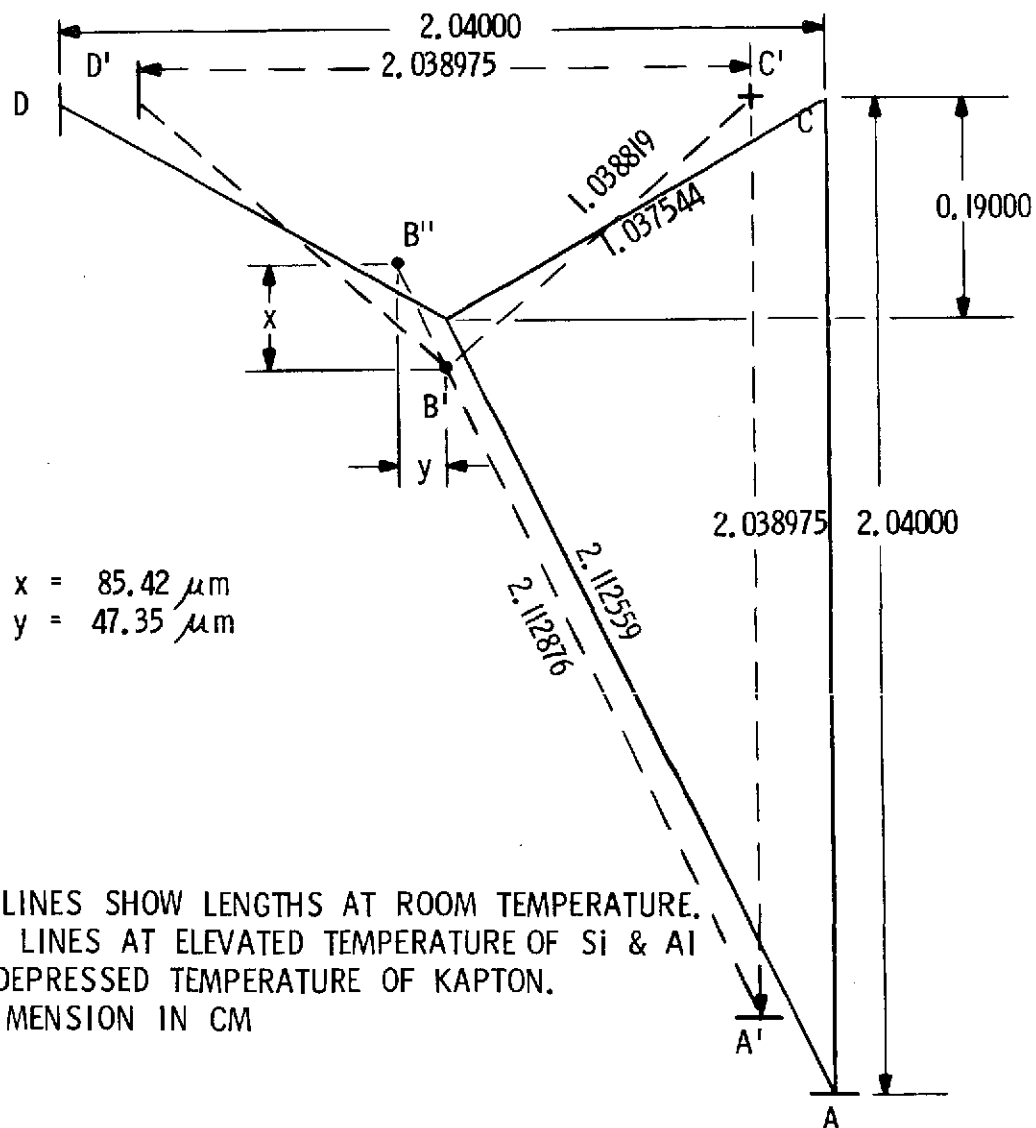
$$l_1 = 2.04 \text{ CM}$$

$$l_2 = \left[ (1.02)^2 + (.19)^2 \right]^{1/2} = 1.037545 \text{ CM}$$

$$l_3 = \left[ (2.04 - .19)^2 + (1.02)^2 \right]^{1/2} = 2.11256 \text{ CM}$$

Figure 3-124. Geometry of Wire Interconnectors at Room Temperature

- Lengths AC, CD, and DA contract dependent upon the  $\alpha$  of the Kapton, becoming lengths A'C', C'D' and D'A', respectively.
- Lengths BC and BD expand dependent upon the  $\alpha$  of the interconnector wire. This establishes point B'.
- Length AB expands dependent upon the  $\alpha$  of the solar cell. This establishes the length of A' to B' ' which extends past point B' which had been located earlier by the  $\alpha$  of the wire.
- Deflections x and y are then calculated to be the deflections necessary to move point B' to B' ' thus changing the distances B' 'D' and B' 'C'.



NOTES: (1) SOLID LINES SHOW LENGTHS AT ROOM TEMPERATURE. DOTTED LINES AT ELEVATED TEMPERATURE OF Si & Al AND DEPRESSED TEMPERATURE OF KAPTON.  
(2) ALL DIMENSION IN CM

Figure 3-125. Thermal Distortion with Aluminum Interconnectors at 73.2°C Solar Cell Temperature

The shear, moment and axial loads in the interconnector wire were calculated assuming the shape of the wire to be that shown in Figure 3-126 and deflecting joint No. 8 in the x and y directions by the amount determined by the steps listed above. These calculations were performed for two wire materials, aluminum and gold, with the solar cell operating at the maximum expected equilibrium temperature ( $73.2^{\circ}\text{C}$ ), and at the minimum expected end-of-eclipse temperature ( $-185^{\circ}\text{C}$ ). Using the combined bending and axial stresses on the wires, it was determined that the ultimate margins of safety are as given in Table 3-43. Based on the same loads, the margins of safety for stresses in the spot bonds were determined to be large in all cases.

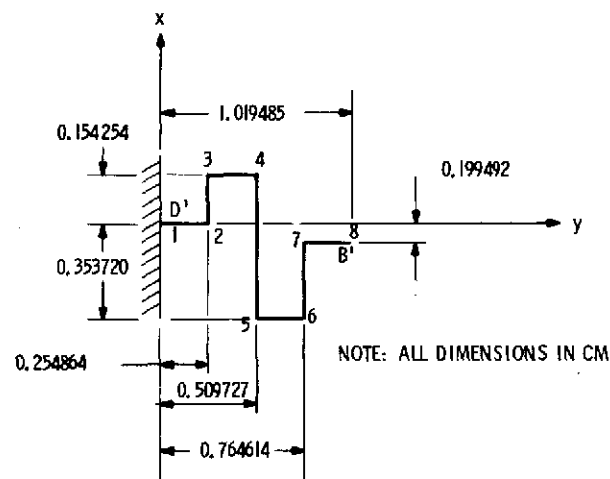


Figure 3-126. Model of Interconnector Wire Loop Configuration

Table 3-43. Margins of Safety for Combined Bending and Axial Stresses in the Wires

Wire Material	Margin of Safety	
	73.2°C Solar Cell Temperature	-185°C Solar Cell Temperature
Al	0.25	1.25
Au	1.50	-0.05

### 3.4.8 THERMOSTRUCTURAL ANALYSIS OF DEPLOYED ASTROMAST BOOM

The structural capability of the selected continuous longeron ASTROMAST boom was evaluated using the analysis method described in Reference 66. The thermostructural loading on a deployed boom is as shown in Figure 3-127. In order to facilitate the integration of the beam-column equation for this case, the unloaded boom deflection curve was assumed to be parabolic and represented by:

$$y_o = \frac{b}{l^2} x^2 \quad (3.4-23)$$

where

$b$  = the tip deflection of the boom which includes the deflection due to thermal bending plus the initial boom out-of-straightness

$l$  = boom length

The differential equation of the elastic curve is given by:

$$EI \frac{d^2 y}{dx^2} = -M = - \left\{ P (y+y_o) + Q l - P (\delta+b) - Q x \right\} \quad (3.4-24)$$

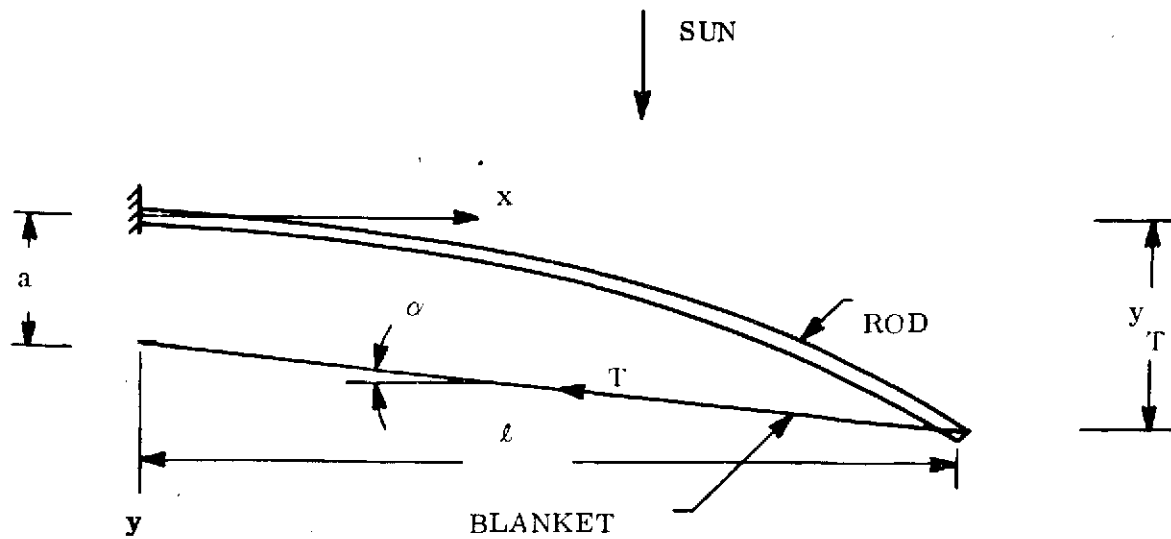
where  $P$  and  $Q$  are the components of the blanket preload  $T$  and  $y$  and  $\delta$  are as shown in Figure 3-127. The solution of equation (3.4-24) for the resultant deflection curve for the boundary conditions of the cantilever beam yields

$$y = -\frac{Q}{kP} \sin kx + \left\{ \frac{Ql}{P} - \delta - b - \frac{2b}{k^2 l^2} \right\} \cos kx - \frac{b}{l^2} x^2 + \frac{Q}{P} x + \delta + b + \frac{2b}{k^2 l^2} - \frac{Ql}{P} \quad (3.4-25)$$

where

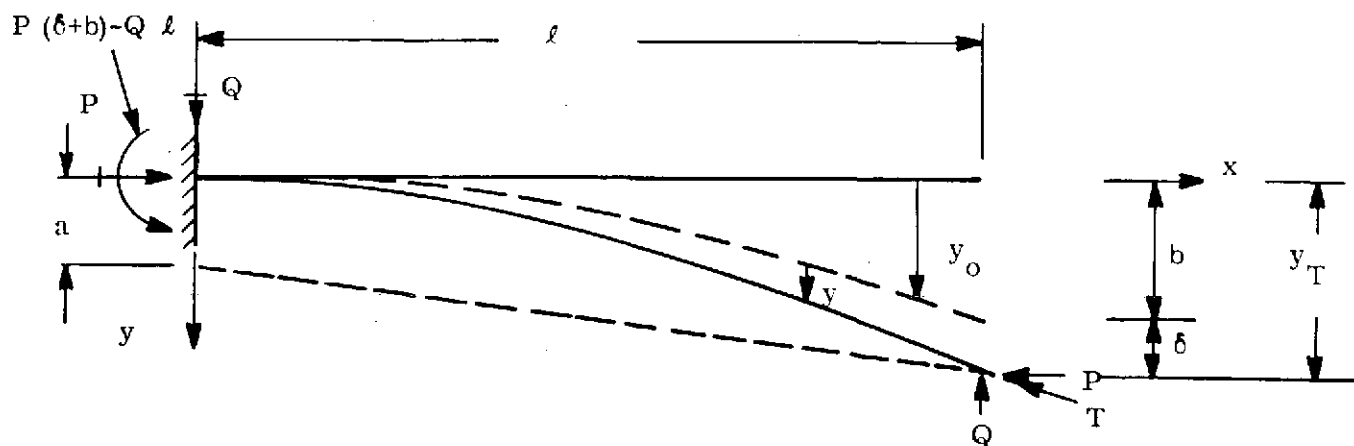
$$k = \sqrt{\frac{P}{EI}}$$

$EI$  = boom bending stiffness



a. SYSTEM SKETCH

P AND Q ARE COMPONENTS OF  
BLANKET TENSION T



b. FREE-BODY DIAGRAM

Figure 3-127. Deployable Boom Orbital Thermostructural  
Loading (from Reference 66)

At this point,  $\delta$  can be determined using the conditions that  $y = \delta$  when  $x = \ell$ , and

$$\frac{Q}{P} = \frac{b + \ell - a}{\ell},$$

$$\delta = b \left\{ \frac{2(1 - \cos k\ell) - k\ell \sin k\ell}{k\ell \sin k\ell} \right\} + a \left\{ \frac{\tan k\ell - k\ell}{\tan k\ell} \right\} \quad (3.4-26a)$$

or

$$\delta = \frac{b \left\{ 2(1 - \cos k\ell) - k\ell \sin k\ell \right\} + a \left\{ k\ell \cos k\ell (\tan k\ell - k\ell) \right\}}{k\ell \sin k\ell} \quad (3.4-26b)$$

It can be seen from this equation that when  $\sin k\ell = 0$ ,  $\delta$  is infinite which defines the critical load as  $k\ell = \pi$  or

$$P_{CR} = \frac{\pi^2 EI}{\ell^2} \quad (3.4-27)$$

which is the critical load for a pin-ended column. The location of the maximum bending moment is obtained by the substitution of equations (3.4-25) and (3.4-26) into (3.4-24) and the solution for  $\frac{dM}{dx} = 0$  to yield

$$x = \frac{1}{k} \tan^{-1} \left\{ \frac{2b(1 - \cos k\ell) - a k^2 \ell^2 \cos k\ell}{[a k^2 \ell^2 + 2b] \sin k\ell} \right\} \quad (3.4-28)$$

Substituting equations (3.4-28), (3.4-29) and (3.4-26) into (3.4-24) gives the magnitude of the maximum bending moment.

These equations were solved using the properties of the continuous longeron ASTROMAST as obtained from Figure 2-128 and 3-129 for the bending stiffness and bending strength, respectively. An ASTROMAST diameter of 19.0 cm (7.5 inches) was selected to provide the bending stiffness ( $3440 \text{ N-m}^2$ ) required to maintain the deployed natural frequency above 0.04 Hz. The critical bending moment for this boom size is approximately 13.0 N-m (115 lb-in.) For a boom length of 18.6m, Figure 3-130 shows the maximum bending moment as a function



of total blanket tension,  $T$ . The offset,  $a$ , of this tension force is equal to zero for the baseline configuration shown in Figure 3-11. With a design load of  $33.3\text{ N}$  ( $7.5\text{ lb}_f$ ), the combined unloaded tip deflection due to out-of straightness and thermal bending,  $b$ , is restricted to approximately  $100\text{ cm}$  ( $39\text{ inches}$ ).

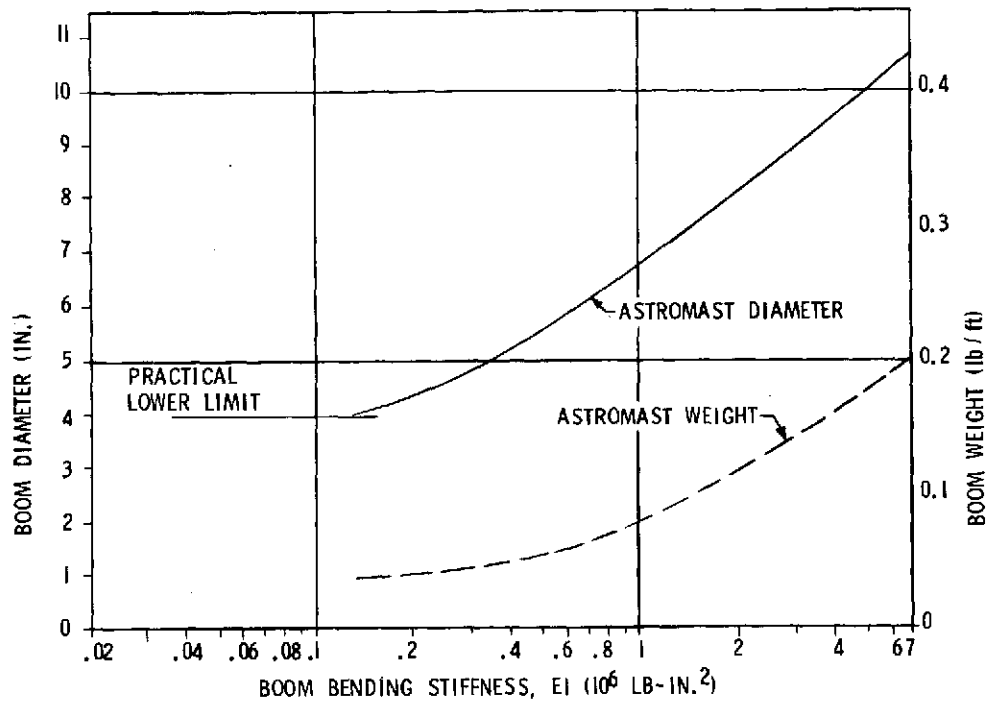


Figure 3-128. Continuous Longeron ASTROMAST Diameter and Weight vs. Bending Stiffness (from Reference 67)

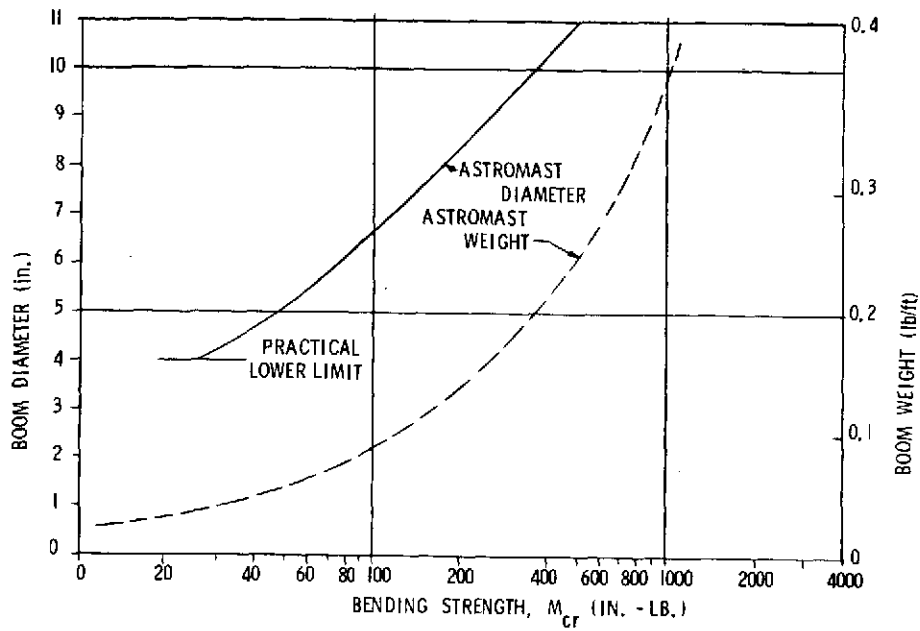


Figure 3-129. Continuous Longeron ASTROMAST Diameter and Weight vs. Bending Strength (from Reference 67)

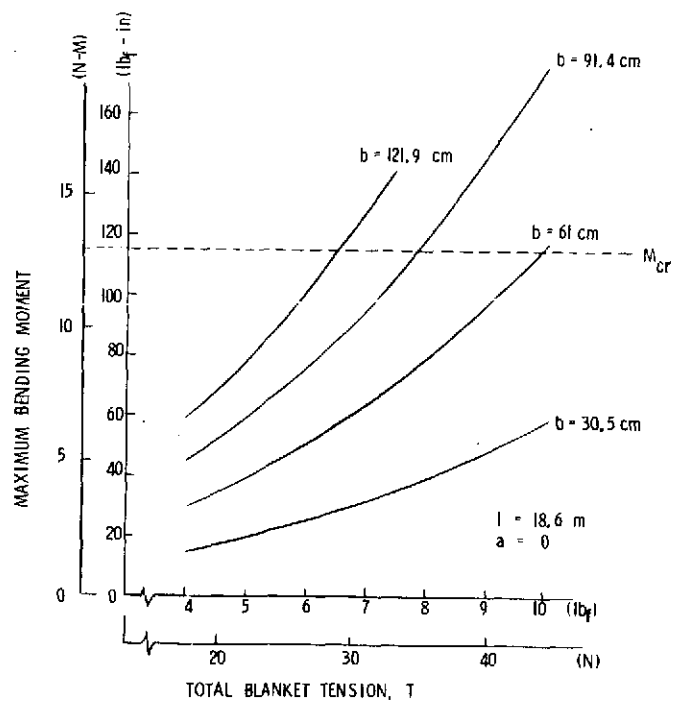


Figure 3-130. Maximum Bending Moment vs Blanket Tension

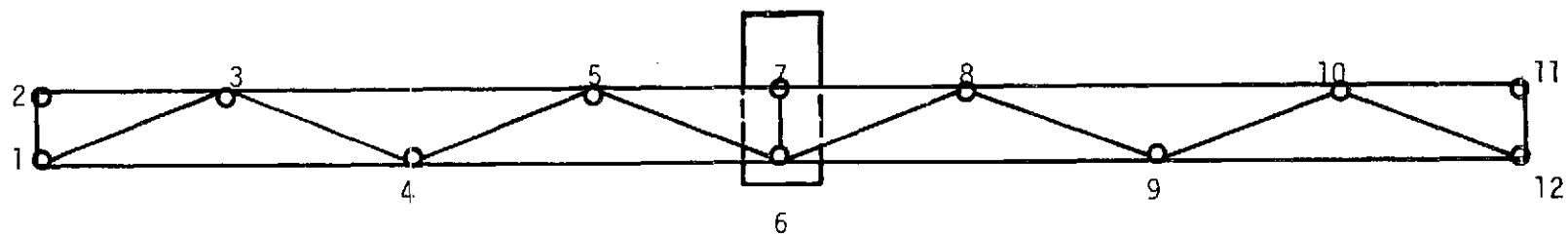
### 3.4.9 STOWED VIBRATION AND LOADS ANALYSIS

#### 3.4.9.1 Introduction and Summary

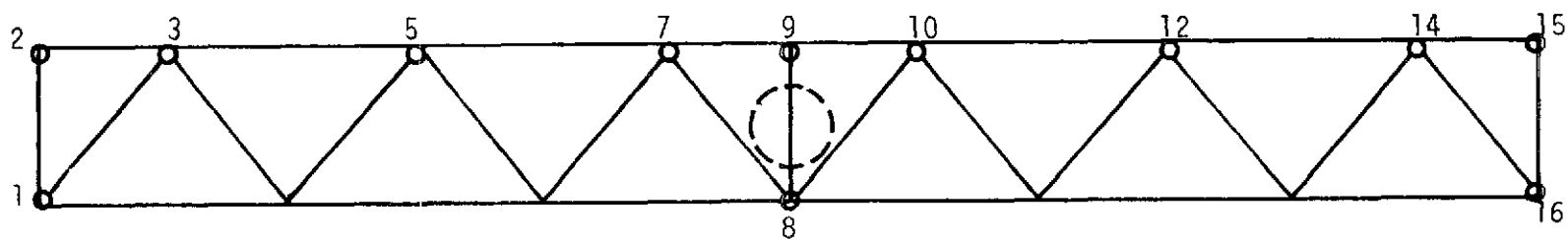
A parametric study was performed to determine the effects of various mounting configurations on the resonant frequencies and dynamic loads of the stowed solar array. Because the choice of a mounting configuration depends on many factors in addition to the solar array configuration, it was considered desirable to vary the method of mounting and determine its effect on the solar array resonant frequencies and loads rather than analyze a fixed configuration. The basic truss configuration was modeled and the support points varied along the span. The configurations analyzed considered two symmetrically spaced supports with and without a center cantilever support, and also an overhung configuration having a center support (either a simple support or a cantilever support) with a second support at various spanwise locations. For those support conditions which were statically determinant, the response to both in-phase and out-of-phase motions of the support points was determined. The results of the study showed that supports near the 10 percent span with a center cantilever support provides the stiffest configuration while two supports at the quarter span points provided the stiffest statically determinant mounting. The quarter span mounting configuration provided the lowest loads and responses for in-phase motion of the support points but relatively large responses occurred for out-of-phase support motions. The overhung configuration was found to be susceptible to out-of-phase support motions providing dynamic magnifications as high as 35 for 5 percent of critical damping in the structure.

#### 3.4.9.2 Analytical Model

The stowed solar array was modeled as a welded truss assembly for both transverse directions. The vertical model investigated the dynamic characteristics for motions along the axis of the boom as shown in Figure 3-131(a). The lateral model of the array, Figure 3-131(b), was used to investigate the transverse resonant frequencies. The free-free stiffness matrix of the array was determined and then the effects of supports at various locations were investigated by deleting the appropriate coordinates. In this manner, a large number of support configurations could readily be investigated.



(a) Vertical Model - Mass at All Grid Points with Inertia at Point 6



(b) Lateral Model - Mass at All Numbered Grid Points, Inertia at Point 9

Figure 3-131. Analytical Models of Stowed Solar Array

The truss member sizes were based on those tube sizes determined for the baseline configuration as shown in the figures. Although these member sizes were optimized for the configuration having center and end supports, they were not changed in the analysis. It was felt that the main effects were the support geometry and could be determined without resizing the truss members for each support condition.

#### 3.4.9.3 Vertical Resonant Frequencies

The fundamental resonant frequencies of the various vertical mounting configurations investigated are summarized in Figure 3-132. The results are presented in terms of the fundamental resonant frequency variation with simple support locations at various distances from the end. Two symmetric supports were considered in the upper portion of the figure while an overhung configuration having a center support is considered in the lower portion of the figure.

In the upper portion of Figure 3-132, the effects of the spanwise location of two symmetric simple supports were evaluated with and without a cantilever center support. For the statically determinant configuration having two simple supports, the optimum spanwise locations is at the quarter span points providing a fundamental resonant frequency of approximately 25 Hertz. This is more than twice the resonant frequency of the array using simple supports at the ends. The configurations analyzed with two simple supports and a center cantilever support showed that very stiff configurations could be obtained by supporting the array at approximately 10 percent span points, over twice the resonant frequency that could be obtained with only two simple supports. These results show that the baseline configuration type of mounting is one of the stiffest configurations having simple supports at the quarter span points, the additional center support does not appreciably increase the resonant frequency.

The various overhung configurations show that the spanwise location of the simple support does not appreciably affect the resonant frequency of the array. The lower curve of Figure 3-132 shows the effect of support location for two simple supports. Although the highest resonant frequency (12 Hertz) is obtained with a support near the quarter span, the vibration in the resonant frequency is small until the supports become close together.

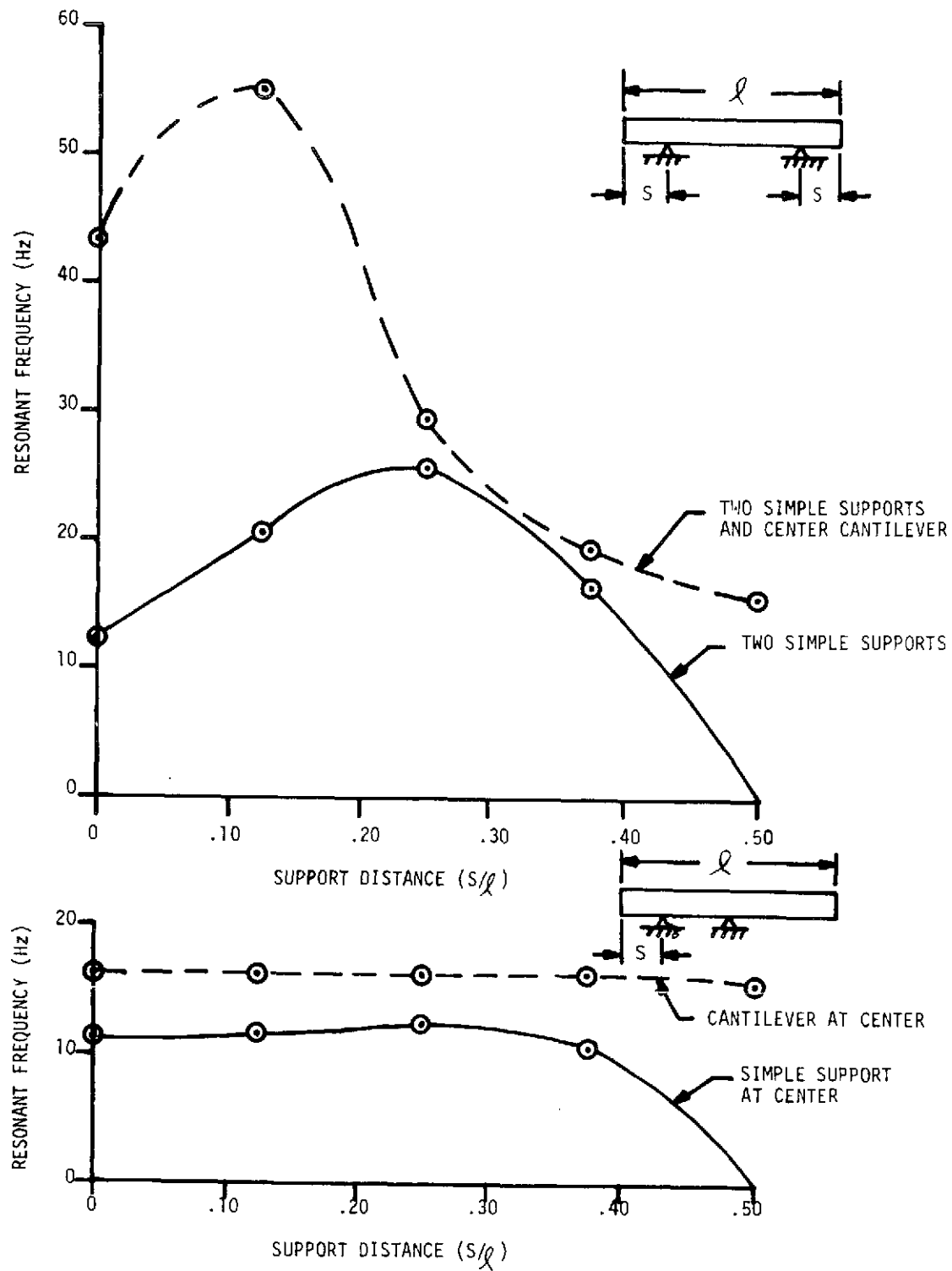


Figure 3-132. Results of Vertical Vibration Analysis

With the center support providing a cantilevered condition as shown by the upper curve, the position of the second support has little effect on the resonant frequency.

The resonant frequency is governed by the stiffness of the unsupported end of the array for these configurations and is not changed appreciably by the position of the second support point at any convenient location with the best position being in the vicinity of the quarter span.

#### 3.4.9.4 Lateral Vibration Analysis

The results of the lateral vibration analysis are shown in Figure 3-133. The trends shown for the lateral vibration analysis are the same as those of the vertical vibration analysis. Although the lateral truss depth is considerably greater than that of the vertical trusses, the frequencies are comparable in that a single truss is used as the main stiffening member for lateral loading.

It will be noted that the simplified planar truss model used for these analyses neglects torsional coupling which may lower the lateral frequencies. The lateral truss is positioned directly beneath the honeycomb panels that support the solar array blankets, the main source of inertial loading. These loads must be transferred to the support points at the base of the truss members. Diagonal members are provided at the center and end sections to provide a rigid load path to the support points so that the effects of this path on the flexibility of the assembly are minimized. However, there will be a tendency for torsional coupling with lateral motion to reduce the resonant frequency.

#### 3.4.9.5 Vertical Response Analysis

Because of the similarity in the trends shown by the lateral and vertical vibration analysis, only the response of the solar array to vertical support motion was investigated. A nominal structural damping of 5 percent of equivalent critical damping was assumed for the structure. The array response was determined for the first ten modes considering the support points to be vibrating in-phase and also out-of-phase. In order to investigate the phasing of the support motions, only selected configurations having statically determinant support conditions were analyzed.

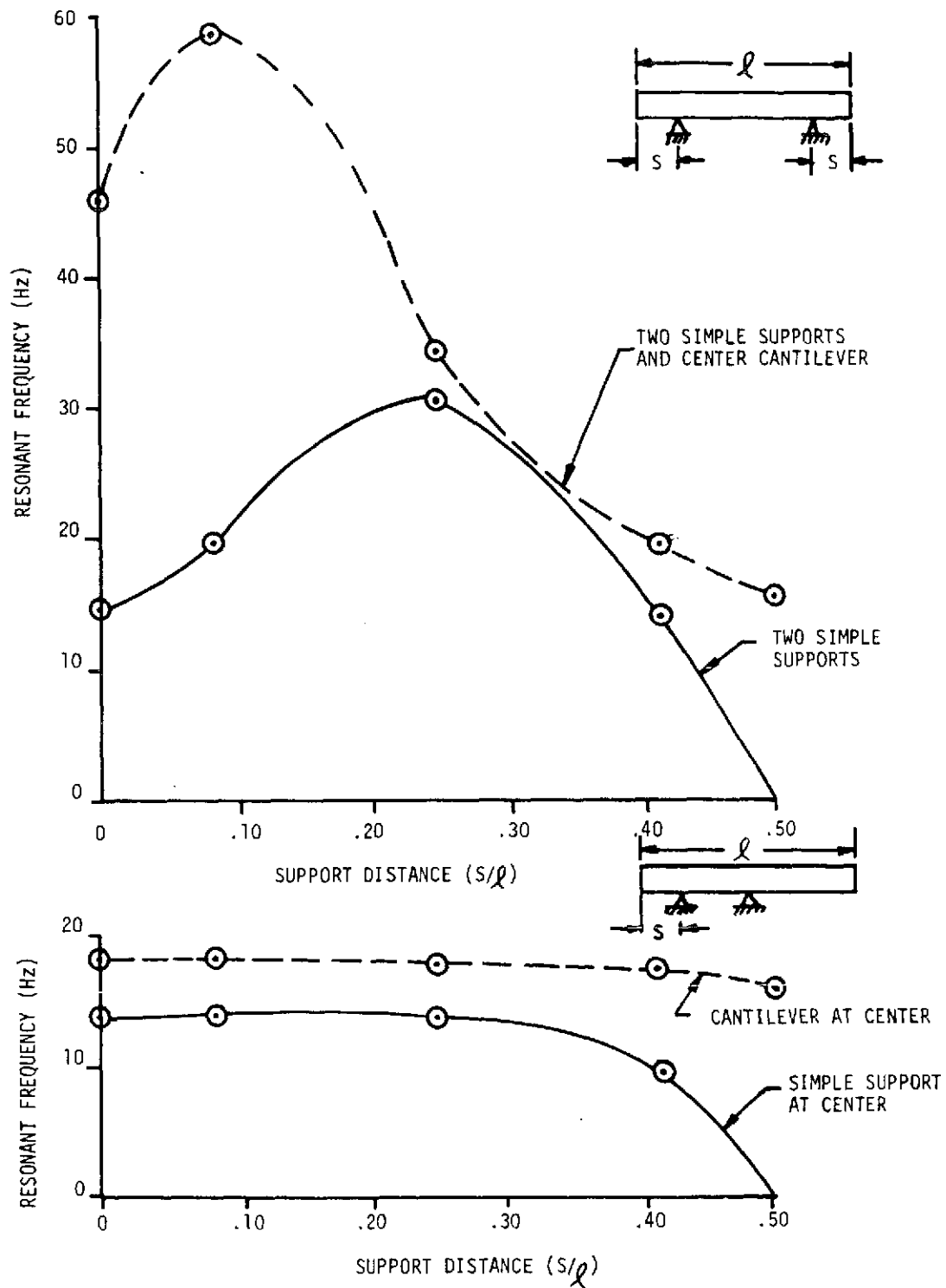


Figure 3-133. Results of Lateral Vibration Analysis



The results of the analysis are shown in Figure 3-134 through 3-137 for the four configurations selected for response analysis. The four configurations were: (1) two simple supports at the ends; (2) two simple supports at the quarter span points; (3) center cantilever; and (4) a center support with an end support. The results show the fundamental mode shape determined from the vibration analysis and the response to a "1" g input acceleration at the support points for in-phase and out-of-phase motions of the supports. For the center cantilever configuration, an out-of-phase condition was analyzed that represents a "1" g out-of-phase acceleration at the ends of the array since it is not defined for a single point support. The total response at various array stations are plotted with some interpretation as to "phasing" for the out-of-phase response plots (in reality, the total response phase is not in or out-of-phase as shown in the figures).

#### 3.4.9.6 Summary of Results

The responses in the fundamental modes to a "1" g excitation are summarized in Table 3-44 and the maximum moments imposed on the array structure and the maximum support loads are given for the in-phase support point motions. For the in-phase excitation, the dynamic loads and response accelerations (6.5g) are lowest for the configuration having two simple supports at the quarter span points. The array response accelerations are maximum at the tip of the array for the center cantilever configuration while the highest bending moment occurs at the center of the end supported configuration. On the other hand, the out-of-phase excitation provides large responses for those configurations having overhung sections. For the configuration with the quarter-span supports, maximum accelerations occur at the tips (23g) while the overhung configuration (center and end supports) has the highest tip response of all the configurations (35g). This is due in part to the increased rotational acceleration of the base resulting from a fixed acceleration of "1" g but at points which are closer together. As indicated in Table 3-44, using a constant rotational acceleration corresponding to  $\pm 1g$  at the ends of the array provides half the response for the overhung configurations although the responses of these configurations are still the highest of the four configurations studied.

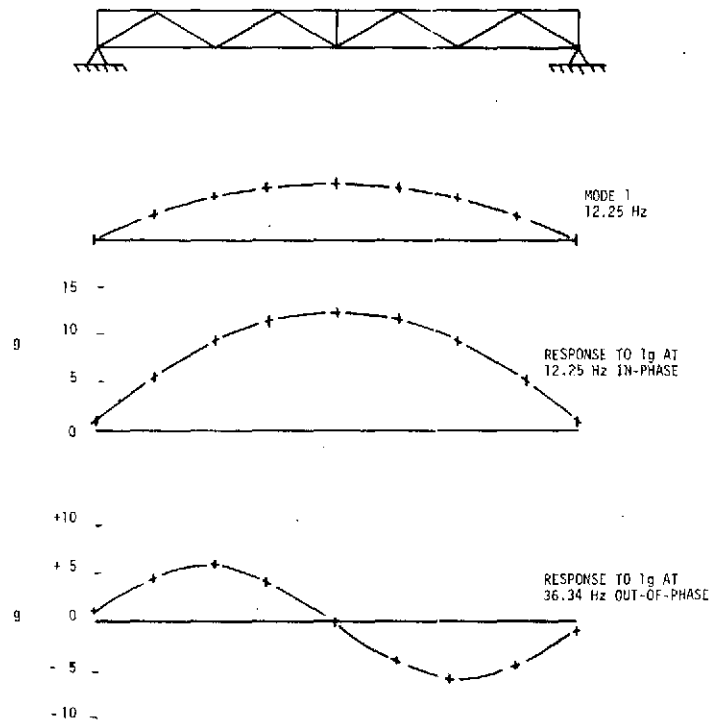


Figure 3-134. Vertical Response Analysis - Simple Supports at Ends

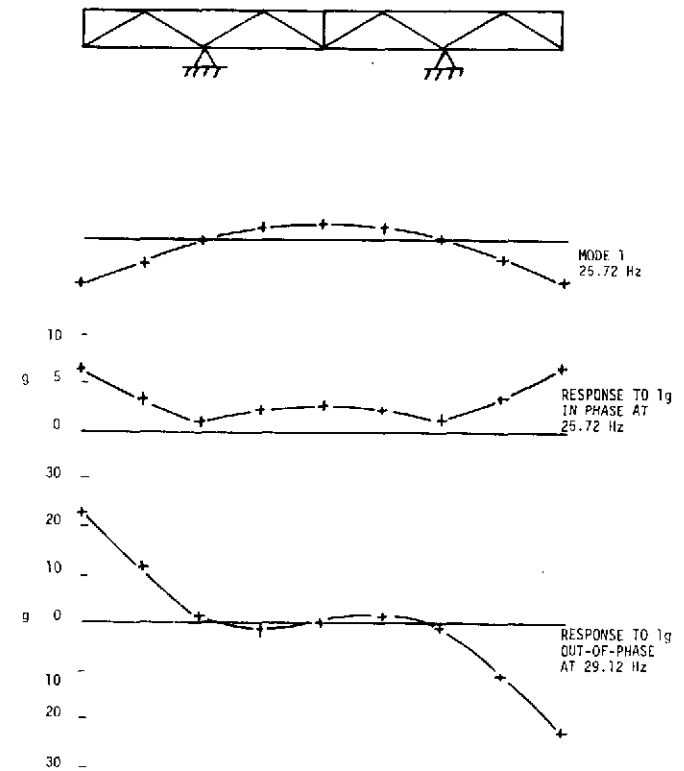


Figure 3-135. Vertical Response Analysis - Simple Supports at Quarter Span

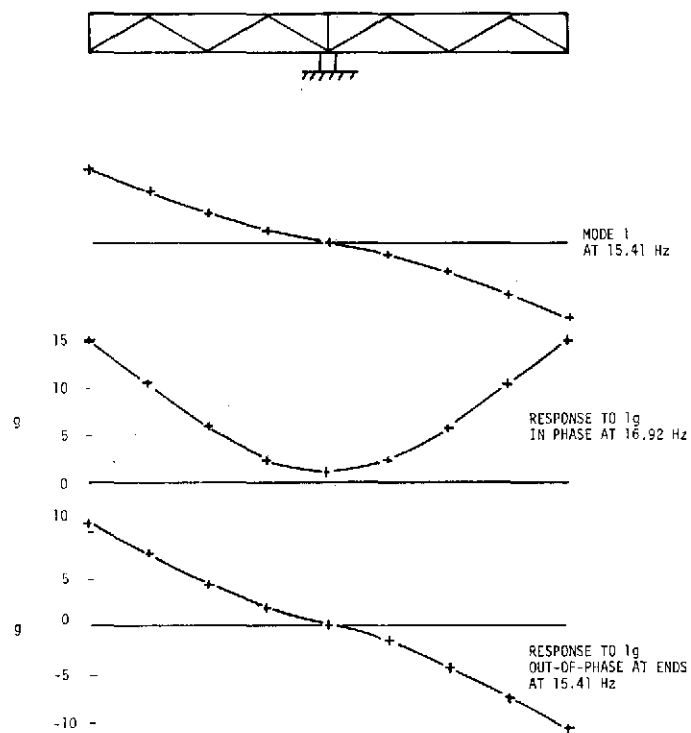


Figure 3-136. Vertical Response Analysis -  
Cantilevered at Center

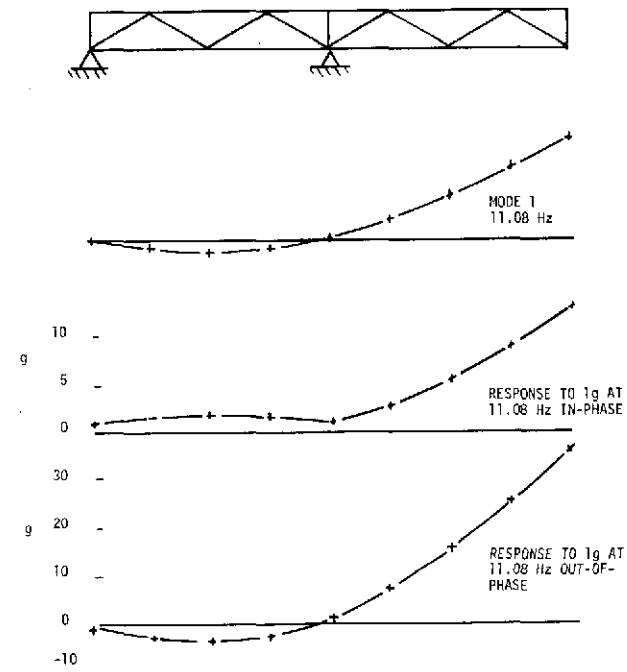
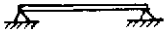

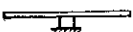



Figure 3-137. Vertical Response Analysis  
End and Center Supports

Table 3-44. Summary of Maximum Loads and Responses for "1" g Excitation

Support Configuration	In-Phase Excitation					Out-of-Phase Excitation	
	Acceleration (g)	Support Force		Array Structural Moment		Acceleration (g)	Normalized * Acceleration (g)
		lb	N	(in - lb)	(N-M)		
	12.2	720	3200	54 700	6180	6.1	6.1
	6.5	240	1066	6 599	735	23.2	11.6
	14.9	1150	5110	49 100	5550	10.8 *	10.8
	12.3	950	4220	43 000	4860	35.0	17.5

\* Normalized to an angular acceleration equivalent to 1g out of phase at the ends of the solar array.

Comparison of the loads and responses indicates that the quarter span support configuration is attractive. For in-phase support motions, this configuration provides the lowest loads and the lowest responses on the array blanket. For out-of-phase support motion equivalent to that of +1g at the array ends, the maximum blanket response is less than that of the other configurations for in-phase support motion. Because it appears more difficult to actually experience high out-of-phase support motion than in-phase support motion, the reduced in-phase responses and loads make this configuration appear attractive.

If differential support motion is not a consideration, the baseline configuration will undoubtedly provide lower array loads and responses. The added supports will enable the inertial loads due to the dynamic response of the blanket to be reacted through shortened spans. In addition, the high stiffness of this configuration (40 Hertz), should result in added damping from the blanket which exhibited a relatively low frequency resonance in previous tests (26 Hertz).

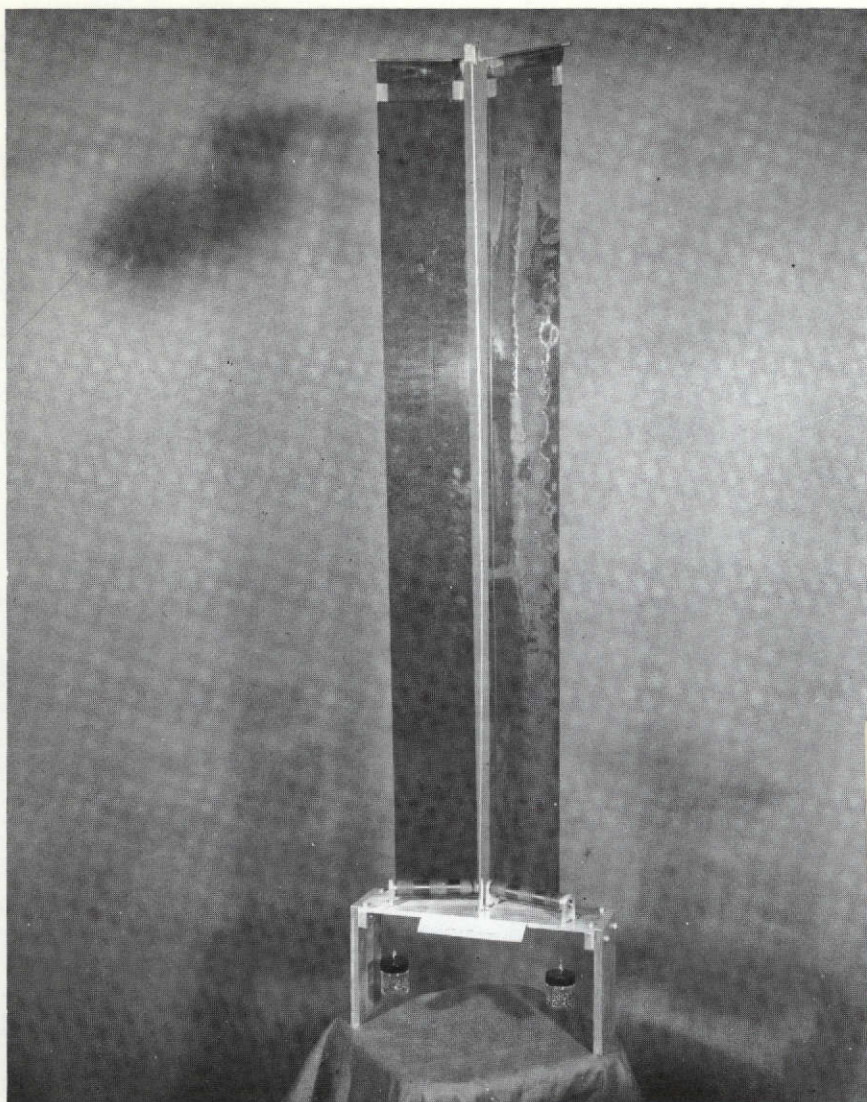
### 3.5 "V" STIFFENED SOLAR ARRAY MODEL DEVELOPMENT

#### 3.5.1 INTRODUCTION

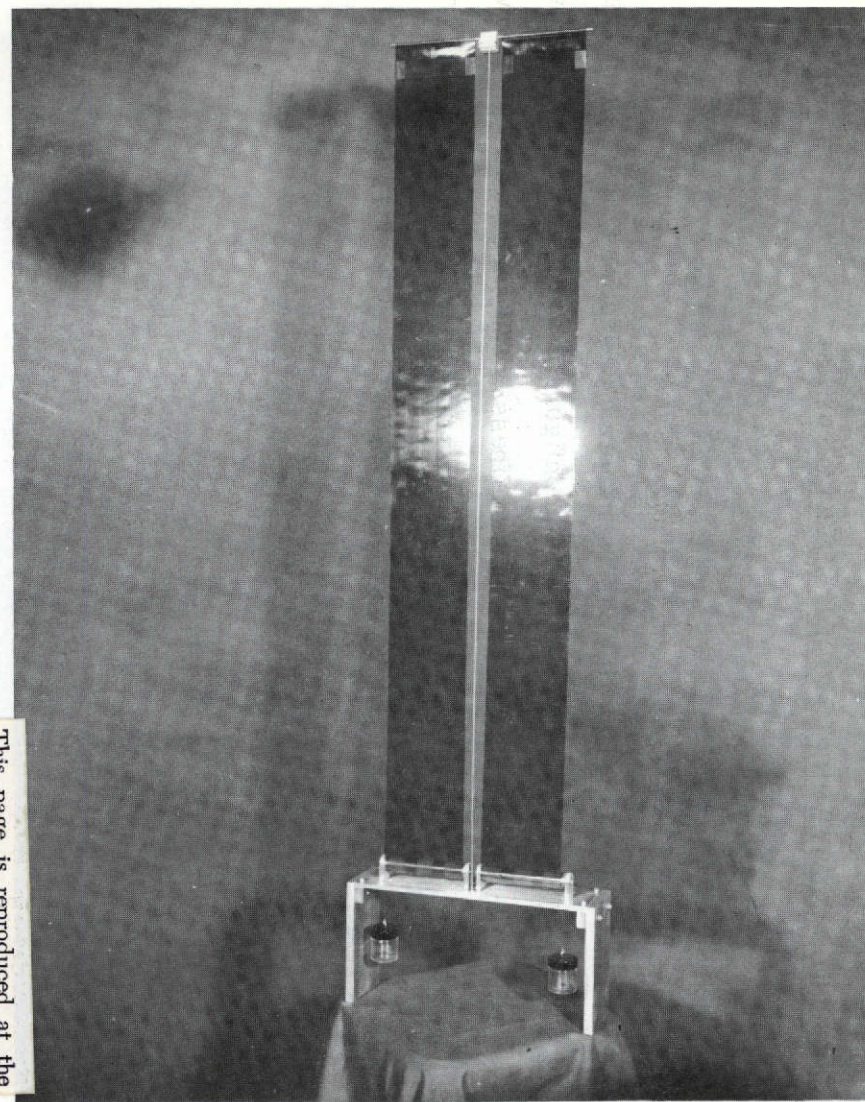
A "V" stiffened single boom solar array configuration was described in Section 3.4.5. This configuration can be significantly stiffer for symmetric deflections, i.e., equivalent to out-of-plane motion, than the conventional planar configuration and so can either provide a higher natural frequency or use a boom with less stiffness. The configuration is shown in Figure 3-110. Analysis showed the critical buckling load was increased by a factor of approximately 3 allowing larger blanket tensions. The symmetric natural frequency was predicted to increase with blanket tension as shown in Figure 3-115 so that the minimum vibration frequency can be increased by a factor of two or more with the "V" configuration. This analysis was preliminary in nature and the system being analyzed is non-linear. Verification of the predicted results was considered important as they literally looked "too good to be true". It was concluded the most effective approach was to construct a model to determine if the system behaved in the predicted manner. This approach was particularly attractive since a low-cost model would provide the desired information.

#### 3.5.2 DESCRIPTION OF MODEL

The basic objective of the model was to evaluate and demonstrate the "V" stiffened configuration. Two models were constructed, each capable of being configured in two "V" angles, so that direct comparisons could be made. The completed models are shown in Figure 3-138. Except for the "V" angle and related differences, the models are similar. Each is mounted on a 6.4 mm (0.25 in) aluminum plate which is supported by end plates to provide working room under the model. Each model consists of a single central boom and two Kapton sheets, which represent the solar array blankets. Each Kapton sheet is wrapped around an aluminum cylinder which is supported by end brackets. A ball bearing at each end of the aluminum cylinder supports the cylinder and allows low friction rotary motion. The central boom is threaded into the base at the center point of the blanket tension. A loop is formed at the outboard end of the Kapton sheets to accommodate the leading edge member assembly. The leading edge member assembly consists of a center fitting and two rods which support the outboard end of the Kapton sheets. The center fitting



(a) 20 Degree "V"



(b) Planar (for reference)

This page is reproduced at the back of the report by a different reproduction method to provide better detail.

Figure 3-138. Solar Array "V" Stiffened Demonstration Models



is drilled so that the two rods are parallel to the drum centerlines and positioned vertically above the line where the Kapton sheets unroll from the cylinders (with a straight rod). A close fitting nylon insert was used in the boom attachment hole and a  $45^\circ$  taper was machined at the outboard end of the boom to allow low friction rotary motion about the boom centerline, but constrain other rotations. Tension in the Kapton sheet is provided by wrapping a small diameter string around the cylinders in a windlass fashion with weights suspended from the other end of the string. Thus each cylinder is free to rotate independently and the static blanket tension is constant and independent of position. Dimensions and other design data are tabulated on Table 3-45.

A set of 6.4 mm (0.25 in) diameter aluminum central booms was fabricated to provide a stiffer system in the event the 3.2 mm (0.125 in) diameter booms were too flexible.

Table 3-45. Design Parameters of Models

Drums:	25.4 mm dia. x 127 mm long A1. rod.
Kapton Sheets:	121 mm wide, 50 $\mu$ m thick, 0.0344 kg/m <sup>2</sup>
Central Boom:	3.2 mm dia stainless steel rod, Length = 1.238 m for 20 deg. "V" = 1.264 m for planar
LEM:	Mass = 95.1 gram 20 deg. "V" = 94.7 gram planar
Geometry:	<u>For Planar System</u> - Inside drum edges are spaced 13 mm and center of boom hole is 13 mm away.  <u>For 20 deg. "V" System</u> - Inside drum edges are 13 mm from intersection of boom centerlines. Boom hole location is 14.13 mm from intersection at center of tension field.  Distance from base surface to drum centerline is 25.4 mm.

### 3.5.3 MODEL TEST RESULTS

The models were assembled and general performance characteristics determined with 3.2 mm (0.125 in) diameter booms by changing strip tensions, displacing the tip of the system and observing the free vibrations of the system, etc. It was noted that the planar system was quite flexible and that the "V" configuration was very much stiffer. Small deviations in straightness of the central boom resulted in large static tip deflections. An example is shown in Figure 3-139. The strip tensions in the "V" configuration is greater than the strip tension in the planar model.

The static buckling tension of the two models was evaluated by determining the maximum strip tension that could be supported. The planar system buckling tension was determined to be approximately 149.5 grams per side\* and the 20 deg. "V" buckling tension was determined to be approximately 914 grams per side.

Observation of the free vibrations of the models lead to a series of measurements involving the relation of natural frequency and strip tension. Results are given in Table 3-46. Note that in-plane vibration data is not presented because attempts to produce this type of motion with initial displacements resulted in motions that are a combination of both torsion and in-plane displacements. These motions quickly decayed to zero and no meaningful data was obtained.

Following tests with the 3.2 mm (0.125 in) diameter booms, the 6.4 mm (0.25 in) diameter boom was installed in the 20 degree "V" model and exploratory investigations conducted. The significantly higher boom stiffness raised the natural frequency of the boom/leading edge member system significantly. For low blanket tensions, a different type of blanket motion was observed and is discussed in the next section. Observed frequencies are given in Table 3-46.

---

\*These values are not exactly equivalent as the planar system would almost sustain this tension and the 20 deg. "V" system sustained the tension, but was on the verge of buckling. Note that the weight of the leading edge member and boom itself are also supported by the boom.



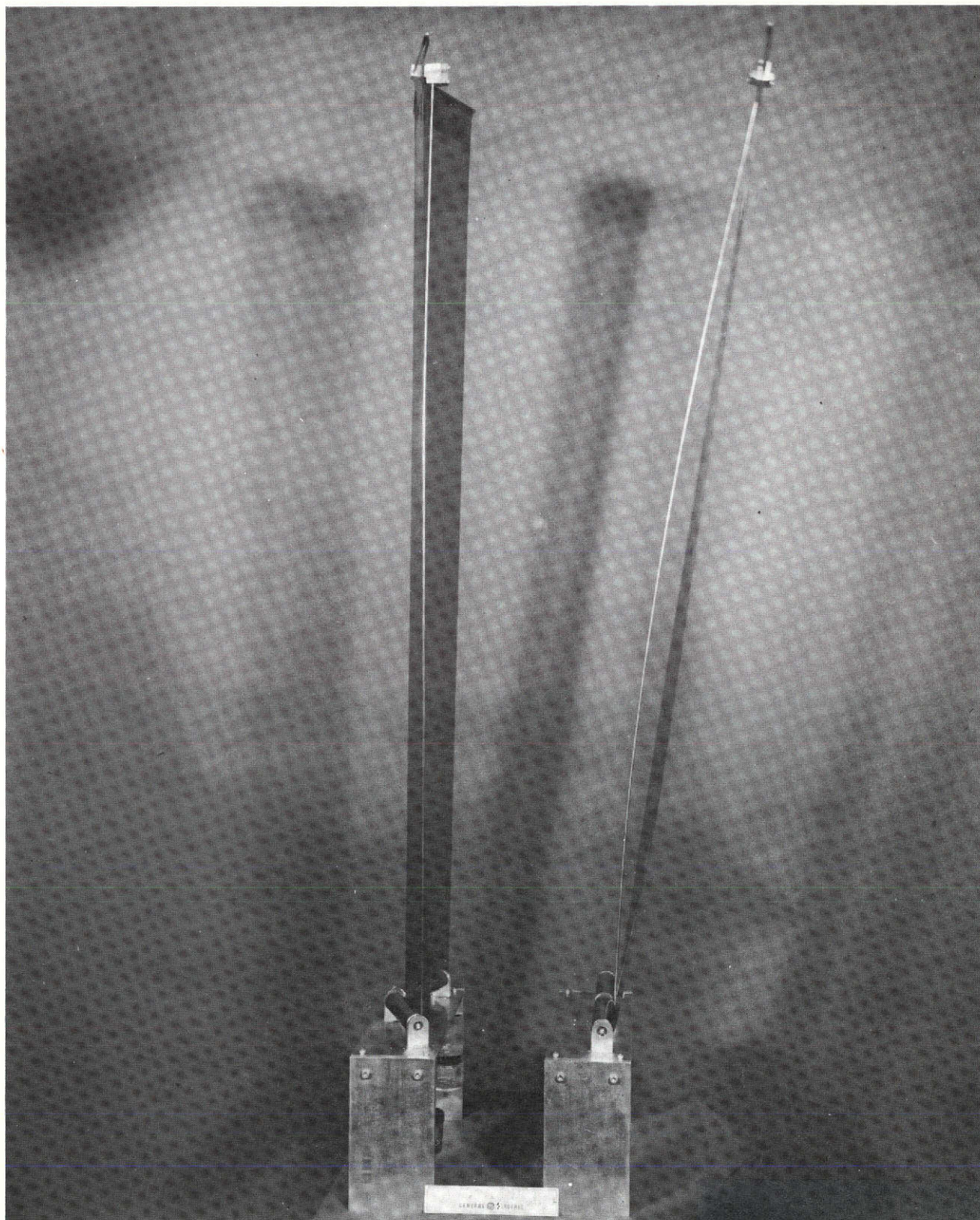


Figure 3-139. Comparison of Static Tip Deflections  
of Planar and "V" Stiffened Models

Table 3-46. Summary of Vibration Test Results

Tension Per Side (gm <sub>f</sub> )	Natural Frequency (Hz)					
	Out of Plane		In Plane		Torsion	
	Hz	No. Cycles*	Hz	No. Cycles*	Hz	No. Cycles*
Planar System - 3.2 mm Diameter Stainless Steel Rod						
0**	.364	15	.364	15	0	
7	.254	2	.336	5	.246	1
92.5	.182	2	.935	6	.52	3
138	.0745	2	1.35	7	.76	2
20° System - 3.2 mm Diameter Stainless Steel Rod						
0**	.374	10				
7	.254	2				
92.5	.52	4			0.7	1
138	.69	5			0.87	1
195.8	.72	5			.885	1
309	1.03	5			1.31	1
416.8	1.18	5				
450	1.16	5				
564	1.26	10				
678	1.21	5				
728	1.15	5				
914	1.06	5				
20° System - 6.4 mm Diameter Aluminum Rod						
0**	1.21	10				
14.95	1.31	10				
450	1.57	10				
914	1.6	10				

\* Number of oscillations upon which the frequency is based.

\*\* LEM only. Blankets removed.



#### 3.5.4 DISCUSSION OF TEST RESULTS

The models demonstrated the dramatic increase in system stiffness that can be obtained with the "V" stiffened configuration. The static buckling load of the model is increased by a factor of at least 4 and the out-of-plane natural frequency is increased by a factor of nearly 3.5 with 450 grams of tension per side.

The observed natural frequency is plotted as a function of strip tension in Figure 3-140. If the results in Figure 3-140 are compared with Figure 3-115, it should be understood the two systems are not the same. Figure 3-115 shows the predicted results for a solar array where most of the system mass is the array blankets and so is distributed over a large area. The inertia forces of the blanket mass are transmitted to the structure at both the leading edge member and the drums. In the model, which was intended to investigate the stiffening effects, most of the mass is in the leading edge member and almost none in the Kapton strips. As a result, the model does not exhibit a mode shape at low tension that approaches that of a stretched string supported at both ends. Thus a mode with a frequency to zero as the tension goes to zero is not shown.

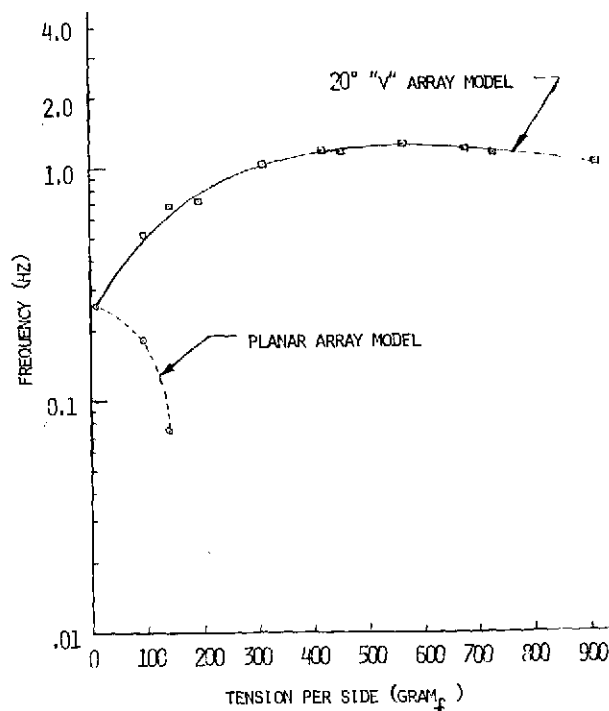


Figure 3-140. Model Vibration Test Results

In all observed vibrations, the blanket appeared to maintain a straight line between the leading edge member and the drum. The model tests were carried out with the same initial displacements and so no effects of displacement on frequency were investigated. However, it was noted that the periods of oscillation were amplitude dependent.

With the 6.4 mm (0.25 in) diameter rod traveling waves were observed in the blanket with 15 grams tension per side. At this frequency, the "stretched string" vibration characteristics are such that the strips can participate in the motion. At higher tensions, the strip tension was sufficiently high so that the strips did not noticeably deviate from a straight line.

### 3.6 SPACECRAFT INTEGRATION STUDIES

#### 3.6.1 MOUNTING CONFIGURATIONS

##### 3.6.1.1 Introduction

The method of mounting the solar array units on the spacecraft can affect the total system weight of the solar array. While it is recognized that an optimum mounting arrangement is a function of a specific spacecraft design, it was the intent of this study to consider the various options and generate designs that are acceptable for typical spacecraft. It was considered particularly important not to assume a mounting arrangement that maximizes the weight performance of the solar array at the expense of total system weight.

From the spacecraft integration standpoint, a statically determinate mounting arrangement would be the simplest to design and analyze. With this arrangement, the loads (or forces) at the array attachment points would be determined from the specified mechanical environment and the relative motion of the attachment points due to structural deflections does not create internal forces in the array structure (on a static basis). The stress analyses and structural design of the array structure can be accomplished without knowledge of the spacecraft structural design. As the number of constraints (or attachment points) is

increased from the minimum number, the array becomes integrated with the spacecraft structure. The loads on the array structural elements are affected by the relative motion and stiffness of the spacecraft structure and a total system analysis is required. A number of possible mounting arrangements have been considered and are discussed in the following paragraphs.

### 3.6.1.2 Present Mounting Arrangement

The mounting configuration of the baseline design is shown schematically in Figure 3-141. There are 14 constraints which are eight more than the six that provide a statically determinate condition. This arrangement is near optimum with respect to the array structure mass as the supports at the corners of the system minimize the internally generated loads which must be carried by the structure. This structure must be flexible enough to tolerate relative motion of these points.

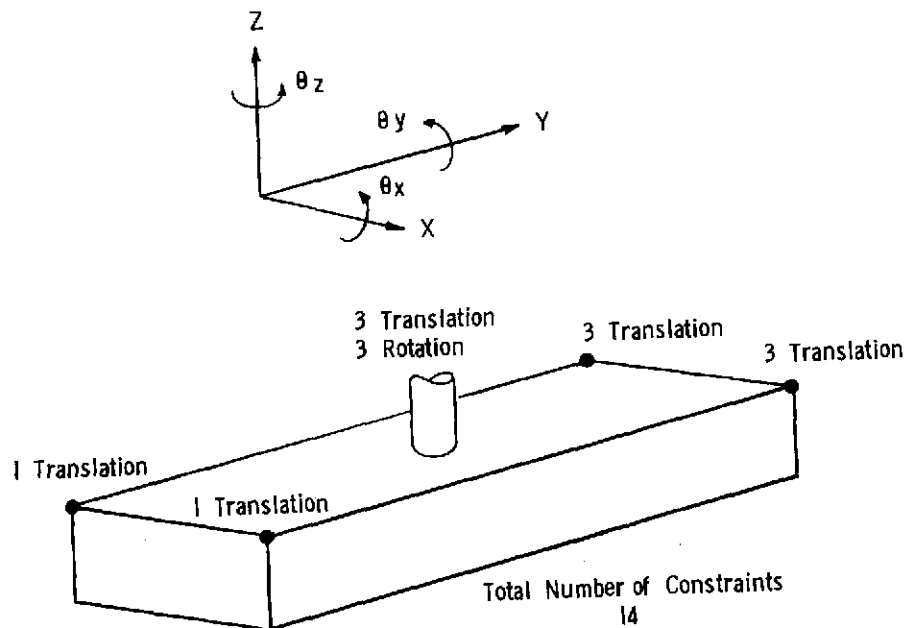


Figure 3-141. Constraints in Baseline Mounting Arrangement

### 3.6.1.3 Alternate Mounting Arrangements

Several possible alternate mounting arrangements using fewer restraints were investigated as shown in Table 3-47. Configuration A eliminates the center support restraints. Such an arrangement does not appreciably increase the solar array weight. However, from a spacecraft viewpoint, it is logical to plan on restraints at the center since the solar array is supported at the center when deployed in order to provide for orientation to the sun.

Configurations B and C show two possible versions of mounting with varying amounts of restraint at the center. Configuration C virtually cantilevers the structure from its midsection for loads in the X direction. These configurations provide support at both ends of the array as well as in the middle and are not very different from the baseline mounting arrangement.

Configuration D has one side of the structure cantilevered from the midsection in the Z direction while Configuration E shows the arrangement with both sides cantilevered. Design considerations for these arrangements with unsupported ends include the accommodation of relatively large tip deflections; avoiding the natural frequencies of the spacecraft which are typically of this order of magnitude; and possibly meeting some minimum frequency design criteria. Configuration D is of interest because spacecraft integration studies (at JPL) show that this is a practical approach to installing large flexible arrays on solar electric spacecraft in the launch configuration.

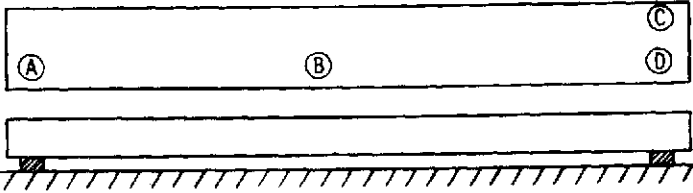
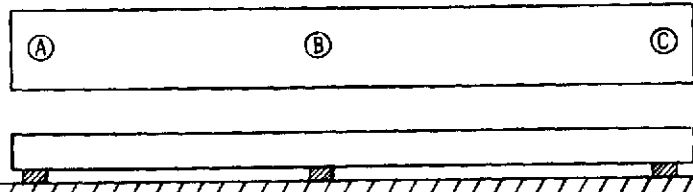
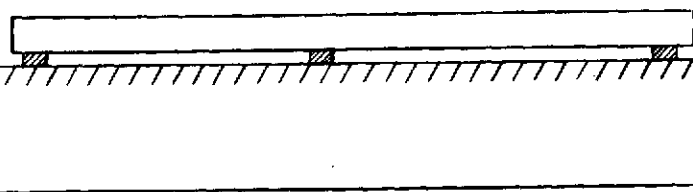
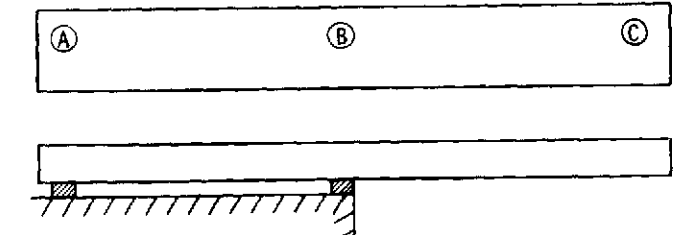
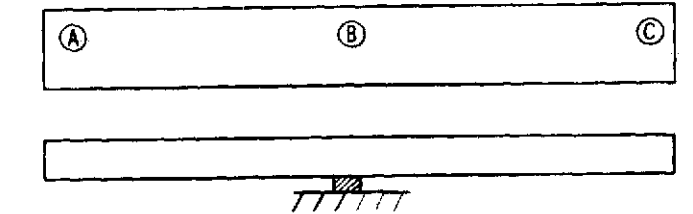
A stowed vibration and load analysis of various spacecraft mounting arrangements is presented in Section 3.4.9.

## 3.6.2 ATTITUDE CONTROL CONSIDERATIONS

### 3.6.2.1 Introduction

Interaction between the vehicle attitude control system and large lightweight solar arrays is a factor in the evaluation and selection of these arrays for space missions. Since the intent of this study was to generate design concepts applicable to future missions it was essential that

Table 3-47. Alternative Mounting Arrangements

CONFIG- URATION	MOUNTING ARRANGEMENT	RESTRAINTS			
		A	B	C	D
A		X <sup>*</sup> Y Z	NONE	X Z	Z
B		X Z	Y $\theta_Y$	X Z	--
C		Z	X Y $\theta_Y$ $\theta_Z$	Z	---
D		X Z	X Y Z $\theta_Y$	NONE	--
E		NONE	X Y Z $\theta_X$ $\theta_Y$ $\theta_Z$	NONE	---

\*Refer to Figure 3-141 for definition of axes

the performance characteristics of the concepts be acceptable to system designers. The approach used in the study was to develop design requirements or guidelines that will provide this performance.

There are no design criteria that both eliminate interaction considerations and allow a large lightweight array for the missions of interest. However, the problem is considered solvable for specific missions and designs with the solution involving the participation of several spacecraft design and analysis disciplines. For example the attitude control of a Solar Electric Multimission Spacecraft (SEMMS) with large solar arrays has been investigated by JPL (see Reference 68) with the conclusion that attitude control of a vehicle with a large flexible solar array can be accomplished for interplanetary missions. Though not as well documented, attitude control specialists have similar opinions with respect to the other two missions included in this study.

This discussion first lists the design guidelines being used by this study with a discussion of the interaction problem following.

#### 3.6.2.2 Design Guidelines

The most important requirement with respect to integrating a large lightweight solar array into a spacecraft with an active attitude control system is to have the capability of adequately modeling the array dynamic characteristics. This allows the design of the attitude control equipment to proceed on a rational basis. The capability to adequately model the array for system dynamics analysis implies that the structural dynamics are understood well enough to analyze the effects of other forcing functions such as propulsion devices on the array system.

The capability to model the solar array does not provide the design constraint needed for the study. The structural rigidity or stiffness constraint adopted for the study is that the solar panel shall have sufficient rigidity so that its lowest natural frequency of vibration is equal to or greater than 0.04 Hz. As discussed in the following section this value has



been used on several lightweight array studies in the past and is an acceptable value for at least the interplanetary and synchronous earth orbit missions.

### 3.6.2.3 Discussion

The structural rigidity design requirements used in previous development programs for large lightweight solar arrays were surveyed as one step in generating a rational design requirement for this study. Results are summarized in Table 3-48. Except for one system, structural rigidity is specified by constraining the natural frequencies of the solar array system. This is as expected since one of the basic attitude control interaction considerations is whether or not there are structural resonances within the bandwidth of the attitude control system. In most systems this is the first problem that is encountered as the structural frequency is reduced. However, other considerations such as the vehicle accelerations can be constraining as is evidently the case for the Flexible Rolled-Up Solar Array (FRUSA).

The relation between the fundamental frequency, an acceleration environment, and the maximum panel deflection for any configuration can be approximated by considering the panel as a single-degree-of-freedom spring mass system. Results are given in Figure 3-142. At the selected lowest natural frequency of 0.04 Hz the static deflection with a 0.1 g force is about 25 meters, an unrealistically large deflection for the size system being considered. Thus, the FRUSA stiffness requirement implies a higher frequency than the value selected for this study.

The preferred approach in control system design is to have all structural resonance outside the bandwidth of the control system. This is the approach used in the CTS program (see Table 3-48) where the "rule of thumb" of a decade of separation was used.

Control system bandwidths for synchronous earth orbits and interplanetary missions are typically in the range of 0.0016 to 0.016 Hz while manned space stations using control moment gyros could have bandwidths of 0.16 to 1.6 Hz. This wide range of bandwidths does not converge on a value for lowest natural frequency that is typical for all missions.

Table 3-48. Structural Rigidity Design Requirements for Large Lightweight Solar Array Programs

Program	Design Requirement	Data Source	Comments
30 Watt per Pound Roll-up Solar Array	First natural frequency equal to or greater than 0.04 Hz	Ref. 12	Artificial "g" conditions provides most severe structural requirement
Large Area Solar Array (20 Watt per Pound)	First natural frequency equal to or greater than 0.04 Hz	Ref. 18	
Space Station Solar Array Technology Program	Fundamental frequency to be less than 0.1 Hz	Ref. 5	
Space Station Solar Array Design Study	No fundamental frequencies in the range of 0.1 Hz to 2 Hz	Ref. 69	
Flexible Rolled-Up Solar Array (FRUSA)	0.1 g acceleration environment	Ref. 13	
Communications Technology Satellite (CTS) Lightweight Solar Array	Fundamental frequency to be greater than 0.1 Hz	Ref. 70	Natural frequency is 10 times the bandwidth of the attitude control subsystem

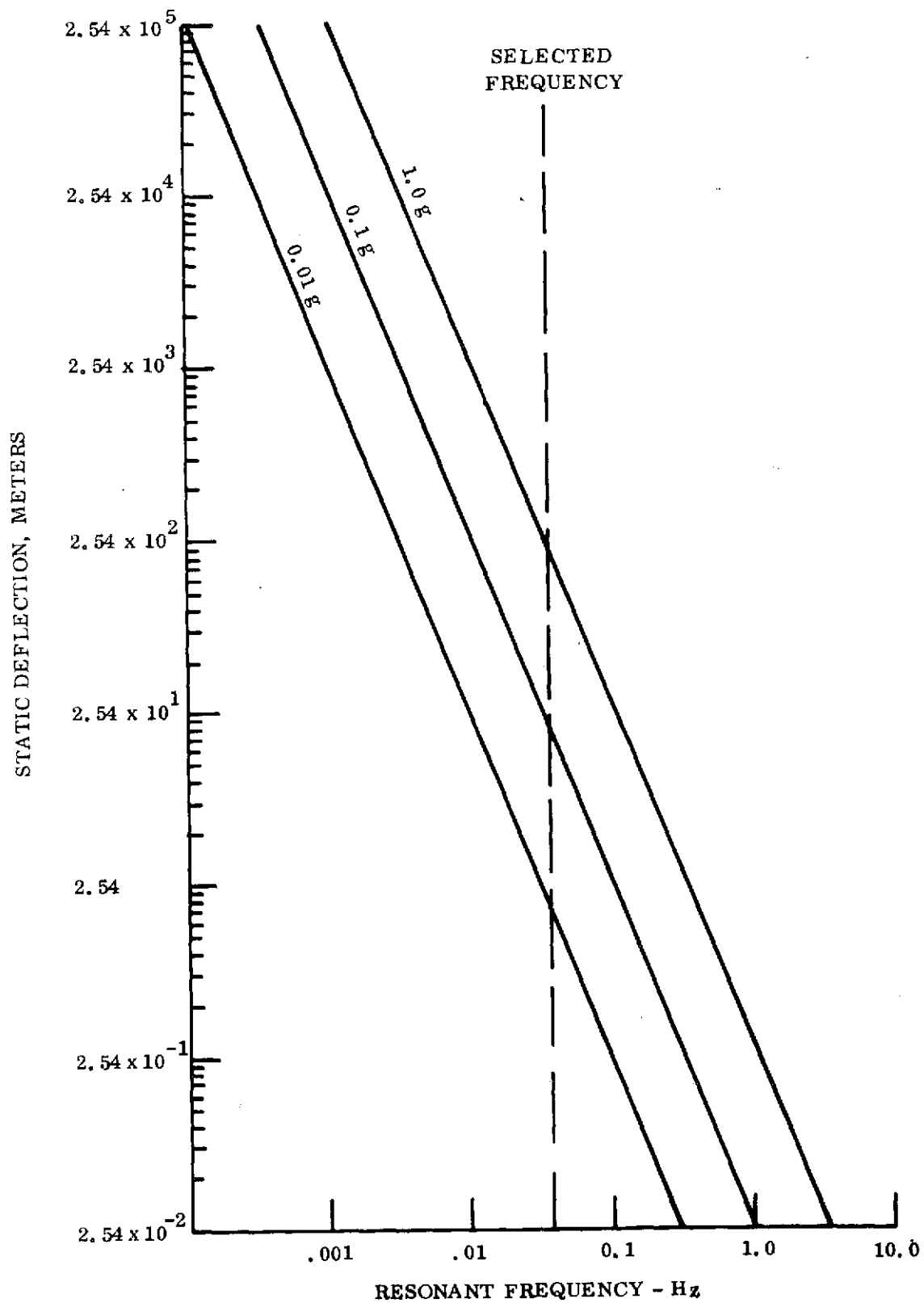


Figure 3-142. Static Deflection vs Frequency

The value of 0.04 Hz was selected as a baseline because it is within the range of interest and because of its use in previous studies. Thus the results of this study are directly comparable with previous studies since the structural stiffness requirement is the same. Parametric studies will be carried out to show the effect of this requirement on weight.

Although a minimum frequency requirement for the general mission categories can be established, integration studies have been carried out for the 0.04 Hz value. Reference 68 concludes that natural frequencies below 0.04 Hz can be accommodated on the SEMMS vehicle designs and unpublished studies at General Electric indicated that 0.04 Hz solar panels could be accommodated on the ATS F and G vehicle with acceptable attitude control performance.

The design of a spacecraft for a particular mission will involve dynamics analysis of the system and it is unlikely that any design requirement adopted in this study will satisfy all mission requirements. It is also likely that at some future date the control system bandwidth will include some of the array natural frequencies. The technique of keeping the frequencies outside the control bandwidth essentially decouples the system and interaction does not occur. There are a number of control system techniques that can be used to maintain stability and control system performance when this is the case. Though they increase the complexity of the control system this may be preferable to the increased weight that results from the simple approach of stiffening the structure to increase its frequency. Reference 72 lists artificially stiffening the structure through the use of special, inner control loops, utilization of a low pass filter within the control amplifier, artificially lowering the bandwidth of the control through use of a special actuator lag which inhibits sign reversal of the control at a rate higher than that needed to follow control commands, or through the use of notch filters. This list should be considered typical rather than all inclusive since the technology of control systems and associated equipment such as on-board computers allows many and varied approaches to the attitude control of a spacecraft.

SECTION 4  
CONCLUSIONS

## SECTION 4

### CONCLUSIONS

Based on the results of this feasibility study, it is concluded that a 10,000 watt solar array with a power-to-mass ratio in excess of 110 watt/kg at the beginning-of-life could be constructed using currently available components and technology. Such a solar array requires the use of ultra-thin solar cells (125  $\mu\text{m}$  thick) coupled with an integral coverglass system. The interconnectors must be welded (or bonded) to the solar cell contacts. The technology exists in all of these areas, but there has never been an attempt to combine them as would be required for this application. This uncertainty is further complicated by the specified thermal shock operating temperature extremes of  $-190$  to  $+140^{\circ}\text{C}$ .

The trade studies and analyses performed during the course of this program have resulted in the following specific conclusions:

1. "Rigid" folding panel design concepts were eliminated from consideration in the 110 watt/kg feasibility study. This conclusion was based on the weight of the Boeing folding panel design. This array is approximately the size required for the 10,000 watt, 110 watt/kg array and has a structural mass-to-area ratio of  $1.486 \text{ kg/m}^2$ . Based on this structural weight, the power-to-mass ratio would be approximately 70 watts/kg if it is assumed that the blanket weight is zero. The addition of a blanket weighing  $0.475 \text{ kg/m}^2$  will reduce the power-to-mass ratio to about 52 watts/kg which is far from the goal of 110 watts/kg. The use of a multiple panel EOS Hollowcore approach offers no potential for improvement of this power-to-mass ratio.
2. A single boom deployment system is lighter than a similar system with two booms. A comparison of the GE roll-up with the Hughes roll-up shows a significant difference in the mass per unit area associated with the deployment related structure. Part of this difference can be attributed to the difference in size and deployed natural frequency. In order to provide a valid comparison between these two concepts, the GE roll-up was scaled down in area and up in deployed frequency using the techniques described by Coyner and Ross in Reference 61. The width of 2.52 m was held constant, and the cell area was reduced to  $13.8 \text{ m}^2$  with the lowest deployed natural frequency increased to 0.25 Hz. Under these conditions, a BI-STEM boom stiffness of  $1200 \text{ N-m}^2$  ( $2.9 \times 10^3 \text{ lb-ft}^2$ ) is required with an associated deployed structure mass of 5.4 kg including the boom, actuator and leading edge member. The resulting deployment equipment mass-to-area ratio of  $0.391 \text{ kg/m}^2$  is still considerably less than the  $0.632 \text{ kg/m}^2$  for the Hughes roll-up.

3. A flat-pack packaging concept offers weight advantages when compared to roll-up stowage. This conclusion is substantiated by comparing the large RAE flat-pack design with either the GE or Hughes roll-up.
4. Improvements in the structural concept of these existing designs is required to meet the 110 watt/kg goal. With a blanket power-to-area ratio of 105.4 watt/m<sup>2</sup> of cell area, it is necessary to have a total mass-to-area ratio of 0.95 kg/m<sup>2</sup> in order to achieve an overall power-to-mass ratio of 110 watt/kg. With a blanket mass of 0.475 kg/m<sup>2</sup>, the remaining 0.475 kg/m<sup>2</sup> is available for deployment and stowage structure. With the present concepts, the best available structure weights are 0.258 kg/m<sup>2</sup> for deployment with the GE roll-up and 0.299 kg/m<sup>2</sup> for the RAE flat-pack stowage system. Thus, improvements in both the deployment and stowage weights are necessary to achieve the 110 watt/kg goal.
5. Nominal solar cell thicknesses of 125 or 100  $\mu$ m appear feasible from an overall weight and electrical performance standpoint. Cell thicknesses of greater than 125  $\mu$ m result in too large a portion of the total allowable system weight being used for the solar cell blankets. This is a manner of judgement based on the distribution of weight in existing lightweight flexible solar array system. Cell thicknesses of less than 100  $\mu$ m have only been produced in very small quantities and there is a complete lack of published performance data for thinner cells. The 125  $\mu$ m thick, 10 ohm-cm, bottom wraparound contact cell manufactured by Ferranti, Ltd., is the best currently available in terms of power-to-mass ratio and has been used as the basis for cell performance predictions. This cell has a power-to-mass ratio of 360 watt/kg at 55°C. By comparison, the cell used on the 30 watt/lb roll-up solar array program had a power-to-mass ratio of 270 watt/kg at 55°C.
6. Pertaining to solar cell covers, a review of existing technology leads to the conclusion that integral glass covers of Corning 7070 glass (with or without ceria stabilization) which are deposited by the Ion Physics HVIBS process or by the ERA's RF sputtering process offer the best approach for performing this function. The low intrinsic stress associated with this glass make it an attractive choice for deposition in thicknesses of 25 to 50  $\mu$ m on 100 to 125  $\mu$ m thick solar cells. More work with cells of this thickness would be required to verify this point. Both of these deposition processes are reported to have produced integral covers with consistently excellent optical and physical properties. It is expected that some amount of ceria doping of the 7070 glass will be required, but this determination will require additional work to optimize the level for a particular particle radiation environment. Both of these processes are capable of depositing some glass on the cell edges to provide a desirable protection against low energy protons.

At the present time, the FEP-Teflon cover does not appear to offer the same degree of environmental stability as the integral glass approaches described above. Further development may reverse this conclusion.

7. For the solar cell blanket substrate, Kapton-H film appears to offer the best solution. With a cementless attachment of the solar cells to the substrate it was found necessary to cut holes in the substrate to allow for direct radiant cooling from the rear solar cell surface. This method was used in the design of the RAE flat-pack solar array substrate. The conductive heat transfer path through the welded interconnectors was found to have only a minor effect in reducing the operating temperature.
8. The continuous fiberglass longeron coilable lattice ASTROMAST is the lightest weight deployable boom system available for the bending stiffness required for this application. The relatively large canister height required for this mast makes integration into the system more difficult when compared to an equivalent BI-STEM type boom and actuator.
9. The application of advanced composite materials, such as graphite/epoxy and boron/aluminum, to the fabrication of deployable boom structures shows promise from a theoretical standpoint. Particular emphasis should be placed in the utilization of Hercules X-3501-AS graphite prepreg material in the continuous longeron ASTROMAST.
10. It is advantageous to select a circuit voltage which is as high as practical. A circuit voltage of less than 100 volts is obviously impractical if the goal is to design a solar array to meet a 110 watt/kg power-to-mass ratio goal. In general, the solar array voltage is predetermined by the power subsystem interface requirements and is beyond the control of the solar array designer. A voltage level of 200 vdc was selected for the baseline design for this study.
11. The "V"-stiffened solar array concept shows the promise of providing increased stiffness to out-of-plane bending when compared to an equivalent planar geometry. This may allow a reduction in the boom stiffness (and weight) required to maintain a specified deployed natural frequency. This concept was not incorporated into the baseline configuration because the associated system weight reduction is not required to achieve the 110 watt/kg objective. The changes required to utilize the "V" stiffened geometry were investigated with the conclusion that it could be implemented with only minor changes in the structural design concept. A different blanket folding pattern would be required, but this also could be easily implemented.



## SECTION 5

### RECOMMENDATIONS

## SECTION 5

### RECOMMENDATIONS

The realization of a power-to-mass ratio of 110 watt/kg is strongly dependent on the ability to utilize ultra-thin ( $\approx 125 \mu\text{m}$  thick) solar cells in conjunction with welded interconnectors and integral covers. Therefore, it is recommended that a development program be initiated to combine the technology in these areas into a solar cell module construction which meets the weight requirements of this application.

The possible application of the two New Technology items reported on this program should be explored in greater depth. The "V" stiffened solar array and the retractable flat-pack stowage concept have potential application to any lightweight solar array design.

SECTION 6

NEW TECHNOLOGY

SECTION 6  
NEW TECHNOLOGY

The following items have been disclosed as New Technology under the terms of this contract:

Item No. 1

Descriptive Title:	Tension Stiffened "V" Shaped Solar Array
Name of Innovator:	C. V. Stahle, Jr.
Date Reported:	14 December 1972
Reference for Discussion:	Sections 3.4.5 and 3.5

Item No. 2

Descriptive Title:	Retractable Flat-Pack Solar Array
Name of Innovator:	A. Kirpich
Date Reported:	26 April 1973
Reference for Discussion:	Section 3.2.1.1.3

## SECTION 7

## REFERENCES

SECTION 7  
REFERENCES

1. Hall, D. F., "Electrostatic Propulsion Beam Divergence Effects on Spacecraft Surfaces," Vol. II, Final Report, TRW Report No. 11985-6002-RU-00, 17 January 1973.
2. Weidner, D. K., "Natural Environment Criteria for the NASA Space Station Program (Second Edition)," NASA TMX-53865, August 20, 1970.
3. Vette, J. I., et al, "Models of the Trapped Radiation Environment, Volume III: Electrons at Synchronous Altitudes," NASA SP-3024.
4. "ATS Power Subsystem Radiation Effects Study, Phase I/Final Report," HAC Report No. SSD80089R, February 1968.
5. "Second Topical Report - Design and Analysis - Space Station Solar Array Technology Evaluation Program," LMSC Report No. A995719, November 1971.
6. "Space Station - A Guide for Experimenters," North American Rockwell - Space Division Document No. SD70-534, October 1970.
7. King, J. H., "Models of the Trapped Radiation Environment, Volume IV: Low Energy Protons," NASA SP-3024.
8. Lavine and Vette, "Models of the Trapped Radiation Environment, Volume V: Inner Belt Protons," NASA SP-3024.
9. Lavine and Vette, "Models of the Trapped Radiation Environment, Volume VI: High Energy Protons," NASA SP-3024.
10. Vette, Lucero, and Wright, "Models of the Trapped Radiation Environment, Volume II: Inner and Outer Zone Electrons," NASA SP-3024.
11. Andrews, J., "Space Radiation Estimates: NASA Space Base," GE Internal Document No. PIR-SB-8014, October 19, 1970.
12. "Final Report - Roll-up Subsolar Array, Volume I - Program Summary," GE-SSO Report No. 70SD4286, February 1971.
13. Wolff, G., "Oriented Flexible Rolled-up Solar Array," AIAA Paper No. 70-738 presented at the 3rd Communication Satellite Systems Conference, April 1970.
14. Wolff, G., "The Flexible Roll-up Solar Array Flight Experiment," paper presented at the 9th Photovoltaic Specialists Conference, May 1972.

15. Treble, F. C., "Status Report on RAE Advanced Solar Array Development," paper presented at the 9th Photovoltaics Specialists Conference, May 1972.
16. Treble, F. C., "Progress in Advanced Solar Array Development," paper presented at the 8th Photovoltaics Specialists Conference, August 1970.
17. Franklin, C. A. and Davison, E. H., "A High-Power Communications Technology Satellite for the 12 and 14 GHz Bands," AIAA Paper No. 72-580 presented at the 4th Communications Satellite Systems Conference, April 1972.
18. "Final Report - Phase II, Large Area Solar Array," Boeing Report No. D2-113355-7, October 1968.
19. Carlson, J. A., "Development of Lightweight Solar Panels," NASA CR-66832.
20. Private communication with R. Lohnes, SPAR Aerospace Products, Ltd., July 18, 1972.
21. Lindmayer, J. and Allison, J., "An Improved Silicon Solar Cell - The Violet Cell," paper presented at the 9th Photovoltaic Specialists Conference, May 1972.
22. Ralph, E. L., et al, "Development of an Integrated Lightweight Flexible Silicon Solar Cell Array," Final Report under JPL Contract 952560.
23. Webb, H., "The Design and Practical Aspects of Maximum Efficiency Silicon Solar Cells for Satellite Applications," paper presented at the 9th Photovoltaic Specialists Conference, May 1972.
24. Crabb, R. L., and Atzec, A., "Environmental Study of European Silicon Solar Cells with Improved Antireflection Coatings," paper presented at the 8th Photovoltaic Specialist Conference, August 1970.
25. Ferranti Catalog entitled, "Satellite Power Sources - Silicon Solar Cells," ESB 581271, December 1971.
26. Private communication with Ira S. Gewant, Ferranti Electric, Inc., June 6, 1972.
27. Ralph, E. L., "Performance of Very Thin Silicon Solar Cells," paper presented at the 6th Photovoltaic Specialists Conference, March 1967.
28. Brackley, G., "Integral Covers for Silicon Solar Cells," paper presented at the 9th Photovoltaic Specialists Conference, May 1972.
29. Stella, P., and Somberg, H., "Integrally Covered Silicon Solar Cells," paper presented at the 9th Photovoltaic Specialists Conference, May 1972.

30. Kirkpatrick, A. R., et al, "Low Stress Integral Cover Slips," paper presented at the 8th Photovoltaic Specialists Conference, August 1970.
31. Fairbanks, J. W., "Evaluation of Integral Covers on Silicon Solar Cells," paper presented at the 1969 Intersociety Energy Conversion Engineering Conference.
32. Kirkpatrick, A. R., et al, "Solar Cell Cover Glass Development," Final Report on Contract NAS 5-10236, March 1971.
33. Ralph, E. L., Somberg, H., and Payne, P., "Manufacturing Methods for Protecting Silicon Solar Cells with Integral Coverslips," Interim Technical Report 504-0(3), Heliotek, Division of Textron, Inc., March 1971.
34. "Stress Free Solar Cell Cover Research," Quarterly Status Report No. 3, Contract No. F33615-71-C-1656, January 1972.
35. Broder, J. D., et al, "Recent Results of FEP Solar Cell Cover Development," paper presented at the 9th Photovoltaic Specialists Conference, May 1972.
36. Forestieri, A. F., and Broder, J. D., "Improvements in Silicon Solar Cell Cover Glass Assembly and Packaging using FEP Teflon," paper presented at the 8th Photovoltaic Specialists Conference, August 1970, also released as NASA TM X-52875.
37. Forestieri, A. F., et al, "FEP Covers for Silicon Solar Cells," paper presented at the 1971 Intersociety Energy Conversion Engineering Conference.
38. Greenberg, S. A., McCargo, M., and Palmer, W. L., "Investigation of FEP Teflon as a Cover for Silicon Solar Cells," NASA CR-72970, August 1971.
39. "Final Review - Space Station Solar Array Technology Program," March 30, 1972.
40. Luft, W., "Solar Cell Interconnector Design," IEEE Transactions on Aerospace and Electronic Systems, Vol. AES-7, No. 5, September 1971.
41. Salama, A. M., et al, "Stress Analysis and Design of Silicon Solar Cell Arrays and Related Material Properties," paper presented at the 9th Photovoltaic Specialists Conference, May 1972.
42. Luft, W., et al, "Hardened Solar Array Panel Segments," Technical Report AFAPL-TR-72-33, May 30, 1972.
43. Eakins, T. C., "Results of Solar Cell Welded Interconnection Development," paper presented at 1972 IECEC.
44. Cohen, D. B., and Schwartz, S., "Engineering Study of Elevated Temperature Solar Cell Panel Fabrication Techniques," paper presented at the 8th Photovoltaic Specialists Conference, August 1970.



45. Reinhartz, K. K., and Capart, J. J., "Status of Welded Solar Cell Module Technology at ESRO," paper presented at the 8th Photovoltaic Specialists Conference, Ausut 1970.
46. "Development of a Flexible Solar Cell Panel," a proposal by Messerschmitt-Bolkow-Blohm, Space Division in response to ESRO RFP AO/335, August 24, 1970.
47. Boller, H. W., et al, "Solar Cells and Generator Technology for the Helios Sun Probe," paper presented at the 9th Photovoltaic Specialists Conference, May 1972.
48. Clarke, D. R., "High-Temperature Annealable Solar Array," paper presented at the 7th Photovoltaic Specialists Conference, November 1968.
49. "First Topical Report - Evaluation of Space Station Solar Array Technology and Recommended Advanced Development Programs," LMSC Report No. A981486, December 1970.
50. Crawford, R. F., "Strength and Efficiency of Deployable Booms for Space Applications," AIAA Paper No. 71-396.
51. "Summary of Stem Characteristics," Spar Aerospace Products, Ltd., June 1969.
52. "Third Topical Report - Design Support, Major Hardware and System Level Testing," LMSC Document No. D153526, September 1972.
53. Advanced Battery Technology, Volume 9, Number 3, March 1973.
54. Toth, I. J., Brentnall, W. D., and Menke, G. D., Fabricating Aluminum Matrix Composites, Journal of Metals, September 1972.
55. Kreider, K., et al, "Plasma Sprayed Metal Matrix Fiber Reinforced Composites," Technical Report AFML-TR-68-119, July 1968.
56. Kreider, K., et al, "Metal Matrix Composite Technology," Technical Report AFML-TR-71-204, December 1971.
57. MIL-HDBK-5A, "Metallic Materials and Elements for Aerospace Vehicle Structures."
58. Final Report, "Feasibility Study for a Solar Electric Propulsion Stage and Integrated SEP Spacecraft," Vo. II, Part 2, Contract NAS8-27360, March 27, 1972.
59. Rasmussen, R., "Calculation of 1 MeV Electron Flux and Irradiation Degradation of Solar Cell I-V Curves by Computer," paper presented at the 6th Photovoltaic Specialists Conference, 1967.
60. Roger, J., "Optimal Bus Bars for Rectangular Solar Arrays," paper presented at the 9th Photovoltaic Specialists Conference, May 1972.

61. Coyner, J. V., Jr., and Ross, R. G., Jr., "Parametric Study of the Performance Characteristics and Weight Variations of Large-Area Roll-up Solar Arrays," Technical Report 32-1502, December 15, 1970.
62. "Design and Development of a Thirty Watt per Pound 250 Square Foot Roll-up Subsolar Array - Final Report," GE Document No. 71SD4239, May 20, 1971.
63. "Gold, Recovery Properties and Applications," E. Merriman Wise, 1964.
64. "Cryogenic Materials Data Handbook," Volume I, AFML-TDR-64-280, August 1968.
65. Technical Information Bulletin H-2, du Pont Kapton Polyimide Film.
66. "Final Report - Feasibility Study - 30 Watts per Pound Roll-up Solar Array," N68-16191, June 21, 1968.
67. "ASTROMASTS for Space Applications," by Astro-Research Corporation, Santa Barbara, California.
68. "Solar Electric Multimission Spacecraft (SEMMS), Phase A Final Report, Technical Summary," Report No. 617-2, 30 July 1971, Jet Propulsion Laboratory, Pasadena, California.
69. Shepard, N. F., Jr., Ferguson, R. C., Jr., Roach, R. E., Jr., Matteo, D. N., "Final Summary Report - Solar Array," Report EL-405, March 16, 1970, General Electric Company, Philadelphia, Pa.
70. Private communication with Canadian Department of Communications Personnel.
71. Martin, J. H., Statler, R. L., and Ralph, E. L., "Radiation Damage to Thin Silicon Solar Cells," paper presented at the 1967 IECEC.
72. "NASA Space Vehicle Design Criteria (Guidance and Control) Effects of Structural Control Systems," NASA SP-8016, April 1969.

APPENDIX A

JPL SPECIFICATION ES506080B

LIGHTWEIGHT SOLAR PANEL SUBSYSTEM,  
110 WATTS PER KILOGRAM,  
DETAIL SPECIFICATION FOR

EQUIPMENT SPECIFICATION

CODE IDENT NO. 23835

SPEC NO. ES506080 REV. R

ISSUE DATE 17 September 1971

SUPERSEDING ES506080 A

DATED 4 August 1971

LIGHTWEIGHT SOLAR PANEL SUBSYSTEM  
110 WATTS PER KILOGRAM  
DETAIL SPECIFICATION FOR

Walter C. Hasbach 14 Sept 71  
ENGINEER W. A. Hasbach DATE  
Section 342 Cognizant Engineer

John V. Goldsmith 14 Sept 71  
APPROVED BY J. V. Goldsmith DATE  
Section 342 Group Supervisor

WRITTEN and G. Inouye 9/17/71  
RELEASED BY G. Inouye DATE  
Section 356 Design Section  
Group Supervisor

Dr. R. G. Ross 16 Sept 71  
APPROVED BY Dr. R. G. Ross DATE  
Section 358 Structures and Dynamics

JET PROPULSION LABORATORY  
CALIFORNIA INSTITUTE OF TECHNOLOGY  
PASADENA, CALIFORNIA

## CHANGE INCORPORATION LOG

CHG LTR	WRITER		AUTHORITY	PAGES AFFECTED	DATE	ENG APPROVAL	
	INITIAL	SECTION				INITIAL	SECTION
A	GI	356			8/4/71	WAH	342
B	GI	356				WAH	342

## 1. SCOPE

1.1 This specification covers the requirements for the design of a 10 kilowatt solar panel having a power-to-weight ratio greater than 110 watts per kilogram.

## 2. APPLICABLE DOCUMENT

2.1 The following document of the issue shown forms a part of this specification to the extent specified herein:

### STANDARD

#### Military

MIL-HDBK 5

Metallic Materials and Elements for  
Flight Vehicle Structures

## 3. REQUIREMENTS

3.1 Conflicting requirements. In case of conflict between the requirements of this specification and the documents referenced herein, the requirements of this specification shall govern.

3.1.1 Deviations from standard practices. Any deviations from generally accepted standard practices will be approved by the Jet Propulsion Laboratory (JPL), after it has been demonstrated by analysis or test that the deviations will not degrade the overall probability of attaining the objectives of this effort. The burden of proof in such circumstances shall rest upon the contractor and not upon JPL.

3.2 Performance requirements. The solar panel shall be designed so that the following performance requirements can be met.

3.2.1 General. In the stowed configuration, the solar panel shall be supported in a manner that will prevent damage to the solar panel under shock

and vibration loads. Upon command and in proper sequence, the release and deployment mechanism shall extend and lock the solar panel into the deployed position at a rate to be defined by the contractor.

3.2.2 Power requirement. Following launch, the deployed solar panel shall be capable of supplying 10 kilowatts of electrical power at the spacecraft interface at a solar intensity of  $140 \text{ mw/cm}^2$  and at the predicted solar array temperature at this intensity.

3.2.3 Lifetime. The solar panel shall be designed to perform over a period of 3 years with no greater than a 20 percent loss of power and with no failures which would prevent the panel from performing successfully in both mechanical and electrical modes.

3.2.4 Solar panel operating temperature. The thermal characteristics of the deployed panel shall be adjusted so that the celled area maintains an operating temperature between 50 and  $70^\circ\text{C}$  at a solar intensity of  $140 \text{ mw/cm}^2$ .

3.2.5 Solar panel weight. The weight of the solar panel, including the release and deployment mechanisms but not including the solar panel gimbaling mechanisms, shall be so that the solar panel specific power exceeds 110 watts per kilogram at a solar intensity of  $140 \text{ mw/cm}^2$ .

3.2.6 Packaging volume envelope. The volume and shape of the stowed solar panel, including the release and deployment mechanisms, shall be determined by the contractor in order to maximize the solar panels adaptability to various spacecraft configurations. In these design considerations, a 2000-pound spacecraft containing two 10-kilowatt solar panels and a Titan-Centaur launch vehicle shall be assumed. The following requirements shall also be included:

- a. Launch vehicle shroud volume restrictions.
- b. Spacecraft structural interface requirements.
- c. Solar panel deployment complexity (reliability).
- d. Solar panel gimbaling (Sun tracking) requirements.

3.2.7 Structural interfaces. The solar panel to spacecraft attachment points shall be considered to provide the most efficient interface capable of performing the mission. Consideration shall be given to the ease with which the deployed solar panel can be gimbaled (tilted or rotated) with respect to the spacecraft as required by the Sun tracking requirements. Consideration shall also be given to the requirements imposed on the spacecraft structure by the solar panel. A solar panel, requiring an extremely rigid support or negligible relative motion between widely spaced support points, would be undesirable because meeting these requirements would result in increased spacecraft weight.

3.2.8 Structural rigidity. In the deployed configuration, the solar panel shall have sufficient rigidity so that its lowest natural frequency of vibration is equal to or greater than 0.04 Hz.

3.2.9 Mass center location. The solar panel shall be designed to minimize displacement of the vehicle mass center and center of solar pressure caused by thermal gradients and solar panel temperatures.

3.2.10 Flatness. In the deployed configuration, the solar panel celled area shall lie in a predetermined plane with a maximum angular deviation of  $\pm 10$  degrees between any portion of the celled area and the plane. This tolerance shall include deflections from the thermal gradients arising from the operation at any heliocentric distance from 0.5 to 5.0 AU, but shall not include deflections due to dynamic load inputs.

3.2.11 Inspection. Release, deployment, and locking mechanisms, not necessarily the assembled solar panel, shall be designed so that, with suitable equipment, their operating functions can be inspected in a one-g Earth field environment.

3.2.12 Reliability. The solar panel design shall incorporate design practices that maximize the probability that the solar panel will operate successfully in both mechanical and electrical modes.



3.3 Environmental requirements. The following environmental requirements shall be considered in the design of the solar panel.

3.3.1 Ground handling. The solar panel's structural, mechanical, and electrical performance shall not be degraded because of ground handling during manufacturing, testing, and transportation operations.

3.3.2 Launch environment. The following environmental constraints, representing the launch environment of the solar panel in the stowed configuration, shall be considered in the solar panel design.

3.3.2.1 Sinusoidal vibration. The sinusoidal vibration input levels at frequencies between 5 and 2000 Hz shall be as specified on Figure 1. These levels are specified at the interface between the solar panel assembly and the spacecraft in each of three axes. For configurations with widely spaced support points, these input levels shall be simultaneously applied at each support point, but the worst case phase relationship shall be assumed for motion perpendicular to the line joining the supports.

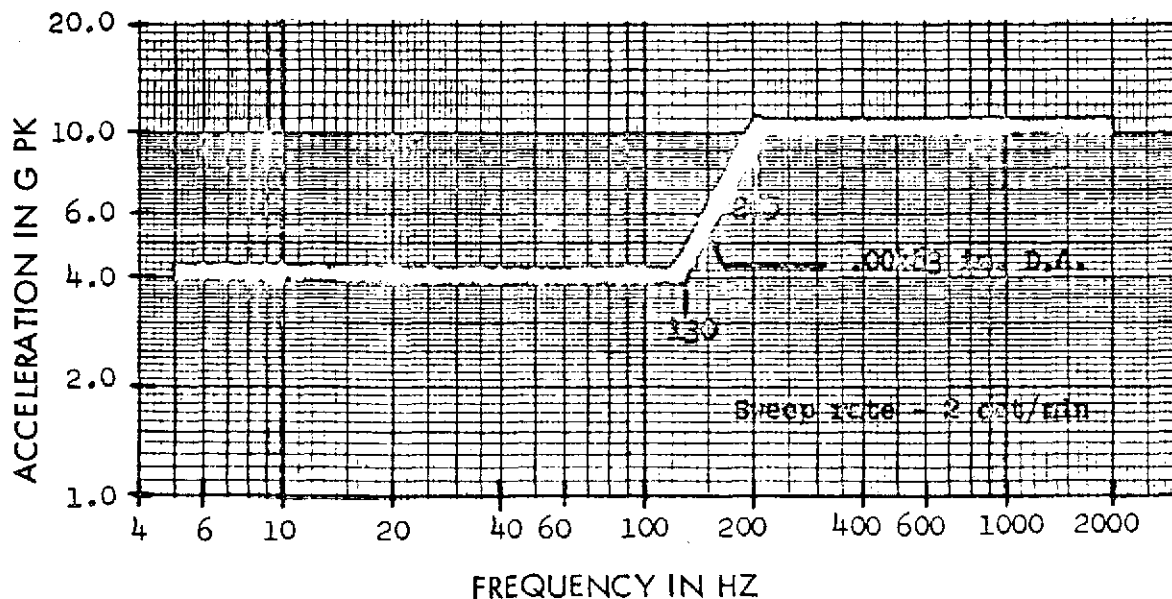


Figure 1. Sinusoidal Vibration Test Requirements

3.3.2.2 Acoustic. The launch acoustics environment shall be 60 seconds of random incidence, reverberant sound field, having the third-octave band sound pressure levels defined in Table I. The overall sound pressure level for the spectrum given in Table I shall be approximately 150 db reference to  $0.0002 \text{ dyne/cm}^2$ ; however, the spectral levels within each one-third octave band defines the basic requirements.

Table I. Acoustic Test Levels

1/3 Octave Band Center Frequency (Hz)	Sound Pressure Level in 1/3 Octave Bands (db ref $2 \times 10^{-4} \text{ dynes/cm}^2$ )
80	132.5
100	136.0
125	138.0
160	140.0
200	142.0
250	142.5
315	143.0
400	142.5
500	141.5
630	140.0
800	138.0
1000	136.0
1250	135.0
1600	133.0
2000	132.0
2500	130.0
3150	128.5
4000	127.0
5000	125.5
6300	124.0
8000	122.5
10,000	120.0

3.3.2.3 Shock. The mechanical shock environment shall be the shock pulse shown on Figure 2 and shall be applicable to each of the three mutually perpendicular axes defined in 3.3.2.1.

3.3.2.4 Static acceleration. The static acceleration environments shall be 9 g's at the approximate center of mass of the solar panel in the stowed configuration. This environment shall be considered equal for each of three mutually perpendicular axes.

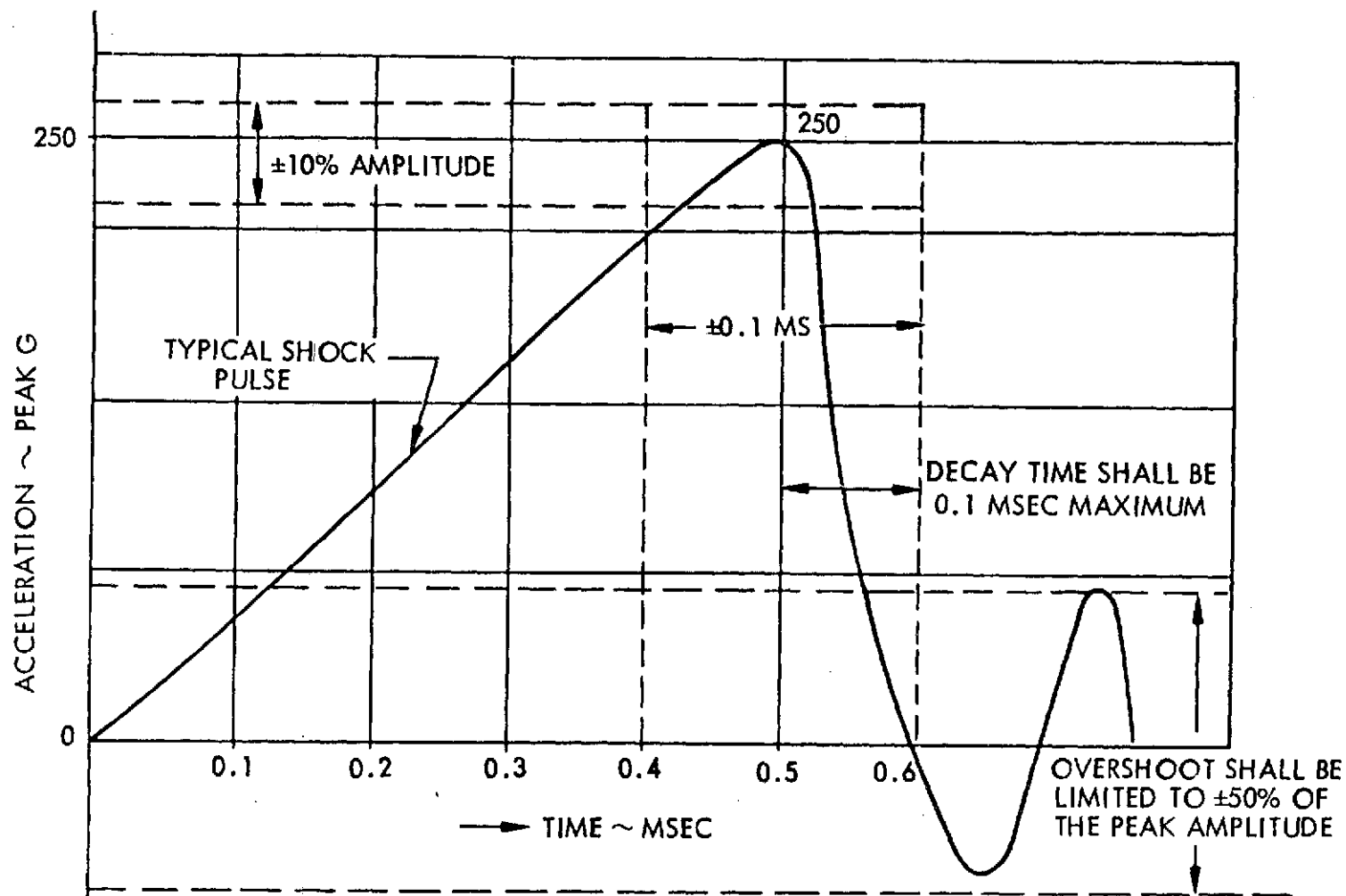
3.3.2.5 Launch pressure profile. The solar panel temperature shall be initially at  $27 \pm 6^\circ\text{C}$  and at atmospheric pressure. The pressure shall be continuously reduced, and the rate of change of pressure shall obtain a maximum of  $116 \pm 8$  torr/second, beginning from a rate of less than 16 torr/second and returning to a rate of less than 16 torr/second in a period of less than 10 seconds, and a minimum pressure level of 20 percent of the atmospheric pressure in less than 65 seconds.

3.3.2.6 Aerodynamic heating. The aerodynamic heating rate of the solar panel's external surface during boost in the stowed configuration shall be considered as  $+30^\circ\text{C}/\text{minute}$  for a period of 200 seconds. Initial temperature shall be taken to be  $27 \pm 6^\circ\text{C}$ .

3.3.3 Space flight environment. The following space flight environmental constraints shall be considered in the solar panel design. These environments are applicable for both the stowed and the deployed configurations.

3.3.3.1 Steady state thermal/vacuum environment. The steady state thermal vacuum environment shall cover the range from  $-130$  to  $+140^\circ\text{C}$  and a pressure of  $10^{-5}$  torr or less.

3.3.3.2 Thermal shock environment. The thermal shock temperature extremes shall be considered to be  $-190$  and  $+140^\circ\text{C}$  and a pressure of  $10^{-5}$  torr or less. The temperature time rates of change during thermal shock shall be at the natural cooling rate of the solar panel in a simulated passage through planetary shadow, and the natural heating rate of the solar panel in a normal solar



NOTE: SOME LATITUDE IS ALLOWABLE FOR THE WAVE SHAPE OF THE SHOCK PULSE. HOWEVER, IT IS DESIRABLE THAT THE SHAPE CONFORM TO THAT OF A TERMINAL PEAK SAWTOOTH AS NEAR AS PRACTICAL.

Figure 2. Shock Pulse

flux of intensity corresponding to a steady state temperature of 140°C on the solar panel. The total thermal shock environment shall consist of 1000 complete cooling and heating cycles.

3.3.3.3 Solar flare proton radiation environment. The proton fluency for the 3 year mission shall be defined in Table II.

Table II. Mission Proton Fluency

Proton Energy (Mev)	Total Fluency (Particles/cm <sup>2</sup> )
1	$2.0 \times 10^{12}$
10	$4.0 \times 10^{10}$
30	$9.0 \times 10^9$
100	$1.0 \times 10^9$

3.3.3.4 Pyrotechnic shock environment. The solar panel assembly shall be capable of withstanding shock environments induced by the firing of any pyrotechnics of the assembly that may be required for the operation of the assembly.

3.4 Materials, parts, and processes. Materials, parts and processes used in the design of the solar panel shall conform to the requirements specified herein. Any materials, parts, and processes that are not so covered shall be subject to the approval of the JPL cognizant engineer. In every case, the contractor's selection shall assure the highest uniform quality of the solar panel.

3.4.1 Material selection criteria. The influence of the following environments and those specified in 3.3 on the design properties of the structural, electrical, thermal control, and lubricant materials in the solar panel shall be considered:

- a. Storage at 95 percent relative humidity at 55 °C for 50 hours.
- b. 150 thermal cycles between -120 and +60 °C at  $10^{-7}$  torr with a rate of change that permits temperature stabilization dwell at the extreme temperatures.
- c. 10,000 thermal cycles between -195 and +140 °C at  $10^{-7}$  torr with a 90 minute cycle, and a temperature stabilization ( $< 2^{\circ}\text{C/hr}$ ) dwell at the extreme temperature.
- d. 1000 thermal shocks of less than 30 °C/minute.

3.4.1.1 Flight environment materials. The materials shall be capable of enduring all space environments without releasing any significant condensing gases which would decrease the solar cell efficiency, or could potentially lead to electrical shorts or degradation to the spacecraft systems operation.

3.4.2 Radiation resistance. The dosage and energy levels of the particulate radiation encountered during a mission shall not produce a significant effect on the metallic structural elements. Polymeric materials shall be either shielded or selected to resist a radiation dosage of  $10^7$  rads without decreasing the critical design properties below the design allowables.

3.4.3 Exposed structural adhesives. When used to bond transparent or partially transparent structural components, the influence of particulate radiation of  $10^7$  rads, and ultraviolet radiation equal to 3650 days of solar radiation at the rate of 2.002 calories/cm<sup>2</sup>/minute, on the adhesive shall be considered.

3.4.4 Solar cell adhesives. A requirement for two separate adhesives can exist in the solar cell area. One requirement shall be for an adhesive used to attach the solar cells to the structure; and the second shall be to bond the solar cell cover glasses to the cells. The adhesive for bonding the cover glasses

to the solar cells shall be transparent to electromagnetic radiation in the wavelengths from 0.4 to 1.0 micron, and shall be resistant to ultraviolet and particulate radiation. The adhesives shall have the following properties:

- a. High thermal conductivity.
- b. Low outgassing in the vacuum environment.
- c. A modulus of elasticity compatible with the thermal motion of the cells and structure.
- d. Repairability during the fabrication phase.

3.4.5 Thermal control coatings. Degradation of the coatings by the ultraviolet and particulate radiation of the flight environment shall be considered.

3.4.6 Bearings and lubricants. In the event bearings and lubricants are required in the solar panel design, the bearing materials shall resist the thermal excursions and particulate radiation of the flight environment. Lubricants shall not degrade: i. e., lose lubricity under flight conditions up to 3650 days, or release any condensing gases, which may potentially cause degradation to the spacecraft system. Possible occurrence of cold welding at hard vacuum shall be evaluated.

3.4.7 Part producibility. Configuration and size of parts shall be compatible with normal tooling practices. Very thin foil gage parts shall be capable of being fabricated with reasonable assurance that damage will not occur; and that the part can be handled without damage when reasonable precautions are taken.

3.4.8 Solar cell adhesive thickness tolerance. Solar panel and solar cell installation normally shall require the extensive use of bonding materials. The thickness and area of application of these materials, if used, shall be accurately controlled. The designs and processes shall include control requirements and tolerances that can be maintained in the fabrication shops.

3.4.9 Solar cell tolerances. The control of solar cell processing through the fabrication shops shall be dependent upon the comparison of initial testing and grading to subsequent cell testing during the fabrication sequence. The tolerances set by the design shall be adequate to allow a high yield of good assemblies.

3.4.10 Solar cell connections. The heat required in joining solar cells by soldering can cause degradation in cell performance. The solar cell electrical connecting technique shall be comparable with solar cell interconnection methods and shall exhibit accurate temperature control for minimum power loss.

3.4.11 Solar cell installation. The installation of solar cell assemblies on to substrate panels, and the assembly of structural components parts shall be accomplished with protective coverings on the operator's hands; or the handling shall be done with suitable mechanical devices. The configuration of these assemblies shall be designed so that the required work can be accomplished while complying with all handling restrictions.

3.4.12 Configuration of the solar panel. The configuration of the solar panel shall be designed so that positioning and holding of components and subassemblies can be accomplished to provide support during solar panel assembly.

3.4.13 Repair and replacement. Fabrication personnel shall be able to repair or replace any components of the solar panel at any time during the fabrication or ground handling sequence. The extent of repairability shall be determined by the ease of access to the damaged part without damage to adjacent parts when the repair is made.

3.5 Mechanical design criteria. The following criteria shall govern the mechanical design of the solar panel.

3.5.1 Strength and deflection requirements. All structures, with minimum material and geometric properties, shall have adequate strength and



rigidity to accomplish all requirements. In the fulfillment of the strength and deflection requirements, the worst possible combination of simultaneously applied loads and environmental conditions shall be used to determine limit loads and design loads. Particular attention shall be given to the following.

3.5.1.1 Dynamic loads. During the loads analysis, consideration shall be given to loads induced by the solar panel's elastic and rigid-body response to dynamic excitation.

3.5.1.2 Quasi-static loads. All quasi-static loads shall be considered, including launch vehicle thrust and flight maneuver loads.

3.5.1.3 Fatigue considerations. Fatigue shall be considered in the design of structural elements by the avoidance of deleterious residual stresses and stress concentrations in conformity with good design practice. Special attention shall be given to elements subjected to repeated load cycles at high stress levels. Material selection shall consider fatigue characteristics in relation to the design requirements of the structural element.

3.5.1.4 Thermal considerations. Consideration shall be given to deterioration of material properties and to stresses and deformation caused by temperature effects, both prolonged and transient.

3.5.2 Limit load. The limit load shall be considered the maximum load a structural element is expected to experience during its required functional lifetime, including fabrication, handling, and ground testing. No structural element with minimum material and geometric properties shall yield at limit loads or impair the required functions of the solar panel.

3.5.3 Design load. The design load shall be considered the limit load multiplied by the safety factor. No structural element with minimum material and geometric properties shall exceed the ultimate stress, failure by instability, or rupture at design load.

3.5.4 Material properties. The allowable material properties shall be selected to satisfy the environmental conditions that affect material properties. Metallic materials shall be in accordance with MIL-HDBK 5.

3.5.5 Safety factors. The following safety factors shall be used:

- a. Structures: 1.25.
- b. Structural joints, fittings, and brittle material: 1.44.

3.5.6 Structural qualification test levels. The environmental levels defined in 3.3 shall be considered as the qualification test levels.

3.5.7 Structural design. Simplicity of the analyses and tests shall be considered in the structural design. All structural components shall be amenable to either analytical or experimental demonstration of adequacy.

3.5.8 Structural nonlinearities. Nonlinear structural characteristics shall be kept to a minimum; however, two types of nonlinearities that are of prime importance are as follows and should be given consideration:

- a. Nonlinearities in energy dissipation mechanisms.
- b. Mechanical backlash.

3.5.8.1 Energy dissipating mechanisms. Where possible, all energy dissipating mechanisms used shall have linear force-velocity relationships over a wide range of frequencies, loads, and temperatures.

3.5.8.2 Mechanical backlash. Particular effort shall be made to avoid any mechanical backlash in all structural connections.

3.5.9 Separation joint preload. Attachment of any component to anchor shall provide for sufficient axial preload so that no physical separation will occur during any ultimate load conditions.

3.5.10 Design flexibility. The solar panel shall be designed so that additional data and advances of technology may be incorporated at later dates.

3.5.11 Thermal gradients. The solar panel shall be designed to minimize thermal gradients in the plane of the solar panel.

3.5.12 Mechanical integrity. The solar panel shall be designed to prevent the release of loose parts or gases that could damage or impair the function of the solar panel or other spacecraft subsystems.

3.5.13 Margins of safety. Margins of safety are defined with respect to the limit load or the design load as:

$$MS = \frac{*}{\text{limit load (design load)}} - 1$$

\*Load corresponding to yield stress of a structure with minimum geometric and material properties with consideration of environmental effects on material properties.

\*\*Load corresponding to ultimate stress, instability, or rupture of a structure with minimum geometric and material properties with consideration of environmental effects on material properties.

3.6 Electrical design criteria. The following criteria shall govern the electrical design of the solar panel.

3.6.1 Solar cell efficiency. The contractor shall establish the power output based on the photovoltaic characteristics of the proposed solar cell and the predicted operating temperature of the solar panel. This design effort shall include the power losses incurred during fabrication, assembly, cabling, and solar panel/spacecraft interfacing considerations.

3.6.2 Electrical insulation. The electrical insulation between the solar cells and the solar panel structure shall provide a maximum dielectric breakdown strength in air, at standard temperatures and pressure conditions,

greater than three times the open circuit voltage of the solar panel. Leakage resistance under the test conditions shall be greater than  $10^9$  ohms per square centimeter of cell area.

3.6.3 Repairability. The solar cell modules shall be constructed, and materials shall be selected so that any defective cell can be replaced in a fabrication repair area without damage to adjacent cells, electrical insulation, or mounting substrate.

3.6.4 Compatibility of materials. The solar cell stack shall be designed to use only materials that are compatible thermally, mechanically, and electrically with each other, with the space environment, and interface requirements of the solar cells substrate.

3.6.5 Interconnections. The solar cells shall be interconnected both in parallel and in series by a metallic conductor. This conductor shall be designed to minimize both thermal and flexural stresses on the solar cell interconnection. The resistance of the interconnection, plus solder, shall not exceed 2 percent of the total series resistance of the solar cells. The joint shall have a strength equal to, or greater than the strength of the bond between the semiconductor material and the ohmic contacts. The joining materials shall exhibit stable physical and electrical characteristics in both space and terrestrial environments.

3.6.6 Magnetic field. Solar cell wiring, interconnecting and structural techniques shall be designed to minimize the magnetic field produced by the flow of current in the solar panel.

3.6.7 Electrical conductors. The size and configuration of electrical conductors shall be determined by the following considerations:

- a. Minimum possible weight.
- b. Minimum resistivity.
- c. Minimum magnetic field.
- d. Mechanical strength to endure design loads.

- e. Exterior finish to be resistant to natural and induced environments.
- f. Process adaptability.
- g. Redundancy.
- h. Thermal coefficient of expansion.
- i. Thermal shock (minimum of 30 °C/minute) on the cells.
- j. Repairability.
- k. Conductor flexibility.

3.6.8 Conductor insulation. Conductor insulating materials shall be selected on the basis of the following considerations:

- a. Mechanical strength.
- b. Flexibility.
- c. Dielectric characteristics.
- d. Ease of forming or fabricating.
- e. Flight environment considerations.
- f. Minimum weight.

3.6.9 Electrical terminals. Terminals shall be used to facilitate maintenance, repair, and replacement of electrical components. The following requirements for terminals shall be met:

- a. Voltage drop across any terminal shall not exceed 25 millivolts at rated load.
- b. The terminals shall withstand 50 cycles of manual mating and unmating without replacement of parts.
- c. The terminals shall be accessible for ease of wiring, installation and for factory or field checkout.
- d. The terminals shall be rigidly attached to primary or secondary structure.
- e. The terminals shall have minimum possible weight.
- f. Exterior finish of the terminals shall be resistant to both natural and induced environments.

3.6.10 Installation. The installation of wires, terminals, electrical connectors, and busses shall conform to the following requirements:

- a. Busses and other wiring shall be installed in order to minimize magnetic fields.
- b. Installation shall withstand the rigors of normal handling and transportation as well as launch and operational maneuvers.
- c. Installation shall be designed to facilitate service and repair activities.

3.6.11 Electrical checkout. Test terminals shall be provided on the solar panel to permit ground testing and checkout prior to launch, in a one-g Earth field, with suitable ground support equipment (GSE).

3.7 Workmanship. Workmanship of the solar panel model shall be of such quality that the model shall be free from any defects that would affect its performance or appearance.

#### 4. QUALITY ASSURANCE PROVISIONS

4.1 Contractor inspection. The contractor shall perform all necessary Quality Assurance control and inspection to assure that compliance with the requirements of this specification have been fulfilled.

4.2 Rejection and resubmittal. Units that do not meet all the test requirements of this specification shall be rejected. Before resubmittal, complete particulars concerning the previous rejection and the action taken to correct the defects shall be furnished.

5. PREPARATION FOR DELIVERY

5.1 Packaging, packing and shipping. The point of inspection, acceptance, and the delivery of all deliverable supplies specified herein shall be made at Jet Propulsion Laboratory, 4800 Oak Grove Drive, Pasadena, California. All deliverable supplies shall be packaged, packed, boxed, or crated in a manner that will assure safe delivery and shall be shipped prepaid to JPL.

6. NOTES

None.

APPENDIX B  
SOLAR CELL RADIATION DAMAGE  
VS  
1-MeV ELECTRON FLUENCE



SOLAR CELL RADIATION DAMAGE  
VS  
1-MeV ELECTRON FLUENCE

The following figures show the degradation in solar cell short-circuit current, open-circuit voltage, and maximum power as a function of 1-MeV electron fluence. Two nominal solar cell base resistivities are shown: Figures B-1, B-2 and B-3 for 2 ohm-cm and Figures B-4, B-5 and B-6 for 10 ohm-cm.

Cell thicknesses from 300 to 86  $\mu\text{m}$  are shown for the 2 ohm-cm resistivity, while thicknesses from 305 to 94  $\mu\text{m}$  are shown for the 10 ohm-cm resistivity. All these curves are based on data obtained from Reference 71.

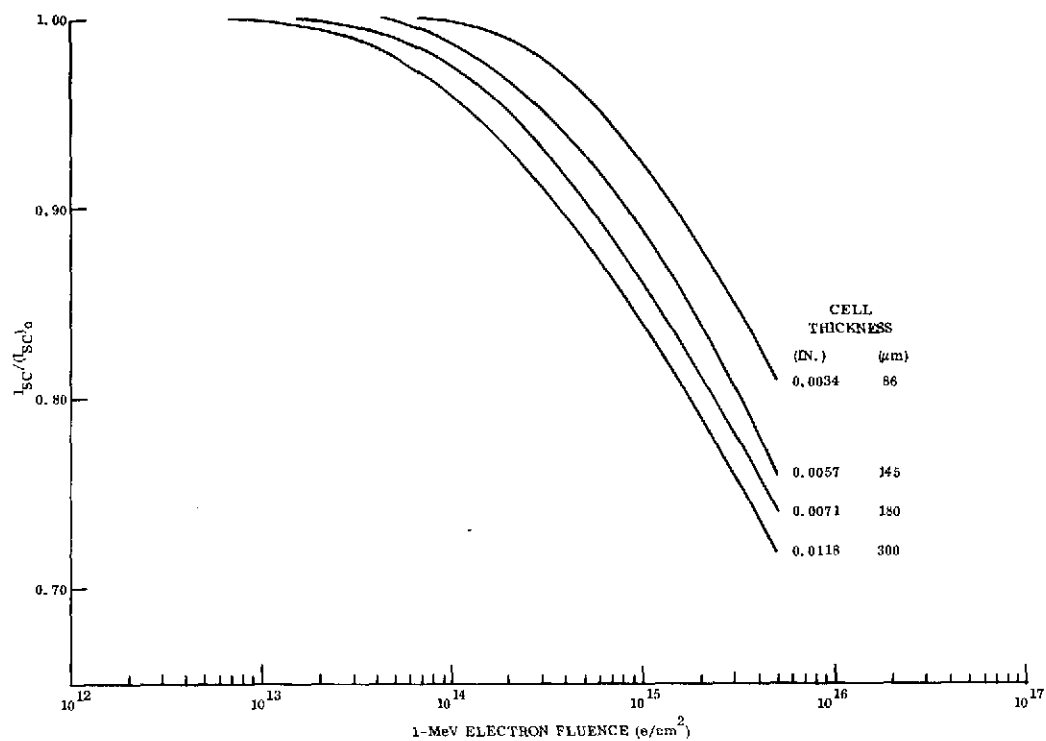


Figure B-1. Short-Circuit Current Degradation for 2 ohm-cm N/P Silicon Solar Cells (from Reference 71)

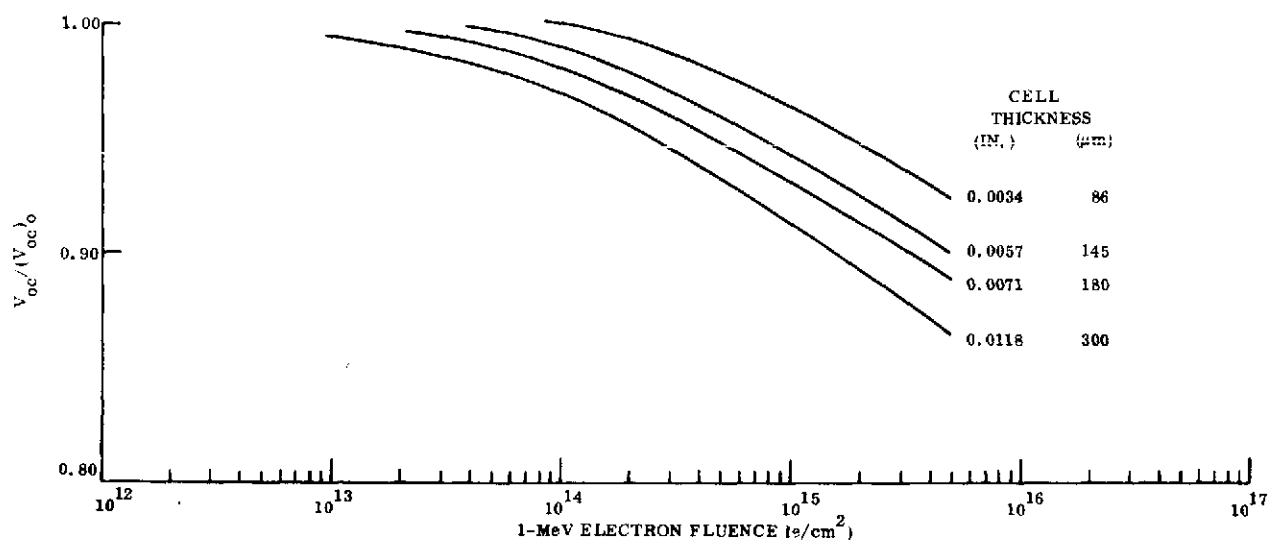


Figure B-2. Open-Circuit Voltage Degradation for 2 ohm-cm N/P Silicon Solar Cells (from Reference 71)

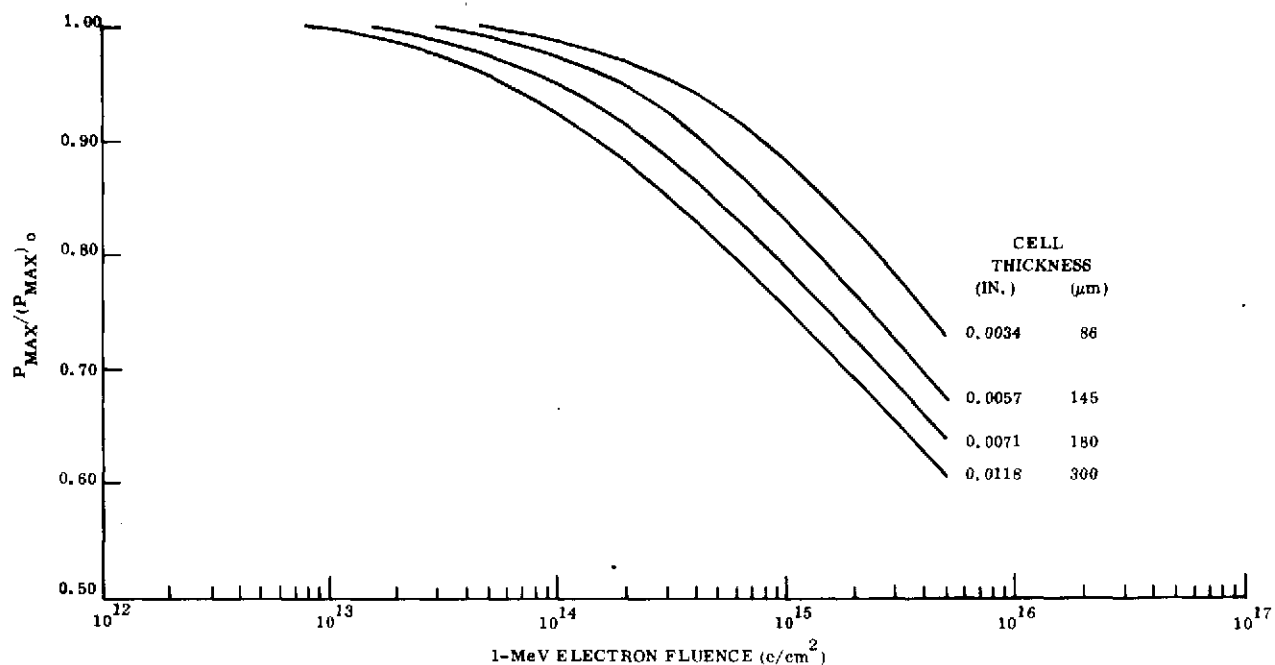


Figure B-3. Maximum Power Degradation for 2 ohm-cm N/P Silicon Solar Cells (from Reference 71)

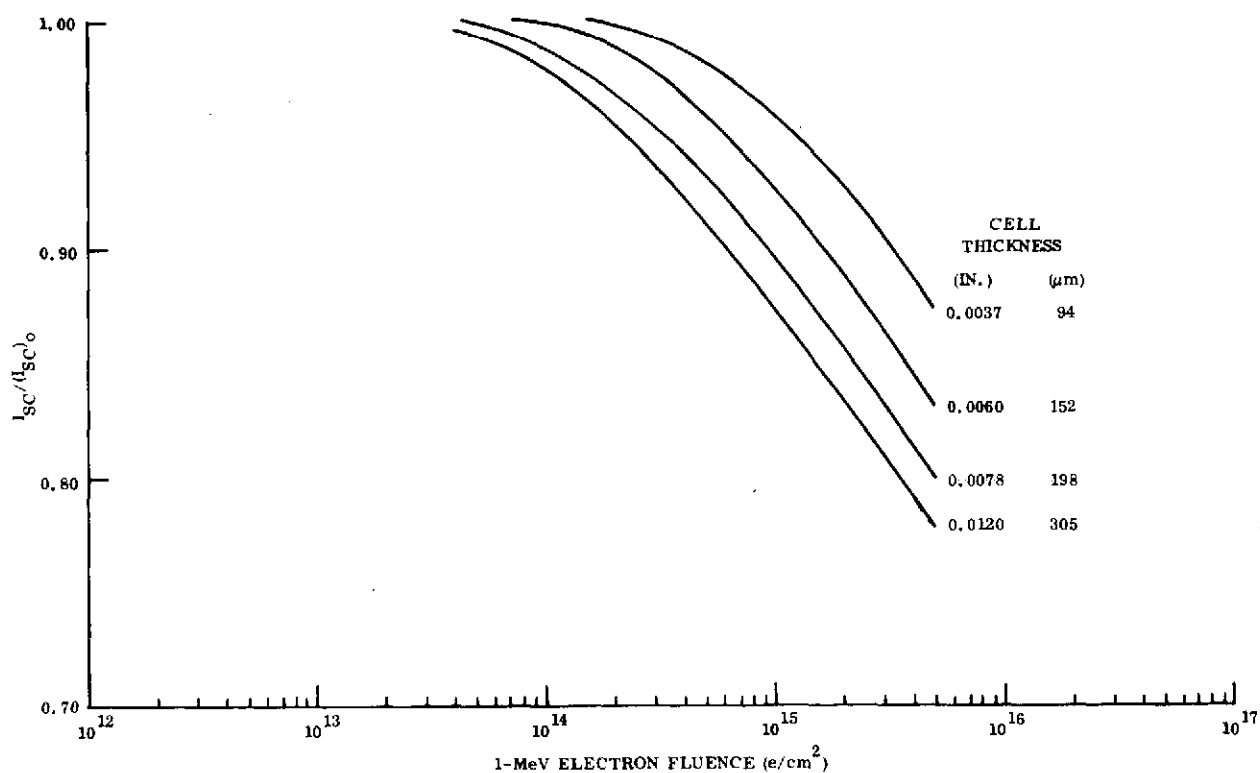


Figure B-4. Short-Circuit Current Degradation for 10 ohm-cm N/P Silicon Solar Cells (from Reference 71)

CA

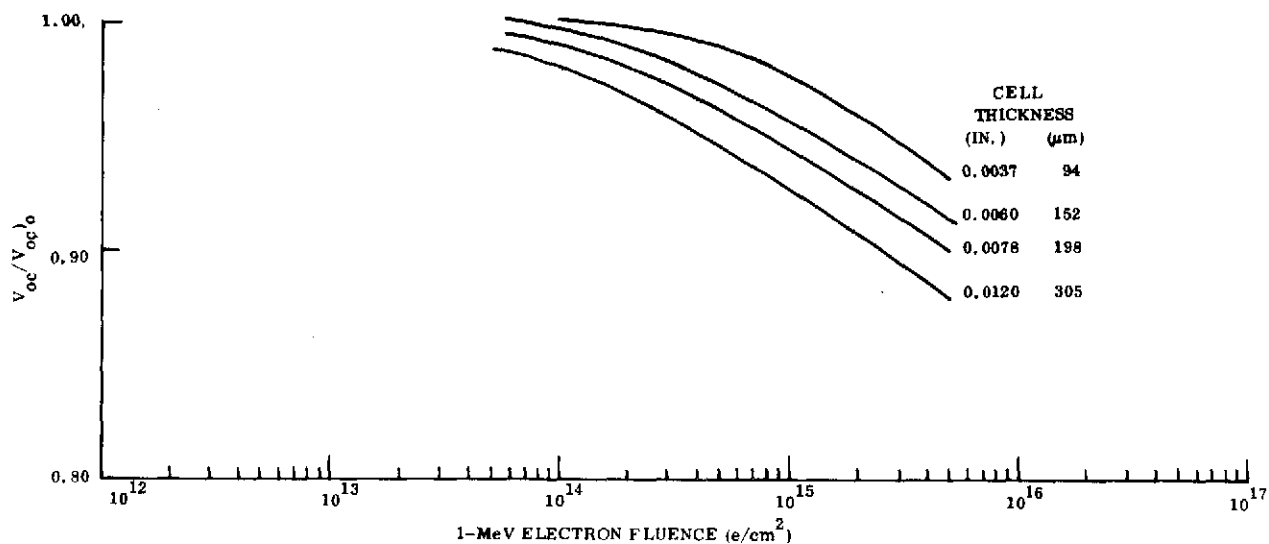


Figure B-5. Open-Circuit Voltage Degradation for 10 ohm-cm N/P Silicon Solar Cells (from Reference 71)

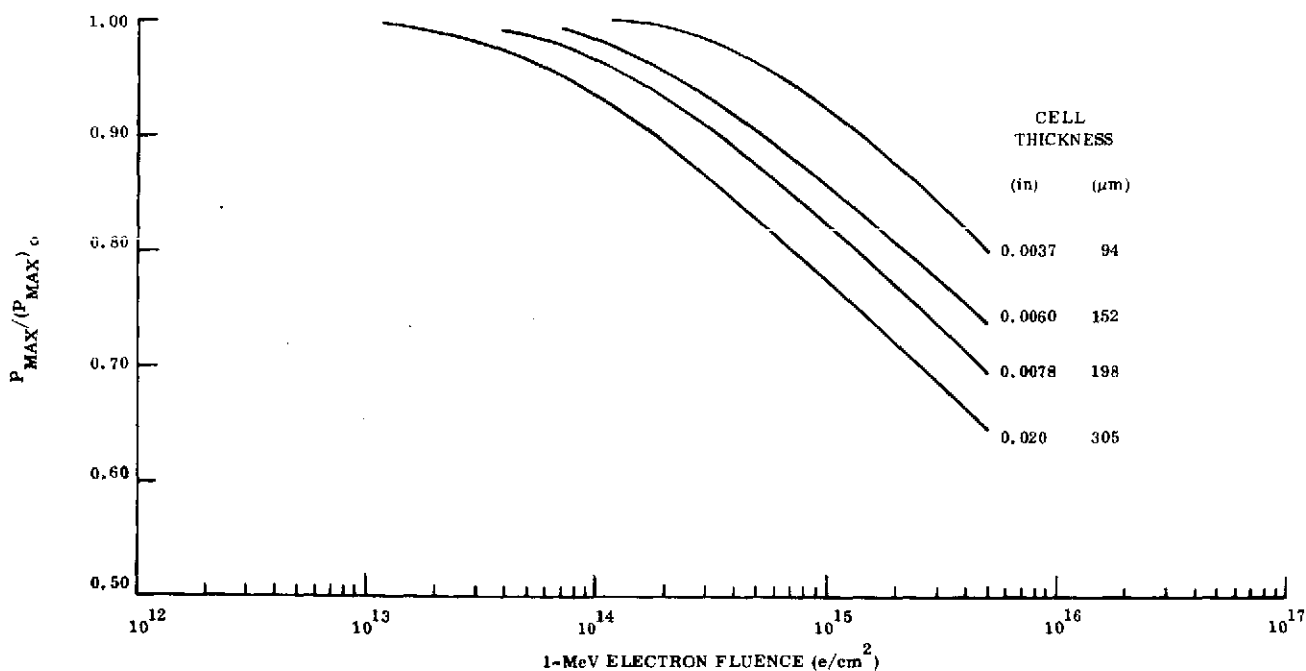


Figure B-6. Maximum Power Degradation for 10 ohm-cm N/P Silicon Solar Cells (from Reference 71)

APPENDIX C  
PRELIMINARY SPECIFICATION  
FOR AN  
ULTRALIGHTWEIGHT  
INTEGRALLY COVERED SOLAR CELL

General Electric Company  
Space Division  
P. O. Box 8555  
Philadelphia, Pa. 19101

Specification No. 1J86-984  
November 29, 1972  
Rev. A

PRELIMINARY SPECIFICATION  
FOR AN  
ULTRALIGHTWEIGHT  
INTEGRALLY COVERED SOLAR CELL

Prepared by: N F Shepard, Jr  
N. F. Shepard, Jr.  
Development Engineer

Date: 11/29/72

Approved by: K L Hanson  
K. L. Hanson  
Program Manager

Date: 11/30/72

REVISION LOG

This log identifies those portions of this specification which have been revised since original issue. Revised portions of each page, for the current revision only, are indicated by marginal striping.

REV.	PAGE NO.	PARAGRAPH NUMBER(S) AFFECTED	REVISED DATE
A	6	3.1.6	30 April 1973
	13	3.3.2 3.3.3	
	18	4.2.6.3	

## SECTION 1

### SCOPE

This specification establishes the design, test, quality assurance and packaging requirements for ultralightweight, integrally covered, N on P silicon solar cells.



SECTION 2  
APPLICABLE DOCUMENTS

The following documents, of the exact issue specified, form a part of this specification to the extent specified herein. In the event of conflict between this specification and any of these referenced documents, this specification shall govern.

SPECIFICATIONS

Military

MIL-Q-9858A 16 December 1963	Quality Program Requirements
MIL-C-45662A 9 February 1962	Calibration System Requirements
MIL-T-10727A 20 May 1959	Tin Plating; Electrodeposited or Hot-Dipped, for Ferrous and Non-ferrous Metals
MIL-E-12397B 18 November 1954	Eraser, Rubber-Pumice (for Testing Coated Optical Elements)
MIL-C-675A Amendment 3 26 March 1971	Coating of Glass Optical Elements (Anti-reflection)

Federal

QQ-C-576b Amendment 1	Copper Flat Products with Slit, Slot and Edge-rolled, Sheared, Sawed or Machined Edges (Plate, Bar, Sheet, and Strip)
--------------------------	---

STANDARDS

Military

MIL-STD-456A Notice 1 15 January 1970	Electronic Parts, Date and Source Coding for
---	--

### SECTION 3 REQUIREMENTS

#### 3.1 BARE SOLAR CELL REQUIREMENTS

The following requirements apply to the bare solar cell prior to deposition of the integral coverglass.

##### 3.1.1 BASE RESISTIVITY

The "P"-doped silicon crystal shall have a bulk material resistivity of 7 to 12 ohm-centimeters.

##### 3.1.2 DIMENSIONS

The cell dimensions shall be  $20.0 \pm 0.15$  mm by  $20.0 \pm 0.15$  mm and shall be  $125 \pm 25$   $\mu$ m thick. Each cell shall fit within a perfect rectangle of the maximum cell dimensions and cover a perfect rectangle of the minimum cell dimensions excluding corner and edge defects. A detailed drawing delineating cell dimensions shall be submitted to GE for approval prior to award of contract. This drawing shall be used for definition of mechanical acceptance criteria.

##### 3.1.3 WEIGHT

The average cell weight measured on a lot basis shall not exceed 0.130 grams.

##### 3.1.4 GRID LINE DISCONTINUITY

The total discontinuity in any grid line shall not exceed 3.5 mm, and the total discontinuity per cell shall not exceed 6.0 mm.

##### 3.1.5 SILICON IMPERFECTIONS

No more than six of the type of imperfections described in this paragraph and its

Rev. A

subsections shall be allowed on a single cell.

#### 3.1.5.1 Edge Imperfections

No edge chip shall be greater than 0.75 mm in depth and 3.8 mm in length. Imperfections less than 125  $\mu$ m in depth and 1.25 mm in length shall not be regarded as imperfections.

#### 3.1.5.2 Corner Chips

No corner chip shall be greater than 1.5 mm along the hypotenuse.

#### 3.1.6 CONTACTS

The solar cells shall have a bottom wraparound contact configuration as shown schematically in Figure 1. The negative contact metallization shall wrap around the cell edge to provide the N contact strip on the rear surface along with the P contact. All contacts and grid lines shall be plated nickel-copper-nickel-gold. The contact strength of each cell shall be sufficient to withstand the contact pull test (paragraph 4.2.6.3) and the tape test (paragraph 4.2.6.2).

#### 3.1.7 ANTI-REFLECTIVE COATING

Each cell shall have a titanium oxide ( $\text{TiO}_x$ ) coating on the active N surface. The optical characteristics of this coating shall be optimized to produce the highest cell electrical output when covered with the integral coverglass system specified in paragraph 3.2. This anti-reflective coating shall be uniform and continuous, and fall within color, void, and stain limits set up by the manufacturer and approved by GE prior to the start of production.

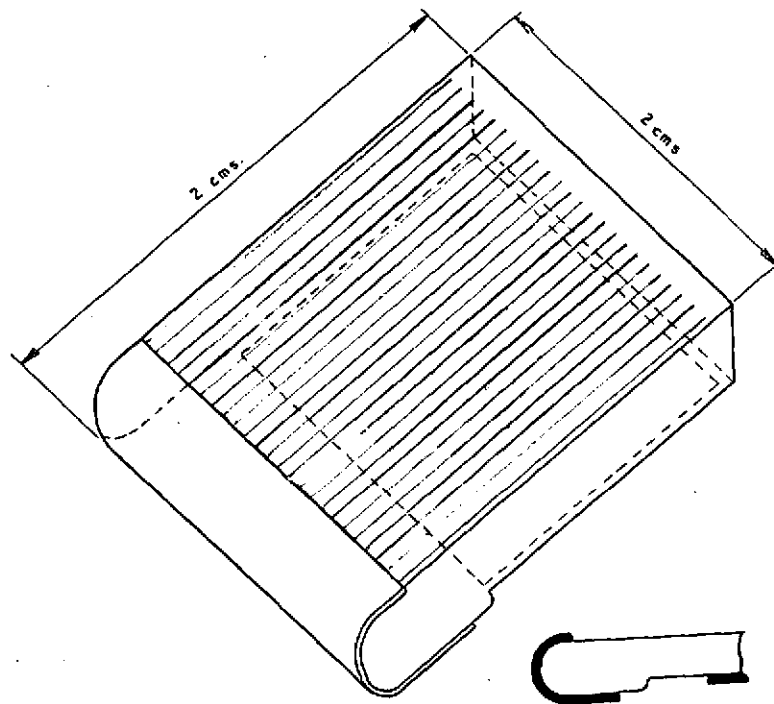


Figure 1. Bottom Wraparound Contact Configuration

### 3.1.8 SPECTRAL RESPONSE

The spectral response of all cells produced during the course of procurement shall be uniform. Controls for production cells shall be instituted to insure uniformity of spectral response and shall be subject to approval by GE.

### 3.1.9 CLEANLINESS

The solar cells shall be clean and free from any finger prints, oil contamination, or other foreign materials.

## 3.2 COVERED SOLAR CELL REQUIREMENTS

The following requirements apply to the integrally covered solar cell.

### 3.2.1 INTEGRAL COVER DEPOSITION PROCESS

Each solar cell shall have an integral coverglass which is deposited by the radio frequency sputtering of Corning 7070 glass.

### 3.2.2 INTEGRAL COVER THICKNESS

The nominal thickness of the deposited glass layer shall be 30 to 37  $\mu\text{m}$ . On any one cell, the thickness variation over the complete front surface shall be less than  $\pm 10\%$ .

### 3.2.3 CELL EDGE COVERAGE

The integral coverglass shall provide some cell edge coverage as specified by the limits on Figure 2.

### 3.2.4 ANTI-REFLECTIVE COATING

The exposed surface of the integral coverglass shall have a single layer  $\text{MgF}_2$  anti-reflective coating which is designed to enhance the transmittance of energy to the

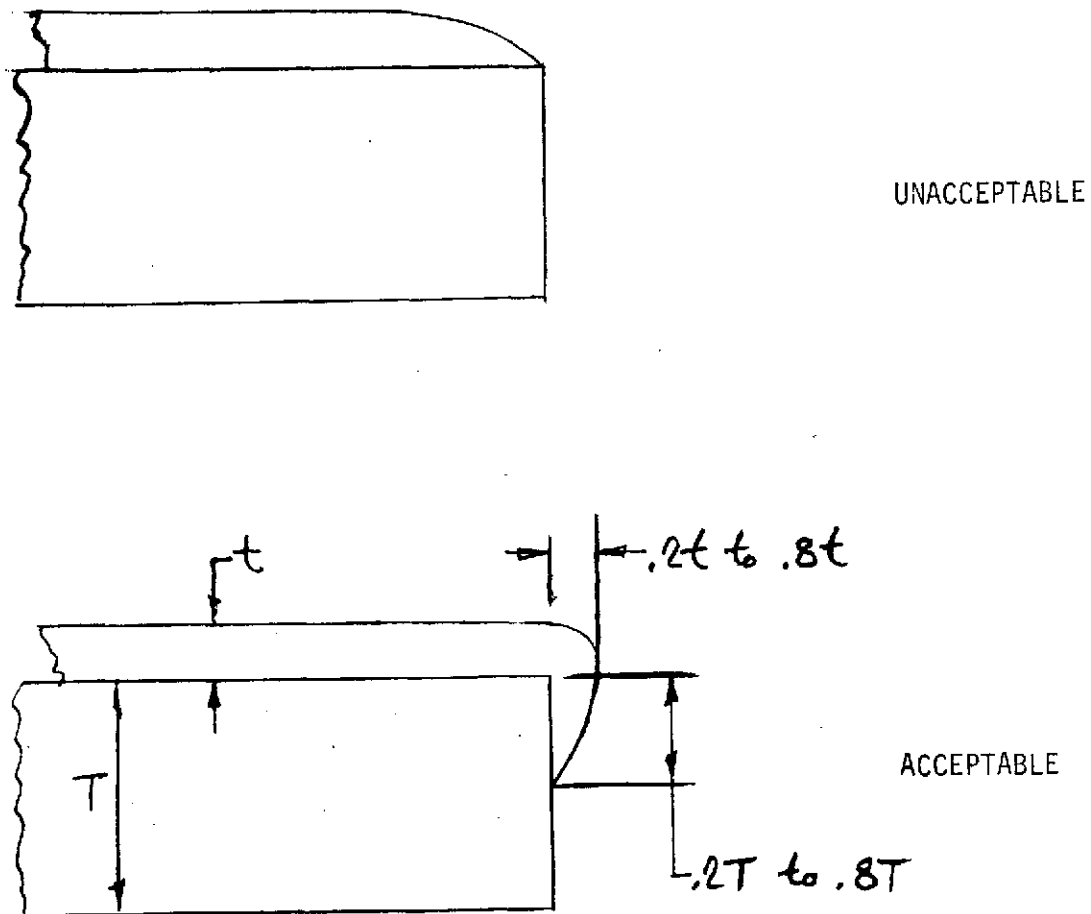


Figure 2. Limits of Acceptable Cell Edge Coverage

solar cell in the region of peak response. There shall be no visible damage to the coated surface when rubbed with an eraser conforming to MIL-E-12397 for 20 strokes with a force of 9 to 11 N.

### 3.2.5 WEIGHT

The average covered cell weight measured on a lot basis shall not exceed 0.162 grams.

### 3.2.6 CELL BOWING

The bowing of the covered solar cells shall be less than 50  $\mu$ m as defined by the "h" dimension on Figure 3 when measured at room temperature.

### 3.2.7 ELECTRICAL OUTPUT REQUIREMENTS

#### 3.2.7.1 Illumination Intensity

The cells shall be tested in an illumination source which supplies an equivalent air mass zero, 1 A.U. intensity as determined by measuring the short-circuit current of two standard cells which have been previously calibrated against balloon flown standards, aircraft flown standards, or an alternate method which shall be subject to GE approval. These standard cells shall be representative of the cells supplied to this specification with respect to spectral response and integral coverglass material and thickness. The standard cells shall be positioned in such a way as to duplicate the position of the cell when under test. The calibration criteria for the illuminator is that the sum of the measured short-circuit currents from the two standard cells shall be less than or equal to the sum of the calibration values of the air mass zero short-circuit currents.

#### 3.2.7.2 Test Temperature

The cell temperature under test shall be 25°C minimum. The cell temperature shall

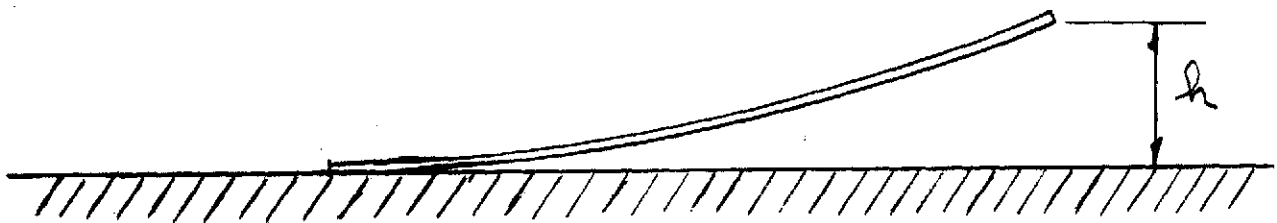


Figure 3. Measurement of Solar Cell Bowing



be determined by controlling and monitoring the cell test fixture block at the test temperature.

### 3.2.7.3 Electrical Output

Each cell and shipping lot supplied to this specification shall meet the minimum output requirements as delineated below when measured at the illumination intensity and temperature as defined in paragraphs 3.2.7.1 and 3.2.7.2, respectively.

Parameter	Value
1. Test Voltage	445 $\pm$ 1.0 mv
2. Individual Cell Minimum Current at Test Voltage	119 ma
3. Shipping Lot Average Minimum Current at Test Voltage	123 ma
4. Individual Cell Minimum Open-circuit Voltage	525 mv
5. Shipping Lot Average Minimum Open-circuit Voltage	535 mv

## 3.3 ENVIRONMENTAL REQUIREMENTS

Except as specified herein, the covered solar cells shall meet all requirements of this specification after exposure to the following environmental conditions.

### 3.3.1 HUMIDITY

Following exposure to 95-100% relative humidity at an ambient temperature of 25  $\pm$  5°C for 336 hours (14 days), the solar cells shall meet the following performance

conditions:

- a. No softening of the I-V curve knee such that the post-humidity test curve current is 2 ma or less than the pre-humidity test curve current at 445 mv.
- b. No presence of a single blister or peel larger than 0.75 mm diameter.
- c. No presence of more than one blister or peel larger than 0.50 mm diameter.

### 3.3.2 LOW ENERGY PROTON IRRADIATION

The covered solar cells shall be capable of surviving a normally incident 1 MeV proton irradiation of a total fluence of  $10^{14}$  protons/cm<sup>2</sup> without experiencing a degradation in electrical performance which exceeds 2 ma at 0.445 volts.

### 3.3.3 THERMAL CYCLING

The solar cells shall be capable of surviving 1,000 thermal cycles between -195 and +140°C at a pressure of  $10^{-7}$  torr or less. The maximum rate of change of temperature shall be 30°C/minute. There shall be no evidence of integral coverglass or contact delamination. The degradation in electrical performance shall not exceed 2 ma at 0.455 volts.

SECTION 4  
QUALITY ASSURANCE PROVISIONS

4.1 QUALITY ASSURANCE PROGRAM

4.1.1 QUALITY CONTROL SYSTEM

The supplier shall provide and maintain a quality control system meeting the requirements of this specification and MIL-Q-9858A.

4.1.2 INSPECTION PLAN

A written inspection plan shall be prepared by the supplier, and shall be maintained and updated during the period of performance under this specification. The inspection plan, and any changes and/or additions shall be submitted to GE for approval at least four weeks before the required and/or intended use.

The inspection plan shall include, but not be limited to, those elements required by the referenced specifications with particular emphasis on the following:

- a. Inspection flow charts indicating sequence of operations, and location of inspection stations.
- b. Inspection instructions, check lists, or equivalent for each inspection station showing method of inspection or test, characteristics checked, acceptance criteria, and measuring or testing equipment used.
- c. Sampling plan if other than 100 percent.

#### 4.1.3 PROCESS CHANGE

Any change in the manufacturing process that may affect the mechanical and/or electrical properties of the cell shall be submitted to GE at least one week prior to implementation and shall be subject to disapproval by GE. All submittals shall indicate the lot or serial number of the "cut-in" point and proposed data of implementation.

#### 4.1.4 SAMPLING PLANS

Sampling plans utilized by the supplier in evaluating or controlling performance against this specification shall be approved by GE prior to implementation.

#### 4.1.5 ACCESS TO SUPPLIER'S FACILITY

GE representatives shall have access to the supplier's facility where work on the cells is being performed and shall be provided with any data necessary to permit evaluation of the manufacturing process and the test methods applicable to this procurement.

#### 4.1.6 IDENTIFICATION AND TRACEABILITY (I&T)

The supplier shall develop a plan for implementing the I&T requirements specified in MIL-Q-9858A. This plan shall be submitted as a part of the Inspection Plan required in paragraph 4.1.2.

### 4.2 TEST PROGRAM

#### 4.2.1 TEST PLAN

The supplier shall prepare a test plan which shall be submitted to GE for review and approval prior to the start of production.

#### 4.2.2 TEST APPARATUS

Gauging, measuring, and other calibration and test equipment must be of the proper type and required accuracy and shall be in conformity with Military Specification MIL-C-45662. Calibration records shall be maintained, dated and signed by the vendor and made available at the supplier's plant for GE review and inspection. Digital voltmeters utilized for cell output readings shall have an accuracy of  $\pm 0.01\%$  with a  $\pm 0.01$  mv resolution. In the event current-voltage curves are required, the X-Y plotter utilized shall have an accuracy of  $\pm 0.25\%$  of full scale.

#### 4.2.3 TEST RECORDS

The supplier shall supply GE with signed and dated documentation (test data and reports) to verify that the completed cells meet all of the in-process test requirements of Section 4.2.6 prior to or upon delivery to GE for each shipping lot.

#### 4.2.4 TEST CONDITIONS

Unless otherwise specified herein, all tests shall be performed at room ambient conditions of  $24 \pm 3^\circ\text{C}$ .

#### 4.2.5 TEST LOCATION

Unless otherwise specified in the contract, tests shall be performed at the supplier's plant. If the use of outside test facilities is required, the use of these facilities shall be subject to approval by GE. GE shall have the right to witness, inspect and review all tests.

#### 4.2.6 IN-PROCESS TESTING

The following tests shall be performed on the solar cells during their fabrication. The purpose of these tests is to insure product quality.

#### 4.2.6.1 Examination of Product

The solar cells shall be mechanically inspected to determine compliance with respect to materials, workmanship, dimensions and weight as specified in paragraphs 3.1.2, 3.1.3, 3.1.4, 3.1.5, 3.1.7, 3.1.9, 3.2.2, 3.2.3, 3.2.5, and 3.2.6.

#### 4.2.6.2 Tape Test

Prior to integral coverglass deposition, each solar cell shall be subjected to a tape test which is performed as follows:

- a. Scotch brand No. 600 Magic Mending tape shall be applied to the "N" surface with the length of the tape normal to the grid lines. The tape shall be pressed onto the cell with sufficient force to insure full transparency.
- b. The tape shall be stripped from the surface at a rate of 5 to 10 cm/sec by applying a force normal to the surface.
- c. This test shall be repeated until the entire "N" surface has been taped.

The failure criteria for this test shall be damage to the grids and/or anti-reflection coating which causes the cell to fall below specified electrical parameters as given in Paragraph 3.2.7.3. Mechanical acceptance criteria for this test is 95% mechanically continuous metallic coverage of the grids. Ten power magnification will be used for this test. All solar cells must be cleaned after performance of this test to insure that no residue of the tape adhesive remains on the solar cell surface.

#### 4.2.6.3 Contact Pull Test

A contact pull test shall be performed on a randomly selected sample of four (4) cells from each production lot. Half of these selected cells shall be subjected to an "N" contact pull test, and the remainder to a "P" contact pull test. The pull tabs shall be flat ribbon  $0.75 \pm .05$  mm wide by  $75 \pm 5$   $\mu$ m thick, and of sufficient length for clamping in the pull tester. The tab shall be bent  $90^\circ \pm 3^\circ$  with a 2.5 mm radius  $0.88 \pm .12$  mm from the end. Tab material shall be copper CR 1/2 hard as per QQ-C-576 tin plated as per MIL-T-10727 Type I and fused. A single tab shall be soldered  $3.0 \pm .75$  mm from the end of the solar cell "N" contact. The tab shall be installed such that the ribbon width is perpendicular to the grid lines and the tab clamping section is on the outboard side of the cell. The outer edge of the "N" contact and the tangent point of radius on the peel tab shall coincide. The tab soldering technique shall be determined by the supplier as long as it accomplishes the test objective. Peel tab installation of the "P" contact shall be accomplished in a similar manner to the "N" contact tab. That is to say, the peel tab shall be soldered  $3.0 \pm 7.5$  mm from any contact edge with the long dimension of the tab edge parallel to this "P" contact edge. The same edge/peel tab radius tangent shall be maintained as previously described for the "N" contact.

The cell shall be clamped to prevent movement in such a manner that the restraining force is distributed over at least 80 percent of the cell surface. The tensile force applied to the tab normal to the face of the cell shall be applied at a uniform rate not exceeding 100 grams per second. The reading of the tensile force indicator shall be recorded at the instant of separation of the tab from the cell. If any contact separation force is less than 500 grams, without cleavage of the silicon, a second sample of 8 cells shall be similarly tested. If this second test correlates

with the initial test results indicating questionable contact band integrity, the particular lot of cells shall be rejected.

#### 4.2.6.4 Abrasion

Three randomly selected covered cells from each production lot shall be subjected to the following abrasion test. The coated surface of the integral coverglass shall be rubbed with an eraser conforming to MIL-E-12397 mounted in a holding device which applies a normal force between 9 and 11 N. Twenty strokes along the same path shall be performed with no visible evidence of damage to the anti-reflective coating. These cells may be subsequently used for the humidity test defined in paragraph 4.2.6.5.

#### 4.2.6.5 Humidity Test

Three randomly selected covered cells from each production lot shall be subjected to the humidity test specified in paragraph 3.3.1. A pre-test and post-test I-V curve shall be obtained for each cell. The acceptance criteria shall be as specified in paragraph 3.3.1.

#### 4.2.6.6 Thermal Shock Test

A thermal shock test shall be performed on a randomly selected sample of three (3) covered cells from each production lot. The test cells, which are initially at room temperature, shall be immersed in liquid nitrogen for a period of 5 minutes, minimum. Following this exposure, the cells shall be transferred to an oven which is maintained at  $140 \pm 5^{\circ}\text{C}$ . The transfer time shall not exceed 30 seconds. After a minimum of 5 minutes in the oven, the cells shall be transferred to the liquid nitrogen bath. The transfer time shall not exceed 30 seconds. This cycle shall be repeated until the cells are removed from the oven for the fifth time. This test



shall produce no evidence of physical damage to the cell or integral coverglass and no delamination of the coverglass from the cell. There shall be no degradation in electrical performance.

#### 4.2.6.7 Electrical Performance Test

Each covered solar cell shall be electrically tested in accordance with the conditions of intensity and temperature specified in paragraphs 3.2.7.1 and 3.2.7.2.

#### 4.2.7 REJECTION OF DEFECTIVE MATERIAL

Any item failing to meet any requirement of this specification may be returned to the supplier's plant at his expense.

#### 4.2.8 NON-CONFORMING MATERIAL

The supplier may offer material having minor non-conformance for review of a decision-making material review board (MRB). Each MRB shall be composed of one supplier representative whose primary responsibility is product quality, and one GE representative. Acceptance of non-conforming material shall be determined by unanimous agreement of the MRB. Pertinent technical competence and thorough knowledge of product quality and functional requirements shall be prerequisite qualifications for all MRB members. Material review board members may consult with other organizations and personnel as required to arrive at optimum decisions. The decisions of the board shall be supported by records of all cases submitted for action, including material that can be reworked to specification, and corrective action taken.

#### 4.2.9 RESUBMISSION OF REJECTED MATERIAL

Any material rejected by GE, either at the vendor's facility or at GE shall bear adequate identification of such rejection if resubmitted. Reference shall be made

Specification No. 1J86-984  
November 29, 1972

to the GE rejection document and evidence given that the causes have been removed.

## SECTION 5

### PREPARATION FOR DELIVERY

#### 5.1 CELL GROUPING

All solar cells comprising a shipping lot shall be grouped according to the value of the current measured at the test voltage as defined in paragraph 3.2.7.3.

Group No.	Current at Test Voltage (ma)
1	119.0 to 120.9
2	121.0 to 122.9
3	123.0 to 124.9
4	125.0 to 126.9
5	127.0 to 128.9

After grouping the shipping lot shall be adjusted to meet the minimum average current requirement as specified in paragraph 3.2.7.3.

#### 5.2 PACKAGING

The solar cells shall be placed in rigid foam boxes with individual slots to prevent the cells from coming in contact with each other. Each box shall contain not more than 100 cells, and cells from more than one electrical group shall not be packaged in the same box.

Each box shall be clearly identified by the following:

- a. Manufacturer's name or trademark

- b. GE part number
- c. Quantity contained in the box
- d. Shipping lot number
- e. Year and week of manufacture/MIL-STD-456A
- f. Box or individual cells marked with the current group number as specified in paragraph 5.1

### 5.3 SHIPMENT

The cells shall be shipped in shipping cartons with adequate protective materials such that surface and/or air transportation will cause no damage or degrade the performance of the cells.

All documentation and certification as mentioned herein shall be submitted to GE Quality Assurance Department prior to or no later than the time of lot shipment.

## SECTION 6

### NOTES

#### 6.1 DEFINITIONS

##### 6.1.1 SHIPPING LOT

A shipping lot is defined as an accumulation, for shipment, of solar cells manufactured under the same conditions and accepted after performance of the tests specified herein. Identification of all production lots contained in each shipping lot shall be specified in the certifications supplied with each lot at the time of shipment.

##### 6.1.2 PRODUCTION LOT

A production lot is defined as a group of solar cells manufactured to this specification which had contacts plated at the same time.

APPENDIX D

PRELIMINARY SPECIFICATION

FOR A

CANISTER DEPLOYED CONTINUOUS

LONGERON ASTROMAST BOOM

General Electric Company  
Space Division  
P. O. Box 8555  
Philadelphia, Pennsylvania 19101

Specification No. 1J86-992  
15 January 1973  
Rev. A

PRELIMINARY SPECIFICATION  
FOR A  
CANISTER DEPLOYED, CONTINUOUS  
LONGERON ASTROMAST BOOM

PREPARED BY: N. F. Shepard, Jr.  
N. F. Shepard, Jr.  
Development Engineer

DATE: Jan 19, 1973

APPROVED BY: K. L. Hanson  
K. L. Hanson  
Program Manager

DATE: Jan 30, 1973

REVISION LOG

This log identifies those portions of this specification which have been revised since original issue. Revised portions of each page, for the current revision only, are indicated by marginal striping.

REV.	PAGE NO.	PARAGRAPH NUMBER(S) AFFECTED	REVISED DATE
A	1 3 5 6 7 8 10	3.2.3, 3.2.4 3.2.5, 3.2.6 Figure 1 3.2.12.1	30 April 1973



## SECTION 1

### SCOPE

This specification covers the design, fabrication and test requirements for a canister deployed, continuous longeron ASTROMAST boom for potential use as part of a lightweight solar array panel system. The boom and associated actuator are herein referred to as the component.

## SECTION 2

### APPLICABLE DOCUMENTS

The following documents, of the exact issue specified, form a part of this specification to the extent specified herein. In the event of conflict between this specification and any of these referenced documents, this specification shall govern.

#### SPECIFICATIONS

##### Military

MIL-E-5400M Amendment 1 16 March 1971	Electronic Equipment, Airborne, General Specification for
---	---

MIL-Q-9858A 16 December 1963	Quality Program Requirements
---------------------------------	------------------------------

MIL-C-45662A 9 February 1962	Calibration System Requirement
---------------------------------	--------------------------------

#### STANDARDS

##### Military

MIL-STD-454C 19 October 1970	Standard General Requirements for Electronic Equipment
---------------------------------	--

MIL-STD-889 25 September 1962	Dissimilar Metals
----------------------------------	-------------------

MS33540F 12 August 1969	Safety Wiring, Cotter Pinning, General Practices for
----------------------------	--

MIL-STD-202D Notice 1 14 April 1970	Test Methods for Electronic and Electrical Component Parts
---	--

MIL-STD-130D 5 March 1971	Identification Marking of US Military Property
------------------------------	--

General Electric Company

146A9560                      Preparation for Delivery of Commercial Shipments - General  
Revision A                      Requirements for

OTHER PUBLICATIONS

National Aeronautics and Space Administration

NHB 5300.4(3A)                Requirements for Soldered Electrical Connections  
May 1968

DRAWINGS

General Electric Company

(TBD)                      Interface Control Drawing, Canister Deployed, Continuous  
Longeron ASTROMAST Boom

## SECTION 3 REQUIREMENTS

### 3.1 GENERAL REQUIREMENTS

The component is intended for use as an actuation device for a lightweight flexible solar array system. It shall consist of two main functional parts: (1) a continuous longeron ASTROMAST structure and (2) the canister and mechanism which houses the stowed mast and permits in-orbit extension by remote command. In-orbit retraction capability is not required, but retraction capability for ground testing must be provided for within the component.

### 3.2 DETAIL PERFORMANCE REQUIREMENTS

#### 3.2.1 FULLY EXTENDED LENGTH

The fully extended length of the mast shall be  $18.6 \pm 0.05$  m ( $61.0$  ft  $\pm 2$  in) measured from the top surface of the canister to the end of the mast at the interface surface with the solar array panel leading edge member.

#### 3.2.2 EXTENSION RATE

The boom extension rate shall be  $4 \pm 2.5$  cm/sec ( $1.5 \pm 1$  in/sec).

#### 3.2.3 MAST DIAMETER

The mast diameter (defined as the diameter of a circle through the center of the longerons) shall have a nominal value of 19.0 cm (7.50 inches)

#### 3.2.4 BENDING STIFFNESS

The bending stiffness of the mast shall be at least  $3440$  N-m<sup>2</sup> ( $1.2 \times 10^6$  lb<sub>f</sub>-in<sup>2</sup>).

### 3.2.5 COMPONENT MASS

The maximum total component mass shall be 7.7 kg (17.0 lbm) including the mass of the canister and boom element.

### 3.2.6 COMPONENT SIZE

The canister diameter, as defined in Figure 1, shall be 22.8 cm (9.0 inches), maximum and the canister height shall be 67.0 cm (26.4 inches) maximum.

### 3.2.7 COMPONENT MOUNTING ARRANGEMENT

The component mounting arrangement shall be as defined in the Interface Control Drawing (GE Drawing No. TBD ).

### 3.2.8 STRAIGHTNESS AND ALIGNMENT

#### 3.2.8.1 Definition of Deployment Axis

The boom deployment axis shall be defined as a straight line which is parallel to the axis of the cylindrical deployment canister and passes through the centroid of the mast longerons at the canister exit plane.

#### 3.2.8.2 Boom Straightness

The tip deflection, measured from the deployment axis as defined in paragraph 3.2.8.1, shall not be greater than 0.457 m (1.5 ft) when measured as specified in paragraph 4.2.6.5.

### 3.2.9 STRUCTURAL LOADING CONDITIONS

When mounted in the solar array panel assembly, the component shall be capable of enduring the following loading conditions without failure or malfunction. These loading conditions shall be considered as acting together under deployment condi-

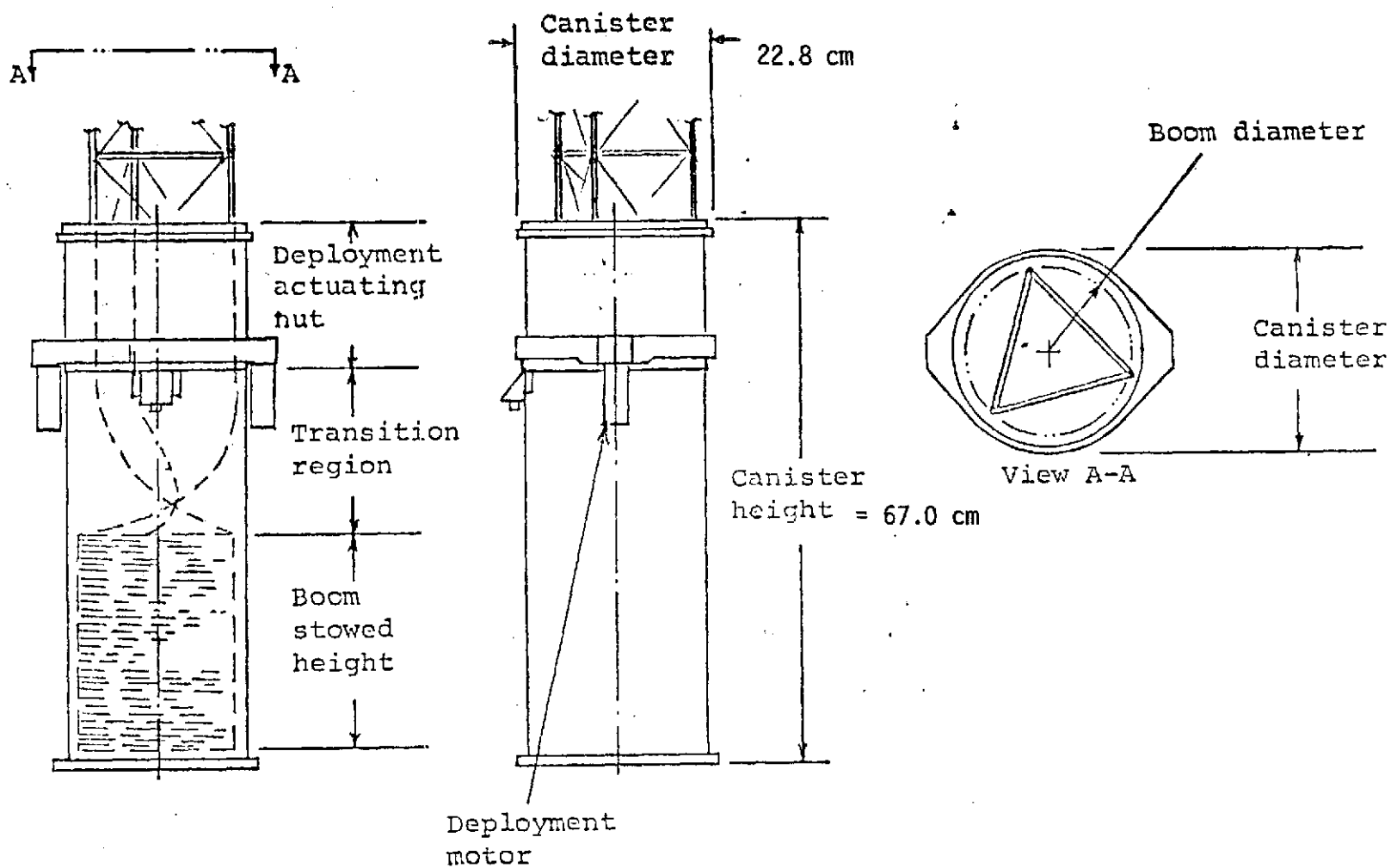


Figure 1. Geometry of Canister Deployed, Continuous Longeron ASTROMAST (not to scale)

tions from 0 to 100% of the fully extended length.

- (a) Tension - A constant tension force shall be applied at the boom tip and directed at a fixed point regardless of boom tip motion. This fixed point is defined as the centroid of the mast longerons at the canister exit plane. The magnitude of this tension force shall be 8.9 N (2.0 lbf) for extensions from 0 to 90% of the fully extended length and 33.4 N (7.50 lbf) for extensions from 90 to 100% of the fully extended length.
- (b) Acceleration - With a tip mass of 2.6 kg (5.74 lb<sub>m</sub>), the mast shall be capable of sustaining a linear steady-state acceleration of  $10^{-4}g$  in any direction.

### 3.2.10 THERMAL BENDING

When subjected to a solar flux of 540 mw/cm<sup>2</sup>, the tip of the unloaded fully deployed mast shall not deflect more than 0.457 m (1.5 ft) from its initial unilluminated position.

### 3.2.11 COMBINED THERMO-STRUCTURAL LOADING

When mounted in the solar array panel assembly, the component shall be capable of enduring, without failure or malfunction, the combined influences of the structural loading conditions specified in paragraph 3.2.9 along with a solar flux input which varies from 140 mw/cm<sup>2</sup> during deployment to a maximum of 540 mw/cm<sup>2</sup> in any direction relative to the solar array panel over the duration of the mission.

### 3.2.12 ELECTRICAL REQUIREMENTS

#### 3.2.12.1 Deployment Motor(s)

The canister shall be motor-driven. The motor shall control the extension rate to the value specified in paragraph 3.2.2 with an input voltage which ranges from 24 to 34 vdc.

#### 3.2.12.2 Limit Switches

The component shall be equipped with two limit switches, one which is mechanically actuated at full extension, and one which is mechanically actuated when the boom is totally stowed within the canister. The wiring for these switches shall be brought out of the component separate from the motor wiring.

#### 3.2.12.3 Wiring and Connectors

No electrical connectors shall be used. Two meter (6 ft) long flying leads shall be provided on all wires requiring external connection. All internal wiring shall be in accordance with MIL-E-5400, paragraphs 3.1.33 through 3.1.33.7. All wire shall be Raychem 44/0411.

#### 3.2.12.4 Dielectric Strength and Insulation Resistance

There shall be no evidence of dielectric breakdown when the component is subjected to 500 VAC, 60 Hz between all terminals shorted together and the case. Insulation resistance shall be a minimum of 100 megaohms when measured at 500 VDC between all mutually insulated points and ground.

#### 3.2.12.5 Continuity

These shall be point-to-point continuity in accordance with the Interface Control Drawing (GE Drawing No. TBD ) in both the fully stowed and fully extended positions.



### 3.2.13 CAGING

The component design shall provide restraint against extension or retraction motions during the launch phases of the mission. For design and test purposes, a tip mass of 1.0 kg (2.2 lb<sub>m</sub>) shall be used as the effective mass which is concentrated at the tip in the stowed configuration.

### 3.2.14 LIFE

The component shall be capable of 100 cycles of full and/or partial extensions and retractions under ground test conditions without malfunction or reduction in the probability of successful deployment in space following the launch environment exposure specified in paragraph 3.3.2. The component shall be capable of performing its structural function for a period of three years in the space flight environment defined in paragraph 3.3.1.

## 3.3 ENVIRONMENTAL CONDITIONS

The component shall be capable of meeting the requirements of paragraph 3.2 under any natural combination of the conditions specified in paragraph 3.3.1 after exposure to any natural combination of the conditions specified in paragraph 3.3.2.

### 3.3.1 SPACE FLIGHT ENVIRONMENT

The following space flight environmental constraints are applicable for both the stowed and the deployed configuration of the component.

#### 3.3.1.1 Steady-State Thermal/Vacuum

The steady state thermal vacuum environment shall cover the range from -130 to +140°C and a pressure of  $10^{-5}$  torr or less.

### 3.3.1.2 Thermal Shock Environment

The thermal shock temperature extremes shall be considered to be -190 to +140°C and a pressure of  $10^{-5}$  torr or less. The temperature time rates of change during thermal shock shall be at the natural cooling rate of the component in a simulated passage through planetary shadow, and to natural heating rate of the component in a normal solar flux of intensity corresponding to a maximum steady state temperature of 140°C on the component. The total thermal shock environment shall consist of 1000 complete cooling and heating cycles.

### 3.3.1.3 Solar Flare Proton Radiation Environment

The solar flare proton radiation environment for the mission duration is defined in Table 1.

Table 1. Solar Flare Proton Environment

Proton Energy -E (MeV)	Total Fluence $\phi > E$ (p/cm <sup>2</sup> )
1	$2.0 \times 10^{12}$
10	$4.0 \times 10^{10}$
30	$9.0 \times 10^9$
100	$1.0 \times 10^9$

### 3.3.2 LAUNCH ENVIRONMENT

The following environmental constraints represent the anticipated launch exposure with the component in the stowed configuration.

#### 3.3.2.1 Sinusoidal Vibration

The sinusoidal vibration input levels at frequencies between 10 and 2000 Hz are

specified in Table 2. The levels are at the interface between the component and the remaining portions of the solar array panel assembly. These input vibration levels shall be applied along each of three mutually perpendicular axes, one of which shall be in the mast deployment direction.

Table 2. Component Level Sinusoidal Vibration

Frequency (Hz)	Input Level
10-13	12.5 mm D.A. Displacement
13-50	4.0 g o-p
50-150	8.0 g o-p
150-380	12.0 g o-p
380-550	.04 mm D.A. Displacement
550-2000	27.0 g o-p

Sweep Rate = 1.0 octave/min

#### 3.3.2.2 Acoustic Noise

The launch acoustic noise environment shall be 60 seconds of a random incidence, reverberant sound field, having the third-octave band sound pressure levels defined in Table 3. The overall sound pressure level of the spectrum given in Table 3 shall be approximately 150 db referenced to  $0.0002 \text{ dyne/cm}^2$ ; however, the spectral levels within each one-third octave band define the basic requirement.

#### 3.3.2.3 Shock

The mechanical shock environment shall be the shock pulse shown on Figure 2 and shall be applicable to each of the three mutually perpendicular axes defined in 3.3.2.1.

Table 3. Acoustic Test Levels

1/3 Octave Band Center Frequency (Hz)	Sound Pressure Level in 1/3 Octave Bands (db ref $2 \times 10^{-4}$ dynes/cm <sup>2</sup> )
80	132.5
100	136.0
125	138.0
160	140.0
200	142.0
250	142.5
315	143.0
400	142.5
500	141.5
630	140.0
800	138.0
1000	136.0
1250	135.0
1600	133.0
2000	132.0
2500	130.0
3150	128.5
4000	127.0
5000	125.5
6300	124.0
8000	122.5
10,000	120.0

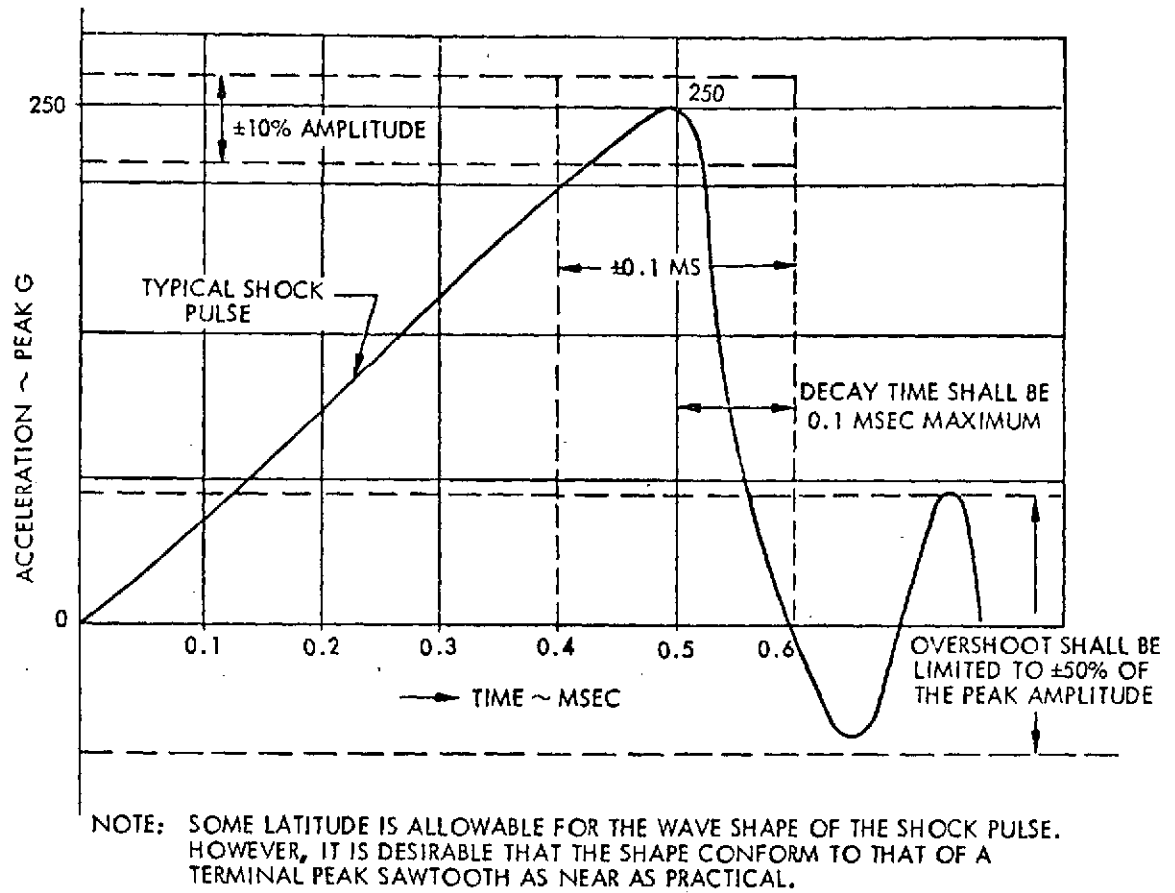


Figure 2. Shock Pulse

#### 3.3.2.4 Static Acceleration

The static acceleration environments shall be 9 g's at the approximate center of mass of the component in the stowed configuration. This environment shall be considered equal for each of three mutually perpendicular axes.

#### 3.3.2.5 Launch Pressure Profile

The component temperature shall be initially at  $27 \pm 6^{\circ}\text{C}$  and at atmospheric pressure. The pressure shall be continuously reduced, and the rate of change of pressure shall obtain a maximum of  $116 \pm 8$  torr/second, beginning from a rate of less than 16 torr/second and returning to a rate of less than 16 torr/second in a period of less than 10 seconds, and a minimum pressure level of 20 percent of the atmospheric pressure in less than 65 seconds.

#### 3.3.2.6 Aerodynamic Heating

The aerodynamic heating rate of the component's external surface during boost in the stowed configuration shall be considered as  $+30^{\circ}\text{C}/\text{minute}$  for a period of 200 seconds. Initial temperature shall be taken to be  $27 \pm 6^{\circ}\text{C}$ .

### 3.4 DESIGN AND CONSTRUCTION

#### 3.4.1 MATERIALS, PROCESSES, AND PARTS

Materials, processes, and parts shall conform to all applicable specifications and standards defined in this specification. Materials, parts, and processes used in the fabrication of equipment previously accepted by the Government shall be acceptable, provided that all of the following are met:

- a. Evidence of prior acceptance of the equipment is submitted to GE-SS.
- b. Prior application(s) included demonstrated capability in equivalent or more severe environments and for longer operational life than

specified herein.

c. The design is approved by GE-SS.

#### 3.4.1.1 Moisture and Fungus Resistance

Component design shall conform to requirement 4 of MIL-STD-454, except paragraph 2 and all references to MIL-STD-810. Wherever possible, non-nutrient materials which resist damage from moisture and fungus shall be used. Protective coatings shall not be acceptable as moisture and fungus preventatives for parts which may lose their coating during the normal course of assembly, inspection, maintenance, and testing.

#### 3.4.1.2 Corrosion of Metal Parts

The use of dissimilar metals, as defined in MIL-STD-889, shall be avoided wherever possible. Materials, techniques, and processes shall be selected and employed with regard to heat treatment procedure, corrosion, protection, finish, and assembly and installation such that sustained or residual surface tensile stress, stress concentrations, and the hazards of stress corrosion, cracking, and hydrogen embrittlement are minimized. Cadmium plating shall not be used. Selected finishes shall be compatible with the thermal requirements of this specification. Materials and surfaces which may be exposed to an effluent shall be selected for compatibility with the effluent insofar as design considerations permit.

#### 3.4.1.3 Material Selection Criteria

The influence of the following environments and those specified in 3.3 on the design properties of the structural, electrical, thermal control, and lubricant materials in the component shall be considered:

- a. Storage at 95 percent relative humidity at 55°C for 50 hours.
- b. 150 thermal cycles between -120 and +60°C at  $10^{-7}$  torr with a rate of change that permits temperature stabilization dwell at the extreme temperatures.
- c. 10,000 thermal cycles between -195 and +140°C at  $10^{-7}$  torr with a 90-minute cycle, and a temperature stabilization ( $2^{\circ}\text{C/hr}$ ) dwell at the extreme temperature.
- d. 1000 thermal shocks of less than  $30^{\circ}\text{C/minute}$ .

#### 3.4.1.4 Outgassing

The materials shall be capable of enduring all space environments without releasing any significant condensing gases which would decrease the solar cell efficiency, or could potentially lead to electrical shorts or degradation to the spacecraft systems operations.

#### 3.4.1.5 Radiation Resistance

The dosage and energy levels of the particulate radiation encountered during a mission shall not produce a significant effect on the metallic structural elements. Polymeric materials shall be either shielded or selected to resist a radiation dosage of  $10^7$  rads without decreasing the critical design properties below the design allowables. In addition, the effects of ultraviolet radiation equal to 3650 days of solar radiation at the rate of  $2.0 \text{ calories/cm}^2/\text{min}$  shall be considered in the selection of polymeric materials.

#### 3.4.1.6 Thermal Control Coatings

Degradation of the coatings by the ultraviolet and particulate radiation of the



flight environment shall be considered.

#### 3.4.1.7 Bearings and Lubricants

Bearings and associated lubricating materials shall resist the thermal excursions and particulate radiation of the flight environment. Lubricants shall not degrade: i.e., lose lubricity under flight conditions up to 3650 days, or release any condensing gases, which may potentially cause degradation to the spacecraft system. Possible occurrence of cold welding at hard vacuum shall be evaluated.

#### 3.4.2 NAMEPLATES AND PRODUCT MARKING

Identification and marking shall be in accordance with the requirements of MIL-STD-130 and MIL-E-5400, Paragraph 3.1.16.

#### 3.4.3 INTERCHANGEABILITY

All components shall be mechanically and electrically interchangeable in accordance with requirement 7 of MIL-STD-454.

#### 3.4.4 SAFETY

Design consideration shall be given to minimize hazardous interaction of equipment, facilities, and facility equipment during component test, and final installation. Suitable precautions shall be specified in component handling, assembly, and test instructions. Ground operating procedures shall incorporate warning and cautionary instructions to preclude inadvertent equipment or personnel injury resulting from electrical shock. Parts which may work loose in service shall be safety wired in accordance with MS33540, or shall have other approved locking means applied.

Personnel safety shall be in accordance with MIL-STD-454, requirement 1.

#### 3.4.5 WORKMANSHIP

Components manufactured under this specification shall be constructed and finished in a manner indicative of good workmanship. Workmanship shall be in accordance with Requirements 9 and 24 of MIL-STD-454 and with NHB 5300.4(3A).

SECTION 4  
QUALITY ASSURANCE PROVISIONS

4.1 QUALITY ASSURANCE PROGRAM

4.1.1 QUALITY CONTROL SYSTEM

The supplier shall provide and maintain a quality control system meeting the requirements of this specification and MIL-Q-9858A.

4.1.2 INSPECTION PLAN

A written inspection plan shall be prepared by the supplier, and shall be maintained and updated during the period of performance under this specification. The inspection plan, and any changes and/or additions shall be submitted to GE for approval at least four weeks before the required and/or intended use.

The inspection plan shall include, but not be limited to, those elements required by the referenced specifications with particular emphasis on the following:

- a. Inspection flow charts indicating sequence of operations, and location of inspection stations.
- b. Inspection instructions, check lists, or equivalent for each inspection station showing method of inspection or test, characteristics checked, acceptance criteria, and measuring or testing equipment used.

4.1.3 PROCESS CHANGE

Any change in the manufacturing process that may affect the mechanical and/or electrical properties of the component shall be submitted to GE at least one week

prior to implementation and shall be subject to disapproval by GE. All submittals shall indicate the lot or serial number of the "cut-in" point and proposed date of implementation.

#### 4.1.4 SAMPLING PLANS

Sampling plans utilized by the supplier in evaluating or controlling performance against this specification shall be approved by GE prior to implementation.

#### 4.1.5 ACCESS TO SUPPLIER'S FACILITY

GE representatives shall have access to the supplier's facility where work on the component is being performed and shall be provided with any data necessary to permit evaluation of the manufacturing process and the test methods applicable to this procurement.

#### 4.1.6 IDENTIFICATION AND TRACEABILITY (I&T)

The supplier shall develop a plan for implementing the I&T requirements specified in MIL-Q-9858A. This plan shall be submitted as a part of the Inspection Plan required in paragraph 4.1.2.

### 4.2 TEST PROGRAM

#### 4.2.1 TEST PLAN

The supplier shall prepare a test plan which shall be submitted to GE for review and approval prior to the start of production.

#### 4.2.2 TEST APPARATUS

Gauging, measuring, and other calibration and test equipment must be of the proper type and required accuracy and shall be in conformity with Military Specification

MIL-C-45662. Calibration records shall be maintained, dated and signed by the vendor and made available at the supplier's plant for GE review and inspection.

#### 4.2.3 TEST RECORDS

The supplier shall supply GE with signed and dated documentation (test data and reports) to verify that the completed component meets all of the test requirements of Section 4.2 prior to or upon delivery to GE of each component.

#### 4.2.4 TEST CONDITIONS

Unless otherwise specified herein, all tests shall be performed at room ambient conditions of  $24 \pm 3^{\circ}\text{C}$ .

#### 4.2.5 TEST LOCATION

Unless otherwise specified in the contract, tests shall be performed at the supplier's plant. If the use of outside test facilities is required, the use of these facilities shall be subject to approval by GE. GE shall have the right to witness, inspect and review all tests.

#### 4.2.6 FUNCTIONAL TESTING

The following tests shall be performed on each component.

##### 4.2.6.1 Examination of Product

The component shall be mechanically inspected to determine compliance with respect to materials, workmanship, dimensions, and mass as specified in paragraphs 3.2.1, 3.2.5, 3.2.6, 3.2.7, 3.4.1, 3.4.2, 3.4.5.

##### 4.2.6.2 Continuity Test

Prior to the first application of power, a continuity test shall be performed to

insure that all point-to-point wiring is in accordance with the interconnection diagram.

#### 4.2.6.3 Dielectric Strength and Insulation Resistance Test

The component shall be subjected to the following tests to verify the requirements of paragraph 3.2.12.4.

1. Dielectric Strength: This test shall be performed in accordance with MIL-STD-202, Method 301, using the following parameters:
  - a. The test voltage shall be 500 VAC, 60 Hertz.
  - b. Application of test voltage shall be for 2 seconds.
  - c. The test voltage shall be applied across all insulation separating circuits from each other, and separating circuits from case and/or ground.
  - d. The equipment shall not be subjected to more than two applications of test voltage.
2. Insulation Resistance: This test shall be performed in accordance with MIL-STD-202, Method 302, using the following parameters:
  - a. The test voltage shall be 500 VDC.
  - b. Electrification time shall be 1 minute.
  - c. The test voltage shall be applied across all insulation separating circuits from each other, and separating circuits from case and/or ground.

#### 4.2.6.4 Ambient Deployment

The component shall be deployed to its fully extended length by floating on a water surface. The tension loading specified in paragraph 3.2.9(a) shall be applied during the deployment. Extension rate and motor voltage and current shall be monitored during the deployment.

#### 4.2.6.5 Boom Straightness

Boom straightness shall be measured with the boom floating in an unloaded condition on a water surface. The displacement of the tip relative to the theoretical boom axis shall be measured for two orientations of the boom relative to the water surface. These orientations shall be with the minimum moment of inertia axis normal to the water surface and parallel to the water surface.

#### 4.2.6.6 Boom Stiffness

With the boom fully deployed and floating on a water surface and static load-tip deflection test shall be performed to determine the effective bending stiffness about the minimum moment of inertia axis.

#### 4.2.7 ENVIRONMENTAL TESTING

##### 4.2.7.1 Vibration

The component shall be tested to demonstrate its ability to withstand the environment defined in Table 2 without structural failure or subsequent malfunction. Attachment of the component to the vibration exciter shall be made by a rigid fixture at the mounting points delineated in GE Drawing No. (TBD) . During vibration, the effective tip mass specified in paragraph 3.2.13 shall be applied. Vibration shall be applied in each of three orthogonal directions, one direction being parallel to the deployment axis.

#### 4.2.8 REJECTION OF DEFECTIVE MATERIAL

Any component failing to meet any requirement of this specification may be returned to the supplier's plant at his expense.

#### 4.2.9 NON-CONFORMING MATERIAL

The supplier may offer material having minor non-conformance for review of a decision-making material review board (MRB). Each MRB shall be composed of one supplier representative whose primary responsibility is product quality, and one GE representative. Acceptance of non-conforming material shall be determined by unanimous agreement of the MRB. Pertinent technical competence and thorough knowledge of product quality and functional requirements shall be prerequisite qualifications for all MRB members. Material review board members may consult with other organizations and personnel as required to arrive at optimum decisions. The decisions of the board shall be supported by records of all cases submitted for action, including material that can be reworked to specification, and corrective action taken.

#### 4.2.10 RESUBMISSION OF REJECTED MATERIAL

Any material rejected by GE, either at the vendor's facility or at GE, shall bear adequate identification of such rejection if resubmitted. Reference shall be made to the GE rejection document and evidence given that the causes have been removed.



SECTION 5  
PREPARATIONS FOR DELIVERY

The component shall be prepared for delivery in accordance with GE Specification 146A9560.